ELECTRON IMPACT EXCITATION OF THE n = 3 LEVELS OF HYDROGEN

by

Robert Francis Syms B.Sc. (Lond.)

A Thesis submitted to the
Faculty of Science of the
University of London for
The Degree of Doctor of Philosophy

Department of Mathematics
Royal Holloway College

1978

ABSTRACT

This thesis is concerned with the study of the excitation of Hydrogen atoms to the $n = 3$ states from the ground state by electrons with incident energies ranging from just above the ionization threshold to energies where the first Born approximation is expected to be valid ($\sim$15 - 200 eV).

The major physical effects in this region are exchange, the distortion of the wave describing the external electron, and the distortion of the atomic system.

A model which includes these effects - the Distorted Wave Polarized Orbital (DWPO) approximation - is generalized for any $1s - n\ell$ excitation and used to investigate the excitation process for $n = 3$ in particular.

Total (integrated) and differential cross sections, not previously calculated using this model, are presented and compared, where possible, with other theoretical and experimental work. Other sensitive indicators of the effects of the model are considered. These include the polarization of Balmer-α ($H\alpha$) radiation and the parameters which describe the orientation and alignment of the atomic system after collision and the coincidence rate for the observation of emitted photons with the ejected electrons (Fano-Macek and Macek-Jaecks parameters). Also studied is the asymmetry in the observed intensity of $H\alpha$ radiation arising on sign reversal of an applied electric field along the interaction direction. There is a serious disparity between the results in this model or the Born approximation and the experimental observations. A number of reasons for this are discussed.

The work here indicates a need for further theoretical and experimental study but that high levels of sensitivity are required in any experimental work particularly with regard to the polarization and asymmetry measurements. Additionally, this work illustrates a very serious failure in the DWPO model caused by the use of the adiabatic polarization potential rather

than an energy dependent potential especially at higher ($\geq$ 150 eV) energies in the 3d excitation where we found that for the total cross section, the results obtained by including full allowance for polarization lie a factor of about 2.5 below the Born result at 200 eV and do not approach the Born cross section even for impact energies measured in keV. The most useful line of future research is expected to be the allowance for coupling to adjacent states by the unitarization method and some preliminary work for this is included.

ACKNOWLEDGEMENTS

I wish to express my thanks and appreciation to all those people who have helped me during the course of this work.

In particular I am deeply indebted to my Supervisor, Professor M.R.C. McDowell, without whose help and guidance this work would not have been done. I also wish to thank Dr. L.A. Morgan for her assistance with the computational aspects and for many useful discussions especially on the coincidence parameters.

I wish to acknowledge the Science Research Council for their patronage in the form of a postgraduate studentship.

My thanks are expressed to Mrs. B. Rutherford - who, despite my writing, has patiently typed this thesis.

Finally, I am very grateful to my wife, Margaret, for her patience, understanding, encouragement and help throughout the course of this work, with the preparation of this thesis and particularly with the graph drawing.

CONTENTS

APPENDICES

LIST OF FIGURES

LIST OF TABLES

CHAPTER I

INTRODUCTION AND ATOMIC SCATTERING THEORY

§1.1 Background to this Study

In this work we have extended and generalised our application of the Distorted Wave Polarized Orbital (DWPO) approximation. The series of previously published reports includes: McDowell et al. 1973; 1974; 1975a,b; Morgan and McDowell 1975; Syms et al. 1975; and these papers are referred to as papers I to VI in the work that follows. In particular we are interested here in the following transitions in hydrogen:

$$e + H(1s) \rightarrow e + H(3\ell : \ell = 0, 1 \text{ or } 2).$$

Since the hydrogen atom and hydrogenic ions are the simplest of all atomic systems, they have been extensively studied both theoretically and experimentally. Published theoretical work on the transitions here includes: the first Born approximation; a modified Born approximation (Morrison and Rudge, 1966); the Ochkur approximation (Gumble, 1969); a two-state distorted wave approximation (Vainshtein, 1961); the Glauber approximation (Tai et al. 1970, Bhadra and Ghosh, 1971); the Second Born approximation (Holt, 1969, Woollings and McDowell, 1973); the unitarized Born approximation (Somerville, 1963); some close coupling results at energies very close to threshold (Burke et al. 1963, Burke et al. 1967); results for 1s - 3p in the second order optical potential method (Bransden et al., 1972); the second order diagonalization method (Baye and Heenan, 1974); a multichannel eikonal approach (Flannery and McCann, 1974); and in paper I (McDowell et al., 1973) results for the 1s - 3s excitation were presented in the DWPO model neglecting target distortion (DWPO I). In paper VI we published total and differential cross sections in the DWPO I and II models. These results are extended and repeated here for the sake of completeness.

Notwithstanding this extensive list of theoretical work, the

$n = 3$ states have not been as well studied as the $n = 2$ states and there has not been a corresponding experimental study. Previous experimental investigations of electron-hydrogen scattering have centred on the $n = 2$ substates mainly because the $2s$ state is metastable and so the substates can be examined separately although they are nearly degenerate in energy. However, the $n = 3$ states are important in astrophysics since they give rise to Balmer alpha radiation (referred to as $H\alpha$). This radiation is emmitted when the $n = 3$ states decay to the $n = 2$ states. Its wavelength is 6563Å - thus it lies in the visible spectrum and is easily detected compared with Lyman alpha (1216 Å in the ultraviolet) which is emmitted when the $n = 2$ states decay to the ground state.

Recently however the experimental position has been greatly improved. The measurement of the total $H\alpha$ cross section by Kleinpoppen and Kraiss (1968) has now been supplemented in an absolute calibration by Walker and St.John (1974). Also Mahan and his colleagues (Mahan 1974, Mahan, Gallaher and Smith 1975; Smith 1975) have used a sophisticated technique to obtain individual cross sections for the $1s - 3\ell$ ($\ell = 0$, 1 or 2) transitions (relative to the Born approximation at 500 eV), and the total $H\alpha$ cross sections. In doing so they discovered some interesting asymmetries (see also Krotkov, 1975) and we discuss these in this work. The only two reported measurements of the optical polarization of the $H\alpha$ line are those of Kleinpoppen and colleagues (Kleinpoppen and Kraiss 1968; Kleinpoppen et al. 1962). We have found no reports of coincidence measurements or measurements of the alignment or orientation parameters for the $n = 3$ states of hydrogen.

There is a thorough review of electron-hydrogen scattering by Moiseiwitsch and Smith (1968) which covers both experimental and theoretical work up to the date of publication.

A comment here is appropriate about the notation used in this thesis. We refer to total cross sections as σ and to differential cross sections as

$\frac{d\sigma}{d\Omega}$ where $\Omega = (\theta,\phi)$ is the scattering angle illustrated in figure F1.1. We work in the centre of mass frame and in atomic units. The position of the bound electron is given by $\underline{r}_1$ and that of the incoming electron by $\underline{r}_2$. The co-ordinate system is chosen so that the incoming electron direction is along the positive z axis. The different models considered here are referred to as: the DWPO model without core polarization (DWPO I) or with core polarization (DWPO II); the BORN approximation or for hydrogenic ions when the nuclear charge ≥ 2 - the COULOMB-BORN approximation; when core polarization is included in these models we add the prefix POLARIZED; and when we include exchange in the BORN and POLARIZED BORN (or COULOMB-BORN or POLARIZED COULOMB-BORN) then the suffix OPPENHEIMER is added. Equations are referenced by the chapter and sequence number. Figures and tables are identified similarly and prefixed by F or T respectively.

The rest of this chapter is devoted to a discussion of general atomic scattering theory and of the features of the models used to study electron hydrogen scattering. In particular we consider the background and equations leading to the polarized orbital approximation. Briefly in section §1.4 we describe Mahan's experimental approach and finally in section §1.5 we present the layout for the rest of this thesis.

§1.2 General Theory of Scattering

For a full and detailed account of formal scattering theory see any of the standard texts - for example Mott and Massey (1971) or Goldberger and Watson (1964). Here we consider the theoretical background to each of the models used to obtain results for the transitions of interest.

The hydrogen atom consists simply of one electron in the Coulomb field of one proton - this system, independent of all interactions, can be described by the time-independent Schrodinger equation:

$$H_o\Psi = E\Psi \qquad (1.1)$$

FIGURE F1·1 POSITION VECTORS : $\underline{r}_1$ and $\underline{r}_2$; AND THE INITIAL AND FINAL MOMENTUM VECTORS : $\underline{k}_i$ and $\underline{k}_f$; (CARTESIAN CO-ORDINATE SYSTEM)

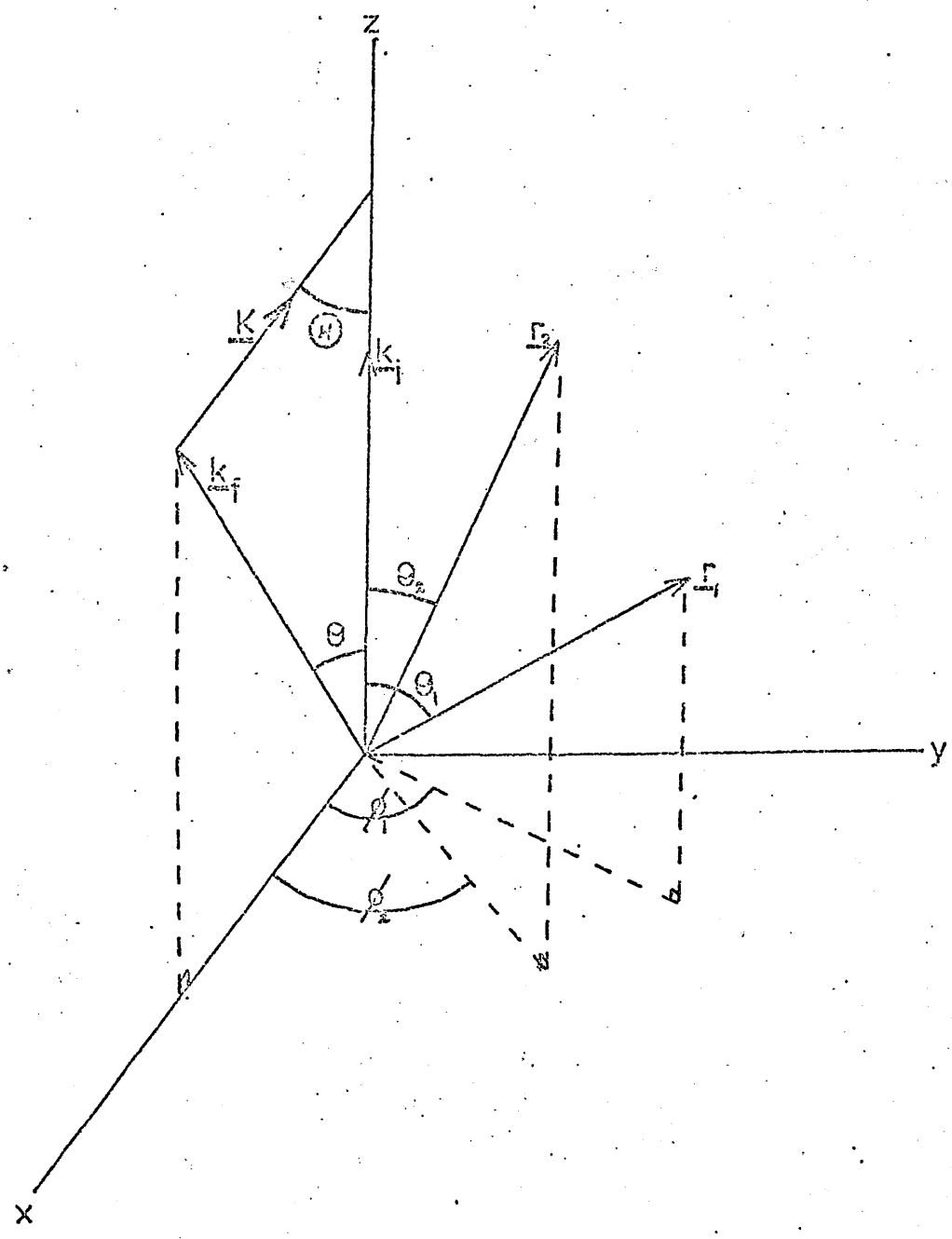

where the Hamiltonian H_o includes only the kinetic and Coulomb potential energies of the electron and in atomic units is given by:

$$H_o = -\tfrac{1}{2}\nabla^2 - \frac{1}{r} \qquad (1.2)$$

This Hamiltonian neglects the various properties of the electron and proton other than their charge and mass. These other properties include electron and nuclear spin and allowance for them can be included by means of a small perturbative correction to the Hamiltonian. The exact solutions to (1.1) yield the energy levels and eigenfunctions of the ground $(1s)$ state and excited $(n\ell)$ states; when the perturbative correction is included then the resultant energy levels and eigenfunctions exactly describe the more complex atomic model including fine and hyperfine structure splittings.

If an external field acts on the atom (which is the case we consider in Chapter 7 below dealing with the asymmetry of $H\alpha$ radiation) then the additional perturbative correction used is one which describes the coupling of the atom to the external field.

If the atom collides with another electron then the system consists of one bound atomic electron with co-ordinates given by $\underline{r}_1$ and a free electron with co-ordinates $\underline{r}_2$ relative to the proton as in figure F1.1. If the incoming electron has sufficient energy that it is scattered inelastically then the scattering process is described by:

$$H(1s) + e^- \rightarrow H(n\ell) + e^- + h\nu \qquad (1.3)$$

When we consider a hydrogenic ion of nuclear charge then all the above still applies with the exception that now we have two electrons moving in a fixed Coulomb potential due to a central charge of Ze units and the equation for the complete system of electron and hydrogenic ion in the initial channel becomes:

$$(H - E)\Psi_i^+ = 0 \qquad (1.4)$$

where the superscript + indicates that the function represents an outgoing wave, and in the final channel:

$$H_f\psi_f = E\psi_f \tag{1.5}$$

where:

$$\left.\begin{aligned} H &= -\tfrac{1}{2}(\nabla_1^2 + \nabla_2^2) - \frac{Z}{r_1} - \frac{Z}{r_2} + \frac{1}{r_{12}} \\ &= H_f + V_f \end{aligned}\right\} \tag{1.6}$$

and

$$\left.\begin{aligned} H_f &= -\tfrac{1}{2}(\nabla_1^2 + \nabla_2^2) - \frac{Z}{r_1} - \frac{z}{r_2}; \quad z = Z - 1 \\ V_f &= -\frac{1}{r_2} + \frac{1}{r_{12}} \end{aligned}\right\} \tag{1.7}$$

The final unperturbed wave function is denoted by ψ_f and V_f is the interaction in the final channel.

Formally, we may write the Green's function operator for the initial channel:

$$G_i^+ = \lim_{\varepsilon \to 0+} \left[\frac{1}{E - H_i + i\varepsilon} \right] \tag{1.8}$$

and with this definition we obtain a formal expansion of Ψ_i^+:

$$\Psi_i^+ = \sum_{p=o}^{\infty} (G_i^+ V_i)^p \psi_i \tag{1.9}$$

(the Lippmann-Schwinger equation)

where

$$\left.\begin{aligned} H &= H_i + V_i \\ \text{and} \\ H_i\psi_i &= E\psi_i \end{aligned}\right\} \tag{1.10}$$

The Green's function operator for the complete system is:

$$G^+ = \lim_{\varepsilon \to 0+} \left[\frac{1}{E - H + i\varepsilon} \right] \tag{1.11}$$

(Note that this differs from (1.8) in that the subscript i has now been dropped). The relation (1.9) can be manipulated so that the solution becomes formally:

$$\Psi_i^+ = (1 + G^+V_i)\psi_i \tag{1.12}$$

Pre-multiplying (1.12) by V_f we obtain:

$$V_f\Psi_i^+ = V_f(1 + G^+V_i)\psi_i = T\psi_i \ . \tag{1.13}$$

T is the transition operator and the T-matrix element, T_{if}, for a transition from state i to state f is defined:

$$T_{if} = \langle\psi_f V_f \Psi_i^+\rangle \tag{1.14}$$

The differential cross section is then defined:

$$\frac{d\sigma}{d\Omega}if = \frac{1}{4\pi^2}\ \frac{k_f}{k_i}\ |T_{if}|^2\ \ a_o^{\,2}\ sr^{-1} \tag{1.15}$$

where $\underline{k}_i$ is the momentum vector of the incoming electron and $\underline{k}_f$ is that of the outgoing electron (see figure Fl.1). When this is integrated over all angles we obtain the probability of scattering given by the total cross sections:

$$\sigma_{if}(k_i^{\,2}) = \frac{1}{2\pi^2}\ \frac{k_f}{k_i}\ \int_{-1}^{1} |T_{if}|^2\ d(\cos\theta)\quad \pi a_o^{\,2} \tag{1.16}$$

By calculating the total cross section we can compare the gross features of one model against another and with experimental measurements. The importance of the differential cross sections lies in the fact that they are a prediction of the probability of scattering at a specific angle and this enables more detailed comparisons to be made.

Closely related to the cross section are the scattering amplitudes defined by

$$f_{if}(k) = -\frac{2}{K^2}\ \langle\psi_f|e^{i\underline{K}.\underline{r}}|\psi_i\rangle \tag{1.17}$$

where $\underline{K} = \underline{k}_i - \underline{k}_f$ is the momentum transferred by the scattered electron to the atom. With this definition, the cross sections can be written:

$$\frac{d\sigma}{d\Omega} = \frac{k_f}{k_i} |f_{if}(K)|^2$$

$$\sigma_{if}(k_i^2) = \frac{2}{k_i^2} \int_{K_{min}}^{K_{max}} |f_{if}(K)|^2 \; KdK \qquad (1.18)$$

and

$$K_{max} = k_i + k_f, \quad K_{min} = k_i - k_f.$$

Returning to (1.9) - if only the first term is used in (1.14) then we obtain the "First Born approximation".

$$T_{if}^{FBA} = \langle \psi_f V_f \psi_i \rangle \qquad (1.19)$$

and the closed terms obtainable for the scattering amplitudes can be used here to readily calculate the cross sections. The obvious improvement to this model is to retain the next highest order term and this results in the "Second Born approximation"

$$T_{if}^{SBA} = \langle \psi_f V_f (\psi_i + G_i^+ V_i \psi_i) \rangle \qquad (1.20)$$

but here the second term cannot be computed exactly and so further subsidary approximations must be utilized. These usually require that the lowest N states are explicitly included and a mean excitation energy together with the closure property of wavefunctions are used to complete the sum. This model has been used by Woollings and McDowell (1973) and Holt (1969) with different choices for the mean excitation energy. In particular, the differential cross section results for inelastic transitions are markedly improved compared with the first Born approximation at large angles and this is attributed to the inclusion of the initial state and $n = 2$ state as intermediate states since elastic scattering and $1s - 2p$ excitation are important intermediate processes (see also Vainshtein and Presnyakov, 1969).

An effective way of improving the Born approximation by making some allowance for coupling to other states and ensuring that the results satisfy the conservation condition is to follow the unitarization method of Seaton (1961) and to use the Born approximation to the reactance matrix. When the initial state wave function is expanded over the angular momentum states, L, of the impact electron then for high values of L exchange and distortion are of lesser importance and so the results obtained by this method can be matched with those of more sophisticated calculations for lower angular momentum states. For this reason we present in Appendix AXII some results which will be useful in such calculations. Somerville (1963) has used this method for the Born approximation to the reactance matrix and presented results for the transitions of interest here. Exchange and distortion effects are still neglected and the transition matrix $\underline{T}_I$ in the Born approximation to the reactance matrix $\underline{R}_B$ is given by

$$\underline{T}_I = -2i\underline{R}_B \tag{1.21}$$

whereas the exact relation between the reactance matrix $\underline{R}$ and the $\underline{T}$ matrix is:

$$\underline{T} = \frac{-2i\underline{R}}{\underline{1}-i\underline{R}} \tag{1.22}$$

By using $\underline{R}_B$ in (1.22) Somerville obtained a better approximation to the $\underline{T}$ matrix given by $\underline{T}_{II}$ and these are the results considered here.

When allowance is included for the exchange of the incoming and bound electron in the Born model we obtain the Born-Oppenheimer model and now the scattering amplitude is written

$$f^{\pm}_{if} = f_{if} \pm g_{if} \tag{1.23}$$

where, as above, f_{if} is the first Born approximation to the scattering amplitude when the hydrogen atom is excited from the initial state i to the final state f and g_{if} is the exchange scattering amplitude for this transition: f^{+}_{if} and f^{-}_{if} are respectively the singlet

and triplet scattering amplitudes. The disadvantage with this method is that it frequently yields results (especially near threshold) which exceed conservation limits (see Bates et al., 1950). Ochkur (1964) has modified the Born-Oppenheimer approximation by expanding g_{if} in a power series of k_i^{-1} and retaining only the first term. In this case, the exchange scattering amplitude becomes

$$g_{if} = \frac{K^2}{k_i^2} f_{if} \tag{1.24}$$

and then the scattering amplitude is:

$$f_{if}^{\pm} = (1 \pm \frac{K^2}{k_i^2}) f_{if} \tag{1.25}$$

This model has been used for the excitations here, by Gumble (1969). Further, Rudge (1965a) has shown that although Ochkur's result satisfies orthogonality conditions between the initial and final states (whereas the Oppenheimer approximation does not) it is not consistent with a choice of trial functions in the variational principle which satisfy the boundary conditions of the problem. In view of this, Rudge (1965b) has modified the Born-Oppenheimer approximation using trial functions in variational expressions for the scattering amplitudes and Morrison and Rudge (1966) have used the resulting expression for the exchange scattering amplitude, which is very similar to Ochkur's, for the $1s \rightarrow 3\ell$ transitions and obtained significantly different results at low incident energies.

The Born and Born-Oppenheimer models treat the impact and scattered electrons as free particles and provided the perturbation V is small or the passage time of the incoming electron in the neighbourhood of the target is small then this may be acceptable. However at lower impact energies the incident wave is distorted and cannot be considered to be a plane wave while at the same time the possibility for exchange becomes greater and so alternative approaches must be considered.

The usual approch is to expand the function Ψ_i^+ in terms of target eigenfunctions:

$$\Psi_i^+(\underline{r}_1,\underline{r}_2) = \sum_q \psi_{iq}(\underline{r}_1)\, F_q(\underline{r}_2) \tag{1.26}$$

where $\psi_{iq}(\underline{r})$ is the orthonormal set of hydrogenic wave functions and $F_q(\underline{r}_1)$ is the free electron scattering function satisfying

$$(\nabla^2 + k_q^2)\, F_q(\underline{r}_2) = 2 \sum_m V_{qm}\, F_m(\underline{r}_2) \tag{1.27}$$

with

$$V_{qm}(\underline{r}_2) = \int \psi_q^*(\underline{r}_1) V(\underline{r}_1,\underline{r}_2)\, \psi_m(\underline{r}_1)\, d\underline{r}_1 \tag{1.28}$$

and $V(\underline{r}_1,\underline{r}_2)$ is therefore the interaction energy between the free electron and the target.

The close-coupling approximation follows when (1.26) is terminated after N terms thus:

$$\Psi_i^+ = \sum_{q=1}^{N} \mathcal{A}\, \psi_{iq}(\underline{r}_1)\, F_q(\underline{r}_2) + \chi(\underline{r}_1,\underline{r}_2) \tag{1.29}$$

where the correlation term χ represents some of the effects of the missing terms and $\mathcal{A}$ is an appropriate antisymmetrizing operator. This method is that used by Burke and co-workers (Burke et al., 1963, Burke et al., 1967).

Alternatively, the lowest N states are treated exactly but for $m > N$ the only terms retained are those coupled with states q where $1 \leq q \leq N$. Then

$$F_m(\underline{r}_2) = 2 \sum_{p=0}^{N} \int G_0^+(k_m^2,\underline{r}_1\underline{r}_2)\, V_{mp}\, F_p(\underline{r}_1)\, d\underline{r}_1 \tag{1.30}$$

where G_o^+ is the free particle Green's function, and the equations for the scattering functions in these retained states are (see Mittleman, and Pöe, 1962)

$$(\nabla^2 + k_q^2)\, F_q(\underline{r}_2) = 2 \sum_{m=0}^{N} V_{q,m}\, F_m(\underline{r}_2) + 4 \sum_{m=0}^{N} \int K_{qm}(\underline{r}_1,\underline{r}_2)\, F_m(\underline{r})\, d\underline{r} \tag{1.31}$$

where the term K_{qm} is the second order non-local potential given by Bransden and Coleman (1972). This is still too complex for an exact

solution so a mean excitation energy for $m > N$ and closure is used and then the optical potential $K_{qm}(\underline{r}_1,\underline{r}_2)$ becomes:

$$K_{qm}(\underline{r},\underline{r}_2) = \sum_{p=N+1}^{\infty} G_o^+(k_p^2,\underline{r},\underline{r}_2)\, V_{qp}(\underline{r}_2)\, V_{pm}(\underline{r}) \tag{1.32}$$

This is the second order optical method used by Bransden et al. (1972).

The eikonal approach is to treat the problem by direct analogy to the potential scattering problem. In this case the function Ψ_i^+ is assumed to have the form

$$\Psi_i^+ = A\, e^{iS} \tag{1.33}$$

where A is a slowly varying real function of the incident wave-number k_i and S satisfies the eikonal equation

$$(\nabla S)^2 = k_i^2 - 2V \tag{1.34}$$

and requires that $\frac{\nabla^2 A}{A} << k_i^2$. Thus the eikonal approximation is a high wave number and high energy (compared with the interaction potential) approximation.

The Glauber model which is based on the Eikonal approximation allows for the target - impact electron interaction although it neglects exchange scattering. The total wave function has the form:

$$\Psi_i^+(\underline{r}_1,\underline{r}_2) = \psi_{1s}(\underline{r}_1)\; e^{i\underline{k}_i\cdot\underline{r}_2}\, \phi(\underline{r}_2) \tag{1.35}$$

and the energy of the impact electron is assumed to greatly exceed the magnitude of the potential so that:

$$\phi(r_2) = \exp\left\{-\frac{i}{V_i}\int_{-\infty}^{Z} V(\underline{r}_1,\underline{r}_2)\, dZ\right\} \tag{1.36}$$

with $\underline{r}_2 = \underline{b} + \underline{Z}$, $\underline{Z}$ lies along $\underline{k}_i + \underline{k}_f$ and $\underline{b}$ is the impact parameter perpendicular to $\underline{Z}$. Thus the free electron scattering function, $F_q(\underline{r}_2)$ is approximated by a straight line along directions making equal angles with $\underline{k}_i$ and $\underline{k}_f$ and the scattering amplitude is given by:

$$f_{if} = \frac{ik_i}{2\pi} \int \psi_f^*(\underline{r})\, \Gamma(\underline{b},\underline{r})\, \psi_i(\underline{r})\, e^{i\underline{K}.\underline{b}}\, d^2b\, d\underline{r} \qquad (1.37)$$

where the phase change χ is given by

$$\chi = -\frac{1}{k_i} \int_{-\infty}^{\infty} V(\underline{r}_1,\underline{r}_2)dZ \qquad (1.38)$$

and

$$\Gamma(\underline{b},\underline{r}) = 1 - \exp(i\chi(\underline{b},\underline{r}_1)) \qquad (1.39)$$

This model has been used by Tai et al. (1970) and Bhadra and Ghosh (1971).

The "coupled-state impact-parameter" method used by Mandelberg (1970) combines both the inclusion of intermediate states as in the close coupling approximation and the simplicity of the impact parameter method where the perturbing electron is assumed to travel in a classical straight-line constant-velocity path with momentum k_i and impact parameter b. This approach thus allows for coupling to intermediate states when direct coupling is weak.

Another impact parameter approximation is that used by Baye and Heenen (1974) using a twenty state basis, while Flannery and McCann (1974) have used an elaborate multichannel eikonal treatment which accounts explicitly for the changes in velocity associated with different channels not acknowledged in earlier semiclassical descriptions such as the eikonal approximation, the impact parameter approach or the Glauber all of which separate the relative motion of the impact electron (described by an eikonal type wavefunction for an electron in a static field) from the internal electronic motions of the atomic system (described by a multistate expansion). This eikonal method readily reduces to the first Born or Glauber approximations.

Vainshtein (1961) has used a two state distorted wave approximation involving only the initial and final states of the atom. The pair of coupled differential equations are obtained from equation (1.25) and are:

$$(\nabla^2 + k_o^2)\, F_o(\underline{r}) = U_{oo}\, F_o(\underline{r}) + U_{o1}\, F_1(\underline{r}) \tag{1.40a}$$

$$(\nabla^2 + k_i^2)\, F_1(\underline{r}) = U_{1o}\, F_o(\underline{r}) + U_{11}\, F_1(\underline{r}) \tag{1.40b}$$

When the coupling potential U_{o1} is small, while U_{oo} and U_{11} are large then the inelastic cross section will be small and so $F_1 << F_o$. Then a good first approximation may be obtained by solving:

$$(\nabla^2 + k_o^2 - U_{oo})\, F_o = 0 \tag{1.41a}$$

$$(\nabla^2 + k_1^2 - U_{11})\, F_1 = U_{o1}\, F_o \tag{1.41b}$$

with the boundary conditions for F_o and F_1 (see Mott and Massey, 1971)

$$F_o \sim e^{ik_o r} + r^{-1} e^{ik_o r} f_o(\theta,\phi) \tag{1.42a}$$

$$F_1 \sim r^{-1} e^{ik_1 r} f_1(\theta,\phi) \tag{1.42b}$$

When the solution for F_o is inserted in (1.41b) we obtain an inhomogeneous equation for F_1 of the form:

$$(\nabla^2 + k_i^2 - U_{11})\, F_1 = g(r,\theta,\phi), \tag{1.43}$$

denoting the solution of the homogeneous equation by $\mathcal{F}_1$ then

$$(\nabla^2 + k_i^2 - U_{11})\, \mathcal{F}_1 = 0 \tag{1.44}$$

and

$$\mathcal{F}_1 \sim e^{ik_1 r\cos\theta} + r^{-1} e^{ik_1 r} f_1(\theta,\phi) \tag{1.45}$$

Therefore in this approximation the function F_o represents the motion of the impact electron in the mean field of the initial atomic state and $\mathcal{F}_1$ that of the outgoing free electron in the mean field of the excited atomic state: thus the scattering wave functions are distorted by the mean fields of the initial and final states of the atom.

By neglecting the coupling potential between the initial and final states but including the polarization distortion of the target by the

incoming electron we come to the distorted wave polarized orbital approximation used here and described below.

§1.3 The Distorted Polarized Orbital Approximation

For a full and detailed description of the polarized orbital method see Drachman and Temkin (1972). The original method by Temkin (1959) and when applied to atomic hydrogen by Temkin and Lamkin (1961) was essentially designed for elastic scattering only. Lloyd and McDowell (1969) applied the method of using the polarized orbital scattering function obtained for elastic scattering to evaluate the 1s - 2s and 1s - 2p cross sections for atomic hydrogen by solving the elastic scattering problem using the extended polarization approximation (EPD) of Callaway et al. (1968) and then used this function to evaluate the T-matrix element for inelastic scattering. The exact wave function Ψ_i^+ satisfies (1.4), so any trial function $\Psi_t(\underline{r}_1,\underline{r}_2)$ which satisfies the correct boundary conditions and the variational principle

$$\delta(I - K) = 0 \tag{1.46}$$

where $$I = \int \Psi_t^*(H - E)\,\Psi_t\, d\underline{r}_1 d\underline{r}_2 \tag{1.46a}$$

and K is the reaction matrix element (see Wu and Ohmura, 1962, p 313) may be used to obtain an approximate solution. Callaway et al. choose a trial function of the form:

$$\Psi_t(\underline{r}_1,\underline{r}_2) = \frac{1}{\sqrt{2}}\mathcal{A}\left[\phi(\underline{r}_1) + \chi(\underline{r}_1,\underline{r}_2)\right] F(\underline{r}_2) \tag{1.47}$$

where $\phi(\underline{r}_1)$ is ground state target wavefunction, $\mathcal{A}$ is the antisymmetrizing operator and $\chi(\underline{r}_1,\underline{r}_2)$ is the first-order perturbed part of the ground state function satisfying

$$(H_o - E_o)\chi(\underline{r}_1,\underline{r}_2) = (V - V_{oo})\phi(\underline{r}_1)$$

and $(H_o - E_o)\phi = 0$, $V_{oo} = \langle\phi|V|\phi\rangle$ and V is given by (1.7)

The EPD method of Callaway et al. is not strictly variantional since if (1.47) is used in (1.46) and the unknown scattering $F(\underline{r}_2)$ is

expanded over the partial waves of the scattered electron thus:

$$F(\underline{r}_2) = \sum_{\ell=0}^{\infty} \frac{u_\ell(r_2)}{r_2} Y_{\ell_o}(\Omega_2) \qquad (1.48)$$

then a set of integro-differential equations for the radial functions $u_\ell(r_2)$ results which would yield bounds on the phase shifts δ_ℓ^+, but the EPD method is applied in two parts:

1. the use of (1.47) with $\mathcal{A} = 1 + P_{12}$ (where $P_{12}f(1,2) = f(2,1)$) replaced by unity in (1.46) to obtain the polarization and distortion effects without exchange; and then
2. the use of (1.47) in (1.46) without the perturbed term $\chi(\underline{r}_1,\underline{r}_2)$ to obtain the exchange effects; this technique does not lead to bounds on the phase shifts

Thus the initial channel only is included in the initial wave function and all other channels are accounted for only by the polarization function $\chi(\underline{r}_1,\underline{r}_2)$. In this model, the integro-differential equation becomes:

$$\left\{\frac{d^2}{dr^2} + k_o^2 - \frac{\ell(\ell+1)}{r^2} - 2V_{oo}(r) - 2V_{pol}(r) + V_d(r)\right\} u_\ell^\pm(r) = \pm X_\ell^\pm(r) r R_o(r) \qquad (1.49)$$

where

$$X_\ell^\pm(r) = (E_o - k_o^2)\delta_{\ell_o}\int R_o(t)u_\ell^\pm(t)tdt + \frac{2}{2\ell+1}\int R_o(t)u_\ell^\pm(t)\gamma_\ell(t,r)tdt$$

and

$$\phi(r) = R_o(r)Y_{oo}(\underline{\Omega}); \quad \gamma_\ell(t,r) = \frac{r_<^\ell}{r_>^{\ell+1}}$$

The potentials are: the polarization potential

$$V_{pol}(r) = \int \phi(r_1)\, V\chi(r_1,r_2)dr_1 \qquad (1.50)$$

and the distortion potential

$$V_d(r) = \int |\nabla_{\underline{r}_2} \chi(r_1,r_2)|^2 \, dr_1 \qquad (1.51)$$

For this work we adopt a simplified version of (1.49) where we neglect distortions other than the dipole component of the polarization potential: in other words we drop $V_d(r)$. Furthermore in the DWPO I model we ignore the effect of the core polarization term in the T-matrix and allow for polarization distortion only when obtaining the scattering wavefunction $F(r_2)$ but this term is explicitly included in the DWPO II model. The effect of this core polarization term will be seen to be quite significant particularly when the 1s - 3d excitation results are considered.

In particular, we use the dipole only Callaway-Temkin potential for $V_{pol}(r)$ since this has been so successful in electron-atom scattering. This is given for hydrogenic systems by:

$$V_{pol}(r) = \frac{-9}{4x^4}\left[1 - e^{-2x}\left(1 + 2x + 2x^2 + \frac{4}{3}x^3 + \frac{2}{3}x^4 + \frac{4}{27}x^5\right)\right] \qquad (1.52)$$

where $x = Zr$.

When we take

$$\chi(\underline{r}_1,\underline{r}_2) = \phi_{pol}(1,2)$$
$$= \frac{-\varepsilon(\underline{r}_1,\underline{r}_2)}{r^2}\,\frac{u_{1s\to p}(r_1)}{r_1}\,\frac{P_1(\cos\theta_{12})}{\sqrt{\pi}} \qquad (1.53)$$

($\varepsilon(\underline{r}_1,\underline{r}_2)$ is a step function which cuts off the polarization term for $r_2 < r_1$) then this gives the Callaway-Temkin potential if $u_{1s\to p}(r)$ satisifies Sternheimer's equation. This equation, which arose originally in the calculation of atomic polarizabilities (Sternheimer 1954) but was subsequently shown to approximately correspond to perturbation theory, is given by:

$$\left[\frac{-d^2}{dr^2} + V_{n\ell\to\ell'}(r)\right] u_{n\ell\to\ell'}(r) = rP_{n\ell}(r) \qquad (1.54)$$

with

$$V_{n\ell\to\ell'}(r) = \frac{1}{P_{n\ell}(r)}\left[\frac{d^2}{dr^2}P_{n\ell}(r)\right] + \frac{\ell'(\ell'+1) - \ell(\ell+1)}{r^2}$$

and $P_{n\ell}(r)$ is the r-multiplied radial part of the hydrogenic $n\ell$ wave function.

Thus we have the basic equation (1.49) on which the DWPO model depends and now our solution corresponds exactly to the adiabatic exchange approximation defined by Drachman and Temkin (1972).

Recently however, Walters (1976) has pointed out some of the deficiencies of this adiabatic model and therefore we consider the implications on our results in Chapter 4 below.

§1.4 Mahan's Experimental Method

The most important experimental work is that of Mahan and co-workers (Mahan, 1974; Mahan et al 1976). They use the different average delays between excitation of the 3ℓ states and the subsequent radiative decay by modulating the beam of impact electrons. This modulation involves turning the electron current on and off sinusoidally at high frequencies, while measuring the resultant amplitude of the modulated photon output as a function of the modulation frequency. The time response of the fluorescence from each directly excited state is described by the same differential equation as is a low pass RC filter. By performing a least squares fit to the modulated amplitudes it is possible to identify the substate cross sections and obtain the relative ratios of the 3s, 3p and 3d cross sections.

In a separate measurement Mahan obtained the intensity of $H\alpha$ radiation at right angles to the electron beam. After correction for the angle of observation and cascade this signal was normalised to the total Born cross section at 500eV to obtain the $H\alpha$ cross section profile and then the total 3ℓ cross sections were derived.

§1.5 Layout of this Thesis

In the next Chapter with the associated appendices we present the generalized formulation for the T-matrix in the DWPO I and II models for hydrogenic systems and indicate how this leads to the differential and total (integrated) cross sections. Also included is the formulation of the polarized Born scattering amplitudes following from the Born approximation when core polarization is explicitly included in the target wave function. In Chapter 3 we discuss the details of the computer programs used to produce the cross sections. In Chapter 4 we present our results for the total and differential cross-sections and compare them with other published results.

At this point in Chapter 5 and 6 we move onto the study of other parameters of the scattering process. In Chapter 5 we consider the optical polarization of $H\alpha$ radiation and then Chapter 6 is devoted to the coincidence and the orientation and alignment parameters. In Chapter 7 we consider the asymmetry of $H\alpha$ radiation in detail and present results using the polarized-Born scattering amplitudes. Finally in Chapter 8 we present our conclusions and suggestions for further study. For the sake of readability we have avoided as much as possible the presentation of detailed mathematical manipulations in the main text and these are to be found in the appendices.

CHAPTER 2.

ELECTRON-ATOM SCATTERING

2.1 General Formulation in terms of the T-Matrix

The cross-section for a transition from an initial state i to a final state f of a hydrogenic system of nuclear charge Z, due to collisions with electrons of initial energy k_i^2 Rydbergs, may be written (McDowell and Coleman 1969 p.307)(using atomic units wherein $\mu_e = e = h = 1$):

$$\sigma_{if}(k_i^2) = \frac{1}{2\pi^2} \cdot \frac{k_f}{k_i} \int_{-1}^{+1} |T_{if}|^2 \, d(\cos\theta) \; \pi a_o^2 \qquad (2.1)$$

where the T-matrix element T_{if} may be defined as:

$$T_{if} = \langle \psi_f | V_f | \Psi_i \rangle \qquad (2.2)$$

with

$$|T_{if}|^2 = \frac{1}{4} \left\{ |T_{if}^{+}|^2 + 3|T_{if}^{-}|^2 \right\} \qquad (2.3)$$

and

$$T_{if}^{\pm} = \langle \psi_f | V_f | \Psi_i^{(\pm)} \rangle \qquad (2.4)$$

(plus and minus signs refer to singlet and triplet contributions respectively) - the T-matrix is a function of the initial and final state wave vectors, $\underline{k}_i$ and $\underline{k}_f$, related by

$$k_i^2 = k_f^2 + \Delta E_{if} \; ; \; \hat{\underline{k}}_i \cdot \hat{\underline{k}}_f = \cos\theta \; . \qquad (2.5)$$

Interest here is centered on transitions from the ground $1s$ state to an excited state $n\ell m_\ell$, although the following may be generalized to account for any initial state.

Here, ψ_f is the unperturbed wave function in the final channel, V_f is the interaction potential in that channel and Ψ_i is the total scattering function in the initial channel, so that Ψ_i satisfies

$$(H - E)\Psi_i = 0 \qquad (2.6)$$

with appropriate boundary conditions as discussed below. The total Hamiltonian for the incident electron-hydrogenic ion(of nuclear charge Z) system may be written

$$H = -\tfrac{1}{2}\nabla_1^2 - \tfrac{1}{2}\nabla_2^2 - \frac{Z}{r_1} - \frac{Z}{r_2} + \frac{1}{r_{12}} \qquad (2.7)$$

$$= H_f + V_f$$

(assuming the target nucleus to have infinite mass) where

$$H_f = -\tfrac{1}{2}\nabla_1^2 - \tfrac{1}{2}\nabla_2^2 - \frac{Z}{r_1} - \frac{z}{r_2}\ ; \quad z = Z - 1 \qquad (2.8)$$

and

$$V_f = -\frac{1}{r_2} + \frac{1}{r_{12}} \qquad (2.9)$$

in the direct channel, defining the position vectors of the initially bound electron and the incident electron to be $\underline{r}_1$ and $\underline{r}_2$ respectively (see figure F1.1).

The final unperturbed state of the whole system is described by

$$H_f\psi_f = E\psi_f \qquad (2.10)$$

and ψ_f is given by

$$\psi_f = \phi_f(Z,1)\ \chi_{\underline{k}_f}(z,2) \qquad (2.11)$$

where $\phi_f(Z,1)$ is the wave function for a hydrogenic ion of nuclear charge Z in the state $n\ell m_\ell$

$$\phi_f(Z,1) = R_{n\ell}(Z,1)Y_{\ell m_\ell}(\underline{\Omega}_1) \qquad (2.12)$$

and $\chi_{\underline{k}_f}(z,2)$ is the outgoing Coulomb wave of an electron in the field of a nucleus of charge z (see McDowell and Coleman 1969 p.239, Gordon 1928, p.180) (note that this reduces to a plane wave when $z = 0$).

$$\chi_{\underline{k}_f}(z,2) = \sum_{\lambda'=0}^{\infty} (2\lambda'+1) i^{\lambda'} \exp(-i\eta_{\lambda'}(k_f)) H_{\lambda'}(k_f r_2) P_{\lambda'}(\cos\theta_{\underline{k}_f}) \qquad (2.13a)$$

$$\cos\theta_{\underline{k}_f} = \hat{\underline{k}}_f \cdot \hat{\underline{r}}_2$$

or in terms of spherical harmonics

$$\chi_{\underline{k}_f}(z,2) = 4\pi \sum_{\lambda'=0}^{\infty} i^{\lambda'} \exp(-i\eta_{\lambda'}(k_f)) H_{\lambda'}(k_f r_2) \sum_{\mu'=-\lambda'}^{\lambda'} Y_{\lambda'\mu'}(\theta,0) Y^*_{\lambda'\mu'}(\underline{\Omega}_2) \qquad (2.13b)$$

where $\hat{\underline{k}}_i \cdot \hat{\underline{k}}_f = \cos\theta$ and the plane $\underline{k}_i, \underline{k}_f$ defines $\phi = 0$ (Fl.1); and where $\eta_\ell(k)$ is the ℓ^{th} partial Coulomb wave phase shift given by

$$\eta_\ell(k) = \arg(\Gamma(\ell+1 - \frac{iz}{k})); \qquad (2.14)$$

and

$$H_\ell(k,r) = G_\ell(k,z,r)/(kr) \qquad (2.15)$$

where $G_\ell(k,z,r)$ is the regular ℓ^{th} order Coulomb function or, in the case when $Z = 1$, it is a (kr) -multiplied Bessel function

$$G_\ell(k,0,r) = krj_\ell(kr). \qquad (2.16)$$

The normalization of $H_\ell(k,r)$ is thus:

$$H_\ell(k,r) \underset{r \to \infty}{\sim} (kr)^{-1} \sin\phi_\alpha(k,r) \qquad (2.17)$$

where $\phi_\alpha(k,r)$ depends on the target polarizability and is given by Burgess (1963) (see equation 2.27).

2.2 The DWPO Model

In the DWPO I model, which neglects target distortion, the total scattering function is taken to be

$$\Psi_i^{(\pm)}(1,2) = \mathcal{A}\phi_i(Z,1)F^{\pm}(2) \qquad (2.18)$$

where the antisymmetrizer $\mathcal{A}$ is

$$\mathcal{A} = 1 + P_{12}$$

and

$$P_{12}f(1,2) = f(2,1) \tag{2.19}$$

Polarization effects in this model are only included in the derivation of the distorted wave scattering function $F^{\pm}(2)$. Working in an uncoupled representation this function is expanded in partial waves

$$F^{\pm}(2) = \sum_{\lambda=0}^{\infty} A_\lambda \frac{u_\lambda^{\pm}(r_2)}{r_2} P_\lambda(\cos\theta_2), \qquad \cos\theta_2 = \hat{k}_i \cdot \hat{r}_2 \tag{2.20}$$

with the radial functions $u_\lambda^{\pm}(r_2)$ satisfying the adiabatic exchange equations (see Temkin and Lamkin 1961, Duxler, Pöe and LaBahn 1971) so that for an initial 1s state

$$\left[\frac{d^2}{dr^2} + k_i^2 - \frac{\lambda(\lambda+1)}{r^2} - 2V_{1s,1s}(r) - 2V_{pol}(r)\right] u_\lambda^{\pm}(k_i r) = \pm X_\lambda(r).r.R_{1s}(Z,r) \tag{2.21}$$

with

$$V_{1s1s}(r) = -\frac{z}{r} - (Z + \frac{1}{r})e^{-2Zr} \tag{2.22}$$

and the Callaway-Temkin polarization potential

$$V_{pol}(r) = -\frac{9}{4Z^4r^4}\left(1 - e^{-2Zr}\left(1 + 2Zr + 2Z^2r^2 + \frac{4Z^3r^3}{3} + \frac{2Z^4r^4}{3} + \frac{4Z^5r^5}{27}\right)\right) \tag{2.23}$$

$$\underset{r\to\infty}{\to} -\frac{\alpha_i}{r^4} .$$

$X_\lambda^{\pm}(r)$ is a non-local zero order exchange interaction, obtained by neglecting polarization

$$X_\lambda^{\pm}(r) = (E_{1s} - k_i^2)\delta_{\lambda o}\int_o^\infty R_{1s}(t)u_\lambda^{\pm}(k_i,t)dt + \frac{2}{(2\lambda+1)}\int_o^\infty R_{1s}(t)u_\lambda^{\pm}(k_i,t) \times \gamma_\lambda(t,r)tdt \tag{2.24}$$

with

$$\gamma_\lambda(r,r') = \frac{r_<}{r_>^{\lambda+1}}, \quad r_< = \min(r,r')$$

$$r_> = \max(r,r') \tag{2.25}$$

Equation (2.21) is solved for $u_\lambda^{\pm}(k_i,r)$ subject to the boundary conditions

$$u_\lambda^{\pm}(k_i,0) = 0$$

$$u_\lambda^{\pm}(k_i,r) \underset{r\to\infty}{\sim} k_i^{-\frac{1}{2}}\sin(\phi_\alpha(r) + \delta_\lambda^{\pm}) \tag{2.26}$$

with

$$\phi_\alpha(r) \underset{r\to\infty}{\sim} k_i r - \tfrac{1}{2}\lambda\pi + \frac{z}{k_i}\,\ell n(2k_i r) + \eta_\lambda \tag{2.27}$$

It follows that the solution for $u_\lambda^{\pm}(k_i,r)$ corresponds to the adiabatic exchange polarization as defined by Drachman and Temkin (1972).

The full expansion for $F^{\pm}(2)$ in terms of spherical harmonics is

$$F^{\pm}(2) = \sum_{\lambda=0}^{\infty}\left[\frac{4\pi(2\lambda+1)}{k_i}\right]^{\frac{1}{2}} i^\lambda \exp(i(\delta_\lambda^{\pm}+\eta_\lambda))\,\frac{u_\lambda^{\pm}(k_i,r_2)}{r_2}\,Y_{\lambda o}(\underline{\Omega}_2) \tag{2.28}$$

and the T-matrix in this model is given by

$$T_{if}^{\pm} = \langle\phi_f(Z,1)\chi_{\underline{k}_f}(z,2)|V_f|(1+P_{12})\phi_i(Z,1)F^{\pm}(2)\rangle \tag{2.29}$$

It is useful to note that by ignoring the local static potential V_{lsls}, the polarization potential V_{pol}, and the exchange term $X_\lambda^{\pm}(r)$ from the integro-differential equation (2.21) the model reduces to the Coulomb-Born-Oppenheimer approximation of Burgess et al. (1970). This is equivalent to simply replacing $F^{\pm}(2)$ by a coulomb wave $\chi_{\underline{k}_i}(z,r_2)$.

Using the expansion

$$\frac{1}{r_{12}} = \sum_{\lambda''=0}^{\infty}\sum_{\mu''=-\lambda''}^{\lambda''}\frac{4\pi}{(2\lambda''+1)}\,\gamma_{\lambda''}(1,2)\,Y_{\lambda''\mu''}(\underline{\Omega}_1)\,Y^*_{\lambda''\mu''}(\underline{\Omega}_2) \tag{2.30}$$

$T_{if}^{\pm}$ reduces, after some algebra (see Appendix AI) to a sum over partial waves of the scattered electron

$$T_{if}^{\pm} = \sum_{\lambda'=0}^{\infty} C_{\lambda'}^{\pm}(m_\ell)\, P_{\lambda'}^{|m_\ell|}(\cos\theta) = \mathcal{G}_{m_\ell}^{\pm} + i\mathcal{D}_{m_\ell}^{\pm} \tag{2.31}$$

where

$$C_{\lambda'}^{\pm}(m_\ell) = \frac{4\pi}{[(2\ell+1)k_i]^{\frac{1}{2}}} \sum_{\lambda=0}^{\infty} i^{\lambda-\lambda'} e^{i\xi_{\lambda\lambda'}^{\pm}}\, \chi_{\lambda\lambda'}^{\ell m_\ell}\Big[I^{\pm}(\lambda,\lambda') \pm \frac{(2\ell+1)}{(2\lambda'+1)}\,(J^{\pm}(\lambda,\lambda') - \delta_{\lambda'o}\,\delta_{m_\ell o}\delta_{\lambda\ell}\, d(\alpha_f)\, K^{\pm}(\ell,0))\Big] \tag{2.32}$$

with

$$\chi_{\lambda\lambda'}^{\ell m_\ell} = (2\lambda+1)(2\lambda'+1)\left[\frac{(\lambda'-|m_\ell|)!}{(\lambda'+|m_\ell|)!}\right]^{\frac{1}{2}} \begin{pmatrix} \lambda' & \ell & \lambda \\ m_\ell & -m_\ell & 0 \end{pmatrix} \begin{pmatrix} \lambda' & \ell & \lambda \\ 0 & 0 & 0 \end{pmatrix} \tag{2.33}$$

the last Wigner 3-j coefficient serving to define the range of λ for given ℓ and λ'.

While

$$\xi_{\lambda\lambda'}^{\pm} = \eta_\lambda(k_i) + \eta_{\lambda'}(k_f) + \delta_\lambda^{\pm}(k_i) \tag{2.34}$$

is a phase factor which for atomic hydrogen reduces to the elastic scattering phase shift $\delta_\lambda^{\pm}(k_i)$.

The first of the basic integrals is

$$I^{\pm}(\lambda,\lambda') = \int_o^{\infty} r f_{ls n\ell}(r)\, H_{\lambda'}(k_f r)\, u_\lambda^{\pm}(k_i r)\, dr \tag{2.35}$$

with

$$f_{ls n\ell}(r) = \int_o^{\infty} R_{ls}(Z,t)\, R_{n\ell}(Z,t)\, \gamma_\ell(t,r)\, t^2\, dt \tag{2.36}$$

(for the evaluation of this, see appendix AII)

The exchange integrals are

$$J^{\pm}(\lambda,\lambda') = \int_o^{\infty} g_{ls\lambda'}(k_f,r)\, R_{n\ell}(Z,r)\, u_\lambda^{\pm}(k_i r)\, dr \tag{2.37}$$

with

$$g_{ls\lambda'}(k_f,r) = r\int_o^{\infty} R_{ls}(Z,t)\, H_{\lambda'}(k_f,t)\, \gamma_{\lambda'}(r,t)\, t^2\, dt \tag{2.38}$$

and (the orthogonality integral)

$$K^{\pm}(\ell,0) = \int_o^{\infty} R_{n\ell}(Z,r)\, u_\ell^{\pm}(k_i r)\, r\, dr \tag{2.39}$$

The coulomb screening factor is:-

$$d(\alpha_f) = \frac{2Z^{3/2}}{(Z^2+k_f^2)} \beta^{\frac{1}{2}}(e^{\beta}-1)^{-\frac{1}{2}} \exp(2\alpha_f \tan^{-1}(\frac{k_f}{Z})) \tag{2.40}$$

with

$$\beta = 2\pi\alpha_f, \quad \alpha_f = -z/k_f \quad \text{and} \quad d(0) = \frac{2}{(1+k_f^2)} \tag{2.41}$$

In the DWPO II model, account of target distortion is included in the direct term of the T-matrix, but, consistent with neglecting exchange polarization terms in (2.24) when obtaining the scattering function, target distortion is neglected in the exchange part of the T-matrix. Thus the T-matrix above is replaced by

$$\tilde{T}_{if}^{\pm} = T_{if}^{\pm} + \langle\psi_f|V_f|\phi_{pol}(1,2)\, F^{\pm}(2)\rangle \tag{2.42}$$

The Callaway-Temkin potential in (2.21) is obtained if $\phi_{pol}(1,2)$ is taken to be

$$\phi_{pol}(1,2) = -\frac{e(r_1,r_2)}{r_2^2} \cdot \frac{u_{1s\to p}(r_1)}{r_1} \cdot \frac{P_1(\cos\theta_{12})}{\sqrt{\pi}} \tag{2.43}$$

where $u_{1s\to p}$ satisfies Sternheimer's Equation:

$$(-\frac{d^2}{dr^2} + \frac{P''_{1s}(r)}{P_{1s}(r)} + \frac{2}{r^2})\, u_{1s\to p}(r) = rP_{1s}(r) \tag{2.44}$$

in which $P_{1s}(r)$ is the r-multipled hydrogenic radial function for the ground state.

It is possible to obtain the solution to (2.44) in closed form: taking $u_{1s\to p}(r) = w(Z,r)\, P_{1s}(r)$ leads to:(see appendixAIII)

$$w(Z,r) = \frac{1}{2Z^3}(Zr + \frac{1}{2}Z^2r^2) \tag{2.45}$$

The term $\varepsilon(r_1,r_2)$ is a step function which cuts off the perturbation for $r_2 \leq r_1$. Thus, more explicitly, we allow the initial state of the target to be perturbed by the dipole component of the interaction with the incident electron to the first order in the interaction, provided that the incident electron is further from the nucleus than the bound electron.

The overall effect of this is to modify (2.32) by replacing $I^{\pm}(\lambda,\lambda')$ by $\tilde{I}^{\pm}(\lambda,\lambda')$ thus (see appendix IV):

$$\tilde{I}^{\pm}(\lambda,\lambda') = I^{\pm}(\lambda,\lambda') + \int r \tilde{\mathcal{J}}_{1sn\ell}(r)\, H_{\lambda'}(k_f r) u_{\lambda}^{\pm}(k_i r)\, dr \qquad (2.46)$$

and

$$\tilde{\mathcal{J}}_{1sn\ell}(r) = \frac{2\ell}{(2\ell-1)} k_{1sn\ell}^{(\ell-1)} + \frac{2(\ell+1)}{(2\ell+3)} k_{1sn\ell}^{(\ell+1)} \qquad (2.47)$$

with (see appendix V).

$$k_{1sn\ell}^{(\lambda'')}(r) = -\frac{1}{r^{\lambda''+3}} \int_0^r u_{1s\to p}(t)\, R_{n\ell}(Z,t)\, t^{\lambda''+1}\, dt \qquad \lambda'' > 0$$

$$= 0 \qquad \lambda'' \leq 0 \qquad (2.48)$$

this is equivalent to replacing $r\, f_{1sn\ell}(r)$ in $I^{\pm}(\lambda,\lambda')$ by $r\, f_{1sn\ell} + r\tilde{\mathcal{J}}_{1sn\ell}(r)$ (note that the leading term of $k_{1sn\ell}^{(1)}$ is, of course, of polarization form $k_{1sn\ell}^{(1)}(r) \underset{r\to\infty}{\sim} -c/r^4$).

2.3 The Coulomb-Born and Coulomb-Born-Oppenheimer Approximations

As stated earlier, replacing $F^{\pm}(2)$ by a coulomb wave $\chi_{\underline{k}_i}(z,r_2)$ leads to the Coulomb-Born-Oppenheimer approximation (CBO). In the DWPO II model, where the polarization term ϕ_{pol} is explicitly included in the atomic wave function, replacing the distorted wave scattering function in this way by a Coulomb wave leads to what we have called the Polarized-Coulomb-Born-Oppenheimer approximation (PCBO). The Coulomb-Born approximation (CB) is achieved by a further simplification whereby exchange is dropped completely - that is the antisymmetrizer, $\mathcal{A}$, in (2.18) is removed.

Again, the corresponding approximation to the DWPO II model is what we have termed the Polarized-Coulomb-Born approximation (PCB). For the results presented here, z = 0, and the Coulomb wave $\chi_{\underline{k}_i}(z,r_2)$ reduces to a plane wave. Strictly therefore, the approximations described above are the Born approximation and variants of it including exchange and core polarization.

The approach described above gives the T-matrix expressed as a sum over partial waves as in equation (2.31). This method still applies for the Coulomb-Born-Oppenheimer and Coulomb-Born approximations although terms arising from $F^{\pm}(2)$ in the basic integrals $I^{\pm}(\lambda,\lambda')$, $J^{\pm}(\lambda,\lambda')$ and $K^{\pm}(\ell,0)$ are replaced by those arising from a Coulomb wave. It is also possible to obtain explicit expressions for the T-matrix in both the Born and, to an increased degree of complexity, the Polarized-Born approximations. Thus, writing

$$f^{B}_{n\ell m_\ell}(\theta,\phi) = -\frac{1}{2\pi} \langle \phi_{n\ell m_\ell}(1)\, e^{i\underline{k}_f\cdot\underline{r}_2} | V(r_1,r_2) | \phi_{1s}(1) e^{i\underline{k}_i\cdot\underline{r}_2} \rangle \quad (2.49)$$

where the superscript B indicates the Born approximation;

then $f_{n\ell m_\ell}(\theta,\phi)$ is the scattering amplitude for the excitation of the $n\ell m_\ell$ state of hydrogen and is related to the T-matrix by:

$$f_{n\ell m_\ell}(\theta,\phi) = -\frac{1}{2\pi}\, T_{if} \quad (2.50)$$

Substituting for $V(r_1,r_2)$, taking $\underline{K} = \underline{k}_i - \underline{k}_f$, $K = |\underline{K}|$ and noting that the contribution due to $\frac{1}{r_2}$ in $V(r_1,r_2)$ drops out due to orthogonality between the hydrogenic wave functions, gives

$$f^{B}_{n\ell m_\ell}(\theta,\phi) = -\frac{1}{2\pi} \int e^{i\underline{K}.\underline{r}_2} \phi^{*}_{n\ell m_\ell}(\underline{r}_1).\, \frac{1}{r_{12}} .\, \phi_{1s}(\underline{r}_1)\, d\underline{r}_1 d\underline{r}_2 \quad (2.51)$$

where both $\phi_{n\ell m_\ell}$ and ϕ_{1s} are given by (2.12).

By use of Bethe's integral (see McDowell and Coleman (1969, p.311)

$$\int \frac{e^{i\underline{K}.\underline{r}_2}}{r_{12}}\, d\underline{r}_2 = \frac{4\pi}{K^2}\, e^{i\underline{K}.\underline{r}_1} \quad (2.52)$$

(2.51) becomes:

$$f^{B}_{n\ell m_\ell}(\theta,\phi) = -\frac{2}{K^2}\int \phi^{*}_{n\ell m_\ell}(\underline{r}_1)\phi_{1s}(\underline{r}_1)e^{i\underline{K}.\underline{r}_1}d\underline{r}_1. \tag{2.53}$$

This reduces, after some algebra (see Appendix VI) to:

$$f^{B}_{n\ell m_\ell}(\theta,\phi) = -\frac{16\sqrt{\pi}i^{\ell}}{n^2K^2}\cdot\frac{2^{\ell}\ell!x^{\ell/2}}{(2\ell+1)!}\left[(n-\ell-1)!(n+\ell)!\right]^{\frac{1}{2}} Y^{*}_{\ell m_\ell}(\theta,0)\ x$$

$$\sum_{s=0}^{n-\ell-1}\frac{(-1)^{s}\left(\frac{2}{n}\right)^{s+\ell}(2\ell+s+2)}{s!(n-\ell-1-s)!(K^2+\gamma^2)^{\frac{\ell+s+3}{2}}}\cdot F\left(\frac{2\ell+s+3}{2},-\frac{(1+s)}{2};\frac{2\ell+3}{2};x^2\right) \tag{2.54}$$

where $\gamma = 1 + \frac{1}{n}$;

$$x^2 = K^2/(K^2+\gamma^2);\cos\theta = \hat{\underline{K}}.\hat{\underline{k}}_i \quad \text{and} \quad \phi = 0, \tag{2.55}$$

and $F(a,b;c;z)$ is a hypergeometric function (see Abramowitz and Stegun (1968), Chapter 15). By substituting for F the familiar forms for $f^{B}_{n\ell m}$ are readily obtained (see Bates (1962), p.552).

When the polarized core term is added to the initial state wave function, the scattering amplitude becomes:

$$f^{PB}_{n\ell m_\ell}(\theta,\phi) = f^{B}_{n\ell m_\ell}(\theta,\phi) + \delta f^{PB}_{n\ell m_\ell}(\theta,\phi) \tag{2.56}$$

where

$$f^{PB}_{n\ell m_\ell}(\theta,\phi) = \frac{2}{3\sqrt{\pi}}\int e^{i\underline{K}.\underline{r}_2}\phi^{*}_{n\ell m_\ell}(\underline{r}_1)\left(\frac{1}{r_{12}}-\frac{1}{r_2}\right)\frac{\varepsilon(1,2)}{r_2^2}\cdot\frac{u_{1s\to p}(r_1)}{r_1}\ x$$

$$\sum_{\mu=-1}^{1} Y_{1\mu}(\underline{\Omega}_1)Y^{*}_{1\mu}(\underline{\Omega}_2)\ d\underline{r}_1 d\underline{r}_2 \tag{2.57}$$

After some algebra (see Appendix VII), this expression reduces to:

$$\delta f^{PB}_{n\ell m_\ell}(\theta,\phi) = 8\sqrt{\pi}\ Y^{*}_{\ell m_\ell}(\theta,0)i^{\ell}\sum_{\lambda'}\int j_\ell(Kr)V^{\lambda'}_{n\ell}(r)dr \tag{2.58}$$

where

$$V^{\lambda'}_{n\ell}(r) = \begin{pmatrix}\ell & 1 & \lambda'\\ 0 & 0 & 0\end{pmatrix}^2\int_0^r R_{n\ell}(t)u_{1s\to p}(t)\gamma_{\lambda'}(t,r)tdt \qquad \lambda' \geq 1$$

$$= 0. \qquad \lambda' \leq 0 \tag{2.59}$$

Obtaining $f^{B}_{n\ell m_\ell}$ and $f^{PB}_{n\ell m_\ell}$ by this approach gives a useful check to the results obtained via §2.1 and §2.2 and is of additional use in the asymmetry analysis described in Chapter 7.

2.4 The Differential and Total Cross Sections

Having obtained the T-matrix as in equation (2.31)

$$T^{\pm}_{if} = \sum_{\lambda'} C^{\pm}_{\lambda'}(m_\ell)\, P^{|m_\ell|}_{\lambda'}(\cos\theta)$$

which may be written

$$T^{\pm}_{if} = \mathcal{C}^{\pm}_{m_\ell} + i\mathcal{D}^{\pm}_{m_\ell}$$

then

$$|T_{if}{}^{\pm}|^2 = |\mathcal{C}_{m_\ell}{}^{\pm}|^2 + |\mathcal{D}_{m_\ell}{}^{\pm}|^2 \tag{2.60}$$

where

$$\begin{aligned} \mathcal{C}_{m_\ell}{}^{\pm} &= \sum_{\lambda'} \mathrm{Re}(C^{\pm}_{\lambda'}(m_\ell)).P^{|m_\ell|}_{\lambda'}(\cos\theta) \\ \mathcal{D}_{m_\ell}{}^{\pm} &= \sum_{\lambda'} \mathrm{Im}(C^{\pm}_{\lambda'}(m_\ell)).P^{|m_\ell|}_{\lambda'}(\cos\theta) \end{aligned} \tag{2.61}$$

the real and imaginary forms of $C^{\pm}_{\lambda'}$ arising only due to the term:

$$i^{\lambda-\lambda'} \exp(i\xi^{\pm}_{\lambda\lambda'}),$$

in equation (2.32) and thus each term is easily separable.

The differential cross section, in atomic units, is

$$\begin{aligned} \frac{d\sigma_{if}}{d\Omega} &= \frac{1}{4\pi^2} \cdot \frac{k_f}{k_i} \cdot |T_{if}|^2 \quad a_o{}^2 \mathrm{str}^{-1} \\ &= \frac{1}{16\pi^2} \cdot \frac{k_f}{k_i} \cdot \left\{ |T_{if}{}^{+}|^2 + 3|T_{if}{}^{-}|^2 \right\} \end{aligned} \tag{2.62}$$

so

$$\frac{d\sigma_{if}}{d\Omega} = \frac{1}{16\pi^2} \cdot \frac{k_f}{k_i}\left\{\left[|\mathcal{C}^{+}_{m_\ell}|^2 + |\mathcal{D}^{+}_{m_\ell}|^2 + 3\left[|\mathcal{C}^{-}_{m_\ell}|^2 + |\mathcal{D}^{-}_{m_\ell}|^2\right]\right\} \quad (2.63)$$

The differential cross section is related to the total cross-section by

$$\sigma_{if} = \int_0^{2\pi} \int_{-1}^{+1} \frac{d\sigma_{if}}{d\Omega} \cdot d(\cos\theta)\, d\phi \quad (2.64)$$

and so

$$\sigma_{if} = \frac{1}{2\pi^2} \frac{k_f}{k_i} \int_{-1}^{+1} |T_{if}|^2 \, d(\cos\theta)$$

(equation 2.1))

in units of πa_o^2.

In (2.31) the θ-dependence of T_{if} arises through the associated Legendre polynomial, $P_{\lambda'}^{|m_\ell|}(\cos\theta)$, only. Furthermore, associated Legendre polynomials are orthogonal with the orthogonality relation:

$$\int_{-1}^{1} P_{\lambda'}^{|m_\ell|} \cdot P_{\lambda}^{|m_\ell|} \, d(\cos\theta) = \frac{2(\lambda'+|m_\ell|)!}{(2\lambda'+1)(\lambda'-|m_\ell|)!} \delta_{\lambda\lambda'} \quad (2.65)$$

(see Abramowitz and Stegun (1968), p.338, equation (8.14.13)),

thus:

$$\sigma_{in\ell m_\ell} = \frac{1}{4\pi^2} \frac{k_f}{k_i} \sum_{\lambda'} \frac{(\lambda'+|m_\ell|)!}{(2\lambda+1)(\lambda'-|m_\ell|)!} \left\{|C^{+}_{\lambda'}(m_\ell)|^2 + 3|C^{-}_{\lambda'}(m_\ell)|^2\right\} \quad (2.66$$

For each sub-level $n\ell m_\ell$ it is possible to describe the cross-section in terms of singlet and triplet contributions

$$\sigma_{in\ell m_\ell} = \sigma^{+}_{in\ell m_\ell} + \sigma^{-}_{in\ell m_\ell} \quad (2.67)$$

where

$$\sigma^{\pm}_{in\ell m_\ell} = \frac{A^{\pm}k_f}{8\pi^2 k_i} \int_{-1}^{+1} |T^{\pm}_{if}|^2 \, d(\cos\theta) \quad (2.68)$$

$$= \frac{A^{\pm}k_f}{4\pi^2 k_i} \sum_{\lambda'} \frac{(\lambda'+|m_\ell|)!}{(2\lambda'+1)(\lambda'-|m_\ell|)!} |C^{\pm}_{\lambda'}(m_\ell)|^2$$

and $A^{+} = 1$, $A^{-} = 3$.

In the Born and Polarized-Born approximations

$$T_{if} = -2\pi\, f_{n\ell m_\ell}(\theta,\phi) \tag{2.50'}$$

so the differential cross section is:

$$\frac{d\sigma_{if}}{d\Omega} = \frac{k_f}{k_i} \left| f_{n\ell m_\ell}(\theta,\phi) \right|^2 \tag{2.69}$$

where $f_{n\ell m_\ell}(\theta,\phi)$ is given by (2.54) or (2.56).

Since

$$\underline{K} = \underline{k}_i - \underline{k}_f$$

$$K^2 = k_i^2 + k_f^2 - 2k_i k_f \cos\theta \tag{2.70}$$

and so (2.1) becomes

$$\sigma_{in\ell m_\ell}(k_i^2) = \frac{2}{k_i^2} \int_{k_i - k_f}^{k_i + k_f} \left| f_{n\ell m_\ell}(K) \right|^2 K\,dK \tag{2.71}$$

Finally, for each state $n\ell$, equations (2.63) and (2.66) are summed over all values of m_ℓ (i.e. $m_\ell = -\ell, -\ell+1, \ldots, -1, 0, 1, \ldots \ell$) and since none of (2.63), (2.66), (2.69) or (2.71) depends explicitly on the sign of m_ℓ:

therefore

$$\frac{d\sigma_{in\ell}}{d\Omega} = \frac{d\sigma_{in\ell o}}{d\Omega} + 2 \sum_{m_\ell=1}^{\ell} \frac{d\sigma_{in\ell m_\ell}}{d\Omega} \tag{2.72}$$

and

$$\sigma_{in\ell} = \sigma_{in\ell o} + 2 \sum_{m_\ell=1}^{\ell} \sigma_{in\ell m_\ell} \tag{2.73}$$

2.5 Summary

This chapter, with the associated appendices, has described in detail the derivation of the T-matrix both in the DWPO I and II models. It has been indicated how, by a simple switch in the scattering function, the models reduce to the (Coulomb-) Born or (Coulomb-) Born-Oppenheimer approximations. Furthermore we have shown how it is possible to make allowance for core polarization in these approximations and to describe

the resulting scattering amplitudes for excitation from the ground state to any excited state in closed form.

We have presented the framework of the calculation of the differential and total cross sections from the T-matrix elements both in terms of the magnetic sublevels and of the singlet and triplet contributions. This calculation was performed, for a range of energies from threshold to the area of validity of the Born approximation and for each of the $n = 3,\ell$ states of hydrogen. The computer programs used to evaluate these results are described in chapter 3 below.

CHAPTER 3

COMPUTATIONAL DETAILS

3.1 Introduction

This chapter describes the computer programs used for both the DWPO I and II models,

a) to evaluate the functions formulated in Chapter 2 and which appear in the integrals $I^{\pm}(\lambda,\lambda')$, $J^{\pm}(\lambda,\lambda')$ and $K^{\pm}(\ell,0)$ in equation (2.32), and then

b) to calculate the values of the cross sections and other parameters of the excitation process which depend on the magnetic sublevel cross sections. These parameters include the polarization fraction of Balmer-α radiation and the coincidence measurements and orientation/alignment parameters which are discussed in Chapter 5 and 6 below.

The basic structure of the computer programs is derived from the program developed by McDowell et al. (paper Ib, 1974) and referred to as POLORB. This program treated the ns (n = 1,5) states of hydrogen and Helium$^+$ in the DWPO I model, and, in practice, very few alterations were necessary to the published version for the 3s state of hydrogen to take account of core polarization effects for the DWPO II model.

Similarly, the program (POLORP) which was used to produce the DWPO I and II results reported for the excitation to the 2p states of hydrogen and Helium$^+$ (see papers III, IV and V) required no further development.

The major computing effort has been expended in programming the calculations relevant to the nd states which involves a sum of three terms for each partial wave corresponding to values for $\lambda = \lambda' - 2$, λ' and $\lambda' + 2$ in equation (2.32) whereas only one term arises for the ns states and only two terms arise for the np states. Because of the nature of the integrals and other functions involved in (2.32) three sets of functions must be retained at each partial wave λ' corresponding to $\lambda = \lambda' - 2$, $\lambda' - 1$ and λ' and the term in $\left[\ \right]$ in (2.32) stored for $\lambda = \lambda' - 2$

and λ'. In general, for any $n\ell$ state, the number of terms involved increases as $\ell + 1$, leading to greater storage requirements and greater complexity in the manipulation of the separate components with increasing orbital angular momentum. The program for the nd states (POLORD) is described in full below and, where applicable, features common to all three programs are indicated. These features include the generation of the radial functions and the calculation of the long range contributions to the direct integral.

Subsequent to the work reported in this thesis, the program suite used to produce the polarized orbital cross sections with or without core polarization and retaining the options for the (Coulomb-) Born or (Coulomb-) Born-Oppenheimer approximations for hydrogen (and Helium$^+$ etc.) has been rationalized into one program using the generalized expressions formulated in Chapter 2.

Descriptions of each polarized orbital computer program

3.2 POLORB

This program has been fully described elsewhere (see McDowell et al. paper I (1973), paper Ib (1974)). The modifications necessary to convert it to include core polarization are made by including an additional subroutine FNEW and computing an additional integral using the integrand FINT. The routine FNEW sets up the coupling function $rk^1_{ns}(r)$ at each mesh point for r. It makes use of the expansion (Ay.6) for values greater than this value. At the cross over point the error involved is negligible. The additional integral corresponds to that in (2.46) where

$$r\mathcal{J}_{lsns}(r) = \frac{2}{3} rk^1_{lsns}$$

and is calculated using Simpson's rule in the same way as the integrals using AINT, etc.

This program does not allow the inclusion of core polarization in the

(Coulomb) Born Approximation since, in this case, the T-matrix calculation is performed using analytic forms for the partial wave contributions expressed in terms of hypergeometric functions. Thus the use of the appropriate switch to generate this approximation produces the (C)B results only. The effect of core polarization in the Born approximation for the 3s state of hydrogen only, has been computed separately using the closed forms for the scattering amplitudes described in Appendix AVII and these results, shown in Chapter 4 indicate that very little difference was evident between the Born and PB models at all energies.

3.3 POLORP

This program was developed from the POLORB program by the authors of papers III - V and includes the calculation, if required, of the rk^2_{lsnp} coupling term in tandem with the calculation of the $rf_{lsn\ell}$ function. Other features include the addition of the long range contributions to the direct integrals and the calculation of the orientation and alignment parameters relevant to the np states. The long range contributions are calculated using the subroutine FARINT together with its associated routines, the orientation and alignment parameters are calculated at the same time as the differential cross sections and these are discussed in Chapter 6.

The implementation of this program for the 3p state calculations required only those modifications dependent on the principal quantum number.

3.4 POLORD

Since this program retains most of the procedures of the POLORB and POLORP programs and yet is a development from them, the program POLORD is more fully described here.

3.4.1 The framework of the program POLORD

The overall structure of the program is given in figure F3.1 and figure F3.2 shows the structure of the major subroutine INTLS.

The functions $r \times f_{ls3d}$ and $r \times k^{\lambda''}_{ls3d}$ ($\lambda'' = 1,3$) all employ short range expansions for $\gamma Zr \leq 0.3$. The difference between the short range expansions and the full expressions at the cross-over point was negligible in all cases.

The calculation of the initial state radial wave function, $u^{\pm}_{\lambda}(k_i,r)$, for varying impact electron energies and for each partial wave λ, has been fully discussed in papers I and Ia. The derivation of the Coulomb function $H_{\lambda'}(k_f,r)$, the phase factors and the function $g_{ls\lambda'}(k_f,r)$ were also all described in the same references.

Essentially, the radial equation for $u^{\pm}_{\lambda}(k_i,r)$ was solved by a non-iterative procedure using a Numerov integration procedure and the normalization and phase shifts were obtained by comparison with JWKB solution (Burgess 1963). The Coulomb or Bessel functions required were generated using a Numerov procedure from the appropriate differential equation:

$$\left(\frac{d^2}{dr^2} + k^2 - \frac{\ell(\ell+1)}{r^2} - \frac{2z}{r}\right) G_{\ell}(k,z,r) = 0.$$

The function $g_{ls\lambda'}(k_f,r)$ was computed directly from the defining integral (2.38).

3.4.2. The long range contributions to the direct integrals

The long range contributions included in the np and the 3d calculations have been discussed in paper III. The importance of these contributions arises in the direct integrals $I^{\pm}(\lambda,\lambda')$ only, wherein

$$rf_{lsn\ell}(r) \underset{r\to\infty}{\sim} r^{-\ell} \qquad \text{(see appendix AII)}$$

$$H_{\lambda'}(k_f,r) \underset{r\to\infty}{\sim} \sin\phi_o(k_f,r)/(k_f r) \qquad \text{(see equation (2.17))}$$

FIGURE (F3.1) STRUCTURE OF THE PROGRAM POLORD

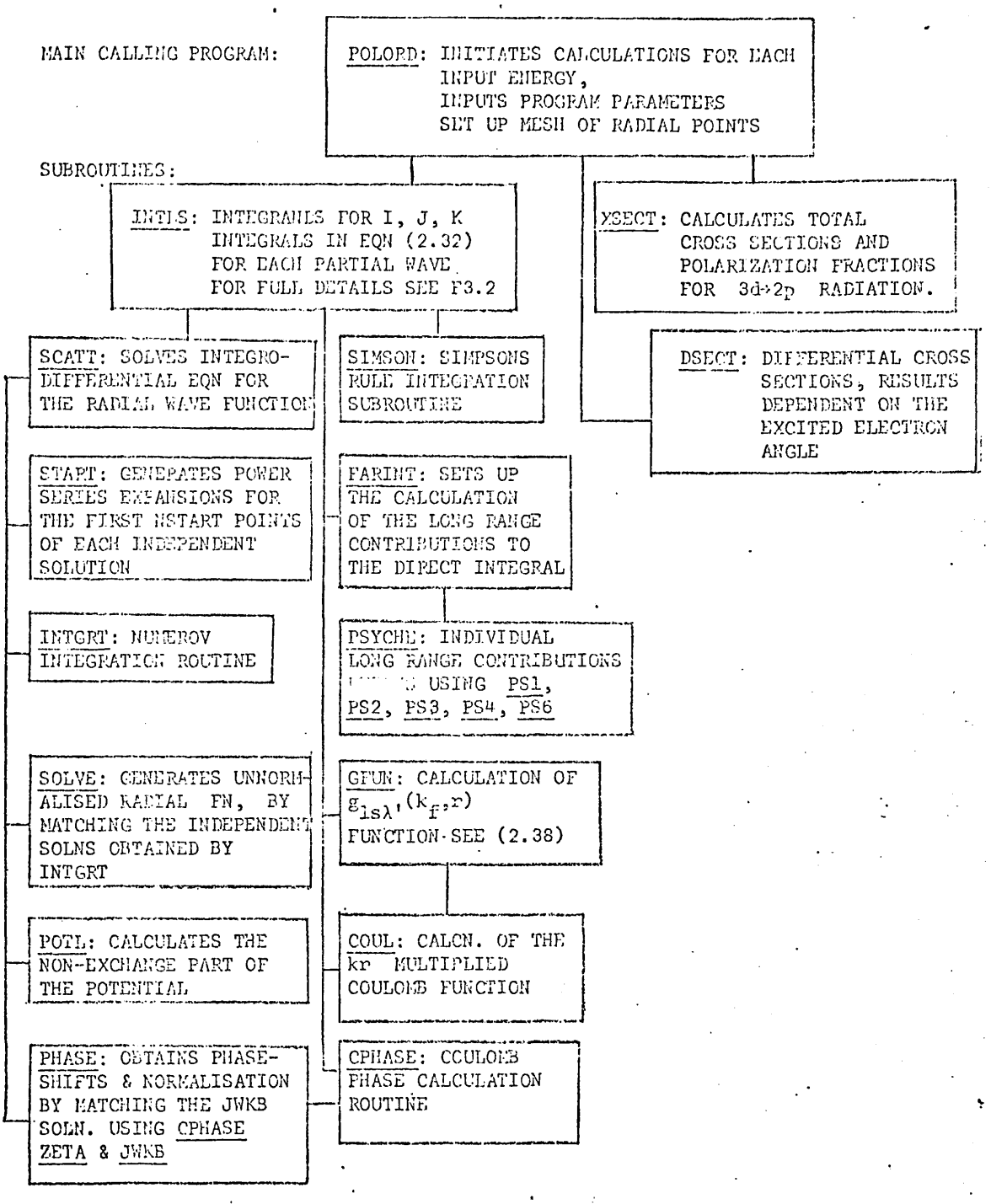

Figure F3.2 Structure of the Subroutine INTLS

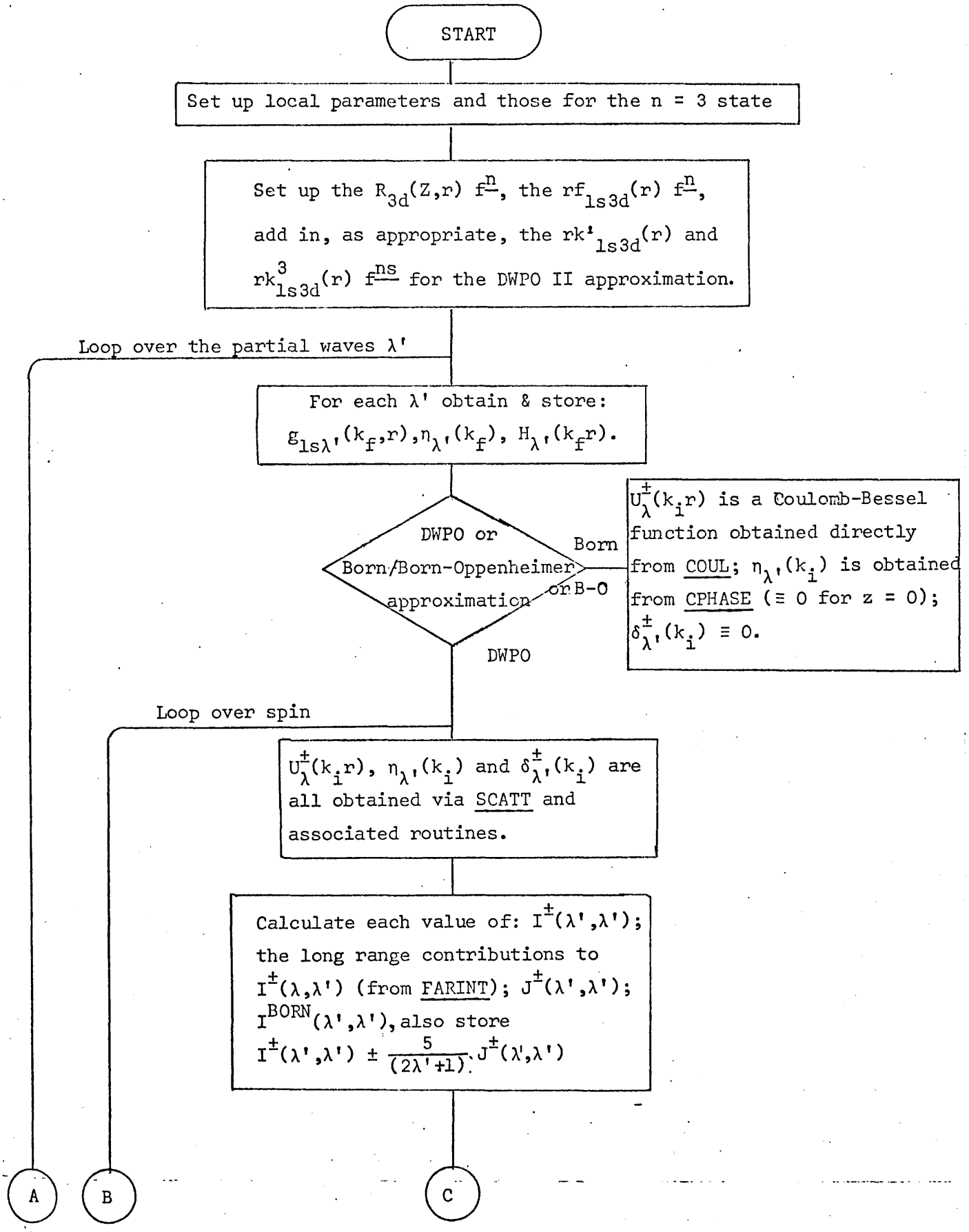

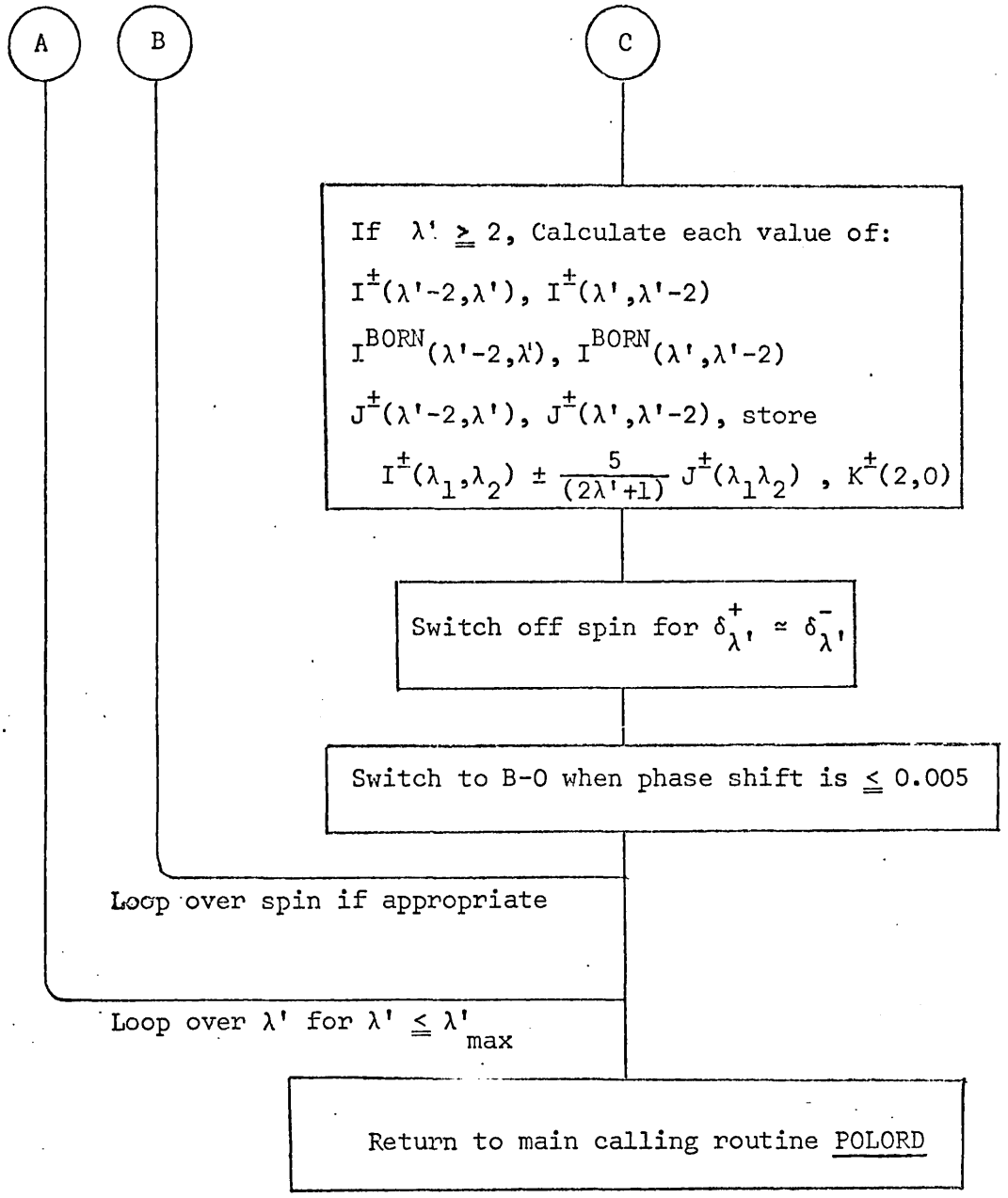
A
B
C
If λ' ≥ 2, Calculate each value of:
$I^{\pm}(\lambda'-2,\lambda')$, $I^{\pm}(\lambda',\lambda'-2)$
$I^{BORN}(\lambda'-2,\lambda')$, $I^{BORN}(\lambda',\lambda'-2)$
$J^{\pm}(\lambda'-2,\lambda')$, $J^{\pm}(\lambda',\lambda'-2)$, store
$I^{\pm}(\lambda_1,\lambda_2) \pm \frac{5}{(2\lambda'+1)} J^{\pm}(\lambda_1\lambda_2)$, $K^{\pm}(2,0)$
Switch off spin for $\delta^{+}_{\lambda'} \simeq \delta^{-}_{\lambda'}$
Switch to B-0 when phase shift is ≤ 0.005
Loop over spin if appropriate
Loop over λ' for $\lambda' \leq \lambda'_{max}$
Return to main calling routine POLORD

and

$$u_\lambda^{\pm}(k_i r) \underset{r\to\infty}{\sim} k_i^{-\frac{1}{2}} \sin(\phi_\alpha(r) + \delta_\lambda^{\pm}) \qquad \text{(see equation (2.26))}$$

Thus, the integrand of $I^{\pm}(\lambda,\lambda')$ converges only as $r^{-(\ell+1)}$ at large r. The subroutine FARINT obtains the integral

$$AINT_{\lambda\lambda'} = \int_{RR(NTOT)}^{\infty} \frac{\sin\phi(r)\sin(\phi(r) + \delta_\lambda^{\pm})dr}{\sqrt{k_i k_f}\, r^{\ell+1}}$$

where RR(NTOT) is the furthest extent of the mesh of radial points at which all the radial functions are calculated.

This integral is calculated using the subroutine PSYCHE and associated routines (PS1, PS2, PS3, PS4 and PS6) using a variant of the method given by Belling (1968).

Additionally, when core polarization is included, the function

$$r \times \mathcal{J}_{lsn\ell}(r) \underset{r\to\infty}{\sim} (A + \frac{B}{r^2}) r^{-(\ell+1)} \qquad \text{(see equation (AV.7) (A,B constants),}$$

therefore, in the POLORD program extra integrals are calculated corresponding to:

$$A \int_{RR(NTOT)}^{\infty} \frac{H_{\lambda'}(k_f,r)\, u_\lambda^{\pm}(k_i,r)dr}{r^3}$$

for all values of λ' and λ.

It was found that any contribution due to the term which included Br^{-2} was negligible and therefore not included.

Note that the exchange integrands converge rapidly for large r due to the $R_{n\ell}(Z,r)$ term (see equation (2.37)) and therefore a similar procedure to the above for $r >$ RR(NTOT) is not necessary for the exchange integrals.

3.4.3 The "Born-Subtraction" technique

The POLORD program also makes full provision for the 'Born-subtraction" technique in the computation of the differential cross sections for both

the DWPO I and II approximations. The method of calculation is outlined below. The technique is used to overcome the need to calculate a large number of partial waves to achieve convergence in the differential cross section particularly since the Born partial waves are used to approximate for the higher orders of partial waves.

Referring to equation (2.31):

$$T^{\pm}_{if}(m_\ell) = \sum_{\lambda'=0}^{\infty} C^{\pm}_{\lambda'}(m_\ell)\, P^{|m_\ell|}_{\lambda'}(\cos\theta) \qquad (3.1)$$

If T^{B}_{if} and T^{PB}_{if} are the Born and Polarized Born approximation to the T-matrix respectively (see equation (2.50), (2.51), (2.56) and (2.57)) and with the expansions:

$$T^{B}_{if}(m_\ell) = \sum_{\lambda'=0}^{\infty} C^{B}_{\lambda'}(m_\ell)\, P^{|m_\ell|}_{\lambda'}(\cos\theta) \qquad (3.2)$$

where the superscript B is taken to refer to either the BORN or the POLARIZED BORN approximation as necessary, then the DWPO T-matrix can be written:

$$T^{\pm}_{if}(m_\ell) = \sum_{\lambda'=0}^{\lambda_o'} \left[C^{\pm}_{\lambda'}(m_\ell) - C^{B}_{\lambda'}(m_\ell)\right] P_\ell(\cos\theta) + T^{B}_{if} \qquad (3.3)$$

The same technique is applied to BORN-OPPENHEIMER and PBO approximations, but the full expansion method is retained for the BORN and PB. approximations as a check of the operation of the computer program.

The expressions for T^{B}_{if} and T^{PB}_{if} are obtained by reference to appendices AVI and AVII and using (2.50'). The choice of λ_o' in equation (3.3) is determined by the requirement that for $\lambda' > \lambda_o'$ the Born approximation to the direct terms of the partial wave T-matrix differs from the DWPO approximation by only a pre-assigned small amount.

The calculation of the differential cross sections follows immediately from the above via (2.62). The Born-subtraction technique is also applicable to the total cross sections and the method of calculation is indicated below.

For both the Born and polarized Born approximations $C^B_{\lambda'}(m_\ell)$ is wholly real and therefore, writing

$$\mathcal{C}^{\pm}_{m_\ell} = \sum_{\lambda'=0}^{\lambda_o'} \left(\mathrm{Re}(C^{\pm}_{\lambda'}(m_\ell)) - C^B_{\lambda'}(m_\ell)\right) P^{|m_\ell|}_{\lambda'}(\cos\theta) + T^B_{if}(m_\ell) \qquad (3.4)$$

the singlet and triplet contributions to the total cross section become:

$$\sigma^{\pm}_{if} = \frac{A^{\pm} k_f}{8\pi^2 k_i} \int_{-1}^{+1} \left[\mathcal{C}^{\pm 2}_{m_\ell} + \mathcal{D}^{\pm 2}_{m_\ell} \right] d(\cos\theta) \qquad (3.5)$$

where, again, $A^+ = 1$ and $A^- = 3$.

Using the expansion (3.2) for $T^B_{if}(m_\ell)$, equation (2.61) for $\mathcal{D}^{\pm}_{m_\ell}$ and the orthogonality condition (2.65), gives

$$\sigma^{\pm}_{if} = \sigma^{\pm}_{if,\lambda'_o} - \frac{A^{\pm}}{4} \sigma^B_{if,\lambda'_o} + \frac{A^{\pm}}{4} \sigma^B_{if} \qquad (3.6)$$

and

$$\sigma_{if} = \sigma_{if,\lambda'_o} - \sigma^B_{if,\lambda'_o} + \sigma^B_{if} \qquad (3.7)$$

where the subscript λ'_o implies that the summation over λ' is taken only as far as $\lambda = \lambda'_o$. The total Born or Polarized Born cross sections σ^B_{if} can be either entered as data in the computer program or calculated by integrating $|T^B_{if}(m_\ell)|$ as in (2.71).

In practice, for most of the results reported here this technique was not applied in the three programs for the total cross sections where the calculation was performed by summing over λ' until the result converged. The description above is included for completeness and because the technique was included in the generalized DWPO program suite referred to earlier.

3.4.4 Other features of the DWPO programs

In the three programs above, exchange is neglected in the computation of the radial wave functions $u^{\pm}_{\lambda'}(k_i,r)$ when for all $\lambda' > \lambda'_o$ the exchange part of the phase shift is such that $|\delta^+_{\lambda'} - \delta^-_{\lambda'}| < 0.01$ and these radial wave functions are replaced by a Bessel function (or Coulomb

function in non-hydrogenic cases) when the non-exchange part of the phase shift $\eta_\lambda(k_i) < 0.01$. We find that the contributions due to the exchange integrals $J^{\pm}(\lambda,\lambda')$ rapidly become negligible for large λ' (typically $\lambda' \simeq O(30)$).

The stability of the results has been tested by varying the initial mesh size to take the values $H = 0.0055$, 0.0060 and 0.0065 so that the mesh of radial points extends to $r = 63.2$, 69.0 and 74.7 respectively. Results for $k_i^2 = 20$, 100 and 200 eV are shown in table T3.1 for both the POLORP and POLORD programs and confirm that the programs are numerically stable. Similar conclusions were reported for the POLORB program (paper Ib).

The values of the phase shifts obtained for a range of impact energies and for the first three partialwaves are given in table T3.2a,b. These agree well with those reported by Drachman and Temkin (1972). Additionally the program (POLORD) was amended so that instead of using the Sloan polarization potential (see equation (2.23)), the simple Buckingham polarization

$$V_{pol}(r) = -\frac{\alpha}{(r^2+d^2)^2} \quad \text{with} \quad d = \frac{1}{Z}$$

could be used in additon to the static potential. Phase shifts for both H and He^+ were produced using the two different polarization potentials for a range of values for k_i between 1.0 and 10.0. These results were used by Bransden et al. (1976) in their comparative study of equivalent exchange potentials in electron scattering wherein the set of the Sloan polarization potential phase shifts were taken as an exact reference set for the adiabatic exchange model. Similarly, the phase shifts referred to therein as those in the static exchange model were produced by excluding any form of the polarization potential in the scattering.

As a general comment on the computing procedures, table T3.3 shows some results obtained using the polarized orbital programs in the Born mode compared with results obtained using the analytic scattering amplitudes integrated in a simple program which used a computer integration package.

Table T3.1 Stability of the DWPO II results for Varying Mesh Sizes.

a) POLORP Program: $\sigma_{3p}(k_i^2)\ \pi a_o^2$

Mesh Size	Extent of r	$\sigma_{3p}(k_i^2$=20eV)	$\sigma_{3p}(k_i^2$=100eV)	$\sigma_{3p}(k_i^2$=200eV)
0.0055	63.2	0.124904	0.109705	0.725109,-1
0.0060	69.0	0.124916	0.109706	0.725107,-1
0.0065	74.7	0.124913	0.109706	0.725105,-1

b) POLORD Program: $\sigma_{3d}(k_i^2)\ \pi a_o^2$

Mesh Size	Extent of r	$\sigma_{3d}(k_i^2$=20eV)	$\sigma_{3d}(k_i^2$=100eV)	$\sigma_{3d}(k_i^2$=200eV)
0.0055	63.2	0.254123,-1	0.397512,-2	0.192892,-2
0.0060	69.0	0.254053,-1	0.397503,-2	0.192886,-2
0.0065	74.7	0.254067,-1	0.397495,-2	0.192881,-2

Table T3.2a DWPO e^-H Phase Shifts (radians):Singlet states

		Partial Waves		
k_i(a.u.)	E(eV)	s	p	d
0.50	3.40	1.158	0.013	0.023
1.00	13.60	0.666	0.019	0.050
1.21	20.00	0.628	0.058	0.060
1.49	30.00	0.624	0.116	0.076
1.72	40.00	0.628	0.160	0.090
1.92	50.00	0.630	0.191	0.103
2.00	54.40	0.629	0.202	0.108
2.43	80.00	0.611	0.240	0.130
2.71	100.00	0.593	0.254	0.141
3.00	122.40	0.575	0.263	0.151
3.32	150.00	0.553	0.268	0.158
3.83	200.00	0.519	0.269	0.166
5.00	340.05	0.454	0.259	0.172
7.00	666.50	0.373	0.232	0.166
10.00	1360.20	0.297	0.200	0.152

Table T3.2b DWPO e^-H Phase shifts (radians): Triplet States

		Partial Waves		
k_i(a.u.)	E(eV)	s	p	d
0.50	3.40	2.146	0.312	0.036
1.00	13.60	1.480	0.503	0.128
1.21	20.00	1.298	0.493	0.157
1.49	30.00	1.122	0.466	0.183
1.72	40.00	1.011	0.442	0.194
1.92	50.00	0.932	0.422	0.200
2.00	54.40	0.904	0.415	0.202
2.43	80.00	0.786	0.383	0.206
2.71	100.00	0.727	0.366	0.206
3.00	122.40	0.676	0.351	0.206
3.32	150.00	0.632	0.337	0.204
3.83	200.00	0.573	0.317	0.201
5.00	340.05	0.480	0.283	0.191
7.00	666.50	0.384	0.242	0.170
10.00	1360.20	0.301	0.200	0.152

Table T3.3a Born results produced by the computer program "POLORP" compared with exact values

Energy	σ(3p0)		σ(3p1)		σ(3p)	
(eV)	P*	E*	P	E	P	E
20	.159847	.159847	.274859.-1	.274859,-1	.214819	.214819
30	.133304	.133304	.429243,-1	.429241,-1	.219153	.219152
40	.108280	.108279	.472148.-1	.472140,-1	.202710	.202707
50	.901142,-1	.901115,-1	.476434,-1	.476415,-1	.185401	.185395
80	.590533,-1	.590461,-1	.433766,-1	.433710,-1	.145807	.145788
100	.478235,-1	.478149,-1	.400080,-1	.400013,-1	.127840	.127818
150	.322901,-1	.322830,-1	.331779,-1	.331763,-1	.986459,-1	.986356,-1
200	.243210,-1	.243190,-1	.283596,-1	.283734,-1	.810402,-1	.810658,-1

*P POLORP computer program in the BORN mode (see text)(πa_o^2)

E Exact values (see text) (πa_o^2)

Table T3.3b Born results produced by the computer program "POLORD" compared with exact values

Energy (eV)	σ(3d0) P*	σ(3d0) E*	σ(3d1) P	σ(3d1) E	σ(3d2) P	σ(3d2) E	σ(3d) P	σ(3d) E
20	.854298,-2	.854297,-2	.588018,-2	.588017,-2	.675509,-3	.675509,-3	.216544,-1	.216543,-1
30	.390470,-2	.390467,-2	.646595,-2	.646592,-2	.152937,-2	.152936,-2	.198953,-1	.198952,-1
40	.216083,-2	.216074,-2	.550024,-2	.550016,-2	.189799,-2	.189795,-2	.169573,-1	.169570,-1
50	.144155,-2	.144141,-2	.453175,-2	.453161,-2	.201863,-2	.201855,-2	.145423,-1	.145417,-1
80	.827227,-3	.828092,-3	.267000,-2	.267229,-2	.191437,-2	.191538,-2	.999597,-2	.100034,-1
100	.714237,-3	.719765,-3	.199181,-2	.200002,-2	.175902,-2	.176344,-2	.821590,-2	.824669,-2
150	.589404,-3	.601244,-3	.111025,-2	.113081,-2	.141320,-2	.142587.-2	.563630,-2	.571460,-2
200	.514703,-3	.530346,-3	.709040,-3	.735201,-3	.116113,-2	.118325,-2	.425504,-2	.436725,-2

*P POLORD computer program in the Born mode (πa_o^2)

E Exact values (see text) (πa_o^2)

Further reference to this computer package is made in Chapter 7 with regard to the program ASYM described therein. Similarly, table T3.4 shows some results produced by the programs in the polarized Born mode together with those produced using the analytic polarized Born expressions. It is not possible to verify directly the computation of the latter results but the Born analytic results agree exactly with published values, while the polarized Born expressions are simply an extension of the Born expressions, and the differential cross sections produced via the polarized Born analytic expressions by the computer program agree with those "manually" calculated from the scattering amplitudes. Thus we have no grounds to doubt the calculation of the polarized Born results. These results in turn agree fully with the polarized orbital computations which rely on a sum over the partial waves of the scattered electron whereas the simple program produces the results directly.

For increasing energies, the DWPO I and Born-Oppenheimer and the DWPO II and PBO results approach the BORN and POLARIZED BORN results respectively. Thus we have good reason to trust the only function not checked by the above calculations - that is the radial wave scattering function $u^{\pm}_{\lambda'}(k_i,r)$.

Finally, to ensure that none of the common subroutines became corrupt when developing the programs, the POLORD program was adjusted so that it produced the I, J and K integrals in the subroutine INTLS which corresponded to those produced by the POLORP program. Again agreement was exact.

3.5 Summary

This chapter has been concerned with the main computational details of the calculation of the cross sections using the polarized orbital programs. The framework of the programs has been described with particular emphasis on the POLORD program. Certain features, such as the long range contributions to the direct integrals and the "Born-Subtraction" technique, have been explained. The stability of the results under varying mesh sizes was

Further reference to this computer package is made in Chapter 7 with regard to the program ASYM described therein. Similarly, table T3.4 shows some results produced by the programs in the polarized Born mode together with those produced using the analytic polarized Born expressions. It is not possible to verify directly the computation of the latter results but the Born analytic results agree exactly with published values, while the polarized Born expressions are simply an extension of the Born expressions, and the differential cross sections produced via the polarized Born analytic expressions by the computer program agree with those "manually" calculated from the scattering amplitudes. Thus we have no grounds to doubt the calculation of the polarized Born results. These results in turn agree fully with the polarized orbital computations which rely on a sum over the partial waves of the scattered electron whereas the simple program produces the results directly.

For increasing energies, the DWPO I and Born-Oppenheimer and the DWPO II and PBO results approach the BORN and POLARIZED BORN results respectively. Thus we have good reason to trust the only function not checked by the above calculations - that is the radial wave scattering function $u^{\pm}_{\lambda'}(k_i,r)$.

Finally, to ensure that none of the common subroutines became corrupt when developing the programs, the POLORD program was adjusted so that it produced the I, J and K integrals in the subroutine INTLS which corresponded to those produced by the POLORP program. Again agreement was exact.

3.5 Summary

This chapter has been concerned with the main computational details of the calculation of the cross sections using the polarized orbital programs. The framework of the programs has been described with particular emphasis on the POLORD program. Certain features, such as the long range contributions to the direct integrals and the "Born-Subtraction" technique, have been explained. The stability of the results under varying mesh sizes was

Table T3.4a Polarized-Born results produced by the computer program "BOLORP" compared with exact values

Energy (eV)	σ(3p0) P*	σ(3p0) E	σ(3p1) P	σ(3p1) E	σ(3p) P	σ(3p) E
20	.127886	.127886	.215501,-1	.215501,-1	.170986	.170986
30	.111063	.111063	.344719,-1	.344717,-1	.180007	.180006
40	.926344,-1	.926332,-1	.385412,-1	.385405,-1	.169717	.169714
50	.785547,-1	.785519,-1	.393597,-1	.393579,-1	.157274	.157268
80	.532687,-1	.532606,-1	.366699,-1	.366634,-1	.126609	.126587
100	.437366,-1	.437256,-1	.341588,-1	.341492,-1	.112054	.112024
150	.301666,-1	.301522,-1	.288003,-1	.287841,-1	.877672,-1	.877204,-1
200	.230091,-1	.229948,-1	.248917,-1	.248695,-1	.727925,-1	.727338,-1

*Notation as in T3.3a

Table T3.4b Polarized-Born results produced by the computer program "POLORD" compared with exact values

Energy (eV)	σ(3d0) P*	σ(3d0) E*	σ(3d1) P	σ(3d1) E	σ(3d2) P	σ(3d2) E	σ(3d) P	σ(3d) E
20	.335529,-2	.335529,-2	.234957,-2	.234957,-2	.273119,-3	.273118,-3	.860067,-2	.860067,-2
30	.163822,-2	.163819,-2	.259038,-2	.259036,-2	.612668,-3	.612661,-3	.804432,-2	.804423,-2
40	.987583,-3	.987513,-3	.224237,-2	.224231,-2	.762813,-3	.762785,-3	.699795,-2	.699770,-2
50	.701281,-3	.701170,-3	.188309,-2	.188298,-2	.816102,-3	.816046,-3	.609967,-2	.609922,-2
80	.416808,-3	.418088,-3	.116481,-2	.116665,-2	.787409,-3	.788227,-3	.432125,-2	.432784,-2
100	.350606,-3	.354946,-3	.889773,-3	.896110,-3	.729497,-3	.732786,-3	.358915,-2	.361274,-2
150	.276944,-3	.280746,-3	.528892,-3	.531938,-3	.587520,-3	.603333,-3	.250977,-2	.255129 ,-2
200	.233910,-3	.240656,-3	.350473,-3	.358030,-3	.484613,-3	.506974,-3	.190408,-2	.197066,-2

*Notation as in T3.3b.

tested and the values for the computed phase shifts presented. Finally, the results obtained by running the programs in the Born and Polarized-Born modes are shown to be in good agreement with exact values.

CHAPTER 4

Total and Differential Cross Sections

§4.1 Introduction

In this chapter we present the results of the calculations performed using the computer programs described above, together with the other available experimental and theoretical results. The individual total 3ℓ cross sections are presented and discussed first, followed by the total $n = 3$ and total $H\alpha$ cross sections. Important comments about the use of the DWPO model are then made and finally we give the differential cross sections.

§4.2 Total Cross Sections for Individual $1s \rightarrow n\ell m_\ell$ Transitions

We show in figure F4.1 the calculated total cross sections for the individual processes

$$e + H(1s) \rightarrow e + H(3\ell); \quad \ell = 0, 1, 2$$

for both the DWPO I and the DWPO II models. The $3p$ cross section dominates throughout the energy range but the $3p$ DWPO II result lies about 10% lower than the DWPO I values. We found (shown below) that at higher energies $\sigma(3p, \text{DWPO I})$ tends to the Born approximation whereas $\sigma(3p, \text{DWPO II})$ tend to the polarized Born approximation. In the $3s$ results, polarization distortion of the core had negligible effect above 100 eV. However, although $\sigma(3d, \text{DWPO I})$ is of the same order of magnitude as the $3s$ cross section, in the case of the $3d$ calculations, polarization distortion effects are now very noticeable. In fact, $\sigma(3d, \text{DWPO II})$ is 50% smaller than the DWPO I results at 200 eV and even at very high energies the DWPO II results, which are equivalent to the polarized-Born results above 200eV, continue to be significantly below the Born approximation. The $\sigma(3d, \text{DWPO I})$ cross section is equivalent to the Born result above 200eV. Similar conclusions about the effect of core polarization have been reached independently by Beigman and Shevel'ko (1974) in a investigation of electron impact induced

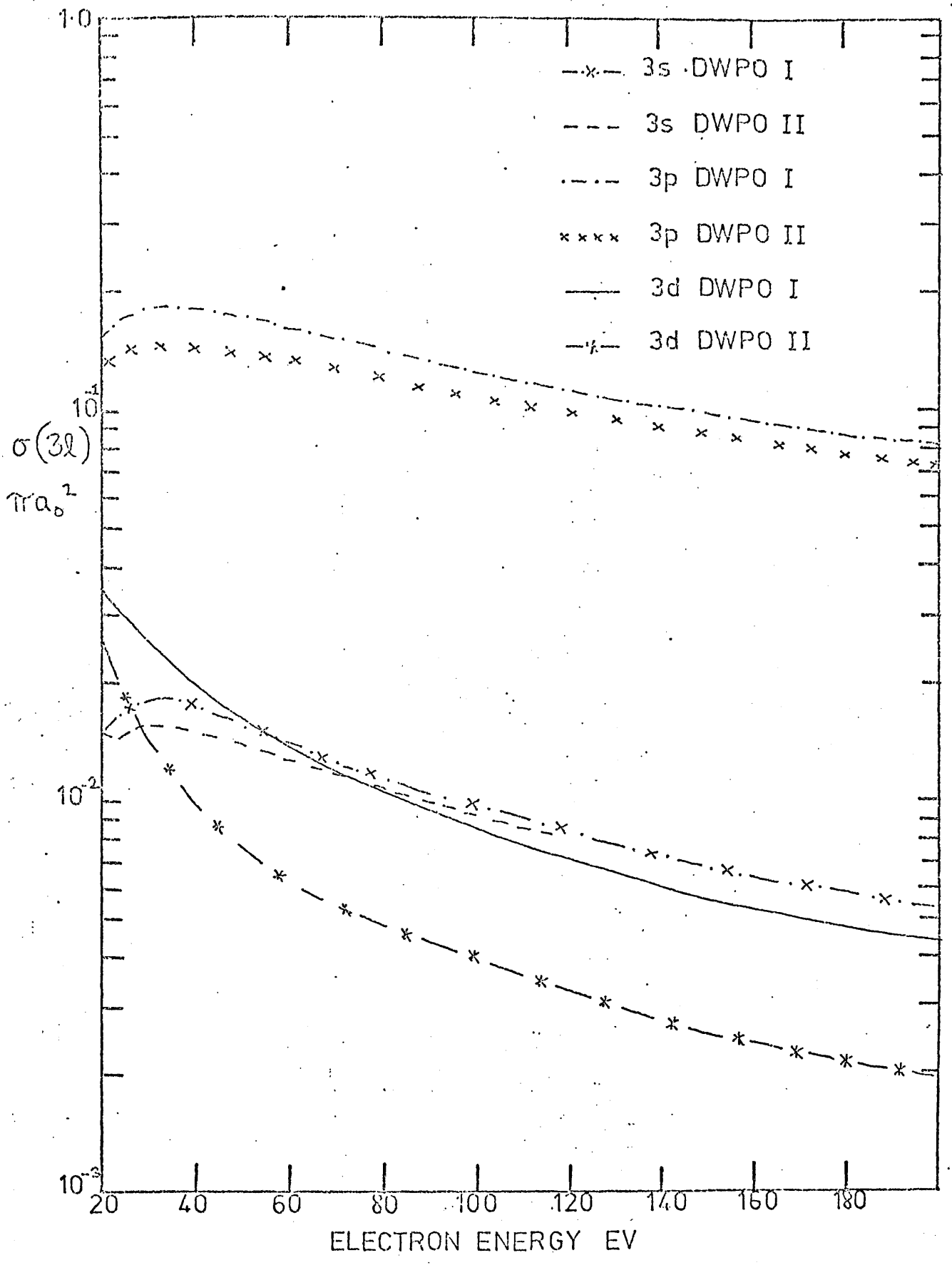

FIGURE F4·1

TOTAL 3s, 3p, 3d CROSS SECTIONS

inelastic transitions in the alkalis.

Figure F4.2 shows our results for the 3s excitation compared with those of other workers. The experimental results are the relative measurements of Mahan (Mahan 1974, Mahan, Gallaher and Smith 1976) obtained via a normalization for the 3p states to the Born 3p cross-section at 500eV. Our results, in either the DWPO I or DWPO II models, are in excellent agreement with this experiment thoughout the energy range. The Glauber calculations of Tai et al. (1970) and the seven-channel eikonal approach of Flannery and McCann (1974) are also in good accord with experiment - the former for energies above 30eV and the latter throughout the energy range. The Born cross section and the modified Born results of Morrison and Rudge (1966) substantially overestimate the cross section below 150eV. An early distorted wave calculation of Vainshtein (1961) is also shown which greatly overestimates the cross section at all energies. The twenty state second-order diagonalization method of Baye and Heenan (1974) and the low energy unitarized Born results of Somerville (1963) are also seen to be in excellent agreement with experiment. The six state close coupling calculation of Burke et al. (1967) at two low energies is also shown but is in poor agreement with experiment. The Ochkur approximation results of Gumble (1969) have not been included since they lie very close to the Born values. Similarly, the Born-Oppenheimer results obtained here which lie above the modified Born results and the simplified second Born approximation of Holt (1969) which lie between the Born and modified Born results are not shown for the sake of clarity. The 3s excitation cross section calculated here in the Born, Born-Oppenheimer and DWPO models with or without core distortion are tabulated for reference purposes in table T4.1. It should be noted that the results referred to in the tables in this chapter have been calculated via equation (2.66) and thus are subject to convergence errors. For this reason the Born results do not exactly agree with published values.

The calculated values for $\sigma(3p)$ are compared with those of other workers and the experimental values of Mahan (1974) in figure F4.3. Our

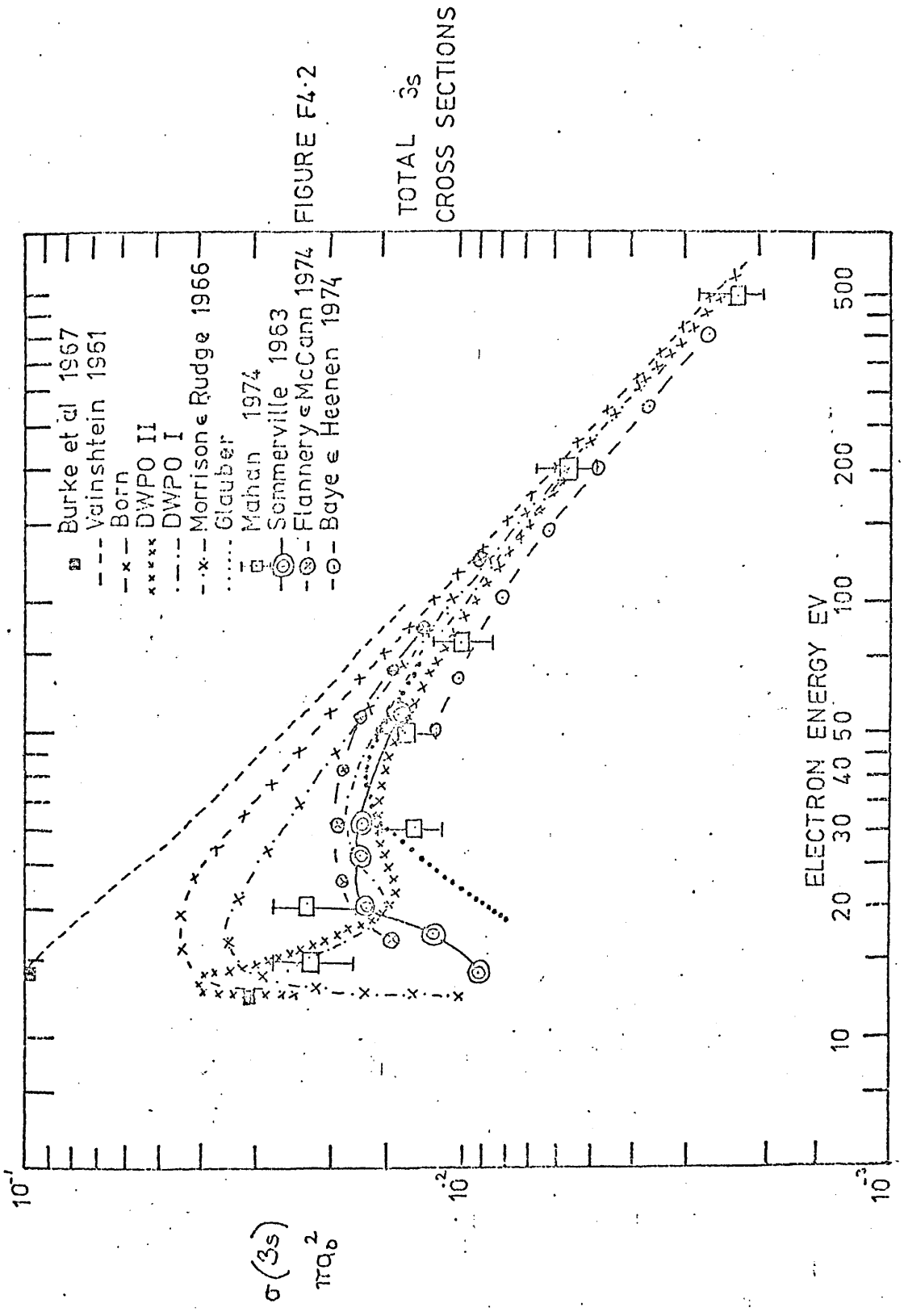
TOTAL 3s CROSS SECTIONS
Burke et al 1967
Vainshtein 1961
Born
DWPO II
DWPO I
Morrison & Rudge 1966
Glauber
Mahan 1974
Sommerville 1963
Flannery & McCann 1974
Baye & Heenen 1974
ELECTRON ENERGY EV
10
20
30
40
50
100
200
500
10^{-1}
10^{-2}
10^{-3}
$\sigma(3s)$
πa_0^2

FIGURE F4·2

T4.1 Cross-sections for transitions from the 1s state to the 3s state

(Units: πa_o^2)

Energy eV	Born	Polarized Born *	Born - Oppenheimer	Polarised Born-Oppenheimer	DWPO I	DWPO II
15	.430,-1	.239,-1	.414	.367	.229,-1	.286,-1
20	.432,-1	.277,-1	.173	.147	.152,-1	.151,-1
30	.335,-1	.250,-1	.499,-1	.407,-1	.181,-1	.155,-1
40	.265,-1	.214,-1	.282,-1	.237,-1	.174,-1	.151,-1
50	.218,-1	.185,-1	.209,-1	.182,-1	.157,-1	.139,-1
80	.142,-1	.130,-1	.130,-1	.122,-1	.115,-1	.107,-1
100	.115,-1	.108,-1	.106,-1	.101,-1	.969,-2	.923,-2
150	.777,-2	.758,-2	.732,-2	.724,-2	.694,-2	.683,-2
200	.587,-2	.584,-2	.560,-2	.564,-2	.539,-2	.541,-2

* The polarized Born results were obtained using the analytic forms for the scattering amplitude (see Chapter 3).

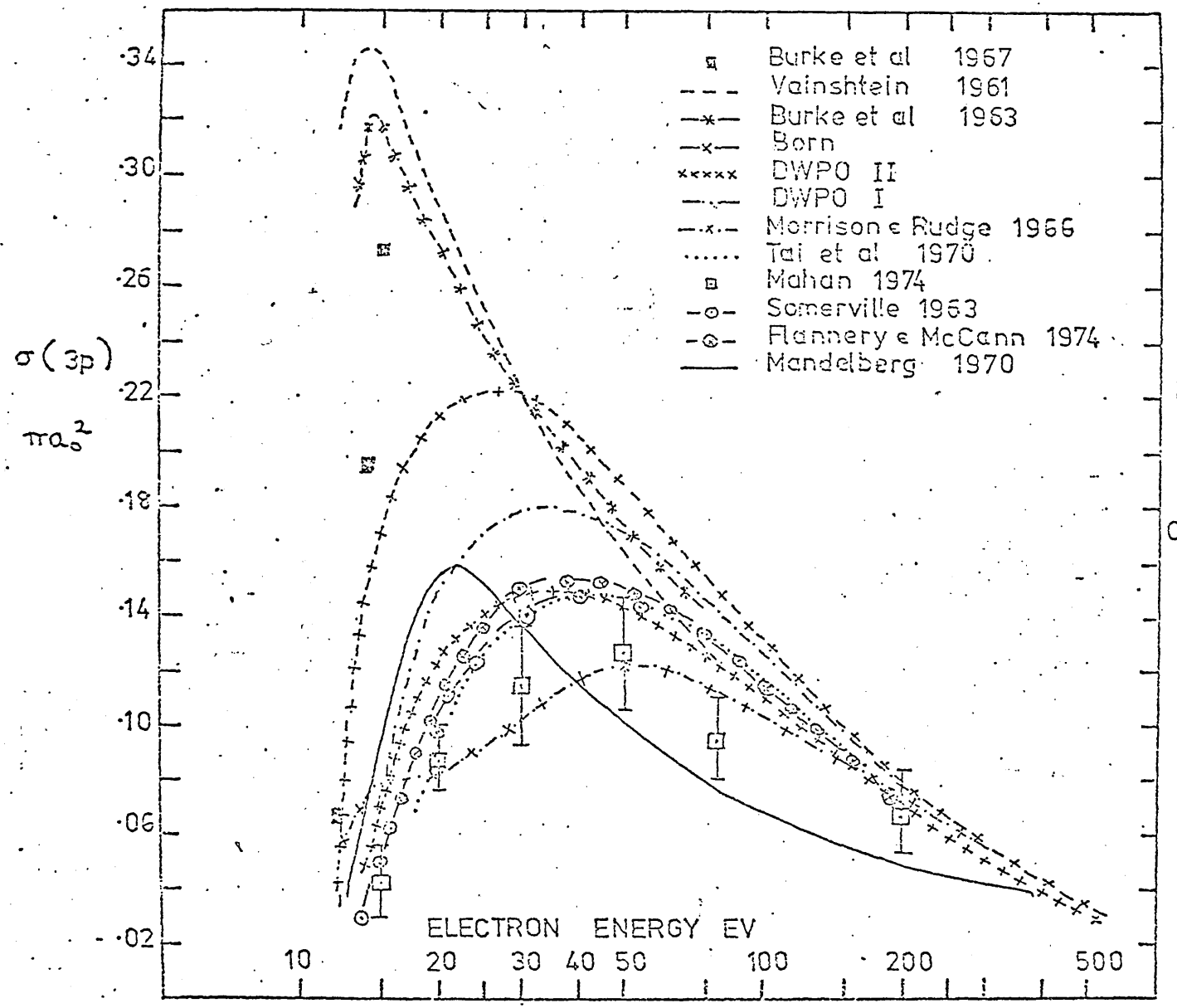

FIGURE F4·3

TOTAL 3p CROSS SECTIONS

DWPO II results are in good general agreement with experiment when this is renormalized to our DWPO II $\sigma(3p)$ value at 500eV as shown rather than to the Born value which is about 8% higher. However with this renormalization we lie slightly above Mahan's estimated r.m.s. errors below 40eV. Once again the low energy unitarized Born results of Somerville (1963) are in excellent agreement with experiment - this agreement is improved when the experimental results are normalized to the Born value at 500eV. Above 20eV, the modified Born resultsof Morrison and Rudge (1966) are also in excellent agreement with experiment. Of the other available theoretical results only the Glauber (Tai et al., 1970) and the eikonal pseudo-state results of Flannery and McCann (1974) give reasonable accord, both in shape and magnitude with experiment. The coupled state impact-parameter method of Mandelberg (1970) lies above the experimental results below 30eV and below these results for higher energies. In particular, the two state (1s - 3p) close-coupling calculation of Burke et al. (1963) gives very large values of $\sigma(3p)$ - possibly because including only these states in a close coupling expansion cannot account for much of the ground state polarizability. Burke et al. (1967) give 6-state close-coupling results for $n = 1$ to $n = 3$ transitons for energies up to the $n = 4$ threshold. Their results for $\sigma(3p)$ also shown in F4.3,increase rapidly above threshold and are in little better agrement with experiment. Burke et al. (1967) remark that they believe their results to be of doubtful validity except for the first point due to resonances below the $n = 4$ threshold whose effect is not included. The second Born approximation results of Holt (1969) and the Ochkur results of Gumble (1969), neither of which are shown, lie between the Born and DWPO I results. The twenty-state diagonalization method of Baye and Heenen (1974) (not shown) lie very close to the Born results; the distorted wave results of Vainshtein (1961) and the one-channel second order potential method of Bransden et al. (1972) (not shown) both greatly overestimate the cross section.

The 3p0, 3p1 and 3p excitation cross sections calculated here are also given in tables T4.2a, b and c. The 3p0 total cross sections in the

T4.2a Cross Sections for transitions from the 1s state to the 3p0 state (units πa_o^2)

Energy eV	Born	Polarised Born	Born-Oppenheimer	Polarised Born Oppenheimer	DWPO I	DWPO II
15	.145	.112	.348	.309	.653,-1	.574,-1
20	.160	.128	.178	.150	.110	.937,-1
30	.133	.111	.116	.960,-1	.114	.954,-1
40	.108	.926,-1	.948,-1	.812,-1	.101	.859,-1
50	.901,-1	.786,-1	.810,-1	.706,-1	.891,-1	.767,-1
80	.591,-1	.533,-1	.558,-1	.503,-1	.625,-1	.557,-1
100	.478,-1	.437,-1	.460,-1	.420,-1	.513,-1	.464,-1
150	.323,-1	.302,-1	.316,-1	.296,-1	.349,-1	.323,-1
200	.243,-1	.230,-1	.240,-1	.227,-1	.262,-1	.245,-1

T4.2b Cross sections for transitions from the 1s state to the 3p1 state (units πa_o^2)

Energy eV	Born	Polarised Born	Born Oppenheimer	Polarised Born Oppenheimer	DWPO I	DWPO II
15	.104,-1	.806,-1	.121,-1	.109,-1	.720,-2	.647,-2
20	.275,-1	.216,-1	.247,-1	.206,-1	.191,-1	.156,-1
30	.429,-1	.345,-1	.369,-1	.296,-1	.329,-1	.265,-1
40	.472,-1	.385,-1	.419,-1	.341,-1	.385,-1	.314,-1
50	.476,-1	.394,-1	.436,-1	.357,-1	.405,-1	.334,-1
80	.434,-1	.367,-1	.411,-1	.347,-1	.393,-1	.332,-1
100	.400,-1	.342,-1	.384,-1	.328,-1	.371,-1	.317,-1
150	.332,-1	.288,-1	.324,-1	.281,-1	.316,-1	.275,-1
200	.284,-1	.249,-1	.279,-1	.245,-1	.274,-1	.241,-1

T4.2c Cross sections for transitions from the 1s state to the 3p state (units πa_o^2)

Energy eV	Born	Polarised Born	Born Oppenheimer	Polarised Born Oppenheimer	DWPO I	DWPO II
15	.165	.128	.373	.528	.797,-1	.703,-1
20	.215	.171	.228	.191	.148	.125
30	.219	.180	.189	.156	.180	.148
40	.203	.170	.179	.149	.178	.149
50	.185	.157	.168	.142	.170	.144
80	.146	.127	.138	.120	.141	.122
100	.128	.112	.123	.108	.125	.110
150	.986,-1	.877, -1	.119	.858,-1	.981,-1	.872,-1
200	.811,-1	.727,-1	.798,-1	.717,-1	.810,-1	.727,-1

Born and DWPO II approximations are plotted in figure F4.4a which also shows the results of Flannery and McCann (1974) and Baye and Heenen (1974). Similarly figure F4.4b shows the corresponding 3pl cross sections. Firstly, these show that although the overall 3p cross section obtained by Baye and Heenen is very similar to the Born approximation to $\sigma(3p)$ (figure F4.4c), the magnetic sublevels contributions are noticeably different. Again, although the Flannery and McCann $\sigma(3p)$ results are in excellent agreement with the DWPO II results above 20eV, comparison of the separate $\sigma(3pm_\ell)$ results would imply a serious discrepancy between their model and our own for their $\sigma(3p0)$ cross section lies well below ours whereas we predict a smaller $\sigma(3p1)$ than they do. This fact significantly affects predictions, using the two models, of the polarization fractions for radiation from the 3p state to the 2s or 1s state (Lyman β) following excitation from the 1s state.

Finally our calculated 3d values are shown in figures F4.5a,b . Firstly, we compare in F4.5a our DWPO I results with Mahan's experimental values (normalized to the Born $\sigma(3d)$ at 500eV) and with certain other theoretical calculations. With this normalization, both the shape and magnitude of the experimental results agree extremely well with the DWPO I results. Additionally, the available results in the unitarized Born approximation (Somerville 1963) agree very well with maximum of the cross section and the twenty state second order diagonalization results for higher energies ($\geq$ 50eV) obtained by Baye and Heenen (1974) are also in line with the experimental results.

However, the experimental results have an energy dependence which is substantially different from that of the Born approximation and Mahan's results lie 50% above the Born at its maximum. The simplified second Born results of Woollings and McDowell (1973) and the Glauber results of Bhadra and Ghosh (1971) are in very close agreement with each other, tend to the first Born at high energies but lie a factor of two below experiment. The modified Born results (Morrison and Rudge 1966) give substantially lower values near the maximum of the cross section and again tend to the Born at high energies.

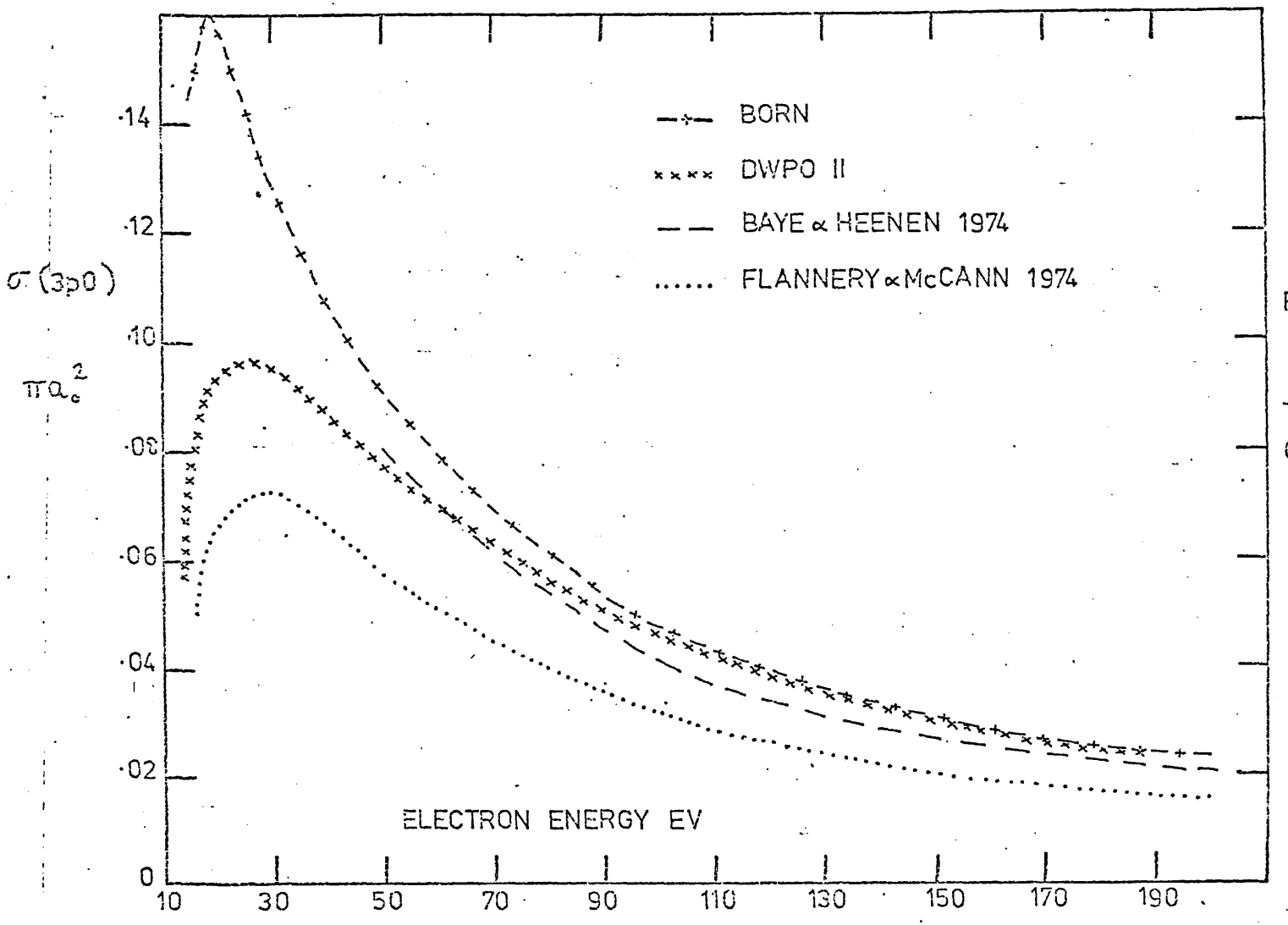

FIGURE F4·4a

TOTAL 3p0
CROSS SECTIONS

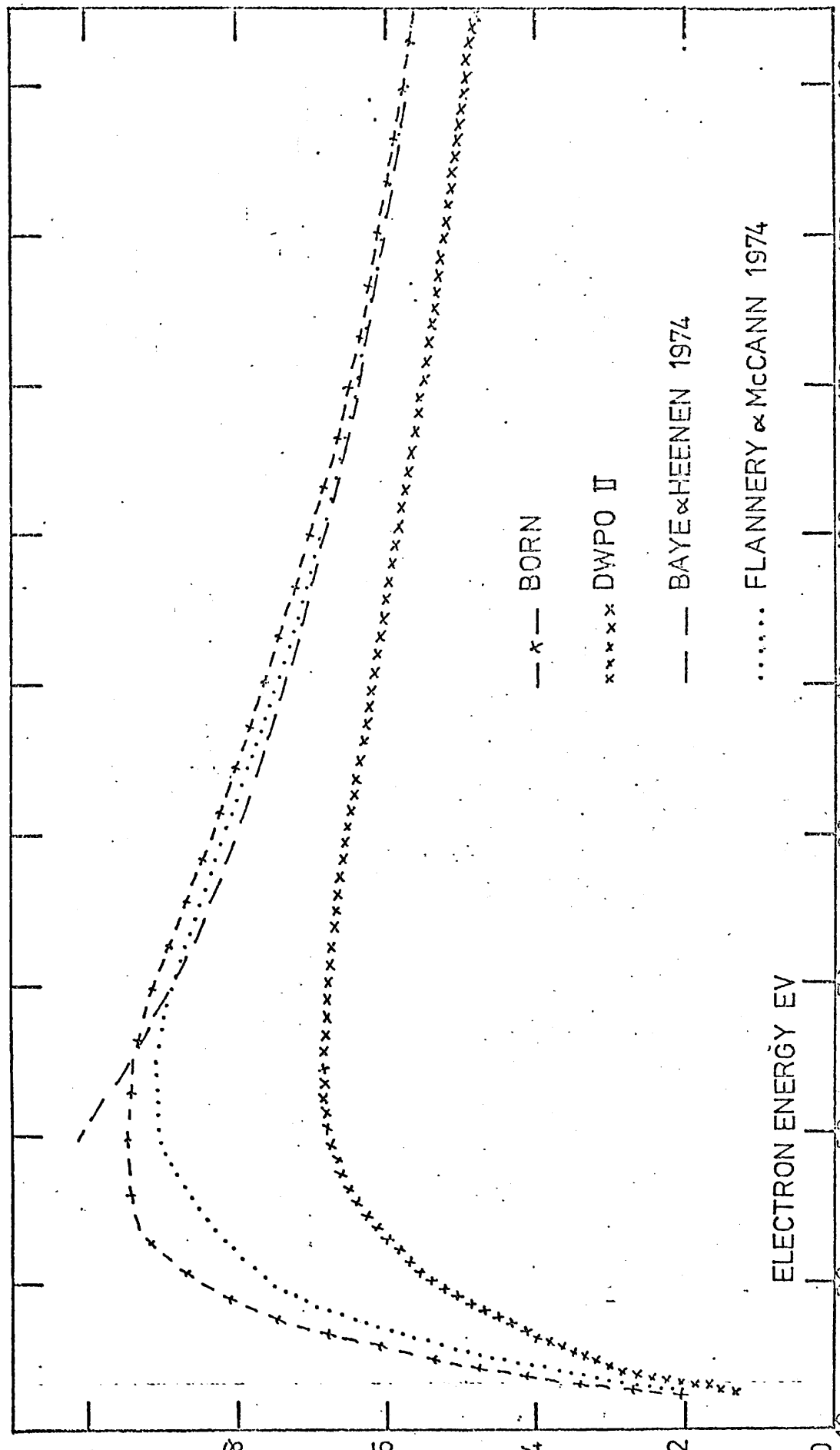

FIGURE F4·4b TOTAL 3p1 CROSS SECTIONS

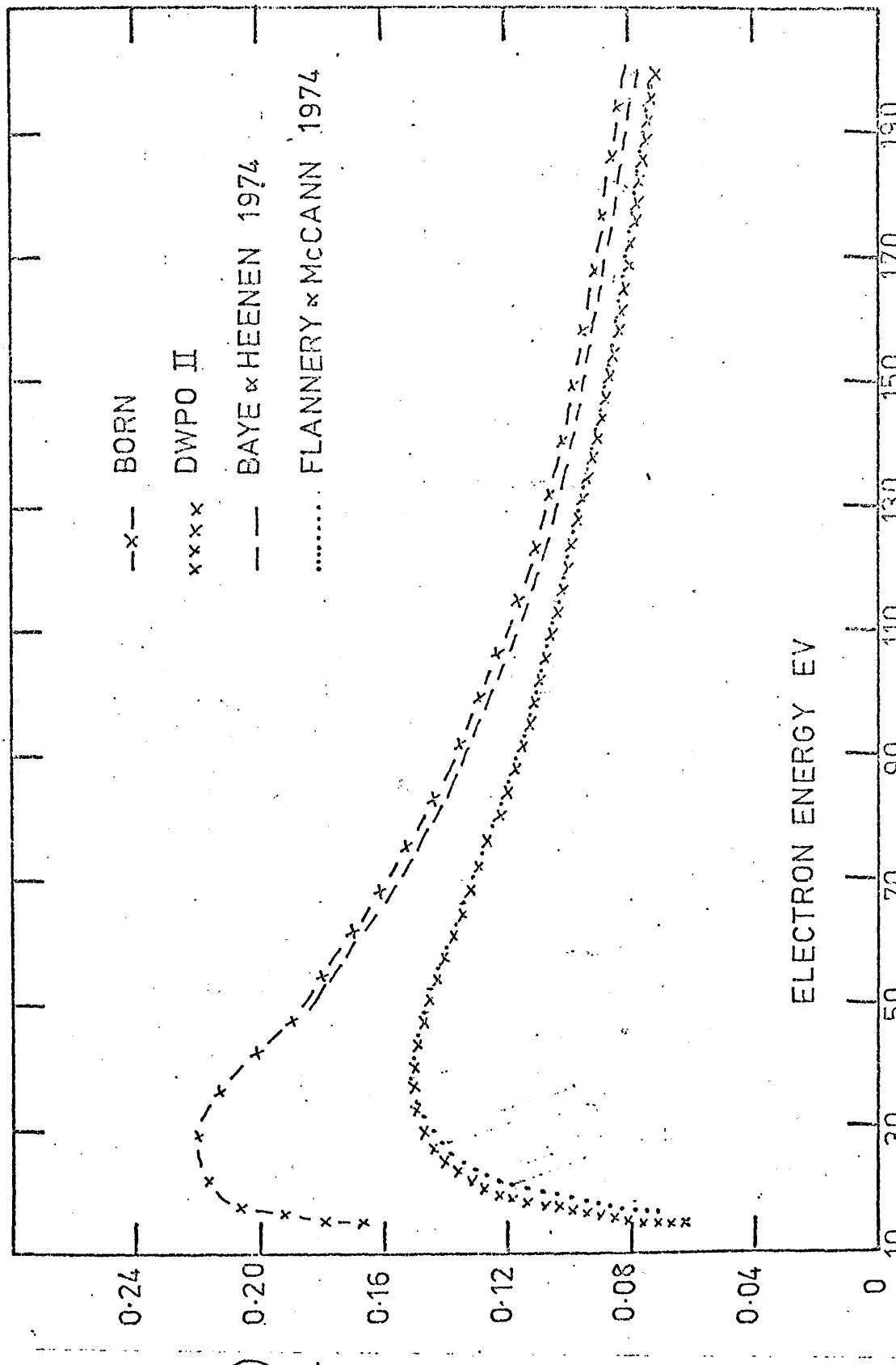

FIGURE F4·4c TOTAL 3p CROSS SECTIONS

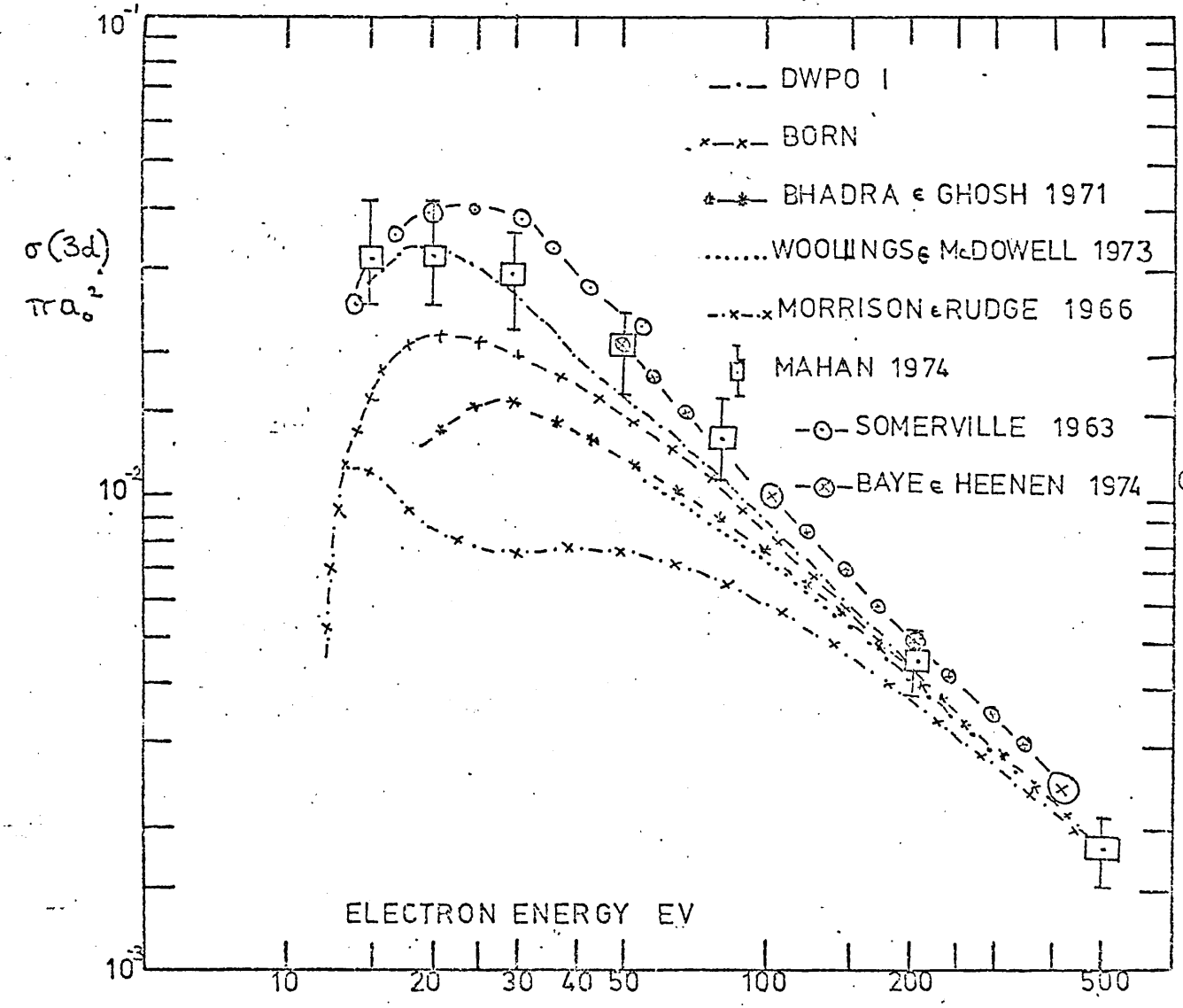

FIGURE F4·5a

TOTAL 3d

CROSS SECTIONS (a)

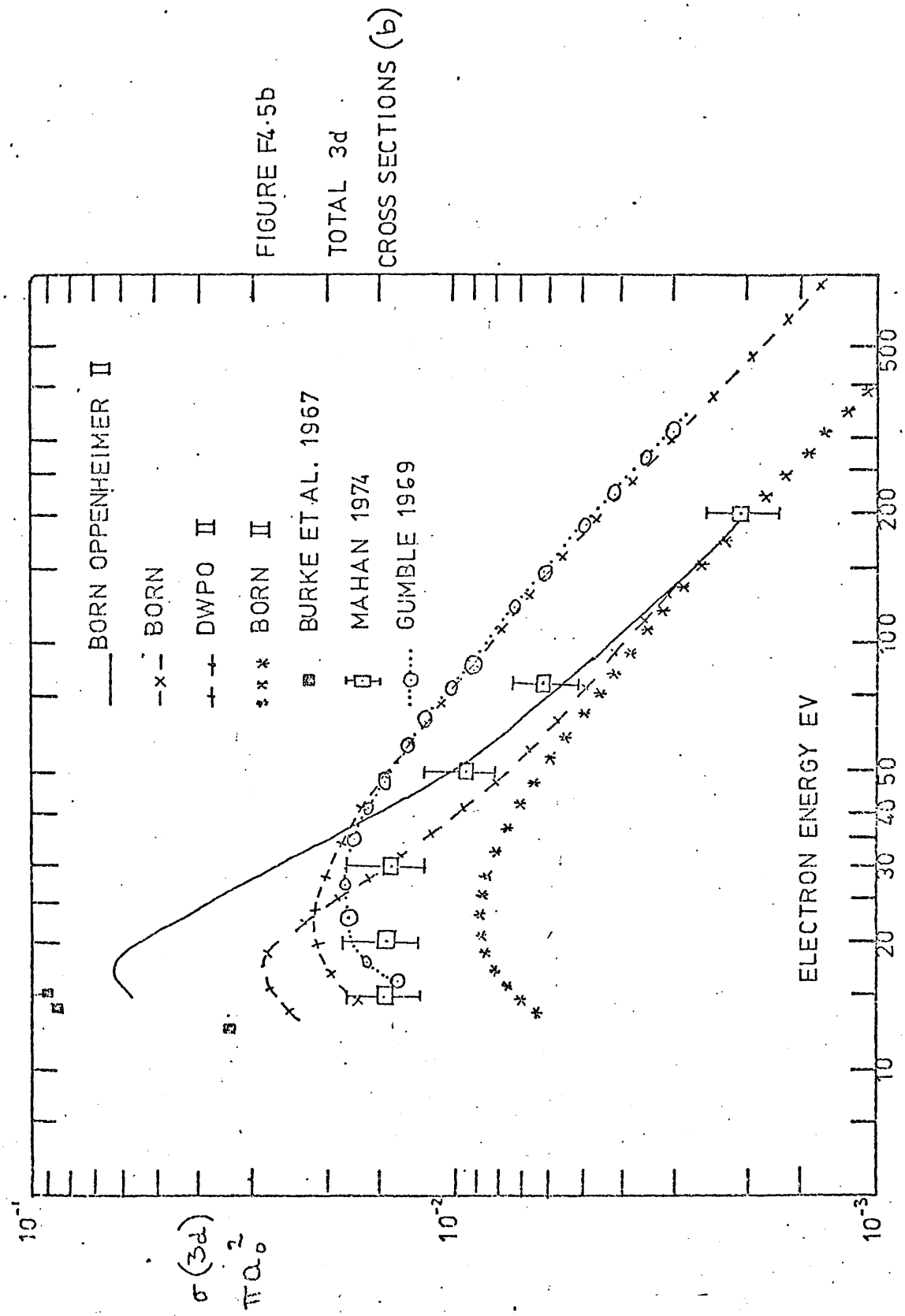
FIGURE F4·5b
TOTAL 3d
CROSS SECTIONS (b)
BORN OPPENHEIMER II
BORN
DWPO II
BORN II
BURKE ET AL. 1967
MAHAN 1974
GUMBLE 1969
ELECTRON ENERGY EV
10
20
30
40
50
100
200
500
10^{-1}
10^{-2}
10^{-3}
$\sigma(3d)$
πa_0^2

As was remarked with respect to figure F4.1, the effectof polarization distortion of the core, incorporated by coupling the 1s - 2p states together in the target wave function, is dramatic in the 1s - 3d case. The DWPO II results, which agree closely with the polarized Born results above 200eV, are shown in figure F4.5b. This shows that the DWPO I results are a factor of about 2.4 below the first Born at 500eV and the separation between the Born and polarized Born results continues even for impact energies measured in KeV. Similar results were found by McDowell et al. (1975b) for the DWPO II 2p cross-section and also found by Beigman and Shevel'ko (1974) for several s - p transitions in the alkalis.

Also, extension of the 3 state close coupling calculation to high energies (Fon, 1975) produces cross sections for the 1s - 2p excitation which are appreciably below the first Born results. This behaviour strongly suggests that p - d coupling, which is not included in this model, may be important and emphasises the advantages of using the unitarization (R-matrix) technique of Seaton (1961).

Choosing to renormalise the experimental results to our DWPO II results at 500eV gives the position shown in F4.5b. Our calculated values remain in good accord with the renormalised experiment at impact energies greater than 30eV. Also shown for reference with F4.5a are the Born results. The Polarized Born results and the polarized-Born-Oppenheimer results are also included - the former lie about 50% below experiment at their maximum while the latter always overestimate the DWPO II results, are a factor of two above them at the cross section maximum and a factor of four abovethe experimental results at this point. This comparison shows that although it is target distortion which lowers the calculated cross section at high energies, it is distortion of the incident wave which dominates at energies below 100eV. Also shown on this graph are the Ochkur results of Gumble (1969) which agree quite well with these renormalised experimental results at low energies but tend to the Born results at 50eV. Nor can these Ochkur results be used for comparison with

the experimental results normalised to the Born results at 500eV as in F4.5a since they always lie below the Born values which have the wrong energy dependence. Not shown on either graph are the coupled state impact parameter results of Mandelberg whose cross sections lie an order of magnitude above the experimental results and other theoretical results - the author states that this feature may be due to the exclusion of higher lying states in the calculations. Remarkably, the shape of the Mandelberg curve closely follows that of the modified Born results of Morrison and Rudge (1966) although there is a difference of a factor of thirty between them and the energy dependence indicated in no way fits that shown by the experimental results.

It should be noticed that the effect of the renormalization adopted for figure F4.5b is that the 3d cross section now always lies below the Born results - contrary to the assumption of Mahan (Thesis 1974). This effect is important when measurements of the Hα polarization are analysed (see chapter 5 below) and when the Hα intensity asymmetry in an applied electric field is considered (see chapter 7 below).

Our calculated 3d results are tabulated in T4.3a,b,c,d.

§4.3 Total n = 3 and total Hα excitation cross sections.

Mahan (1974) actually measured the total Hα cross section

$$\sigma(H\alpha) = \sigma_{3s} + 0.12\sigma_{3p} + \sigma_{3d}$$

relative to the Born value at 500eV together with the ratios of σ_{3s}, σ_{3p} and σ_{3d} to $\sigma(H\alpha)$. From the individual 3ℓ cross sections thus obtained, he computed the total n = 3 cross section according to:

$$\sigma(n = 3) = \sigma_{3s} + \sigma_{3p} + \sigma_{3d}.$$

Figure F4.6 shows his results for this cross section together with the theoretical calculations. The experimental points are insensitive to our suggested renormalization of the 3d cross section at 500eV. They lie between our DWPO II result and the modified Born calculation of Morrison and Rudge while the sum of the individual Glauber cross sections (Tai et al. 1970,

T4.3a Cross sections for transitions from the 1s state to the 3d0 state (units πa_o^2)

Energy eV	Born	Polarised Born	Born Oppenheimer	Polarised Born Oppenheimer	DWPO I	DWPO II
15	.116,-1	.466,-2	.385,-1	.279,-1	.165,-1	.155,-1
20	.854,-2	.336,-2	.345,-1	.237,-1	.149,-1	.133,-1
30	.390,-2	.164,-2	.111,-1	.723,-2	.764,-2	.541,-2
40	.216,-2	.988,-3	.415,-2	.255,-2	.342,-2	.213,-2
50	.144,-2	.701,-3	.203,-2	.118,-2	.214,-2	.128,-2
80	.825,-3	.416,-3	.820,-3	.425,-3	.861,-3	.483,-3
100	.710,-3	.348,-3	.696,-3	.343,-3	.649,-3	.346,-3
150	.569,-3	.257,-3	.572,-3	.260,-3	.520,-3	.252,-3
200	.495,-3	.214,-3	.503,-3	.220,-3	.512,-3	.253,-3

T4.3b Cross sections for transitions from the 1s state to the 3d1 state (units πa_o^2)

Energy eV	Born	Polarised Born	Born Oppenheimer	Polarised Born Oppenheimer	DWPO I	DWPO II
15	.283,-2	.116,-2	.190,-1	.144,-1	.598,-2	.535,-2
20	.588,-2	.235,-2	.222,-1	.152,-1	.822,-2	.563,-2
30	.647,-2	.259,-2	.139,-1	.812,-2	.777,-2	.400,-2
40	.550,-2	.224,-2	.915,-2	.487,-2	.569,-2	.260,-2
50	.453,-2	.188,-2	.656,-2	.331,-2	.479,-2	.215,-2
80	.267,-2	.116,-2	.323,-2	.115,-2	.288,-2	.131,-2
100	.199,-2	.890,-3	.229,-2	.109,-2	.216,-2	.100,-3
150	.110,-2	.509,-3	.119,-2	.572,-2	.121,-2	.581,-3
200	.699,-3	.330,-3	.739,-3	.358,-3	.830,-3	.425,-3

T4.3c Cross sections for transitions from the 1s state to the 3d2 state (units πa_o^2)

Energy eV	Born	Polarised Born	Born Oppenheimer	Polarised Born Oppenheimer	DWPO I	DWPO II
15	.129,-3	.532,-4	.433,-3	.285,-3	.161,-3	.105,-3
20	.676,-3	.273,-3	.158,-2	.942,-3	.832,-3	.419,-3
30	.153,-2	.613,-3	.254,-2	.133,-2	.190,-2	.870,-3
40	.190,-2	.763,-3	.269,-2	.132,-2	.210,-2	.904,-3
50	.202,-2	.816,-3	.263,-2	.123,-2	.225,-2	.972,-3
80	.191,-2	.787,-3	.222,-2	.992,-3	.210,-2	.912,-3
100	.176,-2	.729,-3	.197,-2	.870,-3	.191,-2	.831,-3
150	.140,-2	.587,-3	.151,-2	.656,-3	.150,-2	.657,-3
200	.115,-2	.485,-3	.121,-2	.525,-3	.126,-2	.564,-3

T4.3d Cross sections for transitions from the 1s state to the 3d state (units πa_o^2)

Energy eV	Born	Polarised Born	Born Oppenehimer	Polarised Born Oppenheimer	DWPO I	DWPO II
15	.176,-1	.708,-2	.774,-1	.571,-1	.287,-1	.264,-1
20	.217,-1	.860,-2	.822,-1	.559,-1	.330,-1	.254,-1
30	.199,-1	.804,-2	.441,-1	.261,-1	.270,-1	.151,-1
40	.170,-1	.700,-2	.278,-1	.149,-1	.190,-1	.914,-2
50	.145,-1	.610,-2	.204,-1	.103,-1	.162,-1	.753,-2
80	.999,-2	.432,-2	.117,-1	.550,-2	.108,-1	.493,-2
100	.821,-2	.359,-2	.921,-2	.427,-2	.878,-2	.401,-2
150	.558,-2	.245,-2	.597,-2	.271,-2	.594,-2	.273,-2
200	.420,-2	.184,-2	.440,-2	.198,-2	.469,-2	.223,-2

FIGURE F4.6

TOTAL n=3 CROSS SECTIONS

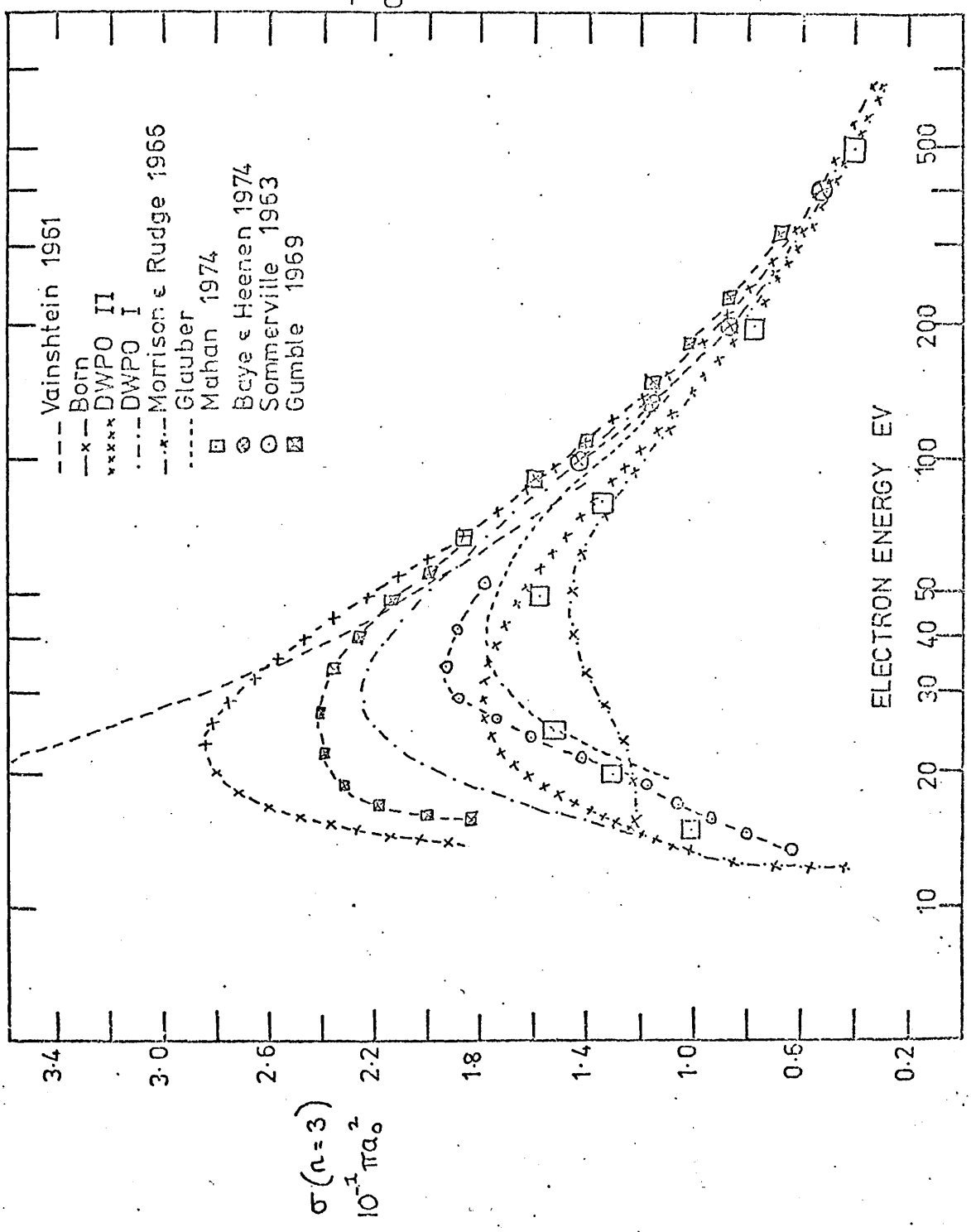

and Bhadra and Ghosh 1971) also gives a result in close agreement with experiment for energies above 20eV. The unitarized Born results of Somerville (1963) are also in reasonable agreement with experiment particularly below 25eV. When target distortion is neglected in our model (as in DWPO I), the resulting cross section, while lower than the first Born results, are nevertheless too large at energies below 150eV. Similarly the Ochkur results of Gumble (1969), the distorted wave results of Vainshtein (1961), and the twenty state second order diagonalization method of Baye and Heenen (1974) all give cross sections which disagree with the experiment. Not shown are the sum of the individual simplied second Born cross sections (Holt 1969, and Woollings and McDowell 1973), which lies between the DWPO I and Born results, and the fourteen coupled states impact parameter method of Mandelberg (1970) which is distorted by the very large 3d cross section.

The total Hα cross section, $\sigma(H\alpha)$, is of more interest since the $\sigma(3p)$ contribution no longer dominates. The available theoretical results are shown in figure F4.7a. Our DWPO II results are in close agreement with those obtained using the individual cross sections of Morrison and Rudge (1966) although the two models exhibit quite different energy dependence at very low energies but where neither approach is expected to be valid. The polarized Born cross sections lie between the DWPO I and II results between 20 and 200eV and are equivalent to the DWPO II results above 200eV. The combined Glauber cross sections of Tai et al. (1970) and of Bhadra and Ghosh (1971) lead to values of Hα which are in good agreement with our DWPO I results at energies above 70eV but predict a maximum at 35eV (higher in energy than the maxima predicted by the other models) and as is usual with Glauber calculations, the cross section below this point rapidly decreases to very small values. The available (above 50eV) combined simplified second Born results (Holt 1969, and Woollings and McDowell 1973) very closely follow our DWPO I results. The remaining theoretical models shown (Born, DWPO I, distorted wave, Born-Oppenheimer, Ochkur and Unitarised Born) all give cross sections which lie higher than our DWPO II results. The

FIGURE F4·7a

TOTAL BALMER α CROSS SECTIONS

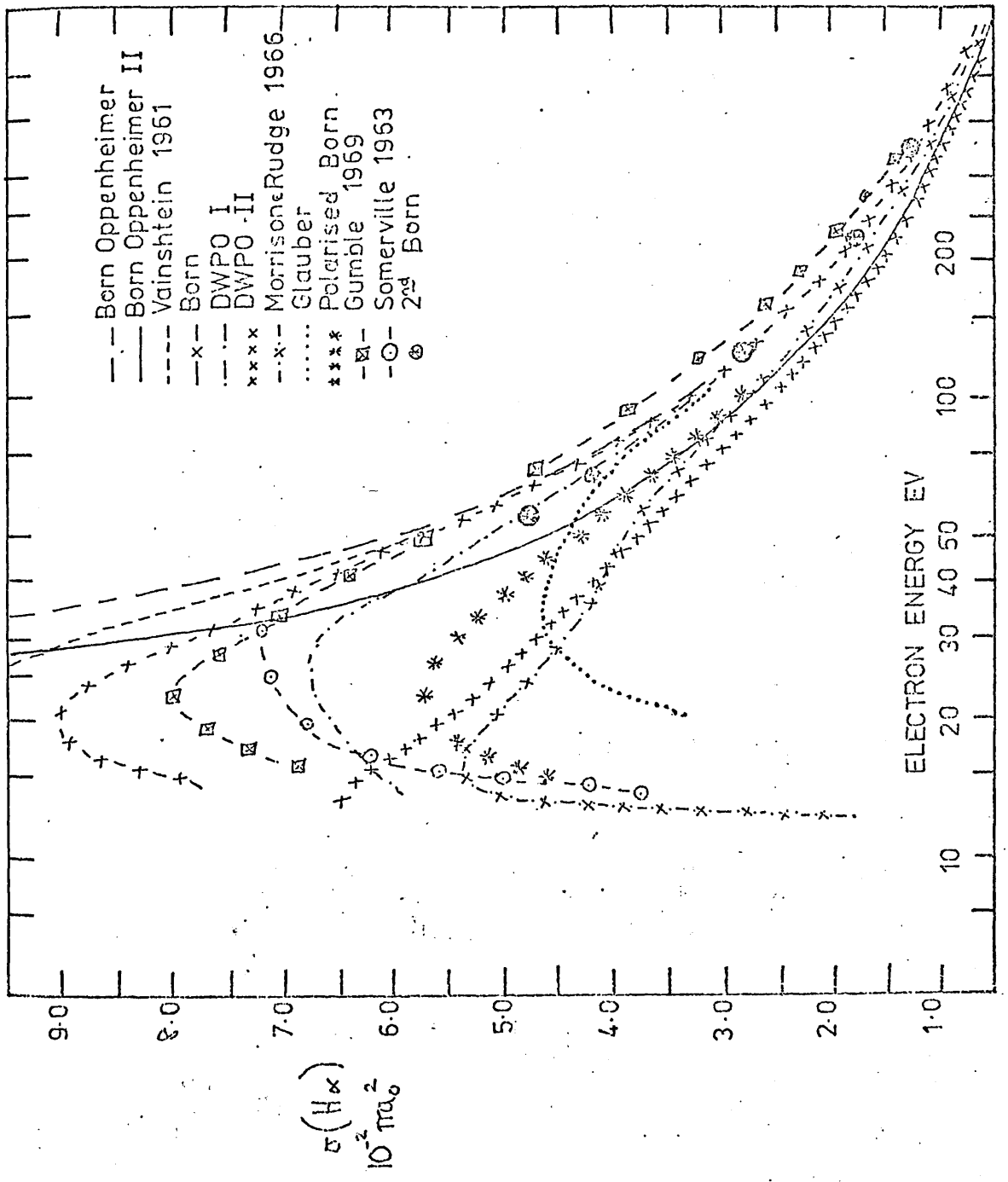

results of Baye and Heenen (1974) are not shown since they are very close to the Born results.

The DWPO I and II results together with the Glauber values are compared with the available experimental data in figure F4.7b. The only absolute experiment is that of Walker and St.John (1974). These results are uncorrected for cascade or for optical polarization. Both these corrections are energy dependent and would reduce the quoted values at energies below 200eV. The other experiments (Kleinpoppen et al. 1962, Kleinpoppen and Kraiss 1968, and Mahan (1974) are all relative measurements and were originally normalised to the first Born Hα cross section at either 200eV or 500eV. We have renormalised them to our DWPO II result at 500eV which lies about 8% below the Born value. With this renormalization, the most recent results (Mahan 1974, Mahan et al. 1976) remain in excellent agreement with our calculated DWPO II results at all energies above 20eV. This fact would suggest that Mahan's 3p results may be 20% too low below 150eV and his 3d values may be 50% too high over this energy range in order that the individual cross sections might agree with our 3p and 3d results and taking the total cross section to be accurate.

The earlier measurements of Kleinpoppen and colleagues (Kleinpoppen et al. 1962, and Kleinpoppen and Kraiss 1968) remain in good agreement with our DWPO II results above 80eV but appear energy independent below this point. These measurements carry large errors (which may be as much as ± 25%)but the general trend is nonetheless imcompatible with that found by Mahan et al., by Walker and St.John or with our theoretical results.

The polarization correction to be applied to Walker and St.John's data arises from the relation (see Chapter 5 below) between the total Hα cross section, $\sigma(H\alpha)$, and that total cross section, $\sigma_{90}(H\alpha)$, which would be measured at 90° and given by:

$$\sigma(H\alpha) = \sigma_{90}(H\alpha)\left[1 - \frac{1}{3} P_{90}(H\alpha)\right]$$

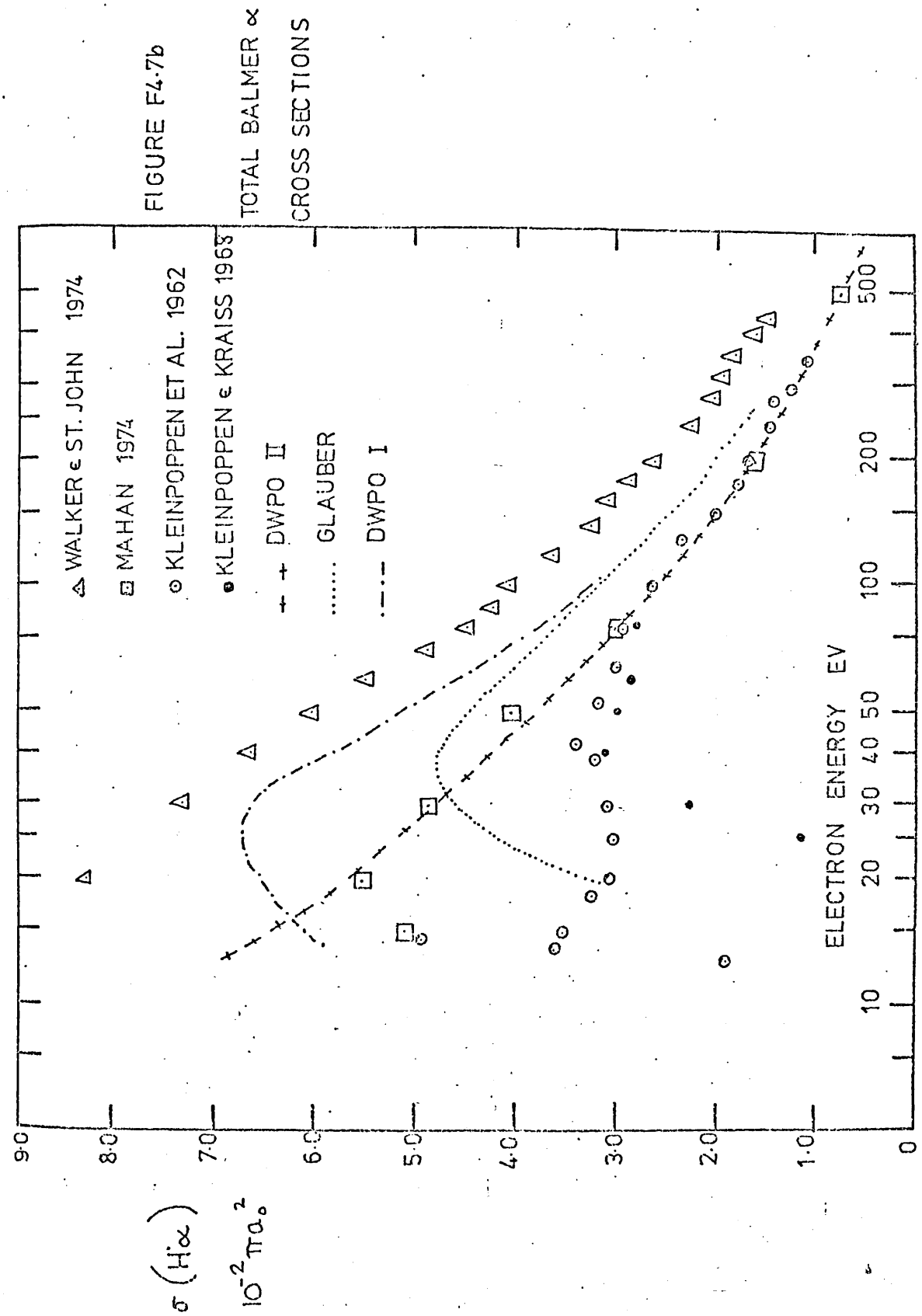
FIGURE F4.7b
TOTAL BALMER α CROSS SECTIONS
△ WALKER & ST. JOHN 1974
⊡ MAHAN 1974
⊙ KLEINPOPPEN ET AL. 1962
● KLEINPOPPEN & KRAISS 1968
+ + DWPO II
..... GLAUBER
-.-.- DWPO I
σ (Hα)
10⁻² πa₀²
ELECTRON ENERGY EV
0
1·0
2·0
3·0
4·0
5·0
6·0
7·0
8·0
9·0
10
20
30
40
50
100
200
500

where $P_{90}(H\alpha)$ is the polarization fraction of $H\alpha$ photons observed at 90° to the incident electron beam. This correction, as will be seen below (chapter 5), is quite small at all energies so that the difference between our results (or Mahan's) and those of Walker and St.John must be attempted to be attributed to cascade effects. But this difference is nearly 50% of our $H\alpha$ cross section at 20eV and increases to about 80% at 500eV. Mahan (1974) attempted a direct experimental determination of the percentage cascade correction to $\sigma(H\alpha)$ as a function of energy by using the different frequency response to the applied r.f. field of states with $n \geq 4$. He found that this percentage correction increased from 4.4% at 15eV to 9.3% at 500eV and thus, if these results are confirmed there remains a serious discrepancy between our results, those of Mahan (however normalised) and those of Walker and St.John.

§4.4 Discussion of the Total 3ℓ, $n = 3$ and $H\alpha$ cross sections.

It is important to note that the most significantly different (from other reported results) contribution to the $H\alpha$ cross section has been the $1s - 3d$ excitation cross section which appears to be too low, particularly at higher energies. It is to be expected that including the coupling to other adjacent levels via the R-matrix unitarization technique of Seaton (1961) (see also Somerville, 1963) would improve this cross section by allowing for cross-population between states. Moreover, as has been explicitly pointed out by Vainshtein and Presnyakov (1969), intermediate states such as the $2p$ state have an important contribution in optically forbidden transitions such as is the case with the $1s - 3d$ excitation.

However, recently an important criticism (Walters, 1976) has been made of the DWPO model as it stands. In particular in this work we have used a simple static polarization potential which is adiabatic in nature. Walters has shown that full account of non-adiabatic effects should be included especially at higher energies. Walters' work dealt specifically with elastic electron-lithium cross sections but the same basic arguement used there applies

equally well to this work: viz the assumpton that the cross section is dominated by the long range interaction of the incident electron with the target atom and that this is best represented by a simple adiabatic polarization potential breaks down at higher energies when non-adiabatic effects are important. Moreover, with Lithium, Walters showed that including non-adiabatic effects leads to an underestimate of the elastic cross section (while the adiabatic potential overestimated the cross section) so that at higher energies the long range interaction no longer can be assumed to dominate and so shorter effects (such as cross population between states) then play an increasingly important role.

With this parallel in mind it is useful to reconsider the results here. For the 3s state, the DWPO results tend to the Born by 200eV and are in excellent agreement with experiment for lower energies. Thus we feel that the dominant effect has been shown to be the long range dipole interaction between the impact electron and the target atom. For the 3p state, the DWPO II results lie about 8% below the Born value at 500eV and this would indicate that at high energies (above 200eV say) shorter range effects should be included. At lower energies (20 - 150eV) when the experimental results are normalized to the Born at 500eV, our DWPO II model is in good general agreement with the experimental results. When the 3d results are considered, there is very wide disagreement at high energies between the DWPO II model and models which ignore core polarization and it is only at low energies ($\leq$ 30eV) that the experimental points (normalized to the Born at 500eV) agree with our results. The high energy effect, as was pointed out earlier, does not disappear when non-adiabatic effects are included. Thus we are forced to conclude that other shorter range effects (such as coupling to other open channels) must be included for this case. Although a re-calculation of the 1s - 3d cross section would not have a major effect on the total n = 3 excitation cross section due to the dominance of the 1s - 3p cross -section, the situation with regard to the Hα cross section, would be altered dramatically and might be expected to go

some way to bringing our results more in line with those of Walker and St.John.

§4.5 Differential Cross Sections

The differential cross sections for the individual and summed 1s - 3ℓ transitions calculated using the formulation of Chapter two are presented next. The individual and summed results in the DWPO II model at 100 and 200eV are shown in figures 4.8a, b; 4.9a, b. These energies were chosen for illustration purposes since some Glauber results at low angles are available for comparison. At small angles ($\leq 45^{o}$) the 3p transition dominates but above 45^{o} the 3s contribution also becomes significant. Glauber 3p cross sections for $\theta \leq 50^{o}$ have been given by Tai et al. (1970) at 100eV and are very close to our results in the forward direction although they lie rather higher at intermediate angles. The Glauber 3s differential cross section at 100eV given by Tai et al. (1970) is always close to our 3s result but lies lower than our values in the near forward direction ($\theta < 10^{o}$) but are higher beyond this direction. The 3d Glauber results, given by Bhadra and Ghosh (1971), are shown in both F4.8b and F4.9b for $\theta \leq 45^{o}$ and for 100 and 200eV. In the forward direction their results lie a factor of two higher than our DWPO II results but the relative difference decreases for intermediate angles for both energies.

The DWPO II results for the complete angular range are shown in figure F4.8a and F4.9a. Our 3d results show some numerical instability for $\theta > 120^{o}$. At large angles our calculated cross sections are many orders of magnitude greater than the first Born results. By comparing the predictions of the DWPO model for the 2p state (McDowell et al., 1975b) with the experimental resultsof Williams and Willis (1975) it is possible to see that failure to allow for final channel distortion leads to an underestimate of $\frac{d\sigma}{d\Omega}$ (n = 2) in the backward direction by about a factor of two. This is confirmed by further comparison of our DWPO results with experiment for $e + He(1^1S) \rightarrow e + He(n^1S)$; n = 2, 3 (Scott and McDowell, 1975). Thus we

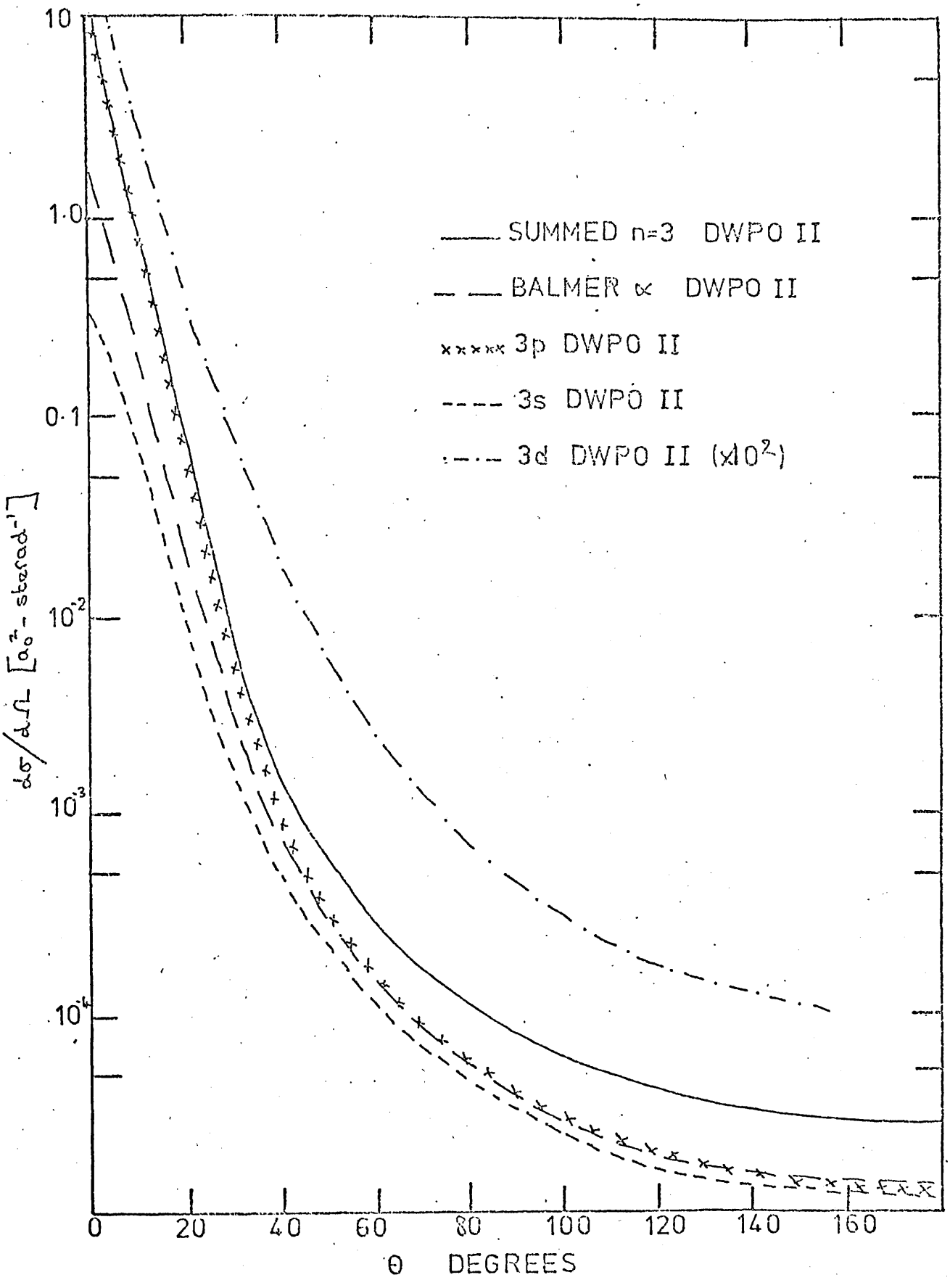

FIGURE F4·8a

DIFFERENTIAL CROSS SECTIONS (100EV)

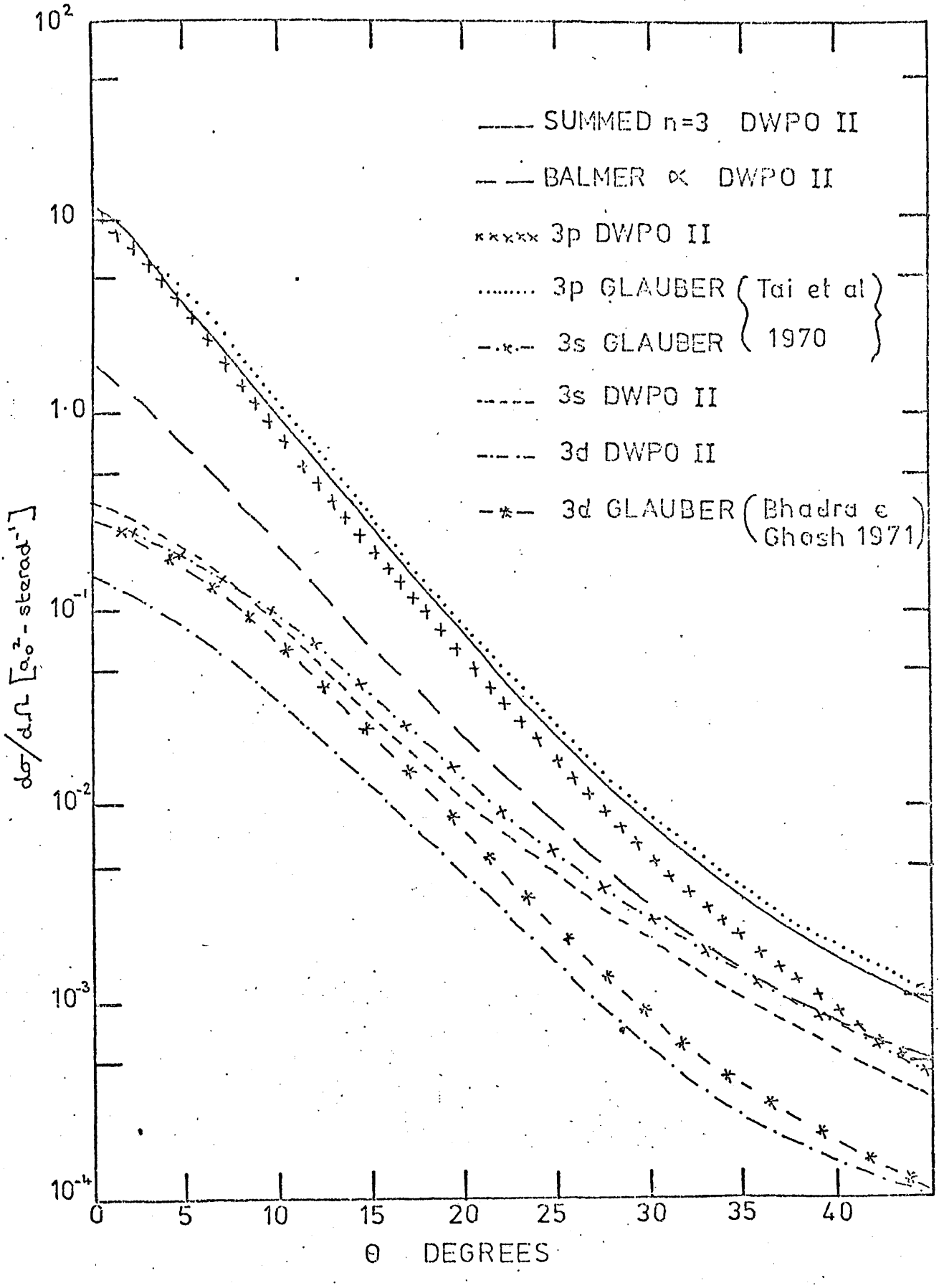

FIGURE F4·8b

DIFFERENTIAL CROSS SECTIONS (100EV)

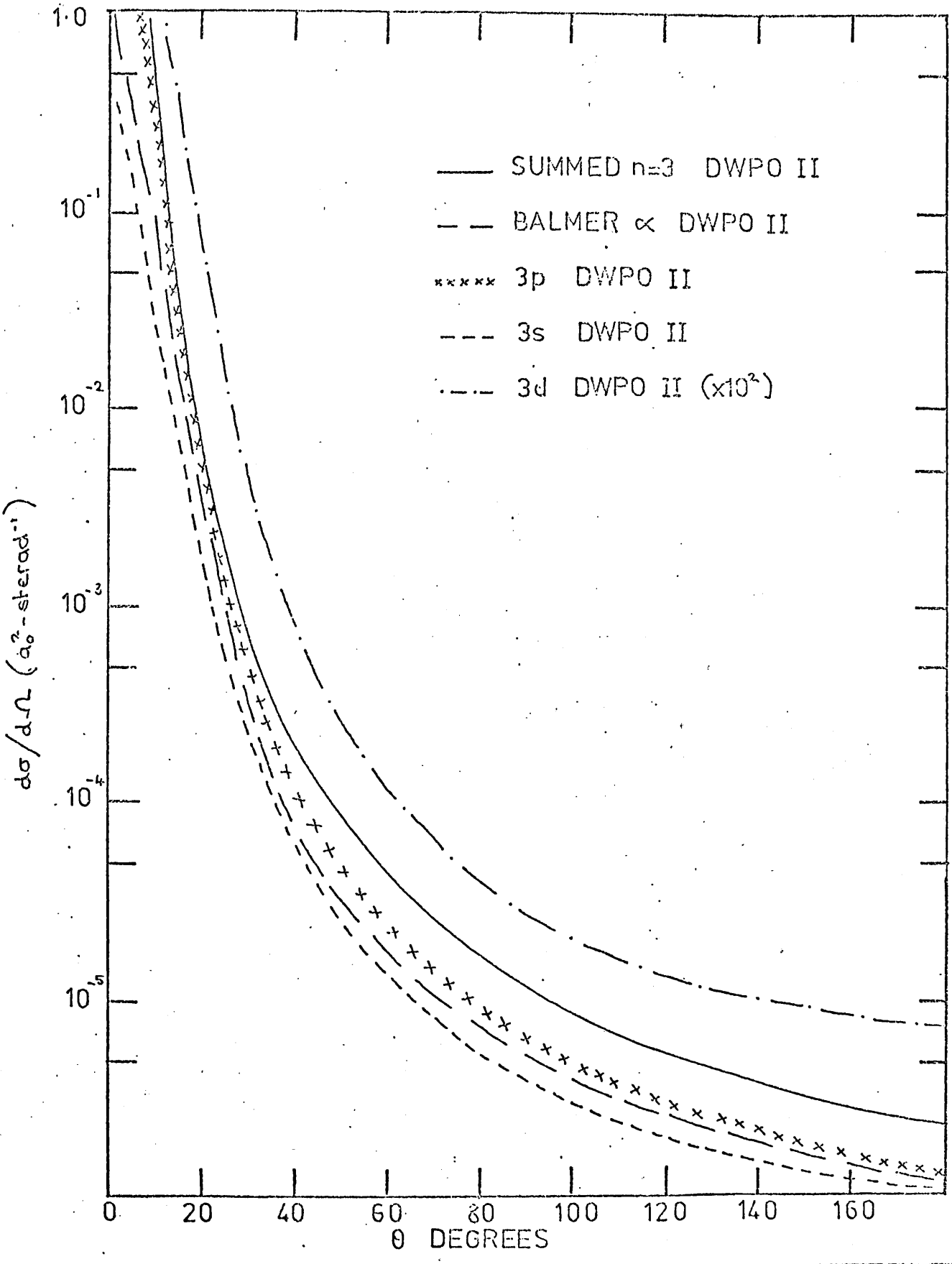

FIGURE F4.9a

DIFFERENTIAL CROSS SECTIONS (200 EV)

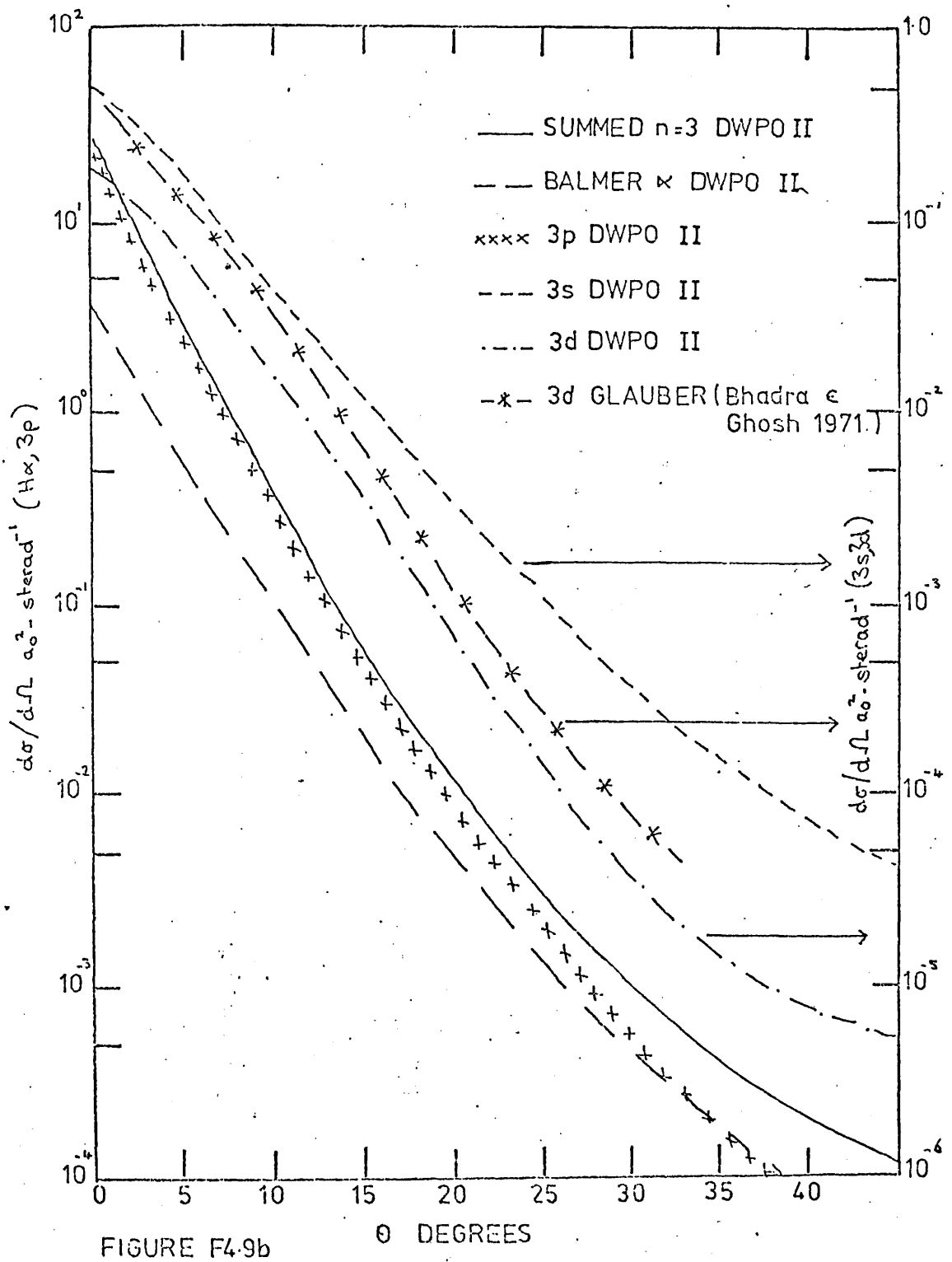

FIGURE F4·9b

DIFFERENTIAL CROSS SECTIONS (200 EV)

N.B. SCALES FOR 3s, 3d CROSS SECTIONS ON R.H.S.

conclude that our current differential cross sections are superior to previously published values for 1s - 3ℓ transitions but that they may well be substantially too low at larger angles and we would expect them to be susceptible to improvement using a unitarization procedure to couple the n = 3 states.

Tables giving the individual total n = 3, and Hα differential cross sections for a range of energies are included below for future reference (tables T4.4a-f DWPO II approximation and T4.5a-f DWPO I approximation). In particular, the $3\ell m_\ell$ differential cross sections are tabulated for reference purposes when the calculations are made of the alignment and orientation parameters discussed in chapter 6 below.

§4.6 Summary

We have presented our calculated total and differential cross sections and compared them where possible with other theoretical and experimental work. Initially (Syms et al. (1975)) our reaction to the disagreement between our total 3ℓ results and the experimental measurements while the total Hα results remained in quite good agreement was ascribed to problems of the experimental procedures. In the light of Walters' work (1976) we now feel that the DWPO model is inconsistent at high energies where an energy dependent perturbation potential should be used and because of the problem of cross-population between states - particularly with regard to the 1s - 3d excitation. Thus we believe that the experimental work is more likely to be correct.

We still believe that the differential cross sections presented here are an improvement on previous work but feel that they would be subject to improvement via a unitarization technique.

The results here all emphasise the need for further experimental and theoretical study.

T4.4a Differential Cross Sections (DWPO II Approximation) 20 eV

θ°	$d\sigma_{3s}/d\Omega$	$d\sigma_{3po}/d\Omega$	$d\sigma_{3p1}/d\Omega$	$d\sigma_{3p}/d\Omega$	$d\sigma_{3do}/d\Omega$	$d\sigma_{3d1}/d\Omega$	$d\sigma_{3d2}/d\Omega$	$d\sigma_{3d}/d\Omega$	$d\sigma_{(H\alpha)}/d\Omega$	$d\sigma(n=3)/d\Omega$
0	.3019,-1	.4623	0	.4623	.2983,-1	0	0	.2983,-1	.1146	.5223
15	.1769,-1	.2456	.2670,-1	.2990	.1703,-1	.4317,-2	.2145,-3	.2609,-1	.7906,-1	.3428
30	.3830,-2	.7764,-1	.2121,-1	.1201	.1084,-1	.5674,-2	.5388,-3	.2327,-1	.4127,-1	.1472
45	.1362,-2	.3240,-1	.8639,-2	.4967,-1	.8993,-2	.5544,-2	.3046,-3	.2069,-1	.2791,-1	.7172,-1
60	.2653,-2	.1565,-1	.3590,-2	.2283,-1	.5012,-2	.4896,-2	.1151,-3	.1503,-1	.2038,-1	.4051,-1
90	.3118,-2	.2138,-2	.7976,-3	.3733,-2	.1072,-4	.1909,-2	.3503,-4	.3900,-2	.7458,-2	.1075,-1
120	.3267,-2	.4413,-2	.2903,-3	.4993,-2	.1199,-2	.1416,-3	.2572,-4	.1534,-2	.5390,-2	.9794,-2
150	.4478,-2	.1119,-1	.1064,-3	.1140,-1	.7677,-3	.5375,-4	.1004,-4	.8952,-3	.6718,-2	.1677,-1
180	.5140,-2	.1433,-1	0	.1433,-1	.6072,-3	0	0	.6072,-3	.7438,-2	.2008,-1

T4.4b Differential Cross Sections (DWPO II Approximation) 30 eV

θ^{o}	$d\sigma_{3s}/d\Omega$	$d\sigma_{3po}/d\Omega$	$d\sigma_{3p1}/d\Omega$	$d\sigma_{3p}/d\Omega$	$d\sigma_{3do}/d\Omega$	$d\sigma_{3d1}/d\Omega$	$d\sigma_{3d2}/d\Omega$	$d\sigma_{3d}/d\Omega$	$d\sigma(H\alpha)/d\Omega$	$d\sigma(n=3)/d\Omega$
0	.1056	.1596,+1	0	.1596,+1	.6861,-1	0	0	.6861,-1	.3625	.1770,+1
15	.4568,-1	.3435	.1170	.5775	.8579,-2	.8931,-2	.2072,-2	.3059,-1	.1444	.6538
30	.8234,-2	.4987,-1	.3022,-1	.1103	.2809,-2	.3391,-2	.1572,-2	.1273,-1	.3398,-1	.1313
45	.3483,-2	.1640,-1	.5797,-2	.2800,-1	.3179,-2	.2238,-2	.3554,-3	.8365,-2	.1515,-1	.3984,-1
60	.2872,-2	.7185,-2	.1507,-2	.1020,-1	.1909,-2	.1685,-2	.6125,-4	.5401,-2	.9476,-2	.1847,-1
90	.1166,-2	.9194,-3	.1952,-3	.1310,-2	.1468,-4	.4118,-3	.8458,-5	.6551,-3	.2175,-2	.3331,-2
120	.8055,-3	.6968,-3	.9646,-4	.8897,-3	.1925,-3	.6718,-5	.1050,-4	.2270,-3	.1137,-2	.1921,-2
150	.1108,-2	.1768,-2	.4068,-4	.1849,-2	.6310,-4	.8769,-4	.1016,-4	.2588,-3	.1585,-2	.3216,-2
180	.1276,-2	.2293,-2	0	.2293,-2	.1979,-3	0	0	.1979,-3	.1744,-2	.3625,-2

T4.4c Differential Cross Sections (DWPO II Approximation) 50 eV

θ°	$d\sigma_{3s}/d\Omega$	$d\sigma_{3po}/d\Omega$	$d\sigma_{3pl}/d\Omega$	$d\sigma_{3p}/d\Omega$	$d\sigma_{3do}/d\Omega$	$d\sigma_{3dl}/d\Omega$	$d\sigma_{3d2}/d\Omega$	$d\sigma_{3d}/d\Omega$	$d\sigma(H\alpha)/d\Omega$	$d\sigma(n=3)/d\Omega$
0	.2207	.4271,+1	0	.4271,+1	.1098	0	0	.1098	.8345	.4602,+1
15	.5276,-1	.1878	.1770	.5418	.3647,-3	.8043,-2	.5372,-2	.2719,-1	.1439	.6218
30	.6591,-2	.1505,-1	.1464,-1	.4434,-1	.6236,-3	.1482,-2	.9721,-2	.5533,-2	.1736,-1	.5646,-1
45	.2104,-2	.3333,-2	.1231,-2	.5795,-2	.3609,-2	.6982,-3	.6168,-4	.1881,-2	.4669,-2	.9780,-2
60	.1017,-2	.1076,-2	.2351,-3	.1546,-2	.4963,-4	.2690,-3	.1298,-4	.6136,-3	.1813,-2	.3177,-2
90	.2658,-3	.1050,-3	.6988,-4	.2447,-3	.1154,-4	.3456,-6	.1306,-5	.1485,-4	.3095,-3	.5254,-3
120	.1526,-3	.6374,-4	.3782,-4	.1394,-3	.2846,-4	.1561,-5	.3633,-6	.3231,-4	.2014,-3	.3243,-3
150	.1603,-3	.1418,-3	.1112,-4	.1641,-3	.9749,-5	.1655,-4	.5727,-5	.5430,-4	.2339,-3	.3787,-3
180	.1697,-3	.1771,-3	0	.1771,-3	.5564,-4	0	0	.5564,-4	.2462,-3	.4025,-3

T4.4d Differential Cross Sections (DWPO II Approximation) 100 eV

θ^{o}	$d\sigma_{3s}/d\Omega$	$d\sigma_{3po}/d\Omega$	$d\sigma_{3p1}/d\Omega$	$d\sigma_{3p}/d\Omega$	$d\sigma_{3do}/d\Omega$	$d\sigma_{3d1}/d\Omega$	$d\sigma_{3d2}/d\Omega$	$d\sigma_{3d}/d\Omega$	$d\sigma(H\alpha)/d\Omega$	$d\sigma(n=3)/d\Omega$
0	.3647	.1092,+2	0	.1092,+2	.1554	0	0	.1554	.1809,+1	.1144,+2
15	.2931,-1	.3932,-1	.9156,-1	.2224	.6906,-3	.1755,-2	.4398,-2	.1300,-1	.6855,-1	.2647
30	.2133,-2	.2319,-2	.1841,-2	.6001,-2	.3575,-4	.1365,-3	.1595,-3	.6277,-3	.3469,-2	.8762,-2
45	.3400,-3	.3689,-3	.4551,-4	.4599,-3	.1146,-4	.4605,-4	.2705,-5	.1090,-3	.5033,-3	.9089,-3
60	.1150,-3	.8925,-4	.2933,-4	.1479,-3	.8821,-6	.1141,-4	.7768,-6	.2526,-4	.1577,-3	.2882,-3
90	.3302,-4	.4329,-5	.1802,-4	.4037,-4	.1273,-5	.7457,-7	.4635,-6	.2349,-5	.4211,-4	.7772,-4
120	.1713,-4	.5265,-5	.7316,-5	.1990,-4	.3090,-5	.3556,-6	.4311,-7	.3887,-5	.2336,-4	.4082,-4
150	.1270,-4	.1092,-4	.1734,-5	.1439,-4	.1310,-5	.1022,-5	.8600,-6	.5074,-5	.1947,-4	.3216,-4
180	.1189,-4	.1352,-4	0	.1352,-4	.1290,-5	0	0	.1290,-5	.1871,-4	.2861,-4

T4.4e Differential Cross Sections (DWPO II Approximation) 150 eV

θ°	$d\sigma_{3s}/d\Omega$	$d\sigma_{3po}/d\Omega$	$d\sigma_{3pl}/d\Omega$	$d\sigma_{3p}/d\Omega$	$d\sigma_{3do}/d\Omega$	$d\sigma_{3dl}/d\Omega$	$d\sigma_{3d2}/d\Omega$	$d\sigma_{3d}/d\Omega$	$d\sigma(H\alpha)/d\Omega$	$d\sigma(n=3)/d\Omega$
0	.4379	.1774,+2	0	.1774,+2	.1733	0	0	.1733	.2705,+1	.1835,+2
15	.1677,-1	.1386,-1	.4352,-1	.1009	.6531,-3	.5855,-3	.2369,-2	.6563,-2	.3523,-1	.1272
30	.8302,-3	.7487,-3	.3220,-3	.1393,-2	.6065,-5	.3755,-4	.2281,-4	.1268,-3	.1121,-2	.2350,-2
45	.9897,-4	.1123,-3	.9710,-5	.1317,-3	.3381,-6	.8230,-5	.7410,-6	.1833,-4	.1328,-3	.2490,-3
60	.3402,-4	.2489,-4	.1238,-4	.4964,-4	.7223,-6	.7362,-6	.1624,-6	.2520,-5	.4240,-4	.8618,-4
90	.1021,-4	.7066,-6	.6958,-5	.1462,-4	.7356,-6	.7078,-8	.6393,-7	.8776,-6	.1281,-4	.2571,-4
120	.4903,-5	.1377,-5	.2623,-5	.6623,-5	.1277,-6	.3786,-6	.1694,-6	.5422,-6	.6627,-5	.1207,-4
150	.3343,-5	.3380,-5	.5018,-6	.4384,-5	.2488,-7	.2588,-6	.1955,-6	.9335,-6	.4854,-5	.8720,-5
180	.3246,-5	.4817,-5	0	.4817,-5	.3332,-7	0	0	.3332,-7	.3848,-5	.8096,-5

T4.4f Differential Cross Sections (DWPO II Approximation) 200 eV

θ°	$d\sigma_{3s}/d\Omega$	$d\sigma_{3po}/d\Omega$	$d\sigma_{3pl}/d\Omega$	$d\sigma_{3p}/d\Omega$	$d\sigma_{3do}/d\Omega$	$d\sigma_{3dl}/d\Omega$	$d\sigma_{3d\ell}/d\Omega$	$d\sigma_{3d}/d\Omega$	$d\sigma(H\alpha)/d\Omega$	$d\sigma(N=3)/d\Omega$
0	.4831	.2410,+2	0	.2410,+2	.1842	0	0	.1842	.3511,+1	.2477,+2
15	.1062,-1	.6438,-2	.2236,-1	.5115,-1	.4082,-3	.2122,-3	.1310,-2	.3452,-2	.2011,-1	.6518,+1
30	.3786,-3	.3382,-3	.7113,-4	.4804,-3	.1002,-5	.9060,-5	.7003,-5	.3313,-4	.4683,-3	.8921,-3
45	.4241,-4	.5018,-4	.6465,-5	.6311,-4	.1964,-4	.2555,-5	.1628,-6	.5632,-5	.5549,-4	.1112,-3
60	.1504,-4	.9813,-5	.6844,-5	.2350,-4	.5241,-7	.4080,-6	.5701,-7	.9825,-6	.1880,-4	.3952,-4
90	.4494,-5	.2456,-6	.3298,-5	.6841,-5	.5289,-7	.1144,-8	.9230,-7	.2398,-6	.5541,-5	.1157,-4
120	.2009,-5	.7612,-6	.1065,-5	.2891,-5	.1573,-6	.4296,-7	.5657,-8	.2546,-6	.2608,-5	.5154,-5
150	.1384,-5	.1420,-5	.3336,-6	.2087,-5	.1382,-6	.2497,-7	.6275,-7	.3137,-6	.1944,-5	.3784,-5
180	.1444,-5	.1176,-5	0	.1176,-5	.2806,-7	0	0	.2806,-7	.1611,-5	.2648,-5

T4.5a Differential Cross Sections (DWPO I Approximation) 20 eV

θ^{o}	$d\sigma_{3s}/d\Omega$	$d\sigma_{3po}/d\Omega$	$d\sigma_{3pl}/d\Omega$	$d\sigma_{3p}/d\Omega$	$d\sigma_{3do}/d\Omega$	$d\sigma_{3dl}/d\Omega$	$d\sigma_{3d2}/d\Omega$	$d\sigma_{3d}/d\Omega$	$d\sigma(H\alpha)/d\Omega$	$d\sigma(n=3)/d\Omega$
0	.2119,-1	.5658	0	.5658	.6680,-1	0	0	.6680,-1	.1548	.6538
15	.1656,-1	.3098	.329,-1	.3755	.3196,-1	.1095,-1	.5154,-3	.5488,-1	.1157	.4469
30	.7548,-2	.9757,-1	.2750,-1	.1526	.1097,-1	.1236,-1	.1288,-2	.3828,-1	.6383,-1	.1984
45	.2100,-2	.3605,-1	.1096,-1	.5797,-1	.7584,-2	.9095,-2	.6724,-3	.2712,-1	.3606,-1	.8719,-1
60	.1358,-2	.1573,-1	.4080,-2	.2389,-1	.4332,-2	.6551,-2	.2001,-3	.1783,-1	.2201,-1	.4308,-1
90	.2781,-2	.1990,-2	.7637,-3	.3517,-2	.1475,-4	.2166,-2	.3326,-4	.4414,-2	.7610,-2	.1071,-1
120	.3610,-2	.440,-2	.2626,-3	.4925,-2	.1164,-2	.1540,-3	.2300,-4	.1518,-2	.5709,-2	.1005,-1
150	.4719,-2	.1139,-1	.9990,-4	.1159,-1	.7335,-3	.5568,-4	.9644,-5	.8641,-3	.6951,-2	.1717,-1
180	.5281,-2	.1467,-1	0	.1467,-1	.5758,-3	0	0	.5758,-3	.7588,-2	.2053,-1

T4.5b Differential Cross Sections (DWPO I Approximation) 30 eV

θ^{o}	$d\sigma_{3d}/d\Omega$	$d\sigma_{3po}/d\Omega$	$d\sigma_{3pl}/d\Omega$	$d\sigma_{3p}/d\Omega$	$d\sigma_{3do}/d\Omega$	$d\sigma_{3dl}/d\Omega$	$d\sigma_{3d2}/d\Omega$	$d\sigma_{3d}/d\Omega$	$d\sigma(H\alpha)/d\Omega$	$d\sigma(n=3)/d\Omega$
0	.5485,-1	.1818,+1	0	.1818,+1	.1469	0	0	.1469	.4163	.2020,+1
15	.4166,-1	.4253	.1414	.7081	.1885,-1	.2696,-1	.4915,-2	.7860,-1	.2038	.8284
30	.1772,-1	.6357,-1	.3992,-1	.1434	.2477,-2	.8670,-2	.3557,-2	.2693,-1	.6157,-1	.1881
45	.5562,-2	.1799,-1	.7221,-2	.3243,-1	.2779,-2	.3681,-2	.6939,-3	.1153,-1	.2092,-1	.4952,-1
60	.2711,-2	.7337,-2	.1656,-2	.1065,-1	.1777,-2	.2166,-2	.9245,-4	.6294,-2	.1026,-1	.1966,-1
90	.1433,-2	.9827,-3	.2393,-3	.1461,-2	.1016,-4	.4529,-3	.9383,-5	.9347,-3	.2540,-2	.3829,-2
120	.1135,-2	.7516,-3	.1221,-3	.9958,-3	.1795,-3	.8701,-5	.9205,-5	.2153,-3	.1468,-2	.2346,-2
150	.1359,-2	.1883,-2	.4887,-4	.1981,-2	.6041,-4	.9342,-4	.9810,-5	.2669,-3	.1850,-2	.3607,-2
180	.1499,-2	.2447,-2	0	.2447,-2	.1918,-3	0	0	.1918,-3	.1980,-2	.4138,-2

T4.5c Differential Cross Sections (DWPO I Approximation) 50 eV

θ°	$d\sigma_{3s}/d\Omega$	$d\sigma_{3po}/d\Omega$	$d\sigma_{3pl}/d\Omega$	$d\sigma_{3p}/d\Omega$	$d\sigma_{3do}/d\Omega$	$d\sigma_{3dl}/d\Omega$	$d\sigma_{3d2}/d\Omega$	$d\sigma_{3d}/d\Omega$	$d\sigma(H\alpha)/d\Omega$	$d\sigma(n=3)/d\Omega$
0	.8837,-1	.4610,+1	0	.4610,+1	.2044	0	0	.2044	.8368	.4903,+1
15	.5853,-1	.2363	.2185	.6733	.4593,-3	.2246,-1	.1332,-1	.7201,-1	.2100	.8038
30	.1570,-1	.1957,-1	.1954,-1	.5865,-1	.6080,-3	.3108,-2	.2066,-2	.1096,-1	.3358,-1	.8531,-1
45	.3074,-2	.3798,-2	.1414,-2	.6625,-2	.3124,-3	.9676,-3	.1018,-3	.2451,-2	.6307,-2	.1215,-1
60	.1128,-2	.1176,-2	.2599,-3	.1695,-2	.4554,-4	.3357,-3	.1312,-4	.7433,-3	.2071,-2	.3566,-2
90	.3872,-3	.1214,-3	.9478,-4	.3110,-3	.8034,-5	.5811,-6	.2960,-5	.1512,-4	.4390,-3	.7133,-3
120	.2332,-3	.7580,-4	.4979,-4	.1754,-3	.3105,-4	.2694,-5	.9379,-6	.3831,-4	.2922,-3	.4469,-3
150	.2199,-3	.1643,-3	.1427,-4	.1928,-3	.1101,-4	.1486,-4	.6167,-5	.5306,-4	.2957,-3	.4658,-3
180	.2234,-3	.2043,-3	0	.2043,-3	.6152,-4	0	0	.6152,-4	.3090,-3	.4892,-3

T4.5d Differential Cross Sections (DWPO I Approximation) 100 eV

θ°	$d\sigma_{3s}/d\Omega$	$d\sigma_{3po}/d\Omega$	$d\sigma_{3p1}/d\Omega$	$d\sigma_{3p}/d\Omega$	$d\sigma_{3do}/d\Omega$	$d\sigma_{3d1}/d\Omega$	$d\sigma_{3d2}/d\Omega$	$d\sigma_{3d}/d\Omega$	$d\sigma(H\alpha)/d\Omega$	$d\sigma(n=3)/d\Omega$
0	.1125	.1148,+2	0	.1148,+2	.2445	0	0	.2445	.1712,+1	.1184,+2
15	.4984,-1	.5146,-1	.1198	.2911	.1999,-2	.5137,-2	.1089,-1	.3405,-1	.1182	.3750
30	.4512,-2	.2891,-2	.2295,-2	.7482,-2	.3686,-4	.2324,-3	.2554,-3	.1012,-2	.6407,-2	.1301,-1
45	.4456,-3	.4351,-3	.4685,-4	.5288,-3	.7698,-5	.6106,-4	.3253,-5	.1363,-3	.6443,-3	.1111,-2
60	.1559,-3	.1055,-3	.3843,-4	.1824,-3	.9247,-6	.1568,-4	.8886,-6	.3405,-4	.2115,-3	.3724,-3
90	.4963,-4	.5112,-5	.2286,-4	.5084,-4	.8793,-6	.6808,-7	.9944,-6	.3004,-5	.5863,-4	.1035,-3
120	.2463,-4	.6463,-5	.9088,-5	.2464,-4	.3310,-5	.6036,-6	.1172,-6	.4752,-5	.3229,-4	.5402,-4
150	.1740,-4	.1341,-4	.2147,-5	.1771,-4	.1693,-5	.7948,-6	.9493,-6	.5181,-5	.2467,-4	.4029,-4
180	.1582,-4	.1678,-4	0	.1678,-4	.1952,-5	0	0	.1952,-5	.1975,-4	.3455,-4

T4.5e Differential Cross Sections (DWPO I Approximation) 150 eV

θ°	$d\sigma_{3d}/d\Omega$	$d\sigma_{3po}/d\Omega$	$d\sigma_{3pl}/d\Omega$	$d\sigma_{3p}/d\Omega$	$d\sigma_{3do}/d\Omega$	$d\sigma_{3dl}/d\Omega$	$d\sigma_{3d2}/d\Omega$	$d\sigma_{3d}/d\Omega$	$d\sigma(H\alpha)/d\Omega$	$d\sigma(n=3)/d\Omega$
0	.1200	.1818,+2	0	.1818,+2	.2525	0	0	.2525	.2518,+1	.1855,+2
15	.3495,-1	.1816,-1	.5765,-1	.1335	.1653,-2	.1551,-2	.5514,-2	.1578,-1	.6648,-1	.1842
30	.1419,-2	.9059,-3	.3618,-3	.1630,-2	.5568,-5	.5373,-4	.3125,-4	.1755,-3	.1787,-2	.3224,-2
45	.1273,-3	.1329,-3	.1250,-4	.1579,-3	.3264,-6	.1156,-4	.8028,-6	.2505,-4	.1710,-3	.3103,-3
60	.4920,-4	.2944,-4	.1610,-4	.6163,-4	.8509,-6	.1421,-5	.3672,-6	.4426,-5	.6090,-4	.1153,-3
90	.1469,-4	.8720,-6	.8588,-5	.1805,-4	.1012,-5	.7436,-8	.1766,-6	.1381,-5	.1820,-4	.3412,-4
120	.6789,-5	.1696,-5	.3189,-5	.8074,-5	.1059,-6	.3610,-7	.2581,-6	.6943,-6	.8436,-5	.1556,-4
150	.4480,-5	.4157,-5	.6166,-6	.5390,-5	.2507,-7	.3475,-6	.1798,-6	.1080,-5	.6196,-5	.1095,-4
180	.3927,-5	.5768,-5	0	.5768,-5	.1056,-6	0	0	.1056,-6	.4713,-5	.9801,-5

T4.5f Differential Cross Sections (DWPO I Approximation) 200eV

θ^{o}	$d\sigma_{3s}/d\Omega$	$d\sigma_{3po}/d\Omega$	$d\sigma_{3p1}/d\Omega$	$d\sigma_{3p}/d\Omega$	$d\sigma_{3do}/d\Omega$	$d\sigma_{3d1}/d\Omega$	$d\sigma_{3d2}/d\Omega$	$d\sigma_{3d}/d\Omega$	$d\sigma(H\alpha)/d\Omega$	$d\sigma(n=3)/d\Omega$
0	.1236	.2457,+2	0	.2457,+2	.2557	0	0	.2557	.3279,+1	.2495,+2
15	.2380,-1	.8305,-1	.2935,-1	.6701,-1	.9351,-3	.5259,-3	.2790,-2	.7568,-2	.3928,-1	.9838,-1
30	.5432,-3	.4026,-3	.7195,-4	.5465,-3	.2512,-5	.1337,-4	.7995,-5	.4524,-4	.6529,-3	.1135,-2
45	.5507,-4	.5969,-4	.8255,-5	.7620,-4	.1636,-6	.3816,-5	.2270,-6	.8250,-5	.7231,-4	.1395,-3
60	.2180,-4	.1150,-4	.8712,-5	.2892,-4	.7250,-7	.7299,-6	.1219,-6	.1776,-5	.2699,-4	.5250,-4
90	.6192,-5	.2872,-6	.4042,-5	.8371,-5	.4705,-7	.2598,-8	.1880,-6	.4282,-6	.7608,-5	.1542,-4
120	.2761,-5	.9206,-6	.1279,-5	.3478,-5	.1681,-6	.7475,-7	.1413,-7	.3458,-6	.3517,-5	.6585,-5
150	.1800,-5	.1754,-5	.4090,-6	.2572,-5	.1872,-6	.1726,-7	.7275,-7	.3672,-6	.2471,-5	.4739,-5
180	.1549,-5	.1696,-5	0	.1696,-5	.3205,-7	0	0	.3205,-7	.1781,-5	.3277,-5

CHAPTER 5

Polarization of Hα Line Radiation

5.1 Introduction

In general the dipole radiation emitted by an atom after excitation by an electron beam is polarized and has an anisotropic angular distribution. With an incident beam of electrons in an Oz direction, this radiation may be regarded as due to an electric dipole in the Oz direction and two equal electric dipoles in the Ox and Oy directions. Letting $I(\theta)$ be the intensity of radiation per unit solid angle in a direction making an angle θ with Oz, and letting I'' and $I^{\perp}$ be the intensities in a direction perpendicular with Oz with electric vectors parallel and perpendicular with Oz, then the polarization fraction at 90°, is defined:

$$P_{90} = \frac{I'' - I^{\perp}}{I'' + I^{\perp}} \tag{5.1}$$

Using the fact that the intensity of dipole radiation, making an angle χ with the dipole axis, is proportional to $\sin^2\chi$, one obtains:

$$I(\theta) = \bar{I} \times \left[\frac{3(1 - P_{90} \cos^2\theta)}{(3 - P_{90})} \right] \tag{5.2}$$

where the total intensity of radiation integrated over all angles is $4\pi\bar{I}$. Therefore, by either measuring I'' and $I^{\perp}$ or by obtaining the photon angular distribution $I(\theta)$, it is possible to determine P_{90}. Further, since $\bar{I} = I'' + 2I^{\perp}$, the percentage polarization can be expressed alternatively:

$$P_{90} = \frac{3I'' - \bar{I}}{I'' + \bar{I}} \tag{5.3}$$

The theory of polarization of impact radiation was first developed by Oppenheimer (1927 a,b, 1928) and further developments and applications were made by Penney (1932). Later, Percival and Seaton (1958) re-examined the problem and extended the analysis. Essentially, the approach is to calculate the probabilities of exciting individual quantum states with the probabilities

of emission of polarized photons in transitions from these states. Penney showed that not only are electron spin and fine structure important, but also it is necessary to consider nuclear spin and hyperfine structure.

Three atomic levels are distinguished: a, the initial level with quantum states α, (and for simplicity it is assumed that it has zero orbital angular momentum which means that the anisotropy of the problem is introduced solely through the motion of the incident electron); b, the upper level with quantum states β populated after collision and before photon emission; c, the final level with quantum states γ reached after photon emission. The cross-sections, $\sigma(\beta)$, for exciting quantum states of the upper level with definite orbital angular momentum component M_L, are calculated where the quantization axis is in the incident beam direction. If the upper level has well defined fine and possibly hyperfine structures then the upper states, β, must be described in a coupled spin-orbital angular momenta representation and the cross sections for excitation of these vector coupled states then expressed in terms of those for excitation of M_L states. The corresponding algebra for radiative transition probabilities is well known (see, for example, Condon and Shortley (1963)).

However Oppenheimer-Penney (O-P) theory, as described above, fails to give unambiguous results in the limit of small fine structure energy or, in the case of non-zero nuclear spin, in the limit of small hyperfine structure energy. That is to say that two different expressions for the polarization fraction can be obtained to describe the same process. These ambiguities arise through the assumption that the probabilities of exciting individual quantum states and the probabilities of emission of polarized photons in transitions from these states, can be calculated separately.

Percival and Seaton adopted the approach of considering the probabilities of photons of definite polarization being emitted by the entire system of atom and colliding electron and obtained an expression involving integrals over the line profiles.

Percival and Seaton theory (P-S) gives the O-P expressions with hyperfine structure (or fine structure) if there is negligible overlap between the profiles of the hyperfine (or fine) structure components and conversely the O-P expressions neglecting nuclear (and electron) spin are obtained if hyperfine (or fine) structure profiles overlap completely.

Thus, to use the O-P theory, it is necessary to decide whether fine or hyperfine structure effects are important: i.e. should the initial and intermediate states, α and β, be expressed

$$\left.\begin{aligned} \alpha &= \Delta'',S'L'M_L'M_S' \\ \beta &= \Delta,SLM_LM_S \end{aligned}\right\} \quad (5.4)$$

or as:

$$\left.\begin{aligned} \alpha &= \Delta',S'L'J'M_J' \\ \beta &= \Delta,SLJM_J \end{aligned}\right\} \quad (5.5)$$

or as:

$$\left.\begin{aligned} \alpha &= \Delta',S'L'J'I'F'M_F' \\ \beta &= \Delta,SLJIFM_F \end{aligned}\right\} \quad (5.6)$$

where Δ,Δ' are used to denote all non-angular momenta quantum numbers, I is the nuclear spin and F is the resultant of J and I.

The relevant criterion adopted by Percival and Seaton is to compare the fine structure separations, the hyperfine structure separations and the line widths (since the polarization in P-S theory directly depends on the ratio: $\varepsilon = 2\pi\nu_{\beta\beta o}/A$ of the separation $\nu_{\beta\beta o}$ of states β,β^o of the level b to the line width).

If the fine structure splitting is much smaller than the line width (i.e. $\varepsilon_{FS} << 1$) then the polarization fraction is derived using (5.4); if the converse holds while at the same time fine-structure energy is not large enough to cause breakdown of LS coupling, then α and β should be taken as described by (5.5) or (5.6) depending on whether $\varepsilon_{HFS} << 1$ or $\varepsilon_{HFS} >> 1$. As mentioned earlier, ambiguities can arise i.e. when ε_{FS} or

$\epsilon_{HFS} \simeq 1$; in such a case to obtain an accurate calculation of the polarization, the expressions to use are those derived by the exact theory of Percival and Seaton.

Percival and Seaton considered $^2P - {}^2S$ transitions and Lyman-α (Ly-α) radiation in particular. Here the hyperfine separations are smaller than the line width but are of the same order of magnitude. Thus they used their exact expressions to obtain the polarizations and found that with O-P theory, neglecting hyperfine structure (i.e. β given by (5.5)), expressions little different from the exact forms were obtained.

5.2 Polarization of radiation from the n = 3 states of Hydrogen

In this work we are interested in transitions from the n = 3 level of hydrogen and in Balmer-α (Hα) transitions in particular: i.e. decay from the n = 3 states to the n = 2 states when the light emitted has wavelength 6563 Å - important since this lies in the visible spectrum and occurs frequently in astrophysics as a strongly emitted line. The decay process of the n = 3 states is illustrated in figure (F5.1). The 3p state decays to either the 2s or 1s state with a probability about seven times greater that it will decay to the 1s state rather than the 2s state: i.e. about 88% of the light emitted from the 3p state is Lyman-β and about 12% is Hα radiation. Both the 3s and 3d states decay to the 2p state only and thus all the radiation from these transitions is Hα.

The polarization of Hα light will depend on the polarization of the light emitted from the separate levels and on the populations of these levels. Thus it is necessary to compare the level separations with the line widths as in table (T5.1). Note that parameters relevant to 3s are ignored since radiation from states with zero orbital angular momentum is unpolarized. Accurate values for all the n = 3 parameters are given in Appendix AVIII. As can be seen $\epsilon_{FS} >> 1$ so fine structure is important and $\epsilon_{HFS} \simeq 1$ for all the $3\ell_j$ states, therefore the exact theory of Percival and Seaton should

FIGURE F5·1 DECAY PATHS OF THE n = 3 LEVELS OF HYDROGEN

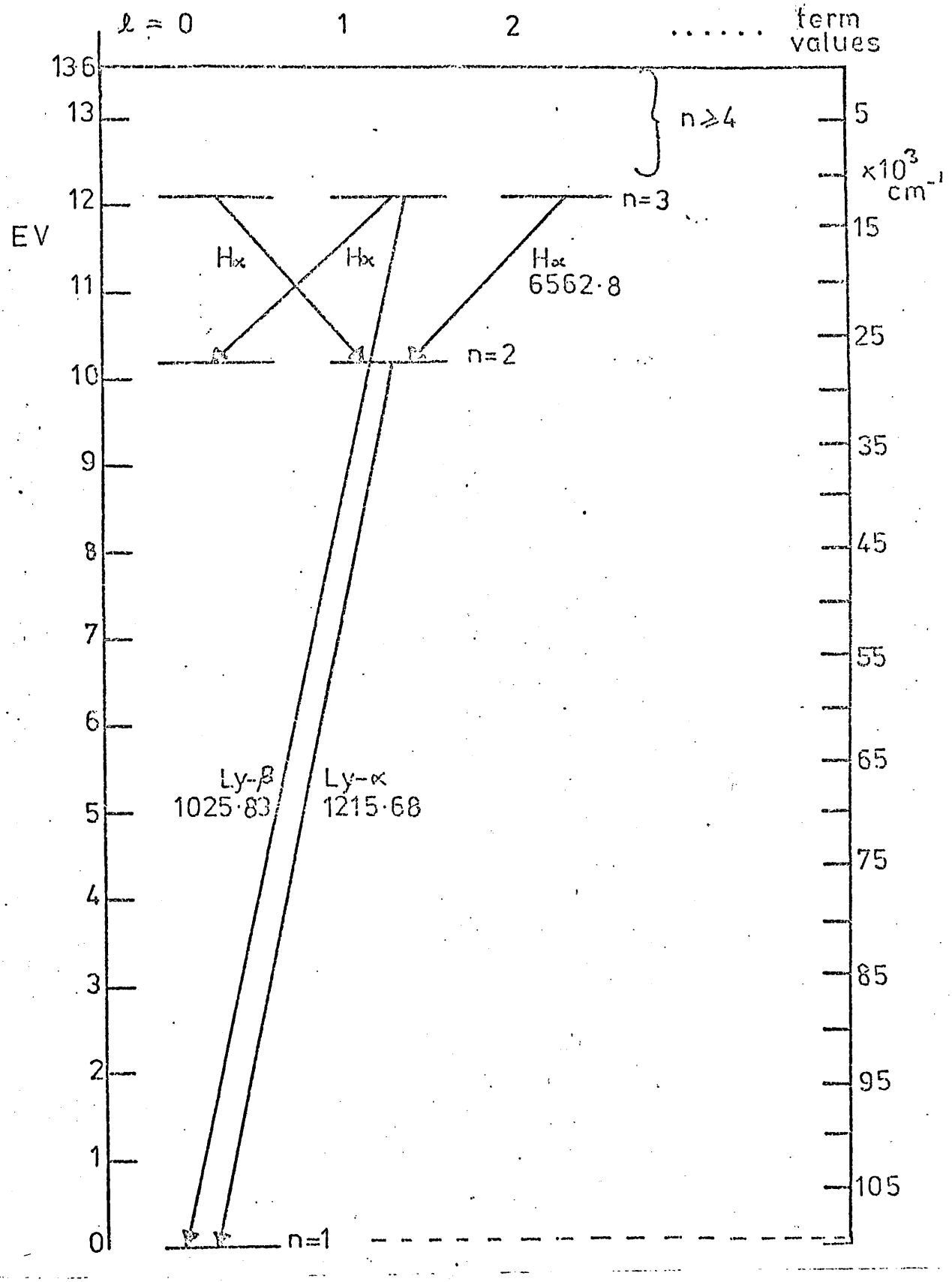

Table T5.1

Fine structure, line widths and hyperfine splittings for the 3p and 3d states of hydrogen

State 3ℓ	3p		3d	
Einstein A coeff for transition $3\ell \rightarrow 2\ell-1$ (1)	2.245,7 sec^{-1}		6.467,7 sec^{-1}	
Line width = $A/2\pi c$	1.192,-4 cm^{-1}		3.434,-4 cm^{-1}	
Fine structure splitting $\Delta\nu_{3\ell}$ (2)	.1084 cm^{-1}		.0361 cm^{-1}.	
$\varepsilon_{3\ell} = 2\pi c\Delta\nu_{3\ell}/A$	9.09,2		1.05,2	
State $3\ell j$:	$3p_{\frac{1}{2}}$	$3p_{3/2}$	$3d_{3/2}$	$3d_{5/2}$
Hyperfine splitting $\Delta\nu_{3\ell j}$ (3)	5.816,-4cm^{-1}	2.326,-4cm^{-1}	1.396,-4cm^{-1}	.8973,-4cm^{-1}
$\varepsilon_{3\ell j} = 2\pi c\Delta\nu_{3\ell j}/A$	4.88	1.95	0.407	.261

(1) Condon and Shortley (1963) p.134.

(2) Garcia and Mack (1965).

(3) Bethe and Salpeter (1957), and see appendix AVIII

be used to obtained the formulae for the polarization fractions. In fact, as indicated by Percival and Seaton (their equations (5.13) and (5.14)), if I''_o and I''_∞ are the light intensities as in (5.1) derived using (5.5) (i.e. for very small $\varepsilon_{3\ell j}$) and (5.6) (i.e. for very large $\varepsilon_{3\ell j}$) respectively, then the exact form for I'' can be written

$$I'' = \frac{I''_o + \varepsilon^2_{3\ell j} I''_\infty}{1 + \varepsilon^2_{3\ell j}} \qquad (5.7)$$

Expressions obtained for the polarization fraction by use of the two O-P formulae and from the explicit formula (5.7) are given in table (T5.2), in terms of the cross-sections for exciting the magnetic sublevels $\sigma(3\ell m_\ell)$ (for details-see appendix AIX). The expressions for $P_{90}(3^2P - 2^2S)$ with and without hyperfine structure are in agreement with those quoted by Percival and Seaton, the expression for $P^{FS}_{90}(3^2D \rightarrow 2^2P)$ is in agreement with that used by Mahan (1974), but obtained after correcting a misprint in Percival and Seaton's paper.

5.3 Polarization Expression for Hα Radiation

To obtain the overall polarization of Hα radiation it is necessary to start from the definition of the perpendicular cross section. Moiseiwitsch and Smith (1968) give the relation

$$\sigma_{TOTAL} = \sigma_{90}(1 - P_{90}/3) \qquad (5.8)$$

where P_{90} is the 90^o polarization of emitted line radiation and σ_{TOTAL} is the total excitation cross section. This also follows directly from (5.2) when $\theta = 90^o$. For the Hα case

$$\sigma_{TOTAL}(H\alpha) = \sigma(3s) + B_{3p}\sigma(3p) + \sigma(3d) = \Sigma\, B_{3\ell}\sigma(3s) \qquad (5.9)$$

where $\sigma(3\ell)$ $(\ell = 1,2,3)$ are the cross-sections for excitation to the 3ℓ state and $B_{3\ell}$ is the branching ratio for radiation from the 3ℓ state to the $2\ell'$ state. Here, $B_{3s} = B_{3d} = 1$ and $B_{3p} = 0.118$ (see appendix AVIII).

Table T5.2 : Linear Polarization Formulae for the s, p and d states of Hydrogen

	$n^2S \rightarrow n'^2P$	$n^2P \rightarrow n'^2S$	$n^2D \rightarrow n'^2P$
0 - P theory (without hfs) P_{90}^{FS}	0	$\frac{3(\sigma(np0) - \sigma(np1))}{(7\sigma(np0) + 11\sigma(np1)}$	$\frac{57(\sigma(nd0) + \sigma(nd1) - 2\sigma(nd2))}{119\sigma(nd0) + 219\sigma(nd1) + 162\sigma(nd2)}$
0 - P theory (with hfs) P_{90}^{HFS}	0	$\frac{15(\sigma(np0) - \sigma(np1))}{53\sigma(np0) + 91\sigma(np1)}$	$\frac{69(\sigma(nd0) + \sigma(nd1) - 2\sigma(nd2))}{183\sigma(nd0) + 343\sigma(nd1) + 274\sigma(nd2)}$
P - S theory; n = 3 states (exact formulae) $P_{90}^{PS}(n = 3)$	0	$\frac{(\sigma(np0) - \sigma(np1))}{(3.18\sigma(np0) + 5.36\sigma(np1)}$	$\frac{\sigma(nd0) + \sigma(nd1) - 2\sigma(nd2)}{2.14\sigma(nd0) + 3.94\sigma(nd1) + 2.94\sigma(nd2)}$

Similarly,

$$\sigma_{90}(H\alpha) = \sigma_{90}(3s) + B_{3p}\sigma_{90}(3p) + \sigma_{90}(3d) = \Sigma B_{3\ell}\sigma_{90}(3\ell) \qquad (5.10)$$

where $\sigma_{90}(3\ell)$ $(\ell = 1,2,3)$ are the individual 90° cross sections and are defined in terms of the 90° polarizations of photons emitted from these states by

$$\sigma_{90}(3\ell) = \sigma(3\ell)\,(1 - P_{90}(3\ell)/3)^{-1} \qquad (5.11)$$

Thus, from the expressions for $P_{90}(3\ell)$ taken from table (T5.2), we obtain the corresponding expressions for σ_{90} as given in table (T5.3).

Since, from (5.9) and (5.11)

$$\sigma_{TOTAL}(H\alpha) = \sigma_{90}(H\alpha) - \frac{1}{3}\Sigma B_{3\ell}\sigma_{90}(3\ell)\,P_{90}(3\ell) \qquad (5.12)$$

then, by substituting for $\sigma_{TOTAL}(H\alpha)$ in (5.8)

$$P_{90}(H\alpha) = 3(\sigma_{90}(H\alpha) - \sigma_{TOTAL}(H\alpha))/\sigma_{90}(H\alpha)$$

$$P_{90}(H\alpha) = \frac{(0.12\sigma_{90}(3p)\,P_{90}(3p) + \sigma_{90}(3d)\,P_{90}(3d))}{\sigma_{90}(H\alpha)} \qquad (5.13)$$

This result is in accord with the intuitive idea that the total polarization of an emitted line should be made up of the sum of the polarizations of the components of the line, weighted according to the populations of the components.

5.4 Polarization results for $3p \rightarrow 2s$, $3d \rightarrow 2p$ and $H\alpha$ radiation

The magnetic sub-level cross sections were combined according to tables T5.2 and T5.3 and the polarization fractions and perpendicular cross sections for the 3p and 3d states produced by the POLORP and POLORD programs respectively. These results were combined according to equation (5.13) via (5.10) to produce the polarization of the $H\alpha$ radiation.

Table T5.3: Perpendicular Cross Sections for the s, p and d States of Hydrogen

		n^2S	n^2P	n^2D
0 - P theory (without hfs)	σ_{90}^{FS}	$\sigma(ns)$	$\frac{7\sigma(np0) + 11\sigma(np1)}{6}$	$\frac{119\sigma(nd0) + 219\sigma(nd1) + 162\sigma(nd2)}{100}$
0 - P theory (with hfs)	σ_{90}^{HFS}	$\sigma(ns)$	$\frac{53\sigma(np0) + 91\sigma(np1)}{48}$	$\frac{183\sigma(nd0) + 343\sigma(nd1) + 274\sigma(nd2)}{150}$
P - S theory; n = 3 states (exact formula)	$\sigma_{90}^{PS}(n = 3)$	$\sigma(ns)$	$1.12\sigma(np0) + 1.88\sigma(np1)$	$1.18\sigma(nd0) + 2.19\sigma(nd1) + 1.63\sigma(nd2)$

Figure F5.2a shows the 90° polarization of the radiation calculated in each of the six approximations (Born, Polarized Born, Born-Oppenheimer, Polarized Born-Oppenheimer, DWPO I and DWPO II), for energies up to 50 eV. Figure F5.2b similarly shows the results from 40 eV to 200 eV. The results in the Born and Polarized Born are equivalent whether produced by the POLORB, POLORP and POLORD programs or from the exact forms of the scattering amplitudes and provide a useful check on the computation.

The DWPO I results show the greatest degree of polarization at near threshold energies - however in this region the polarized orbital results are not expected to be very accurate since coupling between the 1s and 2p states only is included and any other effects are ignored. Above 20 eV DWPO II results lie above all the others with DWPO I being almost indistinguishable from DWPO II up to about 40 eV. At this point, the DWPO I results depart from the DWPO II results and tend to the Born approximation at higher energies. Similarly the DWPO II results tend to the Polarized Born approximation.

The Born and polarized Born results decrease uniformly across the entire energy range shown. Initially the Born polarization fraction is higher than the polarized Born but the position is reversed at nearly 50 eV and by 200 eV, the separation between the two is over two percentage points.

The Born-Oppenheimer and PBO polarization fractions both show a peak at about 25 eV with the B-O results lying slightly higher than the PBO up to about 60 eV where the relative positions are reversed. At higher energies the B-O results tend to the Born results from below and the PB-O polarization fraction tends to the polarized Born results - also from below. Neither the Born nor the Born-Oppenheimer results are expected to have much validity at low energies since they are of course high energy approximations. The effect of the distorted wave polarized orbital model is clearly to increase the calculated polarization fraction. Additionally the inclusion of core polarization leads to significantly higher results especially at higher energies.

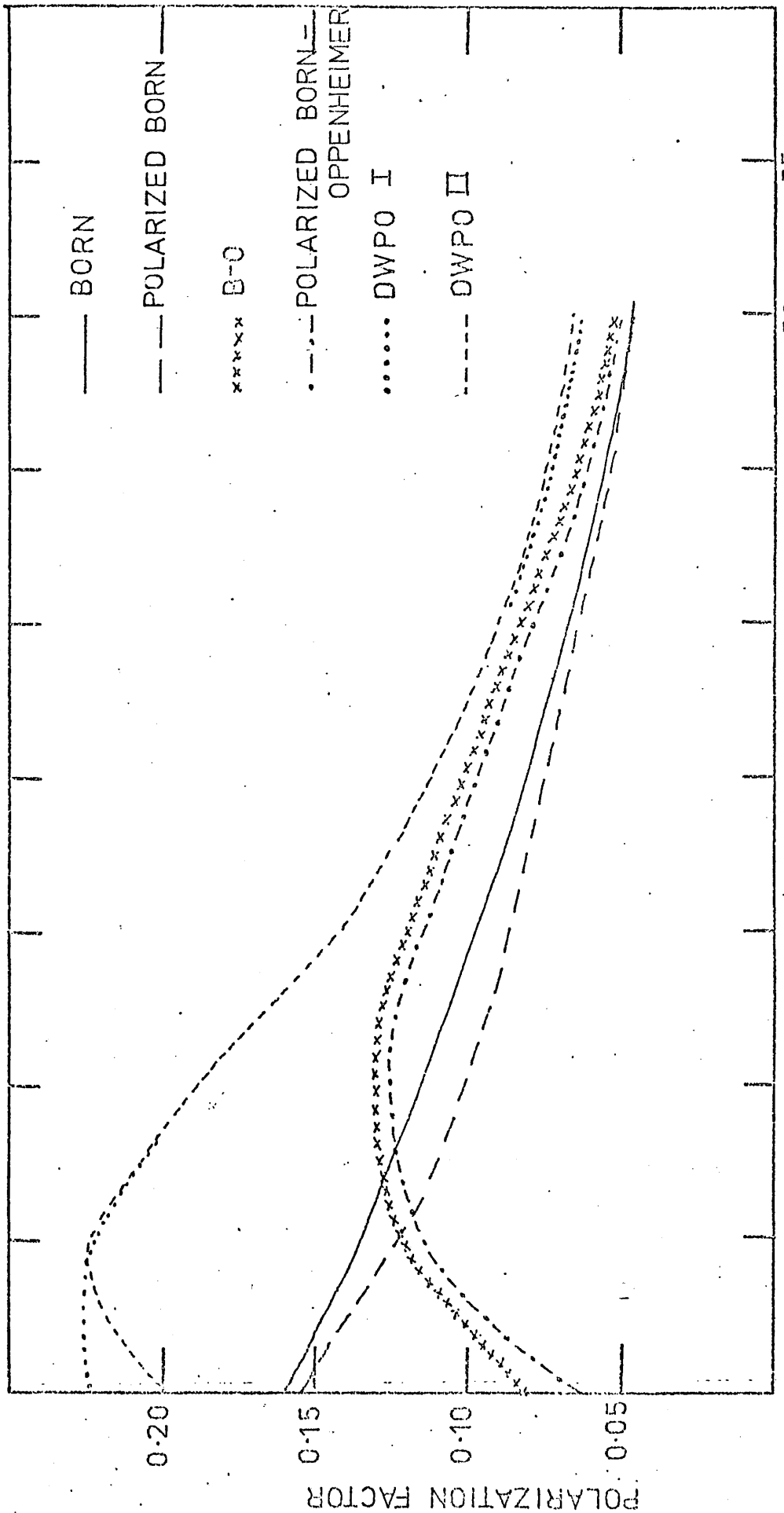

FIGURE F5·2a THE POLARIZATION FRACTION P(90°) CALCULATED IN THE MODELS LISTED FOR $k_i^1 = 15$ TO 50 EV

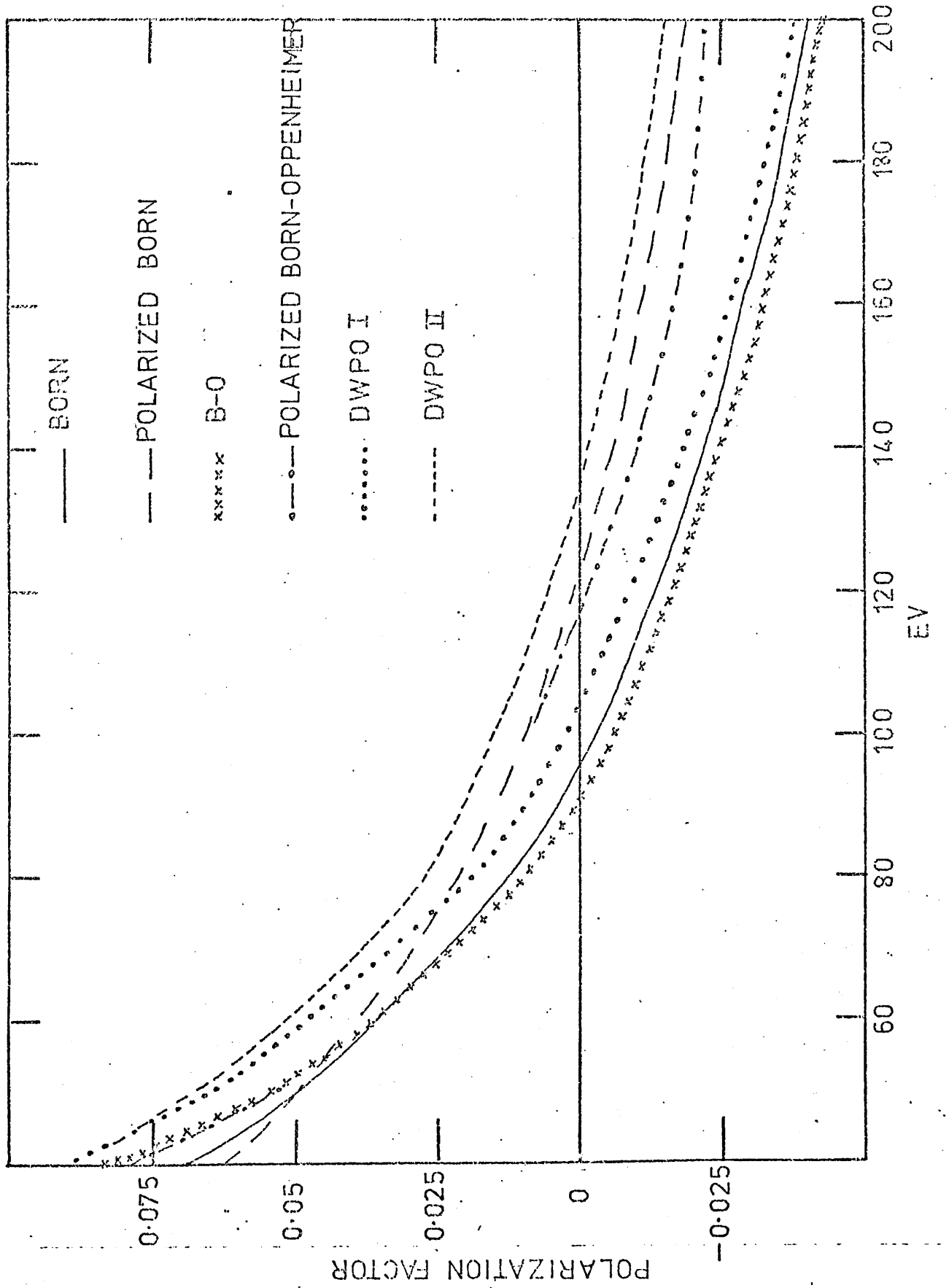

FIGURE F5·2b THE POLARIZATION FRACTION P(90°) CALCULATED IN THE MODELS LISTED FOR $k^2 = 40$ TO 200EV

The explanation of the change of sign of polarization is that it occurs when the emitted radiation changes from right to left polarization. Thus, distortion of the atom and electron system leads to a shift to higher values in the energy at which this occurs. Although the effect of exchange only (i.e. considering the Born-Oppenheimer rather than the Born models) appears to shift the energy slightly to the left, the validity of these models in the region where this occurs is open to doubt.

Figure F5.3 again shows the DWPO II results and the Born values for comparison for energies up to 100 eV. Also shown are the experimental results of Kleinpoppen et al. (1962), of Kleinpoppen and Kraiss (1968) and the calculated values of Mahan (1974). The values given by Mahan do not represent an independent measurement of polarization, but rather are calculated values in which the Born $\sigma(n\ell)$ cross sections are replaced by his measured values while the $\sigma(n\ell m_\ell)$ Born results are retained.

However, although the DWPO II Lyα polarization polarization results were in complete agreement, at energies above 20 eV, with the reported measurements of Ott et al. (1970) our present results for Hα are in strong disagreement with the measurements of Kleinpoppen and his colleagues ((1962) and (1968)). Kleinpoppen believes that the later experiments (Kleinpoppen and Kraiss (1968)) carries errors of at least 25% (private communication 1975), but this does not bring it into agreement with theory. The comments made in Chapter 4 about the DWPO model as a whole apply particularly with respect to the results at higher energies. Therefore the values shown at these energies are not expected to be a reliable prediction of polarization measurements. The model's predictions at lower energies are expected to be more reliable and this is where the available experimental results show the greatest disparity with theory. Further theoretical and experimental studies are clearly required to explain this disparity.

Table T5.4 shows the polarization fractions for the 3p state obtained in each model and using:

FIGURE F5·3

THE POLARIZATION FRACTION P(90°) CALCULATED IN THE BORN AND DWPO II MODELS AND SHOWING THE AVAILABLE EXPERIMENTAL RESULTS

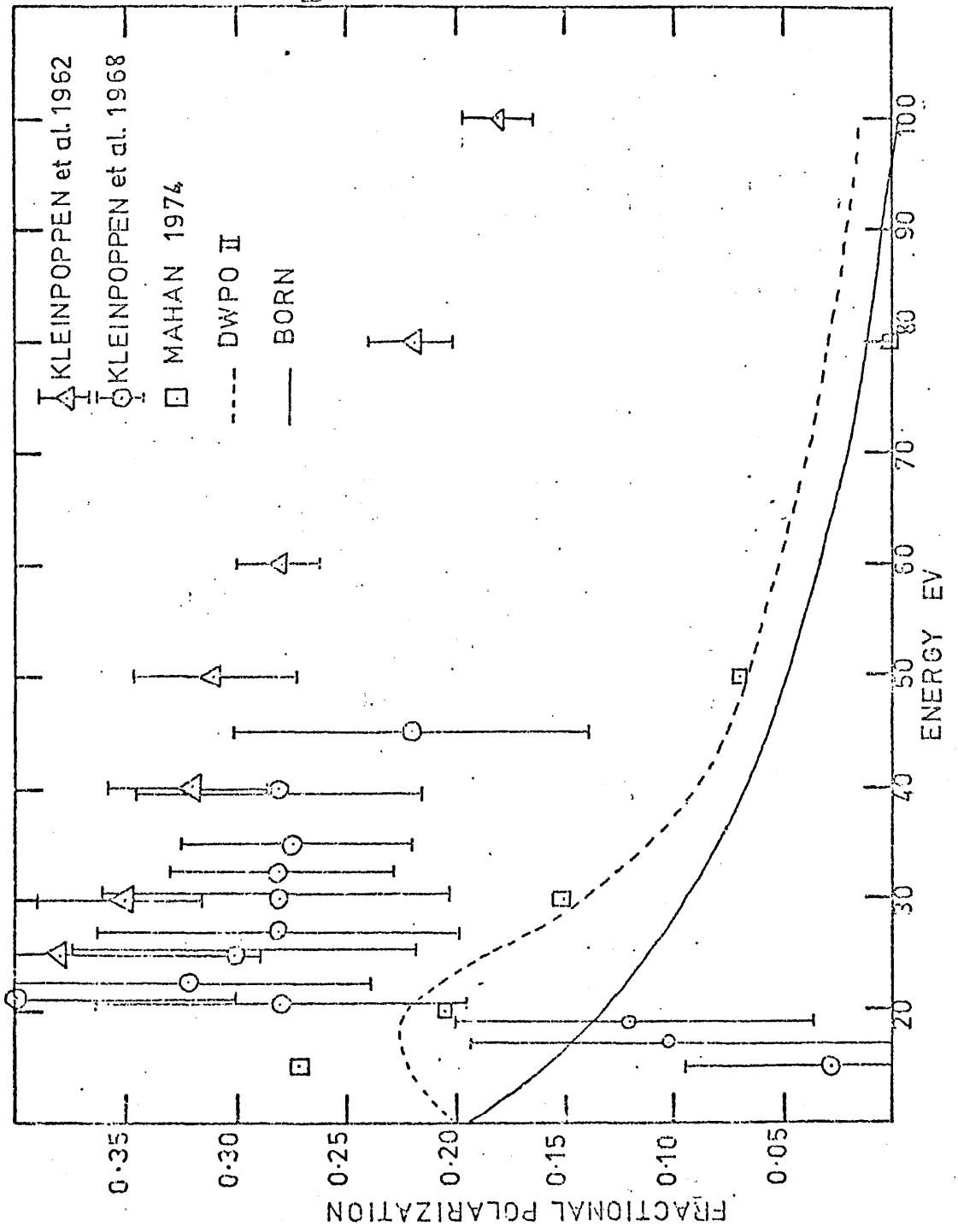

a) O-P theory with fine structure but not including hyperfine structure,

b) O-P theory with hyperfine structure included,

c) P-S "exact" formulation.

These results confirm the importance of hyperfine effects at all energies and for each model since the results under c) are nearest to those under b). However, the differences even here are significant and show that the "exact" formulation of Percival and Seaton should be used. The effect of exchange is to increase the polarization of 3p radiation at low energies - at higher energies the effect is barely discernible. Core polarization leads to higher polarization fractions, particularly at high energies. The full distorted wave polarized orbital model with core polarization gives the highest values for the polarization fraction such that at 200 eV the polarization percentage is nearly 3% higher than the Born value. All models except PBO predict a monotomically decreasing polarization fraction with energy. The exception, PB-O, suggests a peak at about 20 eV but this model is unreliable at such low energies in any case.

It should be noted that these results are also a theoretical calculation of the polarization of Ly-β radiation (wavelength 1025·83 Å) arising through the decay of the 3p state to the ground state. We have not found any reports of theoretical calculations or experimental measurements of this quantity.* However, with other theoretical work it is possible to obtain the 3p polarization by combining the individual $\sigma(3pm_\ell)$ cross sections, when reported, in the appropriate manner as in table T5.3. More usefully though, the separate $\sigma(3pm_\ell)$ may be directly compared and where possible we have considered this in Chapter 4.

Table T5.5 shows the polarization fractions for the 3d state as in table T5.4. It will be noticed that including hyperfine splitting in the O-P theory leads to results which greatly underestimate the polarization fraction at all energies and in all models and that the results using a) are very close to the P-S exact formulation. This is to be expected, in any case, since for the 3d state the parameter $\epsilon_{3\ell j} < 1$ (see section 5.1),

* (note added at binding): ...but see Chan F.T. and Chang C.H., 1977, Phys Rev A15, p 118; for Glauber model theoretical calculations.

Table T5.4 Polarization fractions for the 3p state of Hydrogen; a) O - P theory including fine structure only; OP theory including hyperfine structure; c) PS "exact" formulation.

eV		BORN	P-BORN	B-O	P-B-O	DWPO I	DWPO II
	a)	.3570	.3575	.3923	.1786	.3250	.3230
15	b)	.2336	.2339	.2578	.1142	.2117	.2104
	c)	.2600	.2604	.2868	.1277	.2359	.2344
	a)	.2794	.2818	.3032	.3045	.2783	.2832
20	b)	.1809	.1825	.1970	.1979	.1802	.1835
	c)	.2019	.2036	.2196	.2206	.2011	.2047
	a)	.1929	.1987	.1942	.2004	.2096	.2153
30	b)	.1236	.1273	.1244	.1285	.1345	.1383
	c)	.1382	.1424	.1391	.1436	.1504	.1546
	a)	.1434	.1513	.1414	.1500	.1664	.1725
40	b)	.0913	.0964	.0899	.0955	.1062	.1102
	c)	.1022	.1079	.1007	.1070	.1188	.1233
	a)	.1103	.1196	.1082	.1182	.1364	.1434
50	b)	.0699	.0759	.0686	.0750	.0867	.0913
	c)	.0784	.0851	.0769	.0840	.0971	.1023
	a)	.0528	.0642	.0522	.0639	.0799	.0891
80	b)	.0332	.0404	.0328	.0403	.0504	.0563
	c)	.0373	.0454	.0369	.0452	.0566	.0631
	a)	.0303	.0421	.0302	.0424	.0557	.0656
100	b)	.0190	.0265	.0190	.0266	.0304	.0414
	c)	.0213	.0297	.0213	.0299	.0393	.0464
	a)	-.0045	.0078	-.0040	.0085	.0165	.0273
150	b)	-.0028	.0049	-.0025	.0053	.0104	.0171
	c)	-.0031	.0055	-.0028	.0060	.0116	.0192
	a)	-.0252	-.0129	-.0245	-.0123	-.0077	.0018
200	b)	-.0157	-.0081	-.0153	-.0077	-.0048	.0011
	c)	-.0177	-.0091	-.0172	-.0086	-.0054	.0013

Table T5.5 Polarization fractions for the 3d state of Hydrogen
a) O-P theory including fine structure; b) OP theory including hyperfine structure; c) P-S "exact" formulation.

eV		BORN	P-BORN	B-O	P-B-O	DWPO I	DWPO II
	a)	.3999	.3985	.3663	.3649	.3827	.3879
15	b)	.3127	.3116	.2856	.2845	.2988	.3030
	c)	.3907	.3894	.3578	.3563	.3739	.3790
	a)	.3087	.3069	.3309	.3349	.3299	.3577
20	b)	.2396	.2381	.2572	.2605	.2564	.2787
	c)	.3014	.2996	.3231	.3271	.3220	.3494
	a)	.1958	.1987	.2380	.2534	.2267	.2632
30	b)	.1505	.1528	.1836	.1958	.1748	.2035
	c)	.1910	.1938	.2322	.2473	.2212	.2569
	a)	.1245	.1327	.1537	.1722	.1408	.1719
40	b)	.0952	.1015	.1177	.1322	.1077	.1319
	c)	.1214	.1293	.1498	.1679	.1372	.1677
	a)	.0740	.0864	.0902	.1083	.0833	.1085
50	b)	.0563	.0658	.0688	.0826	.0634	.0828
	c)	.0721	.0842	.0879	.1055	.0811	.1057
	a)	-.0189	.0011	-.0191	-.0013	-.0242	-.0032
80	b)	-.0143	.0008	-.0144	-.0010	-.0183	-.0025
	c)	-.0183	.0011	-.0186	-.0012	-.0236	-.0032
	a)	-.0568	-.0342	-.0602	-.0413	-.0670	-.0456
100	b)	-.0428	-.0258	-.0453	-.0311	-.0504	-.0344
	c)	-.0553	-.0333	-.0586	-.0402	-.0652	-.0444
	a)	-.1160	-.0907	-.1240	-.1043	-.1279	-.1039
150	b)	-.0870	-.0681	-.0928	-.0783	-.0958	-.0780
	c)	-.1128	-.0882	-.1206	-.1015	-.1244	-.1011
	a)	-.1509	-.1251	-.1611	-.1421	-.1506	-.1195
200	b)	-.1128	-.0937	-.1203	-.1063	-.1126	-.0896
	c)	-.1468	-.1217	-.1566	-.1382	-.1465	-.1163

Table T5.6 Polarization fractions for Hα radiation a) O-P theory including fine structure; b) O-P theory including hyperfine structure; c) P-S "exact" formulation

eV		BORN	P-BORN	B-O	P-B-O	DWPO I	DWPOII
	a)	.1874	.1910	.0944	.0713	.2417	.2164
15	b)	.1321	.1308	.0673	.0512	.1800	.1611
	c)	.1590	.1541	.0825	.0632	.2228	.1999
	a)	.1602	.1546	.1344	.1223	.2459	.2479
20	b)	.1123	.1049	.0989	.0892	.1804	.1818
	c)	.1350	.1234	.1231	.1107	.2211	.2227
	a)	.1153	.1106	.1318	.1258	.1627	.1654
30	b)	.0797	.0741	.0958	.0904	.1160	.1166
	c)	.0954	.0867	.1185	.1109	.1410	.1407
	a)	.0836	.0836	.0958	.0950	.1093	.1125
40	b)	.0570	.0554	.0680	.0661	.0754	.0763
	c)	.0678	.0645	.0830	.0798	.0901	.0901
	a)	.0607	.0648	.0659	.0694	.0797	.0861
50	b)	.0407	.0424	.0455	.0470	.0537	.0572
	c)	.0479	.0491	.0548	.0558	.0634	.0668
	a)	.0177	.0302	.0156	.0285	.0281	.0429
80	b)	.0105	.0190	.0091	.0179	.0168	.0269
	c)	.0112	.0214	.0095	.0201	.0180	.0301
	a)	.0000	.0160	-.0029	.0137	.0079	.0261
100	b)	-.0017	.0094	-.0039	.0077	.0027	.0155
	c)	-.0036	.0100	-.0064	.0079	.0009	.0165
	a)	-.0278	-.0070	-.0310	-.0094	-.0221	.0005
150	b)	-.0207	-.0058	-.0231	-.0077	-.0177	-.0015
	c)	-.0264	-.0079	-.0296	-.0103	-.0237	-.0034
	a)	-.0444	-.0213	-.0472	-.0233	-.0385	-.0149
200	b)	-.0319	-.0152	-.0340	-.0168	-.0285	-.0114
	c)	-.0399	-.0189	-.0426	-.0210	-.0364	-.0148

whereas the converse holds for the 3p state leading to the corresponding result discussed above. Again, all models show a monotonically decreasing polarization fraction with energy. Similar effects due to exchange and core polarization at energies above 20 eV are noticeable as in the 3p case and again the DWPO II results predict the highest value for the polarization fraction.

Finally table T5.6 presents, in the same way as T5.4 and T5.5, the full Hα polarization results. The effect of hyperfine structure is seen to underestimate the exact formulation polarization fraction whereas fine structure alone overestimates it by nearly as much. The ambiguity is most marked in the DWPO II results where, although the smaller contribution of the 3d cross section to the total cross section would lead to an expected lesser effect of hyperfine structure, this is balanced by a larger 3p cross section (and despite the branching ratio which reduces this cross section to the same order as the 3d cross section).

5.5 Summary

This chapter has been concerned with the linear polarization of the radiation emitted by the 3p and 3d states and of the Hα radiation emitted by excitation to the $n = 3$ states with subsequent decay to the $n = 2$ states. The background to the theory has been described with particular application to the $n = 3$ states and the formulation of the relevant expressions outlined.

Results, using the DWPO models as well as the Born and Born-Oppenheimer approximations, have been presented and discussed. These results have been compared with the available experimental results but show strong disagreement at all energies and indicate the need for further experimental and theoretical work.

CHAPTER 6

Fano-Macek orientation and alignment parameters and the Macek-Jaecks parameters

6.1 Introduction

Macek and Jaecks (1971) discuss in detail the theory of measurements wherein photons are detected in delayed coincidence with a scattered particle and present a form of analysis specifically applicable to atomic collisions, relating the coincidence rate as measured for given photon and particle orientation to excitation amplitudes. This approach provides an added insight into the physics of electron atom collision processes and taken with the relative phases of excitation, provide a sensitive test of any collision model.

Fano and Macek (1973) further describe the orientation and alighment of the excited atom and show that the alignment of the emitter along the direction of emission is proportional to the anisotropy of emission and that the linear and circular polarizations are proportional to the alignment within the plane of polarization and to the component of orientation in the direction of emission respectively.

Morgan and McDowell (1975) have presented results in the DWPO II model for these Fano-Macek parameters for the case of Lyman α photons and have produced computer generated maps of the coincidence rates. Eminyan et al. (1973, 1974) have made experimental determinations of the coincidence rate for the 2^1P and 3^1P states of Helium. No theoretical or experimental results for the coincidence rates or orientation and alignment parameters have yet been reported for the $n = 3$ states of Hydrogen.* We present here results for the Macek and Jaecks parameters, that is components of the coincidence rate for the $n = 3$ states of hydrogen, and also Fano-Macek parameters for the 3p states of hydrogen.

* (note added at binding): ...but see: Chan F.T. and Chang C.H., 1977, Phys Rev A15, p 118; for Glauber model theoretical calculations.

6.2 Coincidence Rate for the n = 3 states of Hydrogen.

Macek and Jaecks (1971) considered the observation of photons in coincidence with scattered electrons where the scattered electrons on

collision with an atom, excite the atom and then the subsequent decay of the atom gives rise to the emission of the observed photons. The rate, dN_c, for the coincidence observation of the scattered electrons and emitted photons is given by the relation (assuming that LS coupling can be used to describe the atom):

$$dN_c \alpha B(A_{oo} + A_{11} + (A_{11} - A_{oo})\cos^2\theta_\nu - \sqrt{2}\ \mathrm{Re}\ A_{o1} \sin 2\theta_\nu + A_{1-1}\sin^2\theta_\nu)d\Omega_e d\Omega_\nu$$

where B is the branching ratio and where the electron is scattered through $\Omega_e = (\theta_e, \phi_e)$ and the photon is scattered through $\Omega_\nu = (\theta_\nu, \phi_\nu)$. The experimental arrangements treated here is that in which $\phi_e = 0$ and $\phi_\nu = \pi$.

The terms $A_{qq'}$, $(q, q' = 0 \pm 1)$ are given by:

$$A_{qq'} = \sum_{JFJ'F'M_LM_L'} U(qq'M_LM_L'JFJ'F'LL_o) \ \langle a_{M_L'} a_{M_L} \rangle \int_0^{\Delta t} \exp -(\gamma + iw_{JFJF'})t \ dt$$

where

$$U(qq'M_LM_L'JFJ'F'LL_o) = \frac{(2J+1)(2J'+1)(2F+1)(2F'+1)(2L+1)}{(2S+1)(2I+1)} \times (-1)^{L_o - M_L + q} \times$$

$$\sum_{\chi\nu} (2\chi+1)(-1)^\chi \begin{Bmatrix} L & L & \chi \\ J' & J & S \end{Bmatrix}^2 \begin{Bmatrix} J & J' & \chi \\ F' & F & I \end{Bmatrix}^2 \begin{Bmatrix} L & L & \chi \\ 1 & 1 & L_o \end{Bmatrix}$$

$$\begin{pmatrix} L & L & \chi \\ -M_L' & M_L & \nu \end{pmatrix} \begin{pmatrix} 1 & 1 & \chi \\ -q & q' & -\nu \end{pmatrix}$$

Δt is the time resolution of the experimental detection apparatus (generally much longer than the precession periods or mean lifetimes of the excited atom), a_{M_L} is the excitation amplitude for the magnetic sub-level M_L; $1/\gamma$ is the mean lifetime of the excited atom; the frequency $w_{JFJ'F'}(=(E_{JF} - E_{J'F'})/\hbar)$ describes the modulation of the light intensity due to interference of radiation from coherently excited levels of the fine-structure or hyperfine-structure multiplet; L_o is the orbital angular momentum quantum member of the state to which the nL state decays.

For the case of Balmer-α radiation, following Macek and Jaecks and ignoring hyperfine structure, then (to a good approximation):

$$\int_0^{\Delta t} \exp -(\gamma+iw_{JFJ'F'})\, dt \simeq \int_0^{\infty} \exp -(\gamma+iw_{JJ'})t \; dt$$

(independent of F, F')

$$= \left[\gamma + iw_{JJ'}\right]^{-1}$$

$$\simeq \begin{cases} 0 & \text{when } J \neq J' \\ 1/\gamma & \text{when } J = J' \end{cases}$$

so

$$A_{qq'} = \sum_{J,M_L M_L'} \frac{(2L+1)(2J+1)^2}{\gamma(2S+1)} (-1)^{L_o - M_L + q} \langle a_{M_L'} a_{M_L} \rangle \sum_{\chi\nu} (2\chi+1)$$

$$\begin{Bmatrix} L & L & \chi \\ J & J & S \end{Bmatrix}^2 \begin{Bmatrix} L & L & \chi \\ 1 & 1 & L_o \end{Bmatrix} \begin{pmatrix} L & L & \chi \\ -M_L' & M_L & \nu \end{pmatrix} \begin{pmatrix} 1 & 1 & \chi \\ q & -q' & \nu \end{pmatrix}$$

We find for each of the $n = 3\ell$ states as follows (see Appendix AX).

1. 3s-2p: (Balmer-α radiation)

$$A_{oo} = \sigma_o/3\gamma$$

$$A_{11} = \sigma_o/3\gamma$$

$$A_{1-1} = A_{o1} = 0$$

2. 3p-2s: (Balmer-α radiation)
   -1s: (Lyman-β radiation)

$$A_{oo} = (5\sigma_o + 4\sigma_1)/9\gamma$$

$$A_{11} = (2\sigma_o + 7\sigma_1)/9\gamma$$

$$Ao1 = \mathrm{Re}\,\langle a_o a_1 \rangle/3\gamma + 7i\,\mathrm{Im}\,\langle a_o a_1 \rangle/9\gamma$$

and ∴

$$\mathrm{Re}A_{o1} = \mathrm{Re}\,\langle a_o a_1 \rangle/3\gamma$$

$$\mathrm{Im}A_{o1} = 7\mathrm{Im}\,\langle a_o a_1 \rangle/9\gamma$$

$$A_{1-1} = -\sigma_1/3\gamma$$

3. $3d \rightarrow 2p$ (Balmer-α)

$$A_{oo} = (44\sigma_o + 69\sigma_1 + 12\sigma_2)/75\gamma$$

$$A_{11} = (31\sigma_o + 81\sigma_1 + 138\sigma_2)/150\gamma$$

$$A_{o1} = -\frac{\sqrt{2}}{25\gamma}\langle a_1 a_2\rangle - \frac{\sqrt{3}}{6\gamma}\langle a_o a_1\rangle + \frac{21\sqrt{2}}{50\gamma}\langle a_2 a_1\rangle + \frac{22\sqrt{3}}{75\gamma}\langle a_1 a_o\rangle$$

$$\left\{\begin{array}{l} \therefore \\ \mathrm{Re}A_{o1} = \mathrm{Re}\langle a_2 a_1\rangle \frac{19\sqrt{2}}{50\gamma} + \mathrm{Re}\langle a_1 a_o\rangle \frac{19\sqrt{3}}{150\gamma} \\ + \mathrm{Im}A_{o1} = \mathrm{Im}\langle a_2 a_1\rangle \frac{23\sqrt{2}}{50\gamma} + \mathrm{Im}\langle a_1 a_o\rangle \frac{23\sqrt{3}}{50\gamma} \end{array}\right\}$$

$$A_{1-1} = -\frac{19\sigma_1}{50\gamma} + \frac{19\sqrt{6}}{75\gamma}\ \mathrm{Re}\langle a_2 a_o\rangle .$$

It will be recognised that the linear polarization expressions obtained in Chapter 5, where hyperfine structure is excluded, can be equally derived from:

$$P_{90} = (A_{oo} - A_{11})/(A_{oo} + A_{11})$$

and this feature provides a useful check on the calculation of the coefficients in both this chapter and in Chapter 5.

6.3 Alignment and Orientation Parameters for the 3p state of Hydrogen

Morgan and McDowell (1974) following Eminyan et al. (1973, 1974) have used the result that in the collision frame the only non-vanishing components of the alignment tensor A and orientation vector O may be written

$$A_o^c = \langle n|3L_Z^2 - L^2|n\rangle g = \tfrac{1}{2}(1 - 3\lambda)\sigma$$

$$A_{1+}^c = \langle n|L_x L_Z + L_Z L_x|n\rangle g = 2\ \mathrm{Re}\langle a_o a_1\rangle$$

$$A_{2+}^c = \langle n|L_x^2 - L_y^2|n\rangle g = \tfrac{1}{2}(\lambda - 1)\sigma$$

and

$$O_{1-}^c = \langle n|L_y|n\rangle g = -\sqrt{2}\ \mathrm{Im}\langle a_o a_1\rangle$$

where

$$g = L(L+1)^{-1}$$

$$\lambda = \sigma_o/(\sigma_o + 2\sigma_1)$$

and where

$$|np\rangle = a_0|1,0\rangle + a_1(|1,1\rangle - |1,-1\rangle) \quad *$$

and that

$$|a_0|^2 = \sigma_0$$

$$|a_1|^2 = \sigma_1,$$

writing

$$a_\mu = |a_\mu| e^{i\chi_\mu}, \quad (\mu = 0,1)$$

then the relative phase of the excitation amplitudes is given by:

$$\chi = \chi_1 - \chi_0.$$

Thus, to fully describe the coincidence rate as well as the orientation and alignment for the collision, in the case of 3p excitation, all that is required is knowledge of the magnetic sub-levels cross sections (the excitation amplitudes) and of the real and imaginary parts of $\langle a_0 a_1 \rangle$.

The details of the calculation and computation for 3p - 2s, 1s are identical with Morgan and McDowell (paper IV, 1975) and thus are not repeated here.

The orientation and alignment parameters for the ns states are trivial since only one magnetic substate is excited. The corresponding parameters for the nd states at present require further study.

6.4 Results and Discussion

The differential cross sections for the magnetic substates produced by the POLORP and POLORD computer programs have been included in the appropriate expressions and the coincidence parameters for the n = 3 levels of hydrogen calculated, in the DWPO, Born and Born-Oppenheimer models either with or without core polarization included.

Morgan and McDowell (paper IV, 1975) have presented computer generated contour maps to illustrate most effectively the normalised coincidence rate for the 2p state as a function of the scattered electron angle

* This set of equations for $|np\rangle$ is inappropriate for hydrogen when both spin channels are included.

(θ_e) and the emitted photon angle (θ_ν). In that work a symmetrical energy dependent pattern was strongly evident. The production of similar maps for the $n = 3$ states should not present any practical difficulties and could be used to gain extra insight into the models considered for comparison with experimental results when they become available.

For the 3p states we have tabulated the real and imaginary parts of $\langle a_o a_1 \rangle$ divided by the differential cross section. Also tabulated are the results for the parameter $\lambda = \sigma_o/(\sigma_o + \sigma_1)$. The results are presented for a range of energies between 20 and 200 eV and selected electron angles between 0^o and 180^o. Intermediate electron angles to give finer resolution and additional electron angles are also available if required. Using the results presented here together with the differential cross sections given in Chapter 4, a full description of the orientation and alignment of the atom after collision is possible.

The real part of $\langle a_o a_1 \rangle$ for the 3p states calculated by the POLORP program is tabulated in T6.1a for the DWPO I and II models and in T6.1b for the Born and Born-Oppenheimer approximations without core polarization. It was found that core polarization had very little effect on the results in the Born models and therefore the results which include core polarization are not tabulated. Due to cancellation in the differential cross sections at higher angles and for higher energies the results at these levels are not reliable. However this does not detract from the value of the lower energy results particularly since (as was discussed in Chapter 1 and 4) the DWPO model itself is no longer expected to be reliable at higher energies whereas it is felt that it is useful at lower energies where the computer program is more robust.

Referring firstly to T6.1a a similar pattern is evident in both the DWPO I and II results: a primary peak occurs in the near forward direction followed by a trough which deepens with increasing energy and a secondary peak at about 150^o which heightens with increasing energy. The effect of core polarization is barely discernible and tends to dampen slightly any structure.

T6.1a: The Real Part of $\langle a_o a_1 \rangle / \sigma$ For the 3p State In the DWPO Model

	DWPO I						DWPO II					
E(eV) / θ^o	20	30	50	100	150	200	20	30	50	100	150	200
0	0	0	0	0	0	0	0	0	0	0	0	0
15	.272	.339	.333	.266	.238	.228	.258	.339	.331	.265	.238	.229
30	.305	.314	.302	.303	.300	.262	.293	.306	.297	.300	.299	.270
45	.278	.276	.258	.392,-1	-.152	-.229	.263	.271	.265	.682,-1	-.131	-.221
60	.255	.243	.141	-.198	-.276	-.285	.248	.252	.173	-.185	-.260	-.293
90	.264,-1	.141	.127,-1	-.707,-1	-.454,-1	-.647,-1	.127	.150	.246,-1	-.771,-1	-.515,-1	-.700,-1
120	.446,-1	.179	.246,	-.270,-1	.270	.297	.120,-1	.154	.240	.269	.268	.297
150	.298,-1	.118	.216	.298	.294	.327	.851,-1	.105	.204	.296	.294	-
180	0	0	0	0	0	0	0	0	0	0	0	0

T6.1b: The Real Part of $\langle a_o a_1 \rangle / \sigma$ For the 3p State In the Born and Born-Oppenheimer approximations

	BORN						BORN-OPPENHEIMER					
E(eV) / θ^o	20	30	50	100	150	200	20	30	50	100	150	200
0	0	0	0	0	0	0	0	0	0	0	0	0
15	.250	.344	.332	.240	.194	.170	.251	.344	.324	.228	.187	.165
30	.330	.349	.303	.245	.223	.213	.329	.342	.294	.401	.210	.202
45	.345	.348	.316	.285	.271	.252	.328	.347	.317	.285	.272	.250
60	.345	.355	.339	.322	.312	.316	.236	.334	.341	.332	.326	.359
90	.319	.342	.351	.351	.342	.337	-.166	-.172	-.142	-.143	-.166	-.169
120	.250	.277	.292	.324	-	-	-.133	-.166	-.158	-.140	-.105	-.168,-1
150	.131	.156	.162	-	-	-	-.546,-1	-.554,-1	-.510,-1	-.478,-1	-.667,-1	-
180	0	0	0	0	0	0	0	0	0	0	0	0

Considering T6.1b giving the real part of $\langle a_o a_1 \rangle$ in the Born and B-O approximations, the secondary peak noticeable in the DWPO model is no longer apparent and the primary peak has been shifted towards the backwards direction. The energy dependence remains similar to the DWPO results with the greatest effect being evident at about 30 eV followed by a decrease with increasing energy. There is very little difference between the Born and Born-Oppenheimer results in the forward direction. However, in the backward direction the latter results are negative at all energies. All models are zero in the forward and backward directions at all energies.

The imaginary parts of $\langle a_o a_1 \rangle$ are shown in T6.2 for the DWPO I and II models only. The results for the Born and Born-Oppenheimer approximations are all zero since the excitation amplitudes are either purely real or purely imaginary and therefore χ, the relative phase of excitation, is zero or $\pm \pi$. This feature can therefore be used to indicate the valid range for the Born approximation - i.e. when the prediction of other models or when experimental results show very small imaginary parts.

Again, the results are all zero in the forward and backward directins. A single peak is evident at about 60° for low energies and this advances to the forward direction with increasing energy. There is very little difference between the DWPO I and II results particularly at higher energies, with the latter model showing slightly "flatter" features.

The results for λ are given in the DWPO I and II models (Table T6.3a) and for the Born and Born-Oppenheimer approximations (T6.3b). The behaviour of this orientation parameter at three energies (20, 50 and 100 eV) is illustrated in Figures F6.1 when calculated in the DWPO II model and in F6.2 calculated in the Born approximation - both sets of results obtained using the POLORP program. These results can be compared with those for the 2p state of hydrogen (see McDowell et al- paper III (1975)) and a similar behaviour is evident here. A rapid decrease is seen in the forward direction to a minimum which deepens with increasing energy and advances to the forward direction. In the DWPO I model a second minimum

T6.2: The Imaginary Part of $\langle a_o a_1 \rangle$ / σ For the 3p State In the DWPO Model

	DWPO I						DWPO II					
θ° \ E(eV)	20	30	50	100	150	200	20	30	50	100	150	200
0	0	0	0	0	0	0	0	0	0	0	0	0
15	.231,-1	.320,-1	.407,-1	.443,-1	.453,-1	.469,-1	.182,-1	.292,-1	.406,-1	.467,-1	.486,-1	.502,-1
30	.485,-1	.682,-1	.102	.151	.162	.132	.408,-1	.628,-1	.101	.152	.166	.144
45	.734,-1	.903,-1	.136	.635,-1	-.613,-1	-.119	.665,-1	.774,-1	.121	.833,-1	-.324,-1	-.107
60	.881,-1	.659,-1	.146,-1	-.149	-.178	-.179	.940,-1	.658,-1	.274,-1	-.123	-.161	-.165
90	.286,-1	-.747,-1	-.218,-1	-.181	-.138	-.111	.831,-1	-.125,-1	-.192	-.176	-.135	-.111
120	-.189	-.243	-.249	-.151	-.100	-.914,-1	-.180	-.236	-.258	-.152	-.101	-897,-1
150	-.772,-1	-.970,-1	-.118	-.418,-1	-.403,-1	-.355,-2	-.798,-1	-.994,-1	-.122	-.442,-1	-.411,-1	-
180	0	0	0	0	0	0	0	0	0	0	0	0

T6.3a: The Parameter $\lambda = \sigma_o/(\sigma_o + 2\sigma_1)$ For the 3p State In the DWPO Approximation

	DWPO I						DWPO II					
θ^o \ E(eV)	20	30	50	100	150	200	20	30	50	100	150	200
0	1.0	1.0	1.0	1.0	1.0	1.0	1.0	1.0	1.0	1.0	1.0	1.0
15	.825	.601	.351	.177	.136	.124	.821	.595	.347	.177	.138	.126
30	.640	.443	.334	.386	.556	.737	.647	.452	.339	.384	.537	.704
45	.622	.554	.573	.823	.842	.783	.652	.586	.575	.801	.853	.795
60	.659	.689	.693	.579	.478	.398	.686	.705	.696	.601	.501	.418
90	.566	.673	.391	.101	.483,-1	.343,-1	.573	.702	.429	.104	.488,-1	.359,-1
120	.893	.754	.432	.262	.210	.265	.888	.783	.457	.261	.207	-
150	.983	.951	.852	.758	.771	.682	.981	.956	.864	.760	.771	-
180	1.0	1.0	1.0	1.0	1.0	1.0	1.0	1.0	1.0	1.0	1.0	1.0

T6.3b The Parameter $\lambda = \sigma_o/(\sigma_o + 2\sigma_1)$ For the 3p State In the Born and Born-Oppenheimer Approximations

	BORN						BORN-OPPENHEIMER					
θ^o \ E(eV)	20	30	50	100	150	200	20	30	50	100	150	200
0	1.0	1.0	1.0	1.0	1.0	1.0	1.0	1.0	1.0	1.0	1.0	1.0
15	.853	.617	.332	.132	.813,-1	.617,-1	.853	.597	.312	.122	.762,-1	.578,-1
30	.677	.423	.242	.139	.111	.101	.682	.411	.231	.131	.106	.952,-1
45	.609	.408	.280	.205	.180	.149	.608	.419	.318	.246	.218	.184
60	.613	.457	.359	.299	.282	.275	.562	.398	.365	.338	.321	.326
90	.717	.626	.570	.532	.521	.516	.750	.512	.355	.319	.350	.285
120	.854	.811	.782	.767	.760	.758	.952	.939	.939	.952	.962	.965
150	.960	.949	.944	.937	.940	.935	.993	.993	.995	.995	.988	.967
180	1.0	1.0	1.0	1.0	1.0	1.0	1.0	1.0	1.0	1.0	1.0	1.0

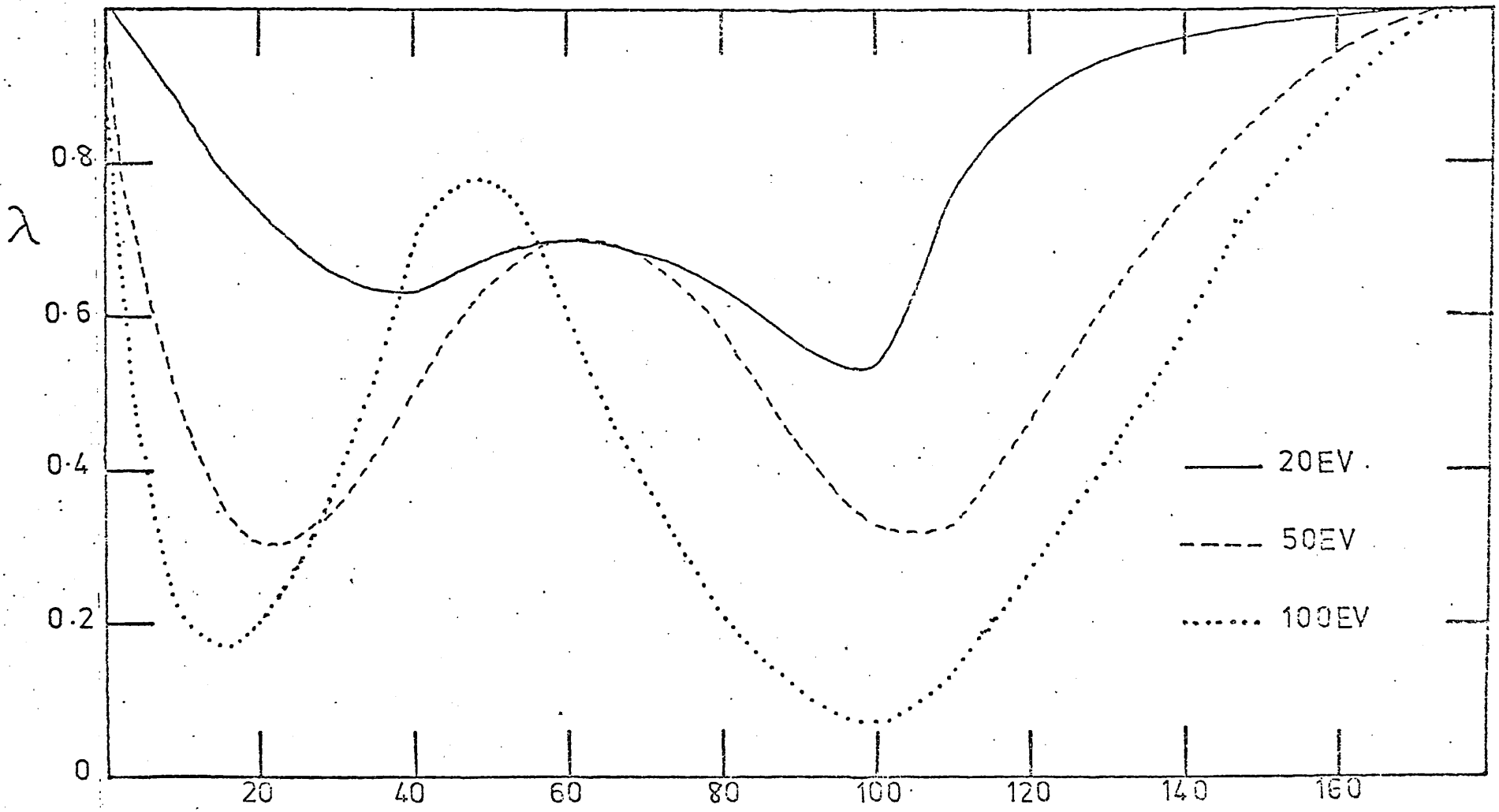

FIGURE F6·1

THE ORIENTATION PARAMETER $\lambda = \sigma_o/\sigma$ AS A FUNCTION OF ANGLE CALCULATED IN THE DWPO II MODEL AT $k_i^2 = 20, 50$ AND 100EV

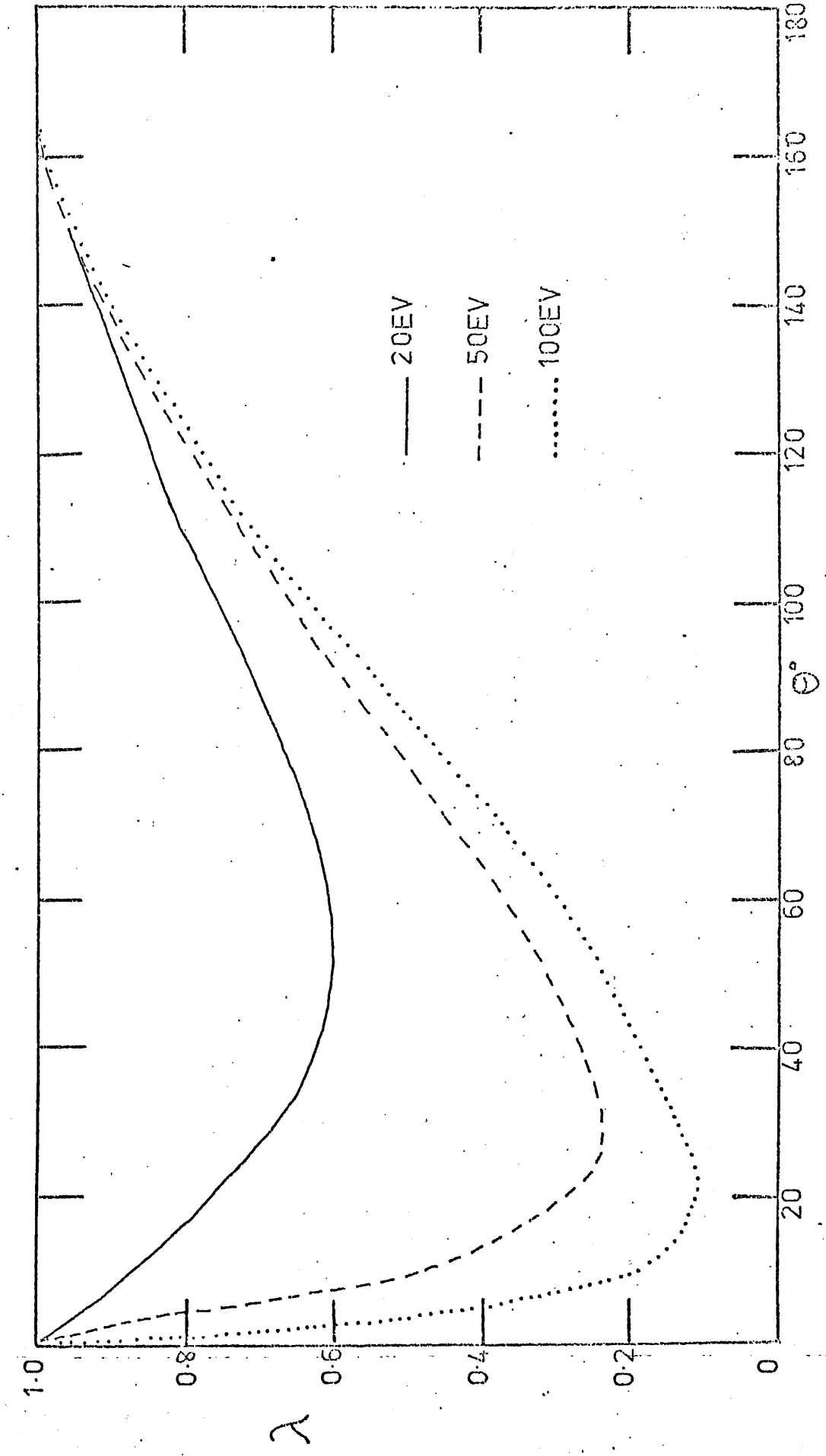

FIGURE F6·2 THE ORIENTATION PARAMETER $\lambda = \sigma_0/\sigma$ AS A FUNCTION OF ANGLE CALCULATED IN THE BORN APPROXIMATION AT $k_i^2 = 20, 50$ AND 100EV

occurs beyond 90^{o} which appears to be almost angle independent followed by a return to unity in the backward direction. When the DWPO I and II results are compared, the minima in the former are deeper though broader than in the latter and the intermediate maximum in the former is less high.

In the Born approximation the second minimum does not occur - the single minimum advances and deepens with increasing energy. In the Born-Oppenheimer a slight second minimum does occur for energies above 30 eV. The effect of core polarization, which is not shown for these models, is to make the minima slightly sharper though less deep.

There are no other experimental or theoretical results for direct comparison to date but the similarity both qualitatively, and to some extent quantitatively, to the 2p results would indicate that experiments to study the detailed behaviour of the coincidence rate will require high levels of sensitivity. However, measurements of λ can provide a more sensitive indication of failure of the Born approximation than straightforward measurements of the differential cross sections, since this approximation does not predict any second minima.

In the 3d case, the coincidence expressions are more complex and therefore the individual components A_{oo}, A_{11} and $A_{1,-1}$ and both the real and imaginary parts of A_{o1} are tabulated separately. Using these results, the coincidence rate can be computed at any scattered photon angle and it is hoped that sufficient information is provided to enable the calculation of the orientation and alignment parameters when the necessary analysis has been completed. Once again, due to cancellation in the differential cross sections, the results for high energies and angles are not considered to be very reliable - they are included however for comparison.

For the 3d state the effect of core polarization is more noticeable and results for DWPO I and II, Born and Born-Oppenheimer and the polarized versions of these approximations are all given except for the imaginary part of A_{o1} in the Born and Born-Oppenheimer approximations. In these models this parameter is zero for all angles and energies since the

excitation amplitudes are either wholly real or wholly imaginary and the relative phases of excitation between the magnetic sublevels is zero or $\pm \pi$.

Referring to Table T6.4a, the parameter A_{oo} is seen to be rapidly decreasing in the Born and polarized Born models, but the inclusion of core polarization leads to a definite reduction (by a factor up to 2.5) particularly in the forward direction and at lower energies. This same feature is apparent in the Born-Oppenheimer and DWPO models. However, in these cases instead of decreasing for all θ_e and E a minimum is evident at about 90^o for energies above 50 eV followed by another minimum in the backward direction. The Born-Oppenheimer and DWPO I results tend to the Born results in the near forward direction with increasing energy but depart from these results for higher values of θ_e with the DWPO I results being about 4-5 orders of magnitude larger than the Born results at higher energies and the B-O results lying intermediate to the Born and DWPO I results. The same effects are noticeable when the polarized Born, polarized B-O and DWPO II results are compared. The effect of increasing energy in each model is to emphasise the forward maximum, and to lower the backward minima.

The parameter A_{11} given in T6.4b exhibits similar characteristics although it does not have an intermediate minimum in any model. Once again at higher energies, where there is little difference in the forward direction between the three models without core polarization, and between those models which include core polarization, the DWPO results lie about five orders of magnitude higher than the Born (or polarized Born) results in the backward direction.

The results for the parameter A_{1-1}, given in T6.4c, continue to show the same behaviour as A_{oo} and A_{11}, but here all models exhibit a maximum at about 90^o. The real part of A_{o1} shown in T6.4d remains negative in the Born models (Born and polarized-Born) apart from in the forward and backward directions where it is zero. All the models show this feature. In the Born models a minimum occurs in the very near forward

T6.4a A_{oo} For the 3d State

	BORN					BORN-OPPENHEIMER				
θ° \ E(eV)	20	30	50	100	200	20	30	50	100	200
0	.416,-1	.736,-1	.104	.129	.143	.102	.121	.126	.136	.144
15	.293,-1	.344,-1	.241,-1	.889,-2	.175,-2	.637,-1	.406,-1	.187,-1	.764,-2	.172,-2
30	.128,-1	.818,-2	.248,-2	.204,-3	.642,-5	.225,-1	.583,-2	.104,-2	.129,-3	.532,-5
45	.449,-2	.153,-2	.201,-3	.522,-5	.630,-7	.729,-2	.115,-2	.664,-4	.179,-5	.270,-7
60	.145,-2	.280,-3	.191,-4	.244,-6	.183,-8	.255,-2	.422,-3	.221,-4	.227,-6	.161,-8
90	.173,-3	.147,-4	.461,-6	.292,-8	.146,-10	.454,-3	.613,-4	.243,-5	.170,-7	.104,-9
120	.341,-4	.183,-5	.398,-7	.190,-1	.823,-12	.914,-3	.847,-4	.276,-5	.185,-7	.649,-10
150	.127,-4	.543,-6	.101,-7	.426,-10	.174,-12	.162,-2	.145,-3	.456,-5	.295,-7	.173,-9
180	.908,-5	.365,-6	.644,-8	.264,-10	.106,-12	.189,-2	.168,-3	.522,-5	.338,-7	.659,-9

	POLARIZED BORN					POLARIZED B-O				
0	.165,-1	.334,-1	.552,-1	.818,-1	.103	.594,-1	.669,-1	.717,-1	.869,-1	.104
15	.112,-1	.134,-1	.911,-2	.335,-2	.772,-3	.372,-1	.193,-1	.619,-2	.262,-2	.760,-3
30	.478,-2	.313,-2	.107,-2	.120,-3	.538,-5	.146,-1	.317,-2	.335,-3	.688,-4	.443,-5
45	.182,-2	.708,-3	.119,-3	.451,-5	.778,-7	.600,-2	.111,-2	.637,-4	.162,-5	.328,-7
60	.676,-3	.162,-3	.148,-4	.274,-6	.302,-8	.256,-2	.474,-3	.244,-4	.216,-6	.133,-8
90	.106,-3	.118,-4	.500,-6	.474,-8	.389,-10	.561,-3	.667,-4	.236,-5	.138,-7	.695,-10
120	.252,-4	.179,-5	.530,-7	.398,-9	.313,-11	.963,-3	.850,-4	.266,-5	.171,-7	.532,-10
150	.103,-4	.590,-6	.150,-7	.104,-9	.824,-12	.164,-2	.145,-3	.447,-5	.283,-7	.161,-9
180	.768,-5	.410,-6	.100,-7	.683,-10	.542,-12	.191,-2	.167,-3	.513,-5	.326,-7	.638,-9

T6.4a A_{oo} For the 3d State

DWPO I

θ° \ E(eV)	20	30	50	100	200
0	.392,-1	.862,-1	.120	.143	.150
15	.289,-1	.348,-1	.231,-1	.764,-2	.148,-2
30	.180,-1	.100,-1	.355,-2	.276,-3	.151,-4
45	.129,-1	.513,-2	.109,-2	.612,-4	.364,-5
60	.860,-2	.305,-2	.338,-3	.151,-4	.734,-6
90	.201,-2	.424,-3	.572,-5	.738,-6	.601,-7
120	.828,-3	.115,-3	.208,-4	.252,-5	.170,-6
150	.483,-3	.123,-3	.211,-4	.188,-5	.137,-6
180	.338,-3	.113,-3	.361,-4	.115,-5	.188,-7

DWPO II

0	.175,-1	.403,-1	.644,-1	.912,-1	.108
15	.140,-1	.136,-1	.847,-2	.272,-2	.648,-3
30	.117,-1	.502,-2	.189,-2	.172,-3	.101,-4
45	.104,-1	.398,-2	.864,-3	.495,-4	.249,-5
60	.746,-2	.268,-2	.279,-3	.111,-4	.415,-6
90	.177,-2	.389,-3	.730,-5	.890,-6	.470,-7
120	.838,-3	.121,-3	.182,-4	.215,-5	.135,-6
150	.501,-3	.119,-3	.219,-4	.185,-5	.114,-6
180	.356,-3	.116,-3	.326,-4	.757,-6	.153,-7

T6.4b A_{11} For the 3d State

DWPO I

20	30	50	100	200
.138,-1	.304,-1	.422,-1	.505,-1	.529,-1
.130,-1	.219,-1	.245,-1	.132,-1	.304,-2
.101,-1	.847,-2	.371,-2	.368,-3	.151,-4
.710,-2	.320,-2	.681,-3	.376,-4	.230,-5
.462,-2	.162,-3	.203,-3	.947,-5	.521,-6
.120,-2	.355,-3	.470,-5	.113,-5	.184,-6
.345,-3	.503,-4	.873,-5	.112,-5	.881,-7
.191,-3	.720,-4	.160,-4	.165,-6	.115,-6
.119,-3	.396,-4	.127,-4	.404,-6	.662,-8

DWPO II

.617,-2	.142,-1	.227,-1	.321,-1	.389,-1
.605,-2	.850,-2	.936,-2	.514,-2	.142,-2
.580,-2	.386,-2	.182,-2	.228,-3	.119,-4
.513,-2	.219,-2	.508,-3	.297,-4	.156,-5
.379,-2	.136,-2	.168,-3	.706,-5	.285,-6
.107,-2	.233,-3	.377,-5	.730,-6	.102,-6
.348,-3	.531,-4	.707,-5	.870,-6	.620,-7
.197,-3	.697,-4	.162,-4	.161,-5	.966,-7
.126,-3	.409,-4	.115,-4	.267,-6	.538,-8

T6.4b A_{11} For the 3d State

	BORN					BORN-OPPENHEIMER				
θ° \ E(eV)	20	30	50	100	200	20	30	50	100	200
0 0	.146,-1	.259,-1	.366,-1	.455,-1	.503,-1	.358,-1	.425,-1	.444.-1	.478,-1	.508,-1
15	.129,-1	.218,-1	.241,-1	.129,-1	.293,-3	.238,-1	.225,-1	.225,-1	.134,-1	.319,-2
30	.739,-2	.704,-2	.291,-2	.291,-3	.994,-5	.982,-2	.635,-2	.296,-2	.357,-3	.131,-4
45	.288,-2	.135,-2	.220,-3	.656,-5	.840,-7	.380,-2	.155,-2	.286,-3	.101,-4	.133,-6
60	.925,-3	.228,-3	.183,-4	.259,-6	.203,-8	.155,-2	.432,-3	.386,-4	.598,-6	.501,-8
90	.943,-4	.918,-5	.315,-6	.211,-8	.109,-10	.329,-3	.480,-4	.202,-5	.148,-7	.141,-9
120	.151,-4	.862,-6	.196,-7	.960,-10	.421,-12	.363,-3	.338,-4	.109,-5	.713,-8	.367,-10
150	.474,-5	.207,-6	.387,-8	.165,-10	.677,-13	.577,-3	.518,-4	.162,-5	.105,-7	.621,-10
180	.320,-5	.129,-6	.227,-8	.930,-11	.373,-13	.667,-3	.593,-4	.184,-5	.119,-7	.232,-9

	POLARIZED BORN					POLARIZED B-O				
0	.582,-2	.118,-1	.194,-1	.288,-1	.363,-1	.209,-1	.236 -1	.253,-1	.306,-1	.367,-1
15	.493,-2	.847,-2	.913,-2	.485,-2	.130,-2	.135,-1	.976,-2	.832,-2	.517,-2	.148,-2
30	.276,-2	.270,-2	.126,-2	.171,-3	.833,-5	.598,-2	.305,-2	.144,-2	.228,-3	.113,-4
45	.117,-2	.625,-3	.131,-3	.566,-5	.104,-6	.299,-2	.115,-2	.216,-3	.917,-5	.154,-6
60	.431,-3	.132,-3	.141,-4	.290,-6	.335,-8	.151,-2	.412,-3	.367,-4	.620,-6	.607,-8
90	.578,-4	.737,-5	.342,-6	.342,-8	.288,-10	.379,-3	.502,-4	.199,-5	.139,-7	.142,-9
120	.111,-4	.842,-6	.261,-7	.201,-9	.160,-11	.383,-3	.339,-4	.105,-5	.656,-8	.307,-10
150	.388,-5	.225,-6	.579,-8	.405,-10	.321,-12	.586,-3	.515,-4	.159,-5	.100,-7	.577,-10
180	.271,-5	.145,-6	.353,-8	.240,-10	.191,-12	.674,-3	.590,-4	.181,-5	.115,-7	.225,-9

T6.4c A_{1-1} For the 3d State

	BORN					BORN-OPPENHEIMER				
θ° E(eV)	20	30	50	100	200	20	30	50	100	200
0	-.269,-1	-.477,-1	-.673,-1	-.837,-1	-.924,-1	-.659,-1	-.782,-1	-.817,-1	-.879,-1	-.935,-1
15	-.104,-1	-.527,-3	-.328,-4	-.468,-2	-.159,-2	-.339,-1	-.649,-2	.181,-2	-.463,-2	-.175,-2
30	-.104,-2	+.504,-3	-.387,-3	-.101,-3	-.440,-5	-.859,-2	.971,-3	.615,-4	-.109,-3	-.578,-5
45	-.375,-4	.865,-4	-.155,-4	-.132,-5	-.223,-7	-.200,-2	.297,-3	.479,-4	-.545,-6	-.290,-7
60	-.173,-4	.186,-4	+.495,-6	-.110,-7	-.163,-9	-.381,-3	.557,-4	.825,-5	.962,-7	.503,-9
90	-.231,-4	-.361,-6	.114,-7	.137,-9	+.798,-12	-.215,-4	-.119,-5	-.651,-7	-.126,-8	-.452,-10
120	-.121,-4	-.511,-6	-.931,-8	-.391,-10	-.159,-12	-.551,-3	-.517,-4	-.173,-5	-.119,-7	-.132,-10
150	-.712,-5	-.293,-6	-.528,-8	-.220,-10	-.888,-13	-.104,-2	-.942,-4	-.296,-5	-.192,-7	-.119,-9
180	-.588,-5	-.237,-6	-.417,-8	-.171,-10	-.687,-13	-.123,-2	-.109,-3	-.338,-5	-.219,-7	-.427,-9

	POLARIZED BORN					POLARIZED B-O				
0	-.107,-1	-.216,-1	-.358,-1	-.530,-1	-.667,-1	-.385,-1	-.434,-1	-.464,-1	-.563,-1	-.676,-1
15	-.340,-2	+.347,-3	-.143,-4	-.176,-2	-.705,-3	-.211,-1	-.480,-2	.105,-2	-.173,-2	-.806,-3
30	-.482,-5	.267,-3	-.188,-3	-.590,-4	-.369,-5	-.634,-2	.220,-3	.134,-3	-.653,-4	-.496,-5
45	.135,-3	.546,-4	-.104,-4	-.114,-5	-.276,-7	-.169,-2	.137,-3	.415,-4	-.397,-6	-.274,-7
60	.480,-4	.155,-4	.443,-6	-.123,-7	-.269,-9	-.319,-3	.346,-4	.737,-5	.990,-7	.502,-9
90	-.602,-5	.197,-6	.226,-7	.223,-9	+.212,-11	-.400,-4	-.187,-5	-.564,-7	-.897,-9	-.379,-10
120	+.768,-5	-.446,-6	-.115,-7	-.818,-10	-.603,-12	-.574,-3	-.518,-4	-.169,-5	-.113,-7	-.105,-10
150	-.567,-5	-.313,-6	-.782,-8	-.538,-10	-.421,-12	-.106,-2	-.937,-4	-.291,-5	-.185,-7	-.111,-9
180	-.497,-5	-.266,-6	-.649,-8	-.442,-10	-.351,-12	-.124,-2	-.108,-3	-.332,-5	-,211,-7	-.413,-9

T6.4c A_{1-1} for the 3d state

DWPO I

θ° \ E(eV)	20	30	50	100	200
0	-.254,-1	-.558,-1	-.777,-1	-.929,-1	-.973,-1
15	-.101,-1	-.157,-2	+.808,-3	-.363,-2	-.134,-2
30	-.332,-2	-.831,-3	-.709,-3	-.658,-4	.146,-6
45	-.289,-2	-.135,-2	-.143,-3	-.193,-5	.417,-7
60	-.158,-2	-.684,-3	-.788,-5	-.216,-6	-.618,-7
90	-.741,-5	-.593,-5	-.203,-5	-.419,-7	-.255,-7
120	-.540,-3	-.923,-4	-.141,-4	-.149,-5	-.804,-7
150	-.315,-3	-.136,-4	.777,-6	+.140,-6	+.524,-9
180	-.219,-3	-.729,-4	-.234,-4	-.742,-6	-.122,-7

DWPO II

0	-.113,-1	-.261,-1	-.417,-1	-.591,-1	-.698,-1
15	-.579,-2	-.107,-2	.234,-3	-.133,-2	-.608,-3
30	-.399,-2	-.125,-2	-.533,-3	-.545,-4	-.556,-6
45	-.344,-2	-.141,-2	-.144,-3	-.320,-5	+.253,-7
60	-.177,-2	-.684,-3	-.639,-5	+.143,-7	-.295,-7
90	-.822,-5	-.899,-5	-.387,-5	-.170,-6	-.382,-8
120	-.562,-3	-.101,-3	-.118,-4	-.123,-5	-.645,-7
150	-.330,-3	-.143,-4	.730,-6	+.160,-6	.269,-8
180	-.231,-3	-.752,-4	-.211,-4	-.490,-6	-.988,-8

T6.4d Real Part of A_{01} for the 3d state

DWPO I

20	30	50	100	200
0	0	0	0	0
-.382,-2	-.102,-1	-.968,-2	-.332,-2	-.498,-3
-.159,-2	-.253,-2	-.100,-2	-.104,-3	-.557,-5
+.438,-3	-.163,-4	.227,-4	.252,-5	-.447,-7
.893,-3	.361,-3	.352,-4	.844,-6	-.681,-7
.676,-4	-.218,-6	-.426,-6	.132,-6	-.248,-8
-.545,-4	-.582,-6	-.103,-5	-.180,-6	-.868,-8
-.120,-6	-.275,-4	-.757,-5	-.658,-6	-.158,-7
0	0	0	0	0

DWPO II

0	0	0	0	0
-.793,-3	-.367,-2	-.362,-2	-.125,-2	-.219,-3
.355,-3	-.642,-3	-.363,-3	-.569,-4	-.399,-5
.112,-2	+.292,-3	.729,-4	.472,-5	+.144,-6
.110,-2	+.403,-3	.416,-4	.137,-5	-.873,-8
.999,-4	.626,-5	-.104,-6	.136,-6	0
-.570,-4	-.140,-6	-.980,-6	-.187,-6	-.126,-7
-.246,-6	-.273,-4	-.782,-5	-.731,-6	-.274,-7
0	0	0	0	0

T6.4d Real Part of A_{01} for the 3d State

	BORN					BORN-OPPENHEIMER				
θ° E(eV)	20	30	50	100	200	20	30	50	100	200
0	0	0	0	0	0	0	0	0	0	0
15	-.524,-2	-.102,-1	-.915,-2	-.315,-2	-.488,-3	-.519,-2	-.109,-1	-.922,-2	-.303,-2	-.465,-3
30	-.347,-2	-.295,-2	-.954,-3	-.731,-4	-.211,-5	-.215,-2	-.228,-2	-.732,-3	-.550,-4	-.159,-5
45	-.134,-2	-.559,-3	-.773,-4	-.199,-5	-.235,-7	.196,-3	.130,-5	-.339,-5	-.148,-6	-.221,-8
60	-.432,-3	-.985,-4	-.718,-5	-.937,-7	-.705,-9	.573,-3	.150,-3	.115,-4	.150,-6	.113,-8
90	-.438,-4	-.430,-5	-.145,-6	-.958,-9	-.489,-11	.873,-4	.156,-4	.680,-6	.479,-8	.371,-10
120	-.610,-5	-.374,-6	-.874,-8	-.435,-10	-.192,-12	-.836,-4	-.755,-5	.232,-6	-.143,-8	-.117,-10
150	-.116,-5	-.565,-7	-.112,-8	-.493,-11	-.205,-13	-.625,-4	-.520,-5	-.144,-6	-.791,-9	-.568,-11
180	0	0	0	0	0	0	0	0	0	0

	POLARIZED BORN					POLARIZED B-O				
0	0	0	0	0	0	0	0	0	0	0
15	-.200,-2	-.396,-2	-.347,-2	-.119,-2	-.216,-3	-.148,-2	-.409,-2	-.341,-2	-.110,-2	-.199,-3
30	-.130,-2	-.113,-2	-.412,-3	-.428,-4	-.177,-5	.209,-3	-.354,-3	-.196,-3	-.262,-4	-.126,-5
45	-.544,-3	-.259,-3	-.460,-4	-.172,-5	-.291,-7	.957,-3	.299,-3	.266,-4	.106,-4	-.725,-8
60	-.201,-3	-.569,-4	-.555,-5	-.105,-6	-.116,-8	.731,-3	.184,-3	.130,-4	.140,-6	.725,-9
90	-.268,-4	-.345,-5	-.158,-6	-.155,-8	-.130,-10	.747,-4	.152,-4	.684,-6	.487,-8	.326,-10
120	-.450,-5	-.365,-6	-.116,-7	-.910,-10	-.727,-12	-.901,-4	-.758,-5	-.218,-6	-.122,-8	-.851,-11
150	-.951,-6	-.614,-7	-.167,-8	-.121,-10	-.971,-13	-.643,-4	-.514,-5	-.138,-6	-.705,-9	-.480,-11
180	0	0	0	0	0	0	0	0	0	0

T6.4e Imaginary Part of A_{ol} for the 3d State

	DWPO I					DWPO II				
θ° \ E(eV)	20	30	50	100	200	20	30	50	100	200
0	0	0	0	0	0	0	0	0	0	0
15	-.837,-4	.163,-3	.977,-3	.865,-3	.280,-3	.156,-3	.185,-3	.395,-3	.331,-3	.121,-3
30	.899,-4	.321,-3	.337,-3	.802,-4	.583,-5	.262,-3	.228,-3	.173,-3	.442,-4	.432,-5
45	.163,-3	.153,-3	.411,-4	.229,-5	-.258,-6	.308,-3	.162,-3	.415,-4	.315,-5	.335,-7
60	.163,-3	.606,-4	-.525,-5	-.219,-5	-.202,-6	.294,-3	.107,-3	.642,-5	-.925,-6	-.879,-7
90	.102,-3	.415,-4	.110,-5	.898,-8	-.155,-7	.103,-3	.365,-4	.662,-6	.442,-7	-.433,-8
120	-.415,-4	-.109,-4	.281,-6	-.108,-6	-.167,-7	-.500,-4	-.967,-5	.290,-6	-.625,-7	-.104,-7
150	-.254,-4	.456,-5	-.138,-5	-.400,-7	.620,-8	-.179,-4	.385,-5	.878,-6	-.150,-7	.535,-8
180	0	0	0	0	0	0	0	0	0	0

direction - thereafter the results increase to zero again by the backward direction. In both the Born and polarized-Born models, the forward minimum deepens with increasing energy. In the forward direction the polarized-Born results are significantly smaller (in absolute terms) than the Born although the position is reversed for energies above 50 eV with θ above 90^{o}. The results in the remaining four models all show an initial minimum in the very near forward direction which deepens to its lowest value at about 30 eV and then decreases with increasing energy. This minimum is followed by a peak at about 45^{o} and then a second minima at about 120^{o}. The B-O and DWPO results are very similar when the models which exclude core polarization and then the models which include polarization are compared in the near forward direction. This is not so at higher angles where the DWPO I and II and the B-O and 'polarized-B-O' results are closer together than the DWPO and B-O models results. The B-O approximations results, at higher energies, tend to zero only slightly less slowly than the Born results while the approach of the DWPO results to zero at 180^{o} is clearly more steep when compared with the Born results. The effect of polarization is seen to be to deepen the initial minima and enhance the subsequent peak.

Finally, T6.4e shows the results in the DWPO I and II models for the imaginary part of A_{o1}. The initial minimum in the DWPO I model vanishes and the peak at about 45^{o} - 60^{o} at 20 eV advances to the forward direction with increasing energy. Additional maxima and minima arise at higher energies with all the results returning to zero in the backward direction. The DWPO II results do not have this initial minimum but otherwise show the same behaviour although beyond about 15^{o} for energies above 30 eV the DWPO II results lie lower than the DWPO I results.

6.5 Summary

In this chapter, the results for the orientation and alignment and coincidence parameters have been presented. For the 3p states, the

effect of the DWPO model is most evident in the parameter λ where an intermediate peak occurs and which does not arise in the Born or Born-Oppenheimer approximations. The effect of core polarization is only slight (as it is for the differential cross sections presented in Chapter 4) and tends to flatten any features. The results indicate that high levels of sensitivity are required in any experimental studies of the coincidence rate. For the 3d results, the DWPO models give values for large angles which are orders of magnitude larger than the Born results for the A_{oo}, A_{11} and A_{1-1} (in absolute terms) parameters. For the A_{oo} and $A_{1,-1}$ parameters, the DWPO models show a trough and peak respectively which do not occur in the Born approximations. The effect of core polarization on all the results is most noticeable at low angles where it causes a reduction of about a factor of two, but towards the backward direction is only slight.

Whether the DWPO models do give an accurate account of the orientation and alignment and coincidence parameters for any range of energies it is not possible to say until other models are tested and the experimental phenomena studied. In view of the results for the $n = 2$ states of hydrogen (discussed elsewhere: papers III, IV and V) and the criticisms of the DWPO model discussed in Chapter 4, the results are known to be less reliable at angles $\theta > 60^{o}$ and for higher energies. However the results are significantly different from the Born results at all energies considered and confirm the unreliability of the Born approximation when calculating these parameters. Work on the differential cross sections for the $n = 2$ states strongly suggests that the inclusion of distortion in the final channel could dramatically improve the results, whereas distortion in this work is only allowed in the initial channel. A development of this work along this line should therefore provide further useful information about the scattering process.

CHAPTER 7

ASYMMETRY OF Hα RADIATION

7.1 Background to the Asymmetry problem

Mahan (1974), in his experimental work on the excitation of the n = 3 levels of hydrogen, recognised that Stark mixing of the magnetic substates of that level could be important. The effect of Stark mixing would be to distort the Hα signal through cross population between states. Only 12% of the 3p state decays with Hα radiation and 88% decays via 4β. The 3s and 3d states emit Hα only on decay. Furthermore, the 3p cross section dominates the excitation process as has been shown earlier. Therefore any cross population out of the 3p state into the 3s or 3d states would be expected to strongly enhance the Hα signal.

The electric field strength required to mix the substates depends mainly on the energy splitting of the states. Referring to the level structure diagram (Figure F7.1), it can be seen that the nearly degenerate pairs of states $P_{3/2} - D_{3/2}$ and $S_{1/2} - P_{1/2}$ are therefore the most important for this mixing effect. Additionally, for an electric field parallel to the electron beam axis, which is assumed to be the situation here, only magnetic substates with the same value for M_J are Stark mixed and therefore only these states need be considered.

Using time dependent perturbation theory Mahan considered the effects on radiation from levels coupled by an electric field and found that fields of 0.1 - 0.2 Volts/cm were the maximum tolerable experimentally. To detect any stray fields in the experimental apparatus, Mahan then applied a known field in three orthogonal directions to the interaction region, using the principle that minimum signal occurs at an overall zero field strength. By observing the position of the minimum signal versus the applied field strength any offset of the minimum implied a stray field which then could be eliminated.

Figure F7.1 Energy level diagram for the n = 3 states of Hydrogen - showing fine structure

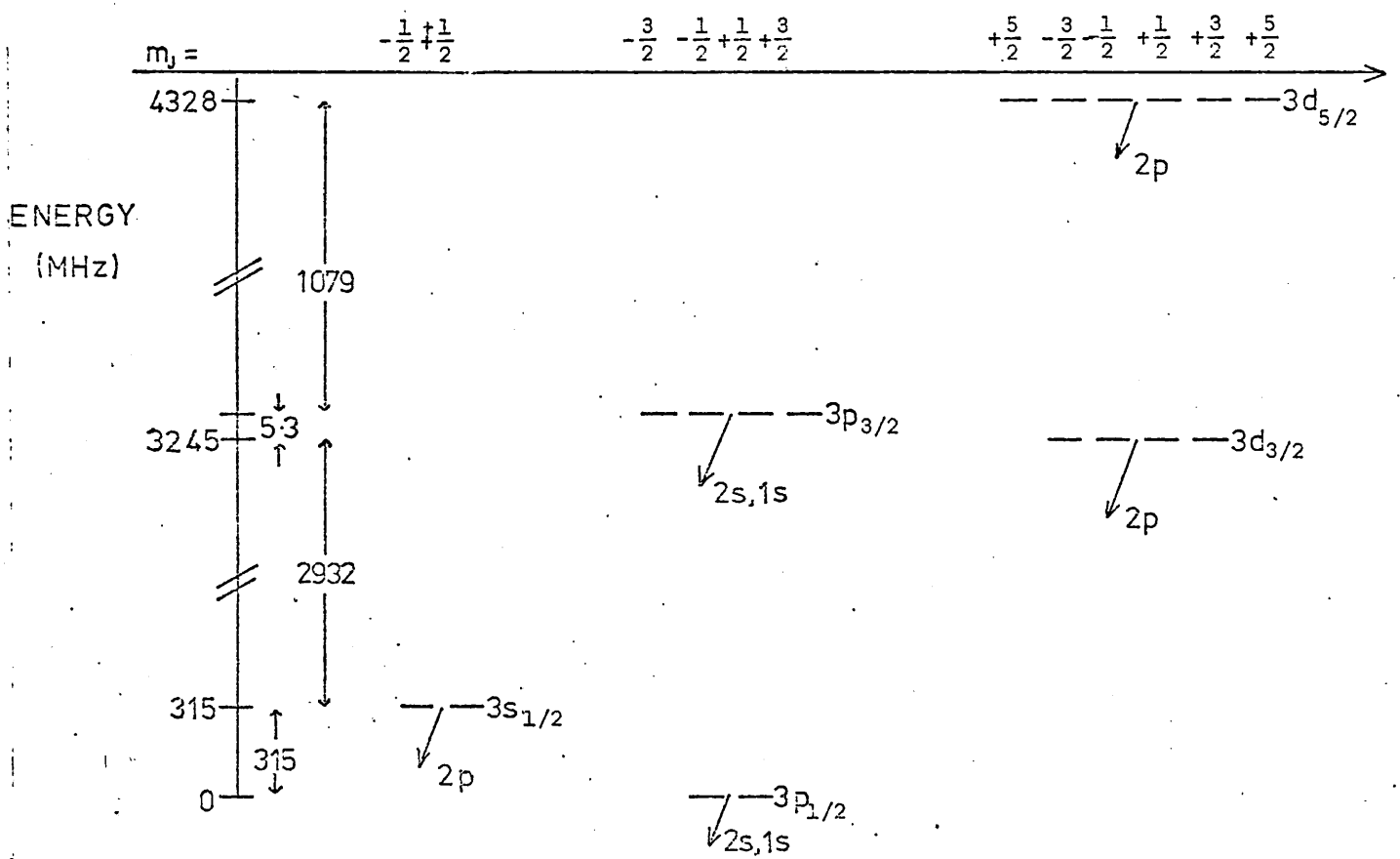

Lifetime τ (nsec)	158·4	5·273	15·46
Transition probability (sec^{-1})	6·313,6	2·245,7	6·467,7

Unexpectedly, when Mahan applied electric fields up to ± 30 V/cm along the beam axis, a strong asymmetry upon sign reversal of the field, as illustrated in Figure F7.2, was observed. It had been assumed that the process involved required that one electron excited one atom to one state only which in turn was Stark mixed by the electric field into a pair of mixed states. The resulting radiation intensity would then be proportional to the square of the electric field and a symmetric intensity curve would be expected. The asymmetry was explained by assuming that a coherent excitation of magnetic substates $n\ell JM_J$ and $n\ell{+}1JM_J$, with a relative non-random phase of excitation could be mixed coherently into each other by the field.

We have repeated the theoretical analysis of Mahan (Thesis 1974) (and see also Smith et al. (1975) and Krotkov (1975)) to eliminate inconsistencies in Mahan's thesis. Using a specially written computer program (ASYM) we have produced calculations of the asymmetry in both the Born approximation (to check with Mahan's work) and the Polarized Born approximation. For the latter we have used the generalised analytic forms derived for the polarized Born scattering amplitudes and described in Chapter 2 of this thesis. These analytic forms were used since both the computed models which include core polarization (DWPO II and PBO) for the $3\ell m$ cross sections had tended to the corresponding $3\ell m$ polarized Born cross sections at energies below 200 eV and therefore can be considered to represent satisfactorily the effect of including (as above) core polarization in any model of the excitation process. Similarly, the DWPO I and BO cross sections have tended to the Born approximation by 200 eV and therefore the analytic Born scattering amplitudes were used in the computations here instead of the DWPO I model. The Hα signal profile was calculated for impact electron energies of 200 eV and 500 eV using the formulation outlined below and the results compared with Mahan's experimental data.

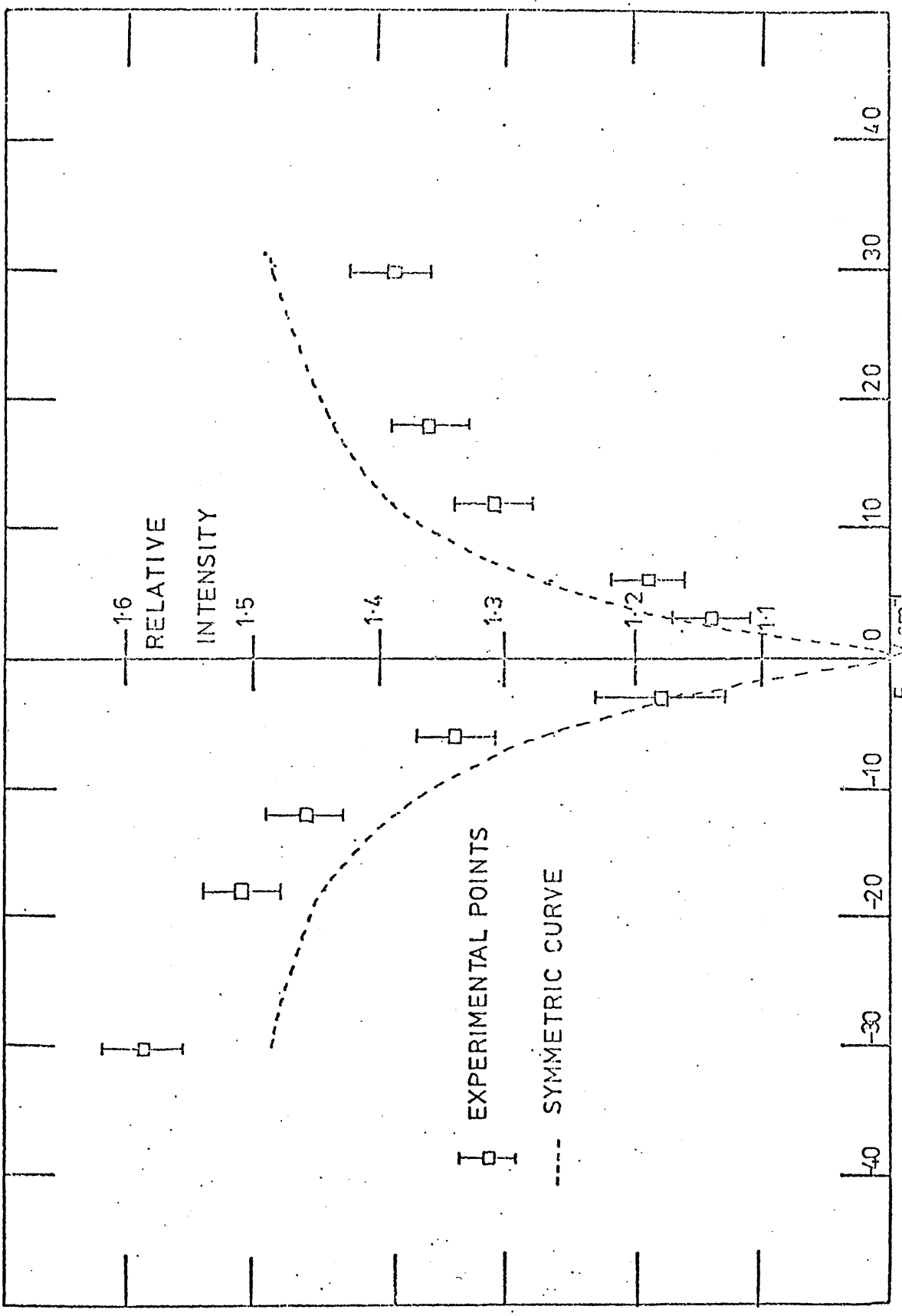

FIGURE F7·2 THE OBSERVED ASYMMETRY ON SIGN REVERSAL OF THE APPLIED ELECTRIC FIELD

7.2 The Calculation of the Hα Signal Intensity

The formulation of Percival and Seaton (1958) as used in the case of polarization of Hα is followed (see also Chapter 5). Three atomic energy levels a, b and c with states α, β and γ are identified and the total intensity of the Hα radiation is given by:

$$I_{TOT} = \int_0^\infty I(t)\, dt$$

$$\sim \frac{1}{k_i^2} \int_{\hat{k}} \sum_{\substack{\alpha,\gamma,\delta \\ \beta,\beta'}} \int_0^\infty F_{\beta\beta'}(\alpha,\hat{k})\, A_{\beta\delta\beta'\delta}(E,t) G_{\delta\gamma}(\hat{e}) dt \; k d\hat{k} d\phi \qquad (7.1)$$

The terms F, A and G may be considered to describe the three processes: coherent excitation; electric field mixing; and decay to lower states with the emission of radiation, in turn. The states δ represent the states into which the electric field mixes the excited states β and β'. The excitation density matrix is expressed in terms of scattering amplitudes:

$$F_{\beta\beta'}(\alpha,\hat{k}) \sim f_\beta(\alpha,\hat{k})\, f^*_{\beta'}(\alpha,\hat{k}) \qquad (7.2)$$

where $f_\beta(\alpha,\hat{k})$ is the scattering amplitude for electron impact excitation of an atom from the initial state, α, to the excited, β or β', with a momentum change vector in the direction $\hat{k}$. These JM_J scattering amplitudes are calculated from the vector coupled LM_L excitation amplitudes and here the Born or polarized-Born scattering amplitudes are used (see Chapter 2). It is important that the relative phases of excitation are maintained throughout the calculation. Mathematically, by allowing for different excited states, β and β', the possibility of coherent excitation is already included. However, in hydrogen the only physically possible mechanism for coherence to occur in the absence of an electric field is for the excited states, β and β', to have the same orbital angular momentum

(e.g. states $P_{3/2}$ and $P_{1/2}$) and then these states can radiate with decay to the same final state - if however β and β' have different L values the two states cannot decay to the same state. But the fine structure splittings of the $n = 3$ sub-levels of hydrogen are so large that any initial relative phasing is lost during the radiation process and thus no coherence effects are observable experimentally in the absence of any electric fields.

In the presence of an external electric field, the two states, β and β', can have different L values because then the possibility exists that they can be mixed into the same state, δ, which decays to the state γ and, provided the initial relative phases of these states for all atoms in the atom beam are non-randomly distributed then the coherence condition of having one state break into two or more intermediate states and recombine into one final state is satisfied. For this reason the density matrix includes the term:

$$A_{\beta\delta\beta'\delta}(\underline{E},t) \sim a_{\beta\delta}(\underline{E},t)\, a^{*}_{\beta'\delta}(\underline{E},t) \qquad (7.3)$$

where the functions $a_{\beta\delta}(\underline{E},t)$ describe the time development of the amplitudes of the states coupled by an external electric field. Bethe and Salpeter (1957, p288) have obtained, from time-dependent pertubation theory, the differential equations coupling the amplitudes, b_1 and b_2, of two states:

$$\frac{\partial b_1}{\partial t} = \left(\frac{-iE_1}{\hbar} - \frac{\Gamma_1}{2}\right) b_1(t) - \frac{i}{\hbar} \langle u_1|V|u_2\rangle\, b_2(t) \qquad (7.4)$$

and

$$\frac{\partial b_2}{\partial t} = -\frac{i}{\hbar} \langle u_2|V|u_1\rangle\, b_1(t) + \left(\frac{-iE_2}{h} - \frac{\Gamma_2}{2}\right) b_2(t) \qquad (7.5)$$

where E_i is the energy of the i^{th} state ($i = 1$ or 2), Γ_i is the reciprocal lifetime and $\langle u_1|V|u_2\rangle = \langle u_1|eE_z|u_2\rangle$ is the Stark mixing element between amplitudes of the two states. The solutions to these equations are detailed in appendix AXI.

The radiation matrix elements connecting the Stark mixed δ levels and the final γ states are given by:

$$G_{\delta\gamma}(\hat{\underline{e}}) \propto g_{\delta\gamma}(\hat{\underline{e}})\, g^{*}_{\delta\gamma}(\hat{\underline{e}}) \qquad (7.6)$$

where $g_{\delta\gamma}(\hat{\underline{e}})$ is the radiation matrix element giving the transition probability in sec^{-1} for emission of an $\hat{\underline{e}}$ photon by an atom in the excited state δ decaying into the final state γ. Thus this matrix includes here the transition probabilities between the $n = 3$ and $n = 2$ states as given by Condon and Shortly (1963, p134) together with a correction term which makes allowance for the experimental arrangement whereby radiation is observed perpendicular to the electron beam. If radiation is detected over the entire solid angle the intensity may be considered to arise from three electric dipoles oscillating along the x, y and z axis where the z axis is in the direction of the electron beam, the x axis is in the observed direction and the y axis is orthogonal to x and z. Viewing along the x axis means that radiation due to this x dipole is not detected and so the corresponding radiation intensity is reduced accordingly. The calculation of the appropriate reduction factors is given in appendix AXI.

The complete situation is summarized in Figure F7.3 where the three stages, treated separately, are illustrated. In Figure F7.3a the incident electron hits the target atom and, since the electric field produced by this moving charge is strong enough during the short period of the impact, the $n = 3, \ell m_\ell$ uncoupled energy levels are directly excited. The electric field strength rapidly decreases as the incident electron is scattered and then spin orbit coupling of the ℓm_ℓ excited levels takes place with the resultant fine structure levels shown with the scattering amplitudes f_β. The coherence excitation arises if two excited states with quantum numbers $(n\ell JM_J)$ and $(n\ell \pm 1 JM_J)$ are produced from the same ground state. In Figure F7.3b the coherent superposition of the two states $\beta\beta'$ are mixed exclusively into one state δ. Figure F7.3c describes the decay process with $H\alpha$

FIGURE F7·3

F7·3A COHERENCE EXCITATION

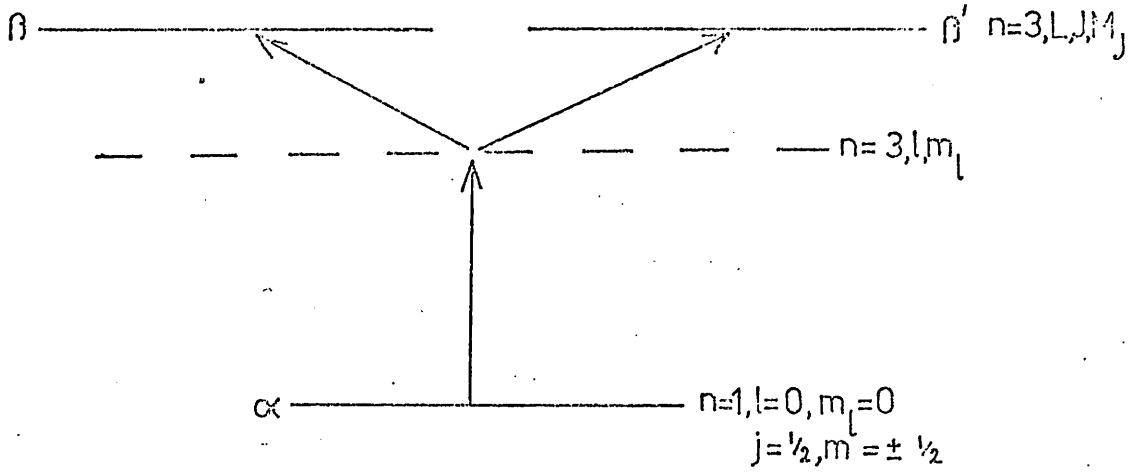

F7·3B ELECTRIC FIELD MIXING

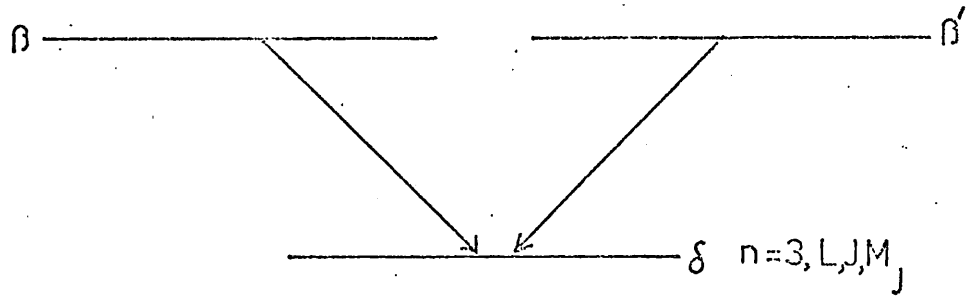

F7·3C DECAY WITH H-α EMISSION

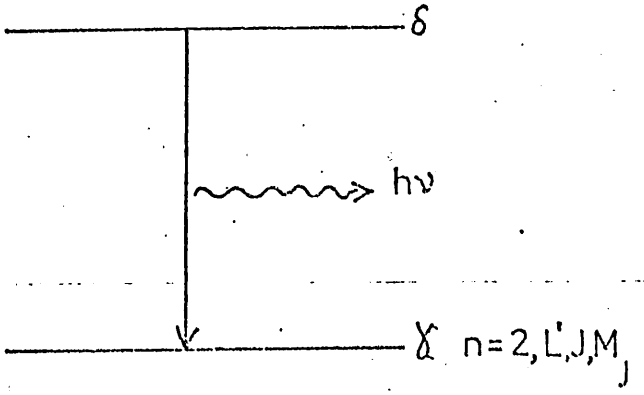

emission. The detailed derivations of elements of each of the matrices F, A and G are covered in appendix AXI. Also given are parameters relevant to the $n = 3$ splitting of hydrogen.

7.3 Computation of the Hα Signal Intensity

A computer program (ASYM) was written to evaluate the expression (7.1) on the ULCC CDC 7600 computer, specifically for the $n = 3$ states of hydrogen. For these states of hydrogen there are 18 separate possibilities for each of β, β' or δ $(\equiv 3\ell jm_j)$; α takes the values $1s\frac{1}{2} \pm \frac{1}{2}$ since the excitations are from the ground-state; and the final state γ takes the values $2\ell'j'm_j'$. The necessary parameters for the electric field mixing calculations are summarized in Table T7.1.

The program is designed for any given value of incoming electron energy and calculates the signal strength for a range of electric field strengths firstly out from zero to 50 volts cm^{-1} and then from -50 to zero volts cm^{-1}: this order of calculation being close to preserve a "base" unit signal at zero field for the intensity to which all values of the signal for non-zero fields can be related.

The essential sequence of the computation is outlined by the flow chart (Figure F7.4) and described below.

Since the excitation matrix, F, is the only function dependent on $\hat{\underline{K}}$, the integration over $\hat{\underline{K}}$ is completed separately. As explained in appendix AXI the computer program uses a numerical integration package (DOIACF) to evaluate these integrals. A check on the computation at this point is provided by comparison of the integration of the Born amplitudes with published values (Morrison and Rudge (1966), Moiseiwitsch and Smith (1968)). Agreement is exact. Furthermore, we have compared with Krotkov (private communication (1975) and P. Rev. (1975)) results of the integrals given by:

Table T7.1 Radiation Parameters for the n = 3 states of Hydrogen

State	Lifetime $T_{3\ell}$ (sec) (1)	Reciprocal Lifetime $\Gamma_{3\ell} = 1/T_{3\ell}$ (sec^{-1})	Transition Probability to a n = 2 state (sec^{-1})
3s	15.84,-8	6.313,6	6.313,6
3p	0.5273,-8	189.65,6	22.45,6
3d	1.546,-8	64.67,6	64.67,6

$$\omega_{sp}^{(2)} = \frac{E_{3s1/2} - E_{3p1/2}}{\hbar} = 1977.26,6 \text{ rad cm}^{-1} \text{ (315 MHz)}$$

$$\omega_{pd}^{(2)} = \frac{E_{3p3/2} - E_{3d3/2}}{\hbar} = 33.55,6 \text{ rad cm}^{-1} \text{ (5.3 MHz)}$$

$$f_{sp}(m_j) = 6\sqrt{2}\ m_j \frac{eE}{\hbar} = 68.22,6 \times m_j E^{(3)} \text{ rad cm}^{-1}$$

$$f_{pd}(m_j) = 0.6\sqrt{5}\ m_j \frac{eE}{\hbar} = 10.79,6 \times m_j E^{(3)} \text{ rad cm}^{-1}$$

(1) Wiese, Smith and Glennon (1966)

(2) Garcia and Mack (1965)

(3) Electric field E measured in volts cm^{-1}.

Figure I7.4 Flow Diagram for the program ASYM

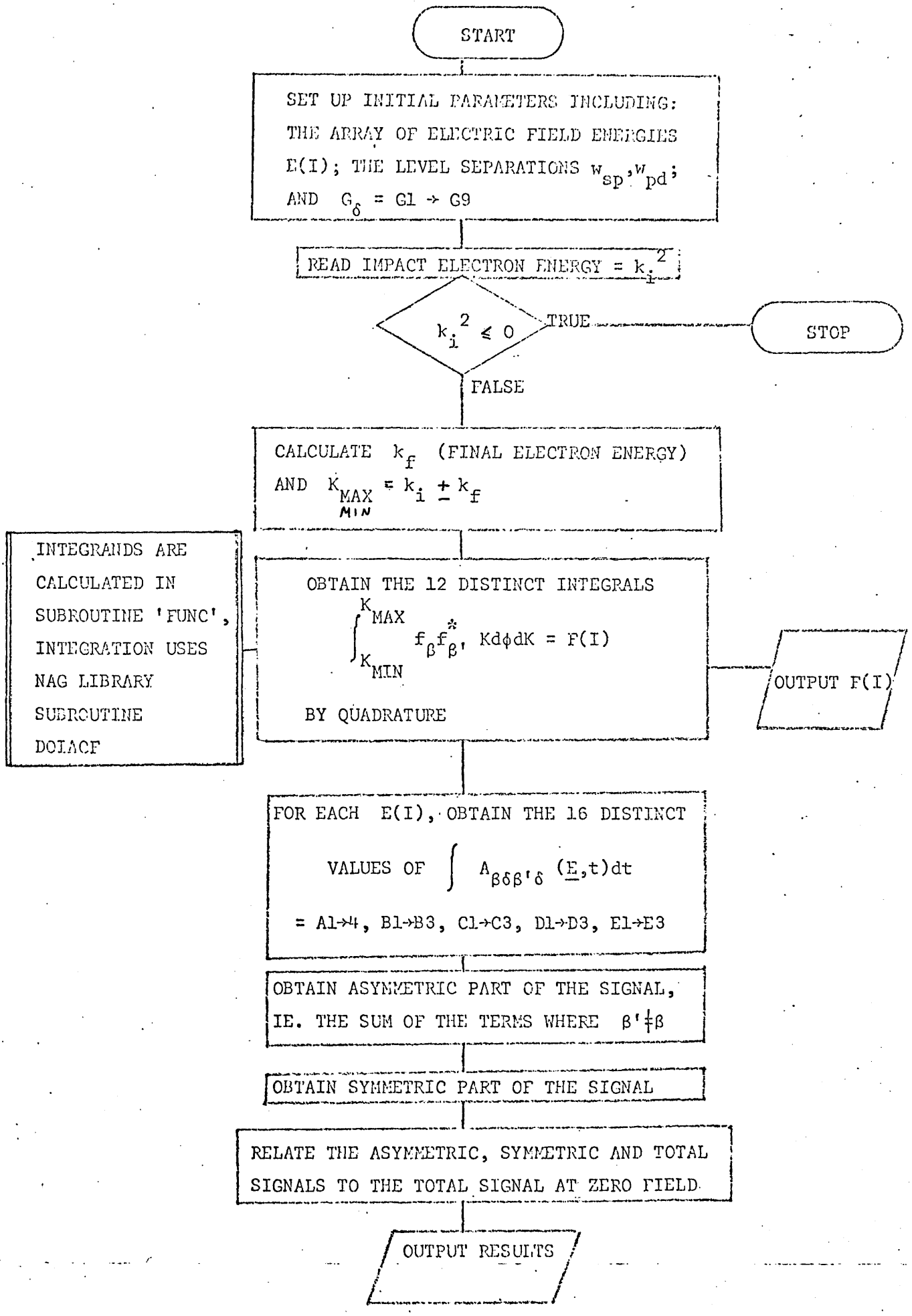

$$2\pi \int f_{\beta} \; f^{*}_{\beta'} \; KdK$$

for different values of β and β'.

Table T7.2 shows our results for the Born amplitudes at 200 eV. The non-zero mixed cross sections can also be compared with figure 4 of Krotkov (1975): again, agreement is exact. For comparison purposes, the corresponding results for the polarized-Born amplitudes at 200 eV are included in T7.2.

We have attempted to reproduce Mahan's results (as shown graphically in his thesis) of the overall asymmetry effect using Born scattering amplitudes but have not been completely successful in obtaining exact quantitative agreement. We cannot tell whether these small differences are due to rounding errors in the computation, slight differences in values of the parameters used or a combination of these effects. We do believe, in the light of the similarity of the plotted results both at 200 eV and 500 eV, that the differences are not significant and that they cannot be ascribed to computer programming or logic errors.

7.4 Results and Discussion

Results are presented in the form of graphs of change in intensity relative to that at zero field against applied field (Figures F7.5 and F7.6). The results are at impact electron energies of 200 and 500 electron volts although there is no computational restriction on the range of impact energies. The applied field ranges from - 50 volts/cm to +50 volts/cm - again there is no computational restriction on this range although it is important that the field is not so large that LS coupling breaks down. Both Born and Polarized-Born approximates for the scattering amplitudes are used.

Table T7.2 Born and Polarized Born Cross sections at 200 eV.

State β	β'	Krotkov[1] BORN X-SECTION		ASYM[2] BORN X-SECTION		ASYM[3] POLARIZED BORN X-SECTION	
$3s_{1/2}$ 1/2	↑	2.94,-3	(50%)[4]	2.94,-3	(50%)	2.92,-3	(50%)
$3p_{1/2}$ 1/2		1.35,-2	(16.7%)	1.35,-2	(16.7%)	1.21,-2	(16.7%)
$3p_{3/2}$ 1/2		1.28,-2	(15.8%)	1.28,-2	(15.8%)	1.18,-2	(16.2%)
$3p_{3/2}$ 3/2		1.42,-2	(17.5%)	1.42,-2	(17.5%)	1.24,-2	(17.1%)
$3d_{3/2}$ 1/2	β	3.27,-4	(7.5%)	3.27,-4	(7.5%)	1.56,-4	(7.9%)
$3d_{3/2}$ 3/2		5.47,-4	(12.5%)	5.47,-4	(12.5%)	2.39,-4	(12.1%)
$3d_{5/2}$ 1/2		3.06,-4	(7.0%)	3.06,-4	(7.0%)	1.44,-4	(7.3%)
$3d_{5/2}$ 3/2		4.13,-4	(9.4%)	4.12,-4	(9.4%)	1.94,-4	(9.8%)
$3d_{5/2}$ 5/2	↓	5.92,-4	(13.5%)	5.92,-4	(13.5%)	2.53,-4	(12.9%)
3s		5.87,-3 [29.6%][4]	{6.4%[4]}	5.87,-3 [29.6%]	{6.4%}	5.84,-3 [35.6%]	{7.3%}
3p		8.11,-2 [48.3%]	{88.8%}	8.11,-2 [48.3%]	{88.8%}	7.27,-2 [52.4%]	{90.3%}
3d		4.37,-3 [22.1%]	{4.8%}	4.37,-3 [22.1%]	{4.8%}	1.97,-3 [12.0%]	{2.4%}
Hα		1.98,-2 [100%]		1.98,-2 [100%]		1.64,-2 [100%]	
n = 3		9.13,-2	{100%}	9.13,-2	{100%}	8.05,-2	{100%}
$3s_{1/2}$ 1/2	$3p_{1/2}$ 1/2[5]	2.02,-3		2.02,-3		2.53,-3	
$3p_{3/2}$ 3/2	$3d_{3/2}$ 3/2	1.02,-3		1.02,-3		6.63,-4	
$3p_{3/2}$ 1/2	$3d_{3/2}$ 1/2	-1.09,-3		-1.09,-3		-6.42,-4	

1. Results under this heading are those given by Krotkov (private communication (1975))

2. Results produced by the program ASYM using the Born scattering amplitudes.

3. Results produced by the program ASYM using the analytic forms for the polarized-Born amplitudes (see Ch. 2).

4. Percentages in:( ) refer to the fraction of the $3\ell J$ cross section; in $\left[\ \right]$ that of the $H\alpha$ cross-section; in $\left\{\ \right\}$ that of the $n = 3$ total cross-section.

5. The mixed cross sections (where $\beta' \neq \beta$) are compared with values taken from Krotkov (Fig. 4 (1975)).

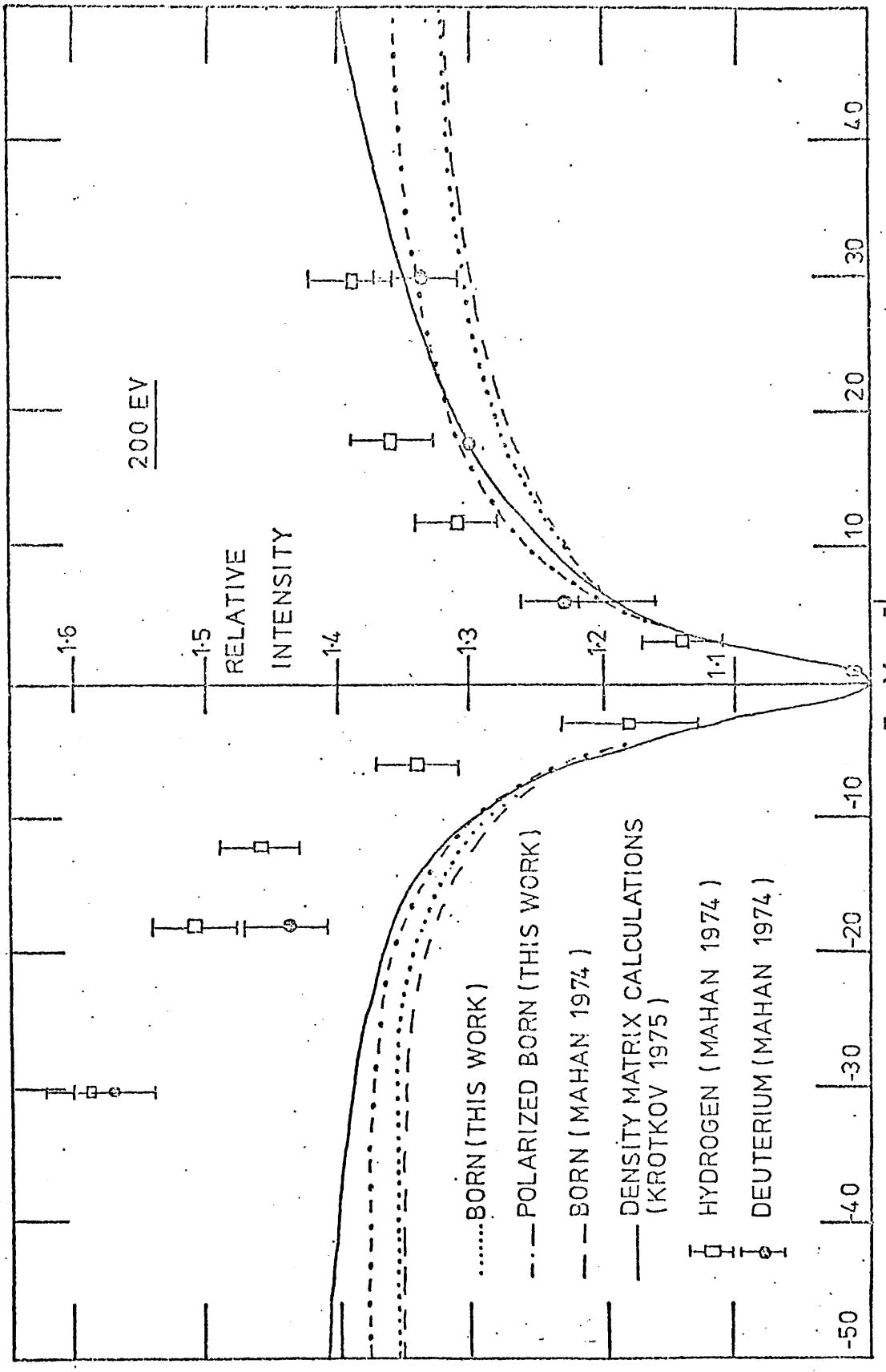

FIGURE F7·5 RELATIVE INTENSITY VS. APPLIED ELECTRIC FIELD (200EV)

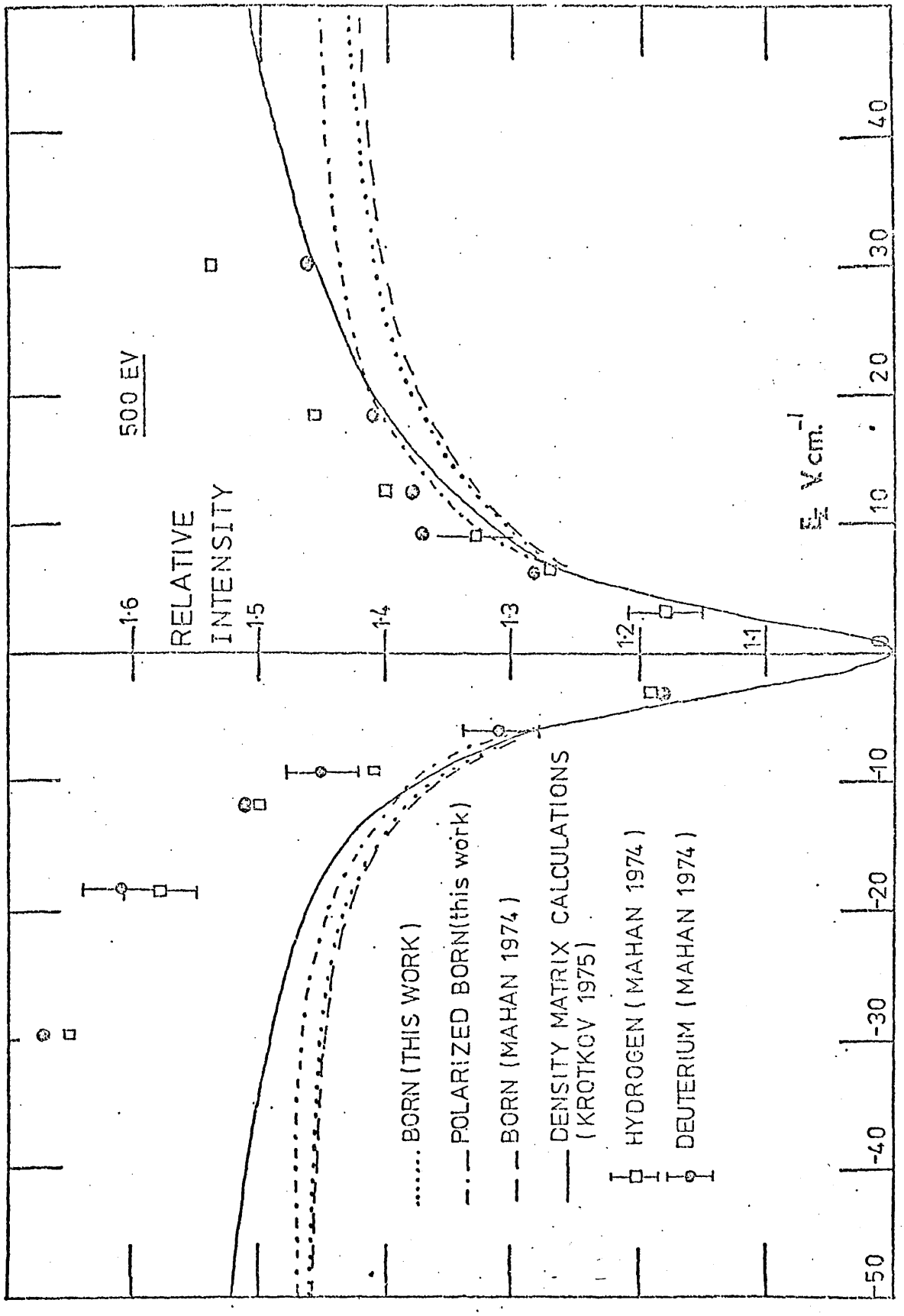

FIGURE F7·6 RELATIVE INTENSITY VS. APPLIED ELECTRIC FIELD (500 EV)

The graphs show that in all cases the predicted signal has field asymmetry in the correct direction - that is: more light is emitted for a negative than for a positive field since a negative field is directed such that it increases the kinetic energy of the impact electron. As was shown in Chapter 4: of the total cross section, the proportion due to the 3p excitation increases, at the expense of decreasing 3s and 3d proportions, with increasing impact energy although the total cross section decreases. Thus, at higher energies there exists a greater proportion of the 3p states to be mixed into 3s or 3d states which can only decay via Hα, whereas if there were a greater proportion of the latter states these would be mixed into the 3p state which is more likely to decay via H_β

For the same reason the signal intensity change is greater at 500 eV than that for 200 eV electrons.

Also shown are Mahan's theoretical and experimental results and Krotkov's theoretical results. The latter results use the description of the atom after the collision in the form of a density matrix with elements $\rho_{nn'}(\theta',\phi')$ and with a basis of a complete set of atomic states u_n such that each atom is described by

$$\psi_{\theta'\phi'} = \sum_n f_u(\theta',\phi')\, u_n;$$

so that

$$\rho_{nn'}(\theta,\phi') = f_n(\theta',\phi')\, f^*_{n'}(\theta',\phi')$$

and the $f_n(\theta',\phi')$ are the Born approximations to the scattering amplitudes. This approach includes all the possible coherent excitations.

Values for the asymmetry are presented in Tables T7.3a and T7.3b and a summary of the results is given in Table T7.4 for applied electrid fields of 30 volts cm^{-1}.

As expected, the effect of core polarization is to increase the overall intensity change while reducing the asymmetry - for the same reason that increased impact energy increases the intensity change since core polarization

Table T7.3a: Value of the asymmetric component, the symmetric component and the total Hα intensity signal - all relative to the total signal at zero applied field. Impact electron energy = 200 eV.

Electric field (Volts cm^{-1})	BORN APPROXIMATION			POLARIZED BORN APPROXIMATION		
	Asymmetric component	Symmetric component	Total signal	Asymmetric component	Symmetric component	Total signal
-50	.1561,-1	.1335,1	.1351,1	.1122,-1	.1363,1	.1374,1
-40	.1893,-1	.1332,1	.1351,1	.1360,-1	.1360,1	.1373,1
-35	.2110,-1	.1329,1	.1351,1	.1515,-1	.1357,1	.1372,1
-30	.2369,-1	.1326,1	.1349,1	.1701,-1	.1353,1	.1370,1
-25	.2674,-1	.1320,1	.1346,1	.1917,-1	.1347,1	.1366,1
-20	.3002,-1	.1310,1	.1340,1	.2148,-1	.1336,1	.1358,1
-15	.3237,-1	.1292,1	.1324,1	.2306,-1	.1318,1	.1341,1
-10	.2924,-1	.1258,1	.1287,1	.2050,-1	.1282,1	.1302,1
- 7	.1962,-1	.1219,1	.1239,1	.1320,-1	.1241,1	.1254,1
- 5	.7814,-2	.1177,1	.1184,1	.4336,-2	.1194,1	.1199,1
- 4	.7023,-3	.1146,1	.1147,1	.9547,-3	.1161,1	.1161,1
- 3	-.5882,-2	.1107,1	.1101,1	-.5777,-2	.1119,1	.1113,1
- 2	-.9609,-2	.1061,1	.1052,1	-.8320,-2	.1068,1	.1059,1
- 1	-.7636,-2	.1019,1	.1011,1	-.6379,-2	.1021,1	.1014,1
0	0.0	.1000,1	.1000,1	0.0	.1000,1	.1000,1
1	.7636,-2	.1019,1	.1026,1	.6379,-2	.1021,1	.1027,1
2	.9609,-2	.1061,1	.1071,1	.8320,-2	.1068,1	.1076,1
3	.5882,-2	.1107,1	.1113,1	.5777,-2	.1119,1	.1124,1
4	-.7023,-3	.1146,1	.1145,1	.9547,-3	.1161,1	.1162,1
5	-.7814,-2	.1177,1	.1169,1	-.4336,-2	.1194,1	.1190,1
7	-.1962,-1	.1219,1	.1200,1	-.1320,-1	.1241,1	.1228,1
10	-.2924,-1	.1258,1	.1228,1	-.2050,-1	.1282,1	.1261,1
15	-.3237,-1	.1292,1	.1260,1	-.2306,-1	.1318,1	.1295,1
20	-.3002,-1	.1310,1	.1280,1	-.2148,-1	.1336,1	.1315,1
25	-.2674,-1	.1320,1	.1293,1	-.1917,-1	.1347,1	.1327,1
30	-.2369,-1	.1326,1	.1302,1	-.1701,-1	.1353,1	.1336,1
35	-.2110,-1	.1329,1	.1308,1	-.1515,-1	.1357,1	.1342,1
40	-.1893,-1	.1332,1	.1313,1	-.1360,-1	.1360,1	.1346,1
50	-.1561,-1	.1335,1	.1320,1	-.1122,-1	.1363,1	.1352,1
Asymmetry at 30 Volts cm^{-1} :	4.74%			3.40%		

Table T7.3b: Values of the asymmetric component, the symmetric component and the total Hα intensity signal - all relative to the total signal at zero applied field. Impact electron energy = 500 eV.

Electric field (Volts cm^{-1})	BORN APPROXIMATION Asymmetric component	Symmetric component	Total signal	POLARIZED BORN APPROXIMATION Asymmetric component	Symmetric component	Total signal
-50	.1478,-1	.1439,1	.1454,1	.1121,-1	.1464,1	.1475,1
-40	.1794,-1	.1435,1	.1453,1	.1361,-1	.1459,1	.1473,1
-35	.2001,-1	.1431,1	.1451,1	.1517,-1	.1456,1	.1471,1
-30	.2250,-1	.1426,1	.1449,1	.1705,-1	.1450,1	.1467,1
-25	.2545,-1	.1418,1	.1443,1	.1928,-1	.1442,1	.1461,1
-20	.2869,-1	.1404,1	.1433,1	.2171,-1	.1428,1	.1450,1
-15	.3123,-1	.1381,1	.1412,1	.2358,-1	.1404,1	.1428,1
-10	.2907,-1	.1334,1	.1364,1	.2177,-1	.1357,1	.1379,1
- 7	.2098,-1	.1283,1	.1304,1	.1542,-1	.1304,1	.1319,1
- 5	.1074,-1	.1227,1	.1237,1	.7491,-2	.1244,1	.1252,1
- 4	.4443,-2	.1187,1	.1191,1	.2565,-2	.1202,1	.1205,1
- 3	-.1583,-2	.1137,1	.1135,1	-.2058,-2	.1148,1	.1146,1
- 2	-.5479,-2	.1078,1	.1073,1	-.4939,-2	.1085,1	.1080,1
- 1	-.4957,-2	.1024,1	.1019,1	-.4254,-2	.1026,1	.1021,1
0	0.0	.1000,1	.1000,1	0.0	.1000,1	.1000,1
1	.4957,-2	.1024,1	.1029,1	.4254,-2	.1026,1	.1030,1
2	.5479,-2	.1078,1	.1084,1	.4939,-2	.1085,1	.1090,1
3	.1583,-2	.1137,1	.1139,1	.2058,-2	.1148,1	.1150,1
4	-.4443,-2	.1187,1	.1183,1	-.2565,-2	.1202,1	.1200,1
5	-.1074,-1	.1227,1	.1216,1	-.7441,-2	.1244,1	.1237,1
7	-.2098,-1	.1283,1	.1262,1	-.1542,-1	.1304,1	.1288,1
10	-.2907,-1	.1334,1	.1305,1	-.2177,-1	.1357,1	.1335,1
15	-.3123,-1	.1381,1	.1350,1	-.2358,-1	.1404,1	.1381,1
20	-.2869,-1	.1404,1	.1376,1	-.2171,-1	.1428,1	.1407,1
25	-.2545,-1	.1418,1	.1393,1	-.1928,-1	.1442,1	.1423,1
30	-.2250,-1	.1426,1	.1404,1	-.1705,-1	.1450,1	.1433,1
35	-.2001,-1	.1431,1	.1411,1	-.1517,-1	.1456,1	.1440,1
40	-.1794,-1	.1435,1	.1417,1	-.1361,-1	.1459,1	.1446,1
50	-.1478,-1	.1439,1	.1424,1	-.1121,-1	.1464,1	.1452,1
Asymmetry at 30 Volts cm^{-1}	4.50%			3.41%		

Table T7.4 Asymmetry at 30 Volts cm^{-1} applied electriv field

200 eV impact energy	BORN	POLARIZED - BORN	EXPERIMENTAL
Mahan (2-state)	4.89%	—	19% (Hydrogen) 23% (Deuterium)
Krotkov (density matrix)	4.1%	—	—
This work (2-state)	4.74%	3.40%	—
500 eV impact energy			
Mahan (2-state)	4.64%	—	13% (Hydrogen) 19% (Deuterium)
Krotkov (density matrix)	3.7%	—	—
This work (2-state)	4.50%	3.41%	—

has been shown to increase the proportion of the 3p cross section mainly through the greatly reduced 3d contribution. Additionally, it is clear that the substitution of polarized-Born for Born scattering amplitudes should not increase the asymmetry values in Krotkov's approach.

However, none of the theoretical approximations come close to the experimental asymmetry observed by Mahan.

This disagreement between theory and experiment could be due to a number of reasons. The first is the exclusion of other off-diagonal elements in the decay matrix G but it should be noted that in the case of Hα radiation, off-diagonal elements linking states such as $3s_{\frac{1}{2}}(m_J = +\frac{1}{2})$ and $3p_{3/2}$ $(m_J = +\frac{1}{2})$ would be field independent since they are too far separated for appreciable mixing by fields of the order of ± 30 Volts/cm. Furthermore, the time integration introduces factors of the order of line width divided by separation making this contribution very small. Other levels with small separations differ in parity and therefore are not linked by the decay matrix G.

Secondly, hyperfine effects have not been considered but shifts, of the order of the hyperfine separations, in the energies of the states considered makes only a very small difference to separations between states apart from the $3^2S_{\frac{1}{2}} - 3^2P_{\frac{1}{2}}$ case where it is only 315 MHz and hyperfine splitting of the two states is 52.6 MHz and 17.5 MHz respectively. Rerunning the computer program with a shift in the separation of about 70 MHz between these states led to no appreciable change in the value of the asymmetry calculated. Full inclusion of hyperfine effects therefore is not expected to affect the results significantly.

Thirdly, the use of the Born amplitudes with or without core polarization may be in error: certainly our results for 3d excitation including core polarization would imply that other coupling effects may be important and that these amplitudes may not adequately describe the excitation process. In particular, the comments in Chapter 4 relating to models which include adiabatic polarization potentials should be considered - but against this, the fact that

even the Born approximation (which is generally expected to be useful at the energies here) fails, suggest the need for deeper study.

Fourthly, cascade contributions from $n > 4$ levels have been ignored. However Mahan quotes the total cascade contributions to the signal to be $\sim$ 10% and estimates that these raise the symmetric part of the intensity signal by only 2-3% with negligible antisymmetric contribution - thus there would be negligible effect on the total asymmetric signal.

Fifthly, it was considered whether the same account had been taken of the electric field contribution to the energy of the impact electron. The theoretical treatment has assumed an electron with an initial impact energy of k_i^2 Rydbergs in a field of E volts cm^{-1}. It is important that experimentally that the electrons selected should be those emitted with the same energy - when these electrons have passed through the interaction region with field strength E, they will have an energy $k_f'^2$ where $k_f'^2 = k_f^2 - E'$ and E' is included to take account of the effect of the electric field. However Mahan in his thesis (p.40) reports that he took into account the energy imparted to the electron by the field. The question remains whether we have the same account.

A sixth reason for the disagreement could be in the theoretical approach since we have assumed the excitation and photon emission processes to be quite distinct. However, in Chapter 5, following Percival and Seaton, we have shown that in the case of the polarization of Hα this assumption leads to ambiguities in the choice of the expressions to use and that the correct forms are obtained by calculating the probability of a photon being emitted by the complete system of atom plus electron. This could imply that the recalculation of the excitation and emission processes including hyperfine structure, as suggested in the second reason above, might lead to a similar ambiguity and that a completely different approach on the lines of Percival and Seaton from a starting point of the Bremsstrahlung formula should be followed. We feel that this might merit further study.

A final source of the discrepancy could be that the experimental results are not correct but we are not in a position to discuss this.

7.5 Summary

We have studied the asymmetry of the radiation upon sign reversal of an applied electric field following closely the work of Mahan. We have been able to closely reproduce his theoretical results in the Born approximation and have presented results in the polarized-Born approximation. We have not been able to reproduce to the full extent the experimentally observed results reported by Mahan and have discussed a number of reasons for this disagreement.

CHAPTER 8

CONCLUSIONS AND SUGGESTIONS FOR FURTHER WORK

§8.1 Conclusions

In this thesis we have generalized the DWPO method for 1s - nℓ transitions in hydrogenic systems in terms of the T-matrix elements and formulated the scattering amplitudes for the polarized Born approximation. We have applied the DWPO method to 1s - 3ℓ transitions in Hydrogen and compared our cross sections (both total and differential) with other theoretical and experimental work. These results have shown the dramatic effect of including core polarization on the 1s - 3d cross sections in particular and indicate the failure of our model to satisfactorily predict cross sections at high energies when dynamic polarization and other effects are clearly important. However the results presented for energies below 150 eV and notably for low energies above the ionization threshold are believed to be a useful addition to existing studies since we have found good agreement with recent experimental work in this region.

We have extended the formulation of polarization of emmitted radiation following excitation to include Hα radiation and presented corresponding results. We found that our model, although it gives significantly different results to the Born approximation, does not give good agreement with the existing experimental results. We have presented tables of results for the parameters describing the orientation and alignment of the atom following excitation and for the coincidence rate for 'photon-scattered electron' observations in anticipation of other work on these topics.

Finally we have re-worked through the formulation of Mahan (1974) on the asymmetry of Hα radiation and presented results in the polarized-Born approximation. These results do not improve agreement with the measured asymmetry compared with the Born approximation and we have

discussed a number of possible reasons for the failure of the theoretical models used.

§8.2 Suggestions for future study

For the theoretical approach to the problem considered here, the most useful development of this work is felt to lie in the more explicit inclusion of coupling to other states. This is particularly so following the success of the simple unitarized Born results of Somerville (1963) and for this reason we have presented some preliminary results in Appendix AXII where we have calculated the R-matrix elements in the Born approximation for large angular momentum states of the scattered electron (following Percival and Seaton, 1957, and see the series of papers starting with Seaton, 1961). By using these elements together with the R-matrix elements obtained via the DWPO model for low angular momentum states a unitarized R-matrix is obtained obeying the conservation condition which should retain the advantages of the DWPO model while including effects at present neglected.

There has not been a great deal of experimental study on the transitions of interest here despite the importance of the $H\alpha$ line. In particular we feel that coincidence experiments would go a long way to help identify the most important features of the scattering process and thus to a better understanding of the best theoretical approach.

Appendix A1.: General form for $T_{if}^{\pm}(K,m)$ in DWPO I model.

Derivation of the partial wave summation for $T_{if}^{\pm}(K)$:

$T_{if}^{\pm}(k,m)$ is defined (2.29):

$$T_{if}^{\pm}(k,m) = \langle \phi_{n\ell m}(Z,1)\ \chi_{\underline{k}_f}(z,2) \left| \frac{1}{r_{12}} - \frac{1}{r_2} \right| \mathcal{A}\, \phi_{1s}(Z,1)\ F^{\pm}(z,2) \rangle \qquad (A1.1)$$

writing

$$T_{if}^{\pm}(k,m) = (T_{D12}^{\pm} - T_{D2}^{\pm}) + (T_{E12}^{\pm} - T_{E2}^{\pm}) \qquad (A1.2)$$

where

$$T_{D12}^{\pm} = \langle \phi_{n\ell m}(Z,1)\ \chi_{\underline{k}_f}(z,2) \left| \frac{1}{r_{12}} \right| \phi_{1s}(Z,1)\ F^{\pm}(z,2) \rangle \qquad (A1.3)$$

$$T_{D2}^{\pm} = \langle \phi_{n\ell m}(Z,1)\ \chi_{\underline{k}_f}(z,2) \left| \frac{1}{r_2} \right| \phi_{1s}(Z,1)\ F^{\pm}(z,2) \rangle \qquad (A1.4)$$

(and this term is always zero by orthogonality of the hydrogenic wave functions)

$$T_{E12}^{\pm} = \langle \phi_{n\ell m}(Z,1)\ \chi_{\underline{k}_f}(z,2) \left| \frac{1}{r_{12}} \right| \phi_{1s}(Z,2)\ F^{\pm}(z,1) \rangle \qquad (A1.5)$$

and

$$T_{E2}^{\pm} = \langle \phi_{n\ell m}(Z,1)\ \chi_{k_f}(z,2) \left| \frac{1}{r_2} \right| \phi_{1s}(Z,2)\ F^{\pm}(z,1) \rangle \qquad (A1.6)$$

The expressions for $\phi_{n\ell m}(Z,1)$, $\chi_{\underline{k}_f}(z,2)$ and $F^{\pm}(z,2)$ - given by (2.12), (2.13b) and (2.28) - and that for r_{12}^{-1} - given by (2.30) - are reproduced below for ease of reference:

$$\phi_{n\ell m}(Z,1) = R_{n\ell}(Z,1)\ Y_{\ell m}(\underline{\Omega}_1) \qquad (A1.7)$$

$$\chi_{\underline{k}_f}(z,2) = 4\pi \sum_{\lambda'=0}^{\infty} i^{\lambda'} \exp(-i\eta_{\lambda'}(k_f)) H_{\lambda'}(k_f, r_2) \sum_{\mu'=-\lambda'}^{\lambda'} Y_{\lambda'\mu'}(\theta,0) Y^{*}_{\lambda'\mu'}(\underline{\Omega}_2) \qquad (A1.8)$$

$$F^{\pm}(z,2) = \sum_{\lambda=0}^{\infty} \left[\frac{4\pi(2\lambda+1)}{k_i} \right]^{\frac{1}{2}} i^{\lambda} \exp(i(\delta_{\lambda}^{\pm} + \eta_{\lambda}))\, \frac{u_{\lambda}^{\pm}(k_i, r_2)}{r_2}\ Y_{\lambda 0}(\underline{\Omega}_2) \qquad (A1.9)$$

$$\frac{1}{r_{12}} = \sum_{\lambda''=0}^{\infty} \frac{4\pi}{(2\lambda''+1)} \gamma_{\lambda''}(1,2) \sum_{\mu''=-\lambda''}^{\lambda''} Y_{\lambda''\mu''}(\underline{\Omega}_1)\, Y_{\lambda''\mu''}(\underline{\Omega}_2) \qquad \text{(A1.10)}$$

Then:

$$T_{D12}^{\pm} = \frac{(4\pi)^{5/2}}{k_i^{\frac{1}{2}}} \sum_{\lambda'} \sum_{\lambda''} \sum_{\lambda} \sum_{\mu'} \sum_{\mu''} \frac{(2\lambda+1)^{\frac{1}{2}}}{(2\lambda''+1)}\, i^{\lambda-\lambda'}\, e^{i\xi_{\lambda\lambda'}^{\pm}}\, Y^*_{\lambda'\mu'}(\theta,0) \times$$

$$\int_{\underline{\Omega}_1} Y^*_{\ell m}(\underline{\Omega}_1) Y_{\lambda''\mu''}(\underline{\Omega}_1) Y_{oo}(\underline{\Omega}_1) d\underline{\Omega}_1 \int_{\underline{\Omega}_2} Y_{\lambda'\mu'}(\underline{\Omega}_2)\, Y^*_{\lambda''\mu''}(\underline{\Omega}_2)\, Y_{\lambda 0}(\underline{\Omega}_2) d\underline{\Omega}_2 \times$$

$$\int_o^{\infty} \int_o^{\infty} r_1^2 r_2\, \gamma_{\lambda''}(1,2)\, R_{n\ell}(Z,1)\, R_{1s}(Z,1)\, H_{\lambda'}(k_f,2)\, u_{\lambda}^{\pm}(k_i,2) dr_1 dr_2 \qquad \text{(A1.11)}$$

where

$$\xi_{\lambda\lambda'}^{\pm} = \eta_{\lambda}(k_i) + \eta_{\lambda'}(k_f) + \delta_{\lambda}^{\pm}(k_i) \qquad \text{(A1.12)}$$

Now

$$\int_{\underline{\Omega}} Y^*_{\ell m}\, Y_{\lambda''\mu''}\, Y_{oo}\, d\underline{\Omega} = \frac{1}{\sqrt{4\pi}} \int_{\underline{\Omega}} Y^*_{\ell m}\, Y_{\lambda''\mu''}\, d\underline{\Omega} \qquad \text{(A1.13)}$$

$$= \frac{1}{\sqrt{4\pi}} \cdot \delta_{\ell\lambda''}\, \delta_{m\mu''}$$

by orthogonality of spherical harmonics (see Edmonds (1960)p.21 equation (2.54)) Combining this result with the integral over $\underline{\Omega}_2$ gives

$$\frac{\delta_{\ell\lambda''}}{\sqrt{4\pi}}\, \delta_{m\mu''} \int_{\underline{\Omega}_2} Y_{\lambda'\mu'}(\underline{\Omega}_2)\, Y^*_{\lambda''\mu''}(\underline{\Omega}_2)\, Y_{\lambda o}(\underline{\Omega}_2) d\underline{\Omega}_2$$

$$= (-1)^m \left[\frac{(2\ell+1)(2\lambda'+1)(2\lambda+1)}{4\pi}\right]^{\frac{1}{2}} \begin{pmatrix} \ell & \lambda' & \lambda \\ -m & \mu' & 0 \end{pmatrix} \begin{pmatrix} \ell & \lambda' & \lambda \\ 0 & 0 & 0 \end{pmatrix} \qquad \text{(A1.14)}$$

and the first of the Wigner 3-j coefficients is non-zero only if $\mu' = m$ (see Edmonds (1960) p.63, equation (4.63)) so

$$T_{D12}^{\pm} = (-1)^m \frac{(4\pi)^{3/2}}{k_i^{\frac{1}{2}}} \sum_{\lambda=0}^{\infty} \sum_{\lambda'=0}^{\infty} (2\lambda+1) \left[\frac{(2\lambda'+1)}{(2\ell+1)}\right]^{\frac{1}{2}} i^{\lambda-\lambda'}\, e^{i\xi_{\lambda\lambda'}^{\pm}}$$

$$\begin{pmatrix} \ell & \lambda' & \lambda \\ -m & m & 0 \end{pmatrix} \begin{pmatrix} \ell & \lambda' & \lambda \\ 0 & 0 & 0 \end{pmatrix} Y^*_{\lambda' m}(\theta,0) \times I^{\pm}(\lambda,\lambda') \qquad \text{(A1.15)}$$

where

$$I^{\pm}(\lambda,\lambda') = \int_o^\infty r\, f_{lsn\ell}(r)\, H_{\lambda'}(k_f,r)\, u_\lambda^{\pm}(k_i r)\, dr \qquad (A1.16)$$

as in (2.35)

with

$$r\, f_{lsn\ell}(r) = r \int_o^\infty t^2\, R_{n\ell}(Z,t)\, R_{ls}(Z,t)\, \gamma_\ell(t,r)\, dt \qquad (A1.17)$$

as in (2.36).

Similarly,

$$T_{E12}^{\pm} = \frac{(4\pi)^{5/2}}{k_i^{\frac{1}{2}}} \sum_{\lambda'} \sum_{\lambda''} \sum_{\lambda} \sum_{\mu'} \sum_{\mu''} \frac{(2\lambda+1)^{\frac{1}{2}}}{(2\lambda''+1)}\, i^{\lambda-\lambda'} e^{i\xi_{\lambda\lambda'}}\, Y^*_{\lambda'\mu'}(\theta,0) \times$$

$$\int_{\Omega_1} Y^*_{\ell m}(\Omega_1)\, Y_{\lambda''\mu''}(\Omega_1)\, Y_{\lambda o}(\Omega_1) d\Omega_1 \int_{\Omega_2} Y_{\lambda'\mu'}(\Omega_2)\, Y^*_{\lambda''\mu''}(\Omega_2)\, Y_{oo}(\Omega_2) d\Omega_2 \times$$

$$\int_o^\infty \int_o^\infty r_1 r_2^2\, \gamma_{\lambda''}(1,2)\, R_{n\ell}(Z,1)\, R_{ls}(Z,2)\, H_{\lambda'}(k_f,2)\, u_\lambda^{\pm}(k_i,1)\, dr_1 dr_2 \qquad (A1.18)$$

Now

$$\int_\Omega Y_{\lambda'\mu'}\, Y^*_{\lambda''\mu''}\, Y_{oo}\, d\Omega = \frac{1}{\sqrt{4\pi}} \int_\Omega Y_{\lambda'\mu'}\, Y^*_{\lambda''\mu''}\, d\Omega = \frac{1}{\sqrt{4\pi}} \cdot \delta_{\lambda'\lambda''}\, \delta_{\mu'\mu''} \qquad (A1.19)$$

so the result of the angular integrations becomes

$$\frac{\delta_{\lambda'\lambda''}\delta_{\mu'\mu''}}{\sqrt{4\pi}} \int_\Omega Y^*_{\ell m}\, Y_{\lambda''\mu''}\, Y_{\lambda o}\, d\Omega = \frac{1}{\sqrt{4\pi}} \int_\Omega Y^*_{\ell m}\, Y_{\lambda'\mu'}\, Y_{\lambda o}\, d\Omega$$

$$= \frac{(-1)^m}{\sqrt{4\pi}} \left[\frac{(2\ell+1)(2\ell'+1)(2\ell+1)}{4\pi}\right]^{\frac{1}{2}} \begin{pmatrix} \ell & \lambda' & \lambda \\ -m & \mu' & 0 \end{pmatrix} \begin{pmatrix} \ell & \lambda' & \lambda \\ 0 & 0 & 0 \end{pmatrix} \qquad (A1.20)$$

and, as in (A1.14), the first Wigner 3-j coefficient is non-zero only if $\mu' = m$, so

$$T_{E12}^{\pm} = (-1)^m \frac{(4\pi)^{3/2}}{k_i^{\frac{1}{2}}} \sum_{\lambda=0}^{\infty} \sum_{\lambda'=0}^{\infty} (2\lambda+1) \left[\frac{(2\ell+1)}{(2\lambda'+1)}\right]^{\frac{1}{2}} i^{\lambda-\lambda'}\, e^{i\xi_{\lambda\lambda'}} \begin{pmatrix} \ell & \lambda' & \lambda \\ -m & m & 0 \end{pmatrix}$$

$$\begin{pmatrix} \ell & \lambda' & \lambda \\ 0 & 0 & 0 \end{pmatrix} Y^*_{\lambda' m}(\theta,0) \times J^{\pm}(\lambda,\lambda') \qquad (A1.21)$$

where

$$J^{\pm}(\lambda,\lambda') = \int_o^\infty g_{ls\lambda'}(k_f,r)\, R_{n\ell}(Z,r)\, u_\lambda^{\pm}(k_i r)\, dr \qquad (A1.22)$$

as in (2.37)

with

$$g_{ls\lambda'} = r \int_o^\infty R_{ls}(Z,t)\, H_{\lambda'}(k_f,t)\, \gamma_{\lambda'}(t,r)\, t^2\, dt \qquad (A1.23)$$

as in (2.38).

Finally,

$$T_{E2}^{\pm} = \frac{(4\pi)^{3/2}}{k_i^{\frac{1}{2}}} \sum_{\lambda'} \sum_{\lambda} \sum_{\mu'} (2\lambda+1)^{\frac{1}{2}}\, i^{\lambda-\lambda'}\, e^{i\xi_{\lambda\lambda'}}\, Y^*_{\lambda'\mu'}(\theta,0) \int_{\Omega_1} Y^*_{\ell m}\, Y_{\lambda 0}\, d\Omega_1$$

$$\int_{\Omega_2} Y_{\lambda'\mu'}\, Y_{oo}\, d\Omega_2 \int_o^\infty \int_o^\infty r_1 r_2\, R_{n\ell}(Z,1)\, R_{ls}(Z,2)\, H_{\lambda'}(k_f,2)\, u_\lambda^{\pm}(k_i,1) dr_1 dr_2 \qquad (A1.24)$$

The angular integrations give $\lambda' = \mu' = 0$, $\lambda = \ell$ and $m = 0$ only

Now

$$\left.\begin{aligned} \int R_{ls}(Z,2)\, H_o(k_f,2)\, r_2 dr_2 &= 2\int_o^\infty e^{-r_2}\, j_o(k_f r_2) r_2 dr_2 && Z = 1 \\ &= \frac{2Z^{3/2}}{k_f} \int_o^\infty e^{-Zr_2}\, G_o(k_f,z,r_2) dr_2 && Z \geq 2 \end{aligned}\right\} (A1.25)$$

Considering the case when $Z = 1$ (i.e. for hydrogen)

$$\int_o^\infty R_{ls}(1,r)\, H_o(k_f,r) r dr = \frac{2}{k_f}\int_o^\infty e^{-r} \sin k_f r\, dr = \frac{2}{(1+k_f^2)} \qquad (A1.26)$$

(Dwight (1961) p.234 equation (860.80))

$$= d(0)$$

(as in (2.41))

If $Z > 1$, then writing

$$I = \frac{2Z^{3/2}}{k_f} \int_o^\infty e^{-2r}\, G_o(k_f,z,r) dr \qquad (A1.27)$$

where $G_o(k_f,z,r)$ satisfies

$$\frac{d^2G_o}{d\rho} + \left(1 - \frac{2\alpha_f}{\rho}\right)G_o = 0 \qquad \text{(A1.28)}$$

(cf Abramowitz and Stegun (1968) p.538. equation (14.1.1))

with

$$\rho = k_f r$$

$$\alpha_f = - z/k_f$$

now

$$G_o(k_f,z,r) = C_o(\alpha_f) \cdot \rho e^{-i\rho} {}_1F_1(1 - i\alpha_f, 2, 2i\rho) \qquad \text{(A1.29)}$$

(Abramowitz and Stegun (1968) p.538 equation (14.1.3))

where

$$C_o(\alpha_f) = e^{-\pi\alpha_f/2}|\Gamma(1 + i\alpha_f)| = [2\pi\alpha_f/(e^{2\pi\alpha_f} - 1)]^{\frac{1}{2}} \qquad \text{(A1.30)}$$

so

$$I = \frac{2Z^{3/2}}{k_f^2}\int_o^\infty c_o(\alpha_f)\rho\, e^{-i\rho}\, e^{-Z\rho/k_f}\, {}_1F_1(1 - i\alpha_f, 2, 2i\rho)\, d\rho \qquad \text{(A1.31)}$$

The integral:

$$J^{\lambda\mu\nu}_{\alpha\beta} = \int_o^\infty e^{-\lambda\rho}\, \rho^\nu\, {}_1F_1(\beta,\gamma,\mu\rho)\, d\rho \qquad \text{(A1.32)}$$

is convergent if $R(\lambda) > |R(\mu)|$ and is equal to

$$\Gamma(\nu+1)\, \lambda^{-\nu-1}\, F(\beta,\nu+1,\gamma,\mu/\lambda)$$

(Laudau and Lifshitz (1958) p.503 equation (f.1)): taking $\lambda = \frac{Z+ik_f}{k_f}$, $\mu = 2i$; the convergence condition is satisfied. With $\nu = 1$, $\beta = 1-i\alpha_f$, $\gamma = 2$, (A1.31) and (A1.32) are equivalent apart from outside factors and:

$$I = \frac{2Z^{3/2}}{k_f^2}\, C_o(\alpha_f) \cdot \frac{k_f^2}{(Z+ik_f)^2}\, F\left(1 - i\alpha_f, 2, 2, \frac{2ik_f}{Z+ik_f}\right).$$

Now

$$F(\beta,2,2,t) = \frac{1}{(1-t)^\beta}$$

so with

$$\beta = 1 - i\alpha_f, \quad t = \frac{2ik_f}{Z+ik_f}$$

$$I = \frac{2Z^{3/2}}{(Z+ik_f)^2} C_o(\alpha_f)\left[\frac{Z+ik_f}{Z-ik_f}\right]^{1-i\alpha_f}$$

$$= \frac{2Z^{3/2}}{(Z^2+k_f^2)} C_o(\alpha_f) \exp\left[2\alpha_f \tan^{-1}(k_f/Z)\right]$$

so

$$\int_o^\infty R_{ls}(Z,r)\, H_o(k_f,r)\, r dr = \frac{2Z^{3/2}}{(Z^2+k_f^2)} \left[\frac{2\pi\alpha_f}{(e^{2\pi\alpha_f}-1)}\right]^{\frac{1}{2}} \exp\left[2\alpha_f \tan^{-1}(k_f/Z)\right] \quad \text{(A1.33)}$$

$$= d(\alpha_f)$$

(as in (2.40))

Thus

$$T_{E2}^{\pm} = \frac{(4\pi)^{3/2}}{k_i^{\frac{1}{2}}} (2\ell+1)^{\frac{1}{2}} i^\ell e^{i\xi_{\ell o}} Y_{oo}^*(\theta,0)\, d(\alpha_f)\, K^{\pm}(\ell,0)\, \delta_{mo} \quad \text{(A1.34)}$$

where

$$K^{\pm}(\ell,0) = \int_o^\infty R_{n\ell}(Z,r)\, u_\ell^{\pm}(k_i r)\, r\, dr \quad \text{(A1.35)}$$

Collecting all the terms together

$$T_{if}^{\pm}(K,m) = (-1)^m \frac{(4\pi)^{3/2}}{k_i^{\frac{1}{2}}} \sum_{\lambda=0}^{\infty} \sum_{\lambda'=0}^{\infty} (2\lambda+1) \left[\frac{(2\lambda'+1)}{(2\ell+1)}\right]^{\frac{1}{2}} i^{\lambda-\lambda'} e^{i\xi_{\lambda\lambda'}} \begin{pmatrix} \ell & \lambda' & \lambda \\ -m & m & 0 \end{pmatrix}^{\pm}$$

$$\begin{pmatrix} \ell & \lambda' & \lambda \\ 0 & 0 & 0 \end{pmatrix} \left[I^{\pm}(\lambda,\lambda') \pm \frac{(2\ell+1)}{(2\lambda'+1)} \left(J^{\pm}(\lambda,\lambda') - \delta_{mo}\delta_{\lambda\ell}\delta_{\lambda' o}\, d(\alpha_f)\, K^{\pm}(\ell,0)\right)\right]$$

$$\times\ Y_{\lambda' m}^*(\theta,0) \quad \text{(A1.36)}$$

or, in terms of associated Legendre functions:

$$T_{if}(k,m) = \frac{4\pi}{[(2\ell+1)k_i]^{\frac{1}{2}}} \sum_{\lambda=0}^{\infty} \sum_{\lambda'=0}^{\infty} (2\lambda+1)(2\lambda'+1)\, i^{\lambda-\lambda'} e^{i\xi_{\lambda\lambda'}^{\pm}}$$

$$\begin{pmatrix} \ell & \lambda' & \lambda \\ -m & m & 0 \end{pmatrix} \begin{pmatrix} \ell & \lambda' & \lambda \\ 0 & 0 & 0 \end{pmatrix} \left[\frac{(\lambda'-|m|)!}{(\lambda'+|m|)!}\right]^{\frac{1}{2}} \times \Big[I^{\pm}(\lambda,\lambda') \pm \frac{(2\ell+1)}{(2\lambda'+1)} \left(J^{\pm}(\lambda,\lambda') - \right.$$

$$\left. \delta_{m0}\delta_{\lambda\ell}\delta_{\lambda'0}\, d(\alpha_f)\, K^{\pm}(\ell,0)\right) \Big] P_{\lambda'}^{|m|}(\cos\theta) \qquad \text{(A1.37)}$$

Appendix AII: Evaluation of $f_{1sn\ell}(r)$

The function $f_{1sn\ell}(r)$ is defined (2.36)

$$f_{1sn\ell}(r) = \int_o^\infty R_{1s}(Z,t)\, R_{n\ell}(Z,t)\, \gamma_\ell(t,r)\, t^2\, dt$$

$$= \frac{1}{r^{\ell+1}} \int_o^r t^{\ell+2}\, R_{1s}(Z,t)\, R_{n\ell}(Z,t)dt + r^\ell \int_r^\infty \frac{1}{t^{\ell-1}} R_{1s}(Z,t) R_{n\ell}(Z,t)dt$$

letting

$$f_{1sn\ell}(r) = I_1 + I_2$$

where

$$I_1 = \frac{1}{r^{\ell+1}} \int_o^r t^{\ell+2}\, R_{1s}(Z,t)\, R_{n\ell}(Z,t)\, dt$$

$$I_2 = r^\ell \int_r^\infty \frac{1}{t^{\ell-1}} R_{1s}(Z,t)\, R_{n\ell}(Z,t)\, dt$$

now

$$R_{1s}(Z,t) = 2Z^{3/2}\, e^{-Zt}$$

and

$$R_{n\ell}(Z,t) = \frac{2Z^{3/2}}{n^2} \left[(n-\ell-1)!(n+\ell)!\right]^{\frac{1}{2}} \left(\frac{2Zt}{n}\right)^\ell e^{-Zt/n}$$

$$\times \sum_{s=0}^{n-\ell-1} \frac{\left(\frac{-2Zt}{n}\right)^s}{s!(n-\ell-1-s)!(2\ell+1+s)!}$$

so, writing $x = Zt$ and $y = Zr$, $\gamma = 1 + \frac{1}{n}$

$$I_1 = \frac{Z}{y^{\ell+1}} \left(\frac{2}{n}\right)^{\ell+2} \left[(n-\ell-1)!(n+\ell)!\right]^{\frac{1}{2}} \sum_{s=0}^{n-\ell-1} \frac{\left(-\frac{2}{n}\right)^s}{(2\ell+1+s)!s!(n-\ell-1-s)!}$$

$$\times \int_o^y x^{2\ell+2+s}\, e^{-\gamma x}\, dx$$

$$I_1 = -\left(\frac{2}{n}\right)^{\ell+2} \left[(n-\ell-1)!(n+1)!\right]^{\frac{1}{2}} \frac{Z}{y^{\ell+1}} \sum_{s=0}^{n-\ell-1} \frac{\left(-\frac{2}{n}\right)^s (2\ell+2+s)}{s!(n-\ell-1-s)!}$$

$$\times \left[\frac{e^{-\gamma x}}{\gamma^{2\ell+3+s}} \sum_{p=0}^{2\ell+2+s} \frac{(\gamma x)^p}{p!} \right]_o^y$$

$$I_1 = \left(\frac{2}{n}\right)^{\ell+2} \left[(n-\ell-1)!(n+\ell)!\right]^{\frac{1}{2}} \frac{Z}{y^{\ell+1}} \sum_{s=0}^{n-\ell-1} \frac{\left(-\frac{2}{n}\right)^s (2\ell+2+s)}{s!(n-\ell-1-s)!\gamma^{2\ell+3+s}} \left[1 - e^{-\gamma y} \sum_{p=0}^{2\ell+2+s} \frac{(\gamma y)^p}{p!}\right]$$

Similarly

$$I_2 = Zy^{\ell} \left(\frac{2}{n}\right)^{\ell+2} \left[(n-\ell-1)!(n+\ell)!\right]^{\frac{1}{2}} \sum_{s=0}^{n-\ell-1} \frac{\left(-\frac{2}{n}\right)^s}{(2\ell+1+s)!s!(n-\ell-1-s)!}$$

$$x \int_y^{\infty} x^{s+1} e^{-\gamma x} dx$$

$$= -\left(\frac{2}{n}\right)^{\ell+2} \left[(n-\ell-1)!(n+\ell)!\right]^{\frac{1}{2}} Zy^{\ell} \sum_{s=0}^{n-\ell-1} \frac{\left(-\frac{2}{n}\right)^s (s+1)}{(2\ell+s+1)!(n-\ell-1-s)!}$$

$$x \left[\frac{e^{-\gamma x}}{\gamma^{s+2}} \sum_{p=0}^{s+1} \frac{(\gamma x)^p}{p!}\right]_y^{\infty}$$

$$= \left(\frac{2}{n}\right)^{\ell+2} \left[(n-\ell-1)!(n+\ell)!\right]^{\frac{1}{2}} Zy^{\ell} \sum_{s=0}^{n-\ell-1} \frac{\left(-\frac{2}{n}\right)^s (\ell+1)e^{-\gamma y}}{(2\ell+s+1)!(n-\ell-1-s)!\gamma^{s+2}} \sum_{p=0}^{s+1} \frac{(\gamma y)^p}{p!}$$

so

$$f_{1sn\ell} = \left(\frac{2}{n}\right)^{\ell+2} \left[(n-\ell-1)!(n+\ell)!\right]^{\frac{1}{2}} \frac{Z}{y^{\ell+1}} \sum_{s=0}^{n-\ell-1} \frac{\left(-\frac{2}{n}\right)^s (2\ell+2+s)}{(n-\ell-1-s)!s!\gamma^{2\ell+3+s}}$$

$$x\left(1 - e^{-\gamma y} \sum_{p=0}^{2\ell+2+s} \frac{(\gamma y)^p}{p!} + \frac{e^{-\gamma y}(s+1)!(\gamma y)^{2\ell+1}}{(2\ell+2+s)!} \sum_{p=0}^{s+1} \frac{(\gamma y)^p}{p!}\right)$$

and

$$rf_{1sn\ell}(r) = \left(\frac{2}{n}\right)^{\ell+2} \frac{\left[(n-\ell-1)!(n+\ell)!\right]^{\frac{1}{2}}}{(\gamma Zr)^{\ell}} \sum_{s=0}^{n-\ell-1} \frac{(2\ell+s+2)(-\frac{2}{n})^s}{s!(n-\ell-1-s)!\gamma^{\ell+s+3}} x$$

$$x\left\{1 - e^{-\gamma Zr}\left[\sum_{p=0}^{2\ell} \frac{(\gamma Zr)^p}{p!} + \sum_{p=2\ell+1}^{2\ell+s+2} (\gamma Zr)^p \left(\frac{1}{p!} - \frac{(s+1)!}{(2\ell+s+2)!(p-2\ell-1)!}\right)\right]\right\}$$

It is important that, for small values of r, the function $rf_{lsn\ell}(r)$ should remain bounded so that the integral $I^{\pm}_{\lambda\lambda'}$ is finite. Using the infinite expansion for $\exp(-\gamma Zr)$ leads to:-

$$rf_{lsn\ell}(r) \underset{r\to 0}{\to} \left(\frac{2}{n}\right)^{\ell+2} \frac{\left[(n-\ell-1)!(n+\ell)!\right]^{\frac{1}{2}}}{(\gamma Z)^{\ell}} \sum_{s=o}^{n-\ell-1} \frac{(2\ell+s+2)\left(-\frac{2}{n}\right)^{s}}{r^{\ell}s!(n-\ell-s-1)!\gamma^{\ell+s+3}}$$

$$\left\{ e^{-\gamma Zr} \left(\sum_{p=2\ell+s+3}^{\infty} \frac{(\gamma Zr)^{p}}{p!} - \sum_{p=2\ell+1}^{2\ell+s+2} \frac{(\gamma Zr)^{p}\,(s+1)!}{(2\ell+2+s)!(p-2\ell-1)!} \right) \right\}$$

Appendix III: Solution of Sternheimer's Equation

The equation to be solved is:

$$\left(-\frac{d^2}{dr^2} + \frac{P''_{1s}(r)}{P_{1s}(r)} + \frac{2}{r^2}\right) y = r\, P_{1s}(r)$$

with

$$P_{1s}(r) = 2Z^{3/2} r e^{-Zr}$$

Taking

$$y = \omega(Z,r)\, P_{1s}(r)$$

then

$$r^2\omega'' + 2r(1 - Zr)\omega' - 2\omega + r^3 = 0$$

Assuming a series solution for ω:

$$\omega = a_o + a_1 r + a_2 r^2 + a_3 r^3$$

gives:

$$a_3 = a_o = 0$$

$$a_2 = \frac{1}{4Z}$$

$$a_1 = \frac{1}{2Z^2}$$

so

$$y = \frac{r^2}{Z^2}\left(1 + \frac{Zr}{2}\right) e^{-Zr}$$

Appendix IV General form for $T_{if}^{\pm}(K,m)$ in DWPO II model

The transition matrix element in the DWPO II model is: (see (2.42))

$$\tilde{T}_{if}^{\pm} = T_{if}^{\pm} + \langle \phi_{n\ell m}(Z,1)\ \chi_{\underline{k}_f}(z,2)\ |V_f|\ \phi_{pol}(1,2)\ F^{\pm}(2) \rangle$$

$$= T_{if}^{\pm} + \delta T_{ifD}^{\pm} .$$

Repeating (2.43) for ease of reference

$$\phi_{pol}(1,2) = -\frac{\varepsilon(r_1,r_2)}{r_2^2} \cdot \frac{u_{1s\to p}(r_1)}{r_1}\ \frac{P_1(\cos\theta_{12})}{\sqrt{\pi}}$$

where

$$\varepsilon(r_1,r_2) = \begin{cases} 0 & r_2 \leq r_1 \\ 1 & r_2 > r_1 \end{cases}$$

and

$$P_1(\cos\theta_{12}) = \sum_{\mu=-1}^{1} \frac{4\pi}{3}\ Y_{1\mu}(\underline{\Omega}_1)\ Y^*_{1\mu}(\underline{\Omega}_2)$$

(Edmonds (1960) p.63, equation (4.66))

now

$$V_f = \frac{1}{r_{12}} - \frac{1}{r_2}$$

(note here that the term corresponding to $T_{D2}^{\pm}$ (A1.4) is not immediately equivalent to zero); because of the effect of $\varepsilon(r_1,r_2)$ on $\gamma_{\lambda''}(1,2)$ (defined equation (2.25) and see (A1.10)), $\varepsilon(r_1,r_2) \times r_{12}^{-1}$ becomes

$$\sum_{\lambda''} \sum_{\mu''} \frac{4\pi}{2\lambda''+1}\ \frac{r_1^{\lambda''}}{r_2^{\lambda''+1}}\ Y_{\lambda''\mu''}(\underline{\Omega}_1)\ Y^*_{\lambda''\mu''}(\underline{\Omega}_2)$$

and for $\lambda'' = 0$ this is simply r_2^{-1}.

Thus

$$\delta T_{ifD}^{\pm} = \sum_{\lambda''=1}^{\infty} \sum_{\mu''=-\lambda''}^{\lambda''} \frac{4\pi}{(2\lambda''+1)}\ \langle \phi_{n\ell m}(Z,1)\ \chi_{\underline{k}_f}(z,2) \left|\frac{r_1^{\lambda''}}{r_2^{\lambda''+1}}\right| \phi_{pol}(1,2)\ F^{\pm}(2)$$

$$Y_{\lambda''\mu''}(\underline{\Omega}_1)\ Y^*_{\lambda''\mu''}(\underline{\Omega}_2) \rangle$$

$$\delta T_{ifD}^{\pm} = -\sum_{\lambda''=1}^{\infty}\sum_{\mu''=-\lambda''}^{\lambda''}\sum_{\lambda'=0}^{\infty}\sum_{\mu'=-\lambda'}^{\lambda'}\sum_{\lambda=0}^{\infty}\sum_{\mu=-1}^{1}\frac{2^7\pi^3}{3k_i^{\frac{1}{2}}}\frac{(2\lambda+1)^{\frac{1}{2}}}{(2\lambda''+1)}\, i^{\lambda-\lambda'}\, x$$

$$\exp(i\xi_{\lambda\lambda'}^{\pm})\, Y^{*}_{\lambda'\mu'}(\Theta,0)\, x \int_{\underline{\Omega}_1} Y_{\lambda''\mu''}(\underline{\Omega}_1)\, Y^{*}_{\ell m}(\underline{\Omega}_1)\, Y_{1\mu}(\underline{\Omega}_1)\, d\underline{\Omega}_1 \int_{\underline{\Omega}_2} Y^{*}_{\lambda''\mu''}(\underline{\Omega}_2)\, x$$

$$Y_{\lambda'\mu'}(\underline{\Omega}_2)\, Y^{*}_{1\mu}(\underline{\Omega}_2)\, Y_{\lambda o}(\underline{\Omega}_2)\, d\underline{\Omega}_2\, x \int_0^{\infty} dr_2 \int_0^{r_2} dr_1 \frac{r_1^{\lambda''+1}}{r_2^{\lambda''+2}}\, R_{n\ell}(r_1)\, u_{1s\to p}(r_1)\, x$$

$$H_{\lambda'}(k_f,r_2)\, u_{\lambda}^{\pm}(k_i^2,r_2)$$

Writing (see Appendix AV)

$$k^{\lambda''}_{1sn\ell}(r) = -\frac{1}{r^{\lambda''+3}}\int_0^r t^{\lambda''+1}\, u_{1s\to p}(t)\, R_{n\ell}(t)\, dt$$

and

$$\delta I^{\pm}(\lambda,\lambda',\lambda'') = \int_0^{\infty} r\, k^{\lambda''}_{1sn\ell}(r)\, H_{\lambda'}(k_f,r)\, u_{\lambda}^{\pm}(k_i^2,r)\, dr$$

then

$$\delta T_{ifD}^{\pm} = \sum_{\lambda''=1}^{\infty}\sum_{\mu''=-\lambda''}^{\lambda''}\sum_{\lambda'=0}^{\infty}\sum_{\mu'=\lambda'}^{\lambda'}\sum_{\lambda=0}^{\infty}\sum_{\mu=-1}^{1}\frac{2^7\pi^3}{3k_i^{\frac{1}{2}}}\frac{(2\lambda+1)}{(2\lambda''+1)}^{\frac{1}{2}}$$

$$i^{\lambda-\lambda''}\exp(i\xi_{\lambda\lambda'}^{\pm})Y^{*}_{\lambda'\mu'}(\Theta,0)\, x \int_{\underline{\Omega}_1} Y_{\lambda''\mu''}\, Y^{*}_{\ell m}\, Y_{1\mu}\, d\underline{\Omega}_1 \int_{\underline{\Omega}_2} Y^{*}_{\lambda''\mu''}\, Y_{\lambda'\mu'}\, Y^{*}_{1\mu}\, Y_{\lambda o}\, d\underline{\Omega}_2$$

$$x\ \delta I^{\pm}(\lambda,\lambda',\lambda'').$$

Integrating over $\underline{\Omega}_1$ gives

$$\int_{\underline{\Omega}_1} Y_{\lambda''\mu''}\, Y^{*}_{\ell m}\, Y_{1\mu}\, d\underline{\Omega}_1 = (-1)^m \left[\frac{3(2\ell+1)(2\lambda''+1)}{4\pi}\right]^{\frac{1}{2}}\begin{pmatrix}\ell & 1 & \lambda''\\ -m & \mu & \mu''\end{pmatrix}\begin{pmatrix}\ell & 1 & \lambda''\\ 0 & 0 & 0\end{pmatrix}$$

Considering this result, the integration over $\underline{\Omega}_2$, and the summations over μ'' and μ:

$$\sum_{\mu''=-\lambda''}^{\lambda''}\sum_{\mu=-1}^{1}(-1)^m\left[\frac{3(2\ell+1)(2\lambda''+1)}{4\pi}\right]^{\frac{1}{2}}\begin{pmatrix}\ell & 1 & \lambda''\\ -m & \mu & \mu''\end{pmatrix}\begin{pmatrix}\ell & 1 & \lambda''\\ 0 & 0 & 0\end{pmatrix}\int Y^{*}_{\lambda''\mu''}\, Y_{\lambda'\mu'}$$

$$Y^{*}_{1\mu}\, Y_{\lambda o}\, d\underline{\Omega}_2$$

$$= \sum_{\mu''=-\lambda''}^{\lambda} \sum_{\mu=-1}^{1} \sum_{\ell'} \sum_{m'} (-1)^{m+\mu+\mu''} \frac{3(2\lambda''+1)}{4\pi} \left[(2\ell+1)(2\ell'+1)\right]^{\frac{1}{2}}$$

$$\begin{pmatrix} \ell & 1 & \lambda'' \\ -m & \mu & \mu'' \end{pmatrix} \begin{pmatrix} \ell & 1 & \lambda'' \\ 0 & 0 & 0 \end{pmatrix} \begin{pmatrix} \ell' & 1 & \lambda'' \\ m' & -\mu & -\mu'' \end{pmatrix} \begin{pmatrix} \ell' & 1 & \lambda'' \\ 0 & 0 & 0 \end{pmatrix} \times \int Y_{\lambda'\mu'} Y_{\lambda 0} Y^{*}_{\ell' m'} \, d\underline{\Omega}_2$$

$$= \sum_{\substack{\ell', m', \\ \mu'', \mu}} (-1)^{m+m'+\mu+\mu''} \frac{3(2\lambda''+1)(2\ell'+1)}{4\pi} \left[\frac{(2\ell+1)(2\lambda'+1)(2\lambda+1)}{4\pi}\right]^{\frac{1}{2}} \begin{pmatrix} \ell & 1 & \lambda'' \\ -m & \mu & \mu'' \end{pmatrix}$$

$$\begin{pmatrix} \ell & 1 & \lambda'' \\ 0 & 0 & 0 \end{pmatrix} \begin{pmatrix} \ell' & 1 & \lambda'' \\ m' & -\mu & -\mu'' \end{pmatrix} \begin{pmatrix} \ell' & 1 & \lambda'' \\ 0 & 0 & 0 \end{pmatrix} \begin{pmatrix} \lambda' & \lambda & \ell' \\ \mu' & 0 & -m' \end{pmatrix} \begin{pmatrix} \lambda' & \lambda & \ell' \\ 0 & 0 & 0 \end{pmatrix}$$

It is immediately possible to say something of the relationships between the different indices. The penultimate Wigner 3-j coefficient is non-zero only if $\mu'=m'$, futhermore $\mu+\mu'' = m' = m$ from the first and third 3-j coefficients and $\ell' + 1 + \lambda''$ and $\ell + 1 + \lambda''$ are even, from the second and fourth.

Now taking the first and third 3-j coefficients

$$\sum_{\mu''=-\lambda''}^{\lambda} \sum_{\mu=-1}^{1} (-1)^{m+\mu+\mu''} \begin{pmatrix} \ell & 1 & \lambda'' \\ -m & \mu & \mu'' \end{pmatrix} \begin{pmatrix} \ell' & 1 & \lambda'' \\ m' & -\mu & -\mu'' \end{pmatrix}$$

$$= \sum_{\mu'' \mu} (-1)^{2m+\ell'+1+\lambda''} \begin{pmatrix} \ell & 1 & \lambda'' \\ -m & \mu & \mu'' \end{pmatrix} \begin{pmatrix} \ell' & 1 & \lambda'' \\ -m' & \mu & \mu'' \end{pmatrix} = \frac{\delta_{\ell,\ell'} \delta_{mm'}}{(2\ell+1)}$$

so

$$\delta T^{\pm}_{ifD} = \sum_{\lambda''=1}^{\infty} \sum_{\lambda'=0}^{\infty} \sum_{\lambda=0}^{\infty} (-1)^{m} \frac{2^4 \pi^{3/2}}{k_i^{\frac{1}{2}}} (2\lambda+1)\left[(2\lambda'+1)(2\ell+1)\right]^{\frac{1}{2}} i^{\lambda-\lambda'}$$

$$\exp(i\xi^{\pm}_{\lambda\lambda'}) Y^{*}_{\lambda' m}(\theta,0) \, \delta I^{\pm}(\lambda,\lambda',\lambda'') \times \begin{pmatrix} \ell & 1 & \lambda'' \\ 0 & 0 & 0 \end{pmatrix}^2 \begin{pmatrix} \lambda' & \lambda & \ell \\ m & 0 & -m \end{pmatrix} \begin{pmatrix} \lambda' & \lambda & \ell \\ 0 & 0 & 0 \end{pmatrix}$$

and

$$\mathcal{T}_{if}^{\pm} = (-1)^m \frac{(4\pi)^{3/2}}{k_i^{\frac{1}{2}}} \sum_{\lambda=0}^{\infty} \sum_{\lambda'=0}^{\infty} (2\lambda+1) \left[\frac{(2\lambda'+1)}{(2\ell+1)}\right]^{\frac{1}{2}} i^{\lambda-\lambda'} \exp(i\xi_{\lambda\lambda'}^{\pm})$$

$$\begin{pmatrix} \ell & \lambda' & \lambda \\ -m & m & 0 \end{pmatrix} \begin{pmatrix} \ell & \lambda' & \lambda \\ 0 & 0 & 0 \end{pmatrix} Y^*_{\lambda' m}(\theta,0) \times \left[\mathcal{I}^{\pm}(\lambda,\lambda') \pm \frac{(2\ell+1)}{(2\lambda'+1)} \left(J^{\pm}(\lambda,\lambda') \right.\right.$$

$$\left.\left. - \delta_{m0}\, \delta_{\lambda\ell}\, \delta_{\lambda'0}\, d(\alpha_f)\, K^{\pm}(\ell,0) \right) \right]$$

with

$$\mathcal{I}^{\pm}(\lambda,\lambda') = I^{\pm}(\lambda,\lambda') + 2 \sum_{\lambda''=1}^{\infty} (2\ell+1) \begin{pmatrix} \ell & 1 & \lambda'' \\ 0 & 0 & 0 \end{pmatrix}^2 \delta I^{\pm}(\lambda,\lambda',\lambda'')$$

$$= I^{\pm}(\lambda,\lambda') + \int_0^{\infty} r \mathcal{J}_{lsn\ell}(r)\, H_{\lambda'}(k_f r)\, \mu_{\lambda}^{\pm}(k_i r)\, dr$$

and

$$\mathcal{J}_{lsn\ell}(r) = 2 \sum_{\lambda''=1}^{\infty} (2\ell+1) \begin{pmatrix} \ell & 1 & \lambda'' \\ 0 & 0 & 0 \end{pmatrix}^2 k_{lsn\ell}^{\lambda''}(r)$$

now

$$\begin{pmatrix} \ell & 1 & \lambda'' \\ 0 & 0 & 0 \end{pmatrix}^2 \begin{cases} = \dfrac{\ell}{(2\ell+1)(2\ell-1)} & \lambda'' = \ell - 1 \\ = \dfrac{(\ell+1)}{(2\ell+3)(2\ell+1)} & \lambda'' = \ell + 1 \\ = 0 & \text{otherwise} \end{cases}$$

so

$$\mathcal{J}_{lsn\ell}(r) = \frac{2\ell}{(2\ell-1)}\, k_{lsn\ell}^{\ell-1}(r) + \frac{2(\ell+1)}{(2\ell+3)}\, k_{lsn\ell}^{\ell+1}(r)$$

Recalling equations (2.35) or (A1.16), $\mathcal{I}^{\pm}(\lambda,\lambda')$ may be written

$$\mathcal{I}^{\pm}(\lambda,\lambda') = \int_0^{\infty} r(f_{lsn\ell}(r) + \mathcal{J}_{lsn\ell}(r))\, H_{\lambda'}(k_f r)\, u_{\lambda}^{\pm}(k_i r) dr$$

Appendix AV: Evaluation of $\mathcal{J}_{1sn\ell}(r)$

The function $\mathcal{J}_{1sn\ell}(r)$ is defined (2.47):

$$\mathcal{J}_{1sn\ell}(r) = \frac{2\ell}{(2\ell-1)} k^{(\ell-1)}_{1sn\ell}(r) + \frac{2(\ell+1)}{(2\ell+3)} k^{(\ell+1)}_{1sn\ell}(r) \qquad \text{(AV.1)}$$

with

$$k^{(\ell')}_{1sn\ell}(r) = -\frac{1}{r^{\ell'+3}} \int_o^r u_{1s\to p}(t)\, R_{n\ell}(Z,t)\, t^{\ell'+1} dt \qquad \ell' > 0$$

$$= 0 \qquad \ell' \leq 0 \qquad \text{(AV.2)}$$

$$u_{1s\to p}(r) = Z^{-\frac{1}{2}} r^2 e^{-Zr} \left(1 + \frac{Zr}{2}\right) \qquad \text{(AV.3)}$$

and $R_{n\ell}(Z,r)$ is as given in Appendix AII. Then putting,

$$y = Zr, \quad x = Zt, \quad \gamma = 1 + 1/n \qquad \text{(AV.4)}$$

$$k^{(\ell')}_{1sn\ell}(r) = -\left(\frac{2}{n}\right)^{\ell+2} \frac{\left[(n-\ell-1)!(n+\ell)!\right]^{\frac{1}{2}}}{2y^{\ell'+3}} \sum_{s=o}^{n-\ell-1} \frac{\left(-\frac{2}{n}\right)^s}{(2\ell+1+s)!s!(n-\ell-1-s)!} \times$$

$$\int_0^y x^{\ell+\ell'+s+3} e^{-\gamma x} \left(1 + \frac{x}{2}\right) dx = \left(\frac{2}{n}\right)^{\ell+2} \frac{\left[(n-\ell-1)!(n+\ell)!\right]^{\frac{1}{2}}}{2y^{\ell'+3}} \qquad \text{(AV.5)}$$

$$\sum_{s=o}^{n-\ell-1} \frac{\left(-\frac{2}{n}\right)^s}{(2\ell+1+s)!s!(n-\ell-1-s)!} \left[e^{-\gamma x} \left\{ \sum_{p=o}^{\ell+\ell'+s+3} \frac{x^p(\ell+\ell'+s+3)!}{p!\gamma^{\ell+\ell'+s+4-p}} \right.\right.$$

$$\left.\left. + \frac{1}{2} \sum_{p=o}^{\ell+\ell'+4+s} \frac{x^p(\ell+\ell'+s+4)!}{p!\gamma^{\ell+\ell'+s+5-p}} \right\} \right]_0^y$$

Therefore

$$k^{(\ell')}_{1sn\ell}(r) = \left(\frac{2}{\gamma n}\right)^{\ell+2} \frac{\left[(n-\ell-1)!(n+\ell)!\right]^{\frac{1}{2}}}{4(\gamma Zr)^{\ell'+3}} \sum_{s=0}^{n-\ell-1} \left(-\frac{2}{\gamma n}\right)^{s} \times$$

$$\frac{(\ell+\ell'+s+3)!(2\gamma+\ell+\ell'+s+4)}{s!(2\ell+1+s)!(n-\ell-1-s)!} \left\{ e^{-\gamma Zr} \sum_{p=0}^{\ell+\ell'+s+3} \frac{(\gamma Zr)^p}{p!} + \right.$$

$$\left. + \frac{e^{-\gamma Zr}(\gamma Zr)^{\ell+\ell'+s+4}}{(\ell+\ell'+s+3)!(2\gamma+\ell+\ell'+s+4)} - 1 \right\} \qquad \text{(AV.6)}$$

and so

$$\mathcal{J}_{1sn\ell}(r) = \left(\frac{2}{\gamma n}\right)^{\ell+2} \frac{\left[(n-\ell-1)!(n+\ell)!\right]^{\frac{1}{2}}}{2(\gamma Zr)^{\ell+2}} \sum_{s=0}^{n-\ell-1} \left(-\frac{2}{\gamma n}\right)^{s} \frac{(2\ell+2\gamma+s+3)(2\ell+s+2)}{s!(n-\ell-1-s)!}$$

$$\times \left\{ \frac{\ell}{(2\ell-1)} \left[e^{-\gamma Zr} \sum_{p=0}^{2\ell+s+2} \frac{(\gamma Zr)^p}{p!} + \frac{e^{-\gamma Zr}(\gamma Zr)^{2\ell+s+3}}{(2\ell+s+2)!(2\gamma+2\ell+s+3)} - 1 \right] \right.$$

$$+ \frac{(\ell+1)(2\gamma+2\ell+s+5)(2\ell+s+4)(2\ell+s+3)}{(2\ell+3)(2\gamma+2\ell+s+3)(\gamma Zr)^2} \left[e^{-\gamma Zr} \sum_{p=0}^{2\ell+s+4} \frac{(\gamma Zr)^p}{p!} + \right.$$

$$\left. \left. + \frac{e^{-\gamma Zr}(\gamma Zr)^{2\ell+s+5}}{(2\ell+s+4)!(2\gamma+2\ell+s+5)} - 1 \right] \right\} \qquad \text{(AV.7)}$$

For computational purposes it is necessary that $\mathcal{J}_{1sn\ell}(r)$ is well behaved for small values of r and can be expressed in terms of a rapidly convergent sum of increasing powers of r. Considering the integral in (AV.5)

$$\int_o^y x^{\ell+\ell'+s+3} e^{-\gamma x} \left(1 + \frac{x}{2}\right) dx = \sum_{p=0}^{\infty} \frac{(-\gamma)^p}{p!} \int_o^y x^{\ell+\ell'+s+3+p} \left(1 + \frac{x}{2}\right) dx$$

$$= \sum_{p=0}^{\infty} \frac{(-\gamma)^p}{p!} \left[\frac{x^{\ell+\ell'+s+4+p}}{(\ell+\ell'+s+4+p)} \left(1 + \frac{(\ell+\ell'+s+4+p)x}{2(\ell+\ell'+s+5+p)}\right) \right]_o^y$$

$$= \frac{(Zr)^{\ell+\ell'+s+4}}{(\ell+\ell'+s+4)} \left\{ 1 + \sum_{p=1}^{\infty} \frac{(-\gamma Zr)^p (\ell+\ell'+s+4)(2\gamma-p)}{2\gamma.p!(\ell+\ell'+s+4+p)} \right\}$$

therefore

$$k^{(\ell')}_{1sn\ell}(r) = -\left(\frac{2}{n}\right)^{\ell+2} \frac{\left[(n-\ell-1)!(n+\ell)!\right]^{\frac{1}{2}}}{2} \sum_{s=0}^{n-\ell-1} \frac{\left(-\frac{2}{n}\right)^{s} (Zr)^{\ell+s+1}}{s!(2\ell+1+s)!(n-\ell-1-s)!(\ell+\ell'+s+4)}$$

$$\times \left\{ 1 + \sum_{p=1}^{\infty} \frac{(-\gamma Zr)^{p}(\ell+\ell'+s+4)(2\gamma-p)}{2\gamma.p!(\ell+\ell'+s+4+p)} \right\} \qquad \text{(AV.8)}$$

and so

$$\mathcal{J}_{1sn\ell}(r) = -\left(\frac{2}{n}\right)^{\ell+2} \left[(n-\ell-1)!(n+\ell)!\right]^{\frac{1}{2}} \sum_{s=0}^{n-\ell-1} \frac{\left(-\frac{2}{n}\right)^{s} (Zr)^{\ell+s+1}}{s!(2\ell+1+s)!(n-\ell-1-s)!} \left\{ \frac{\ell}{(2\ell-1)} \right.$$

$$\left[\frac{1}{(2\ell+s+3)} + \sum_{p=1}^{\infty} \frac{(-\gamma Zr)^{p}(2\gamma-p)}{2\gamma.p!(2\ell+s+3+p)} \right] + \frac{(\ell+1)}{(2\ell+3)} \left[\frac{1}{(2\ell+s+5)} + \sum_{p=1}^{\infty} \right.$$

$$\left. \left. \frac{(-\gamma Zr)^{p}(2\gamma-p)}{2\gamma.p!(2\ell+s+5+p)} \right] \right\} \qquad \text{(AV.9)}$$

The infinite sum in (AV.8) can be terminated after only a few terms without severe loss of accuracy since the ratio of the m^{th} term of the sum to the first term is:

$$\frac{(\ell+\ell'+s+5)}{(\ell+\ell'+s+4+m)} \cdot \frac{(2\gamma-m)}{(2\gamma-1)} \cdot \frac{(-\gamma Zr)^{m-1}}{m!} : 1$$

and for $\gamma Zr < 1$ this diminishes at least as fast as $\frac{(\gamma Zr)^{m-1}}{(m-1)!}$

Appendix VI : Evaluation of the Born Scattering Amplitude $f^{B}_{n\ell m}(\theta,\phi)$

Equation (2.53) defines $f^{B}_{n\ell m}(\theta,\phi)$ thus:

$$f^{B}_{n\ell m}(\theta,\phi) = -\frac{2}{k^2} \int \phi^{*}_{n\ell m}(\underline{r})\, \phi_{1s}(\underline{r})\, e^{i\underline{K}.\underline{r}} dr$$

where

$$\phi_{n\ell m}(\underline{r}) = R_{n\ell}(1,r)\, Y_{\ell m}(\underline{\Omega}_1)$$

(equation (A1.7) with Z = 1)

$$R_{n\ell}(1,r) = \frac{2}{n^2}\left[(n-\ell-1)!(n+\ell)!\right]^{\frac{1}{2}} \left(\frac{2r}{n}\right)^{\ell} e^{-r/n} \sum_{s=0}^{n-\ell-1} \frac{\left(-\frac{2r}{n}\right)^{s}}{s!(n-\ell-1-s)!(2\ell+1+s)!}$$

and

$$e^{i\underline{K}.\underline{r}} = 4\pi \sum_{\ell'} i^{\ell'} j_{\ell'}(Kr) \sum_{m'=-\ell'}^{\ell'} Y_{\ell'm'}(\underline{\Omega}_1)\, Y^{*}_{\ell'm'}(\theta,0) \qquad \text{(AVI.1)}$$

(see McDowell and Coleman (1969), equations (5.2.9) and (5.2.18)),

where

$$\cos\theta = \hat{\underline{K}}.\hat{\underline{k}}_i = \frac{k_i - k_f \cos\theta}{(k_i^2 - 2k_f\cos\theta + k_f^{\,2})^{\frac{1}{2}}} \qquad \text{(see Figure F1.1)}$$

Therefore

$$f^{B}_{n\ell m}(\theta,\phi) = -\frac{8\pi}{k^2} \sum_{\ell',m'} i^{\ell'} \int j_{\ell'}(Kr) R_{n\ell}(r) R_{1s}(r) r^2 dr \times$$

$$\int Y^{*}_{\ell m}(\underline{\Omega}_1)\, Y_{\ell'm'}(\underline{\Omega}_1)\, Y_{oo}(\underline{\Omega}_1)\, d\underline{\Omega}_1\, Y^{*}_{\ell'm'}(\theta,0) \qquad \text{(AVI.2)}$$

The angular integration gives

$$\int Y^{*}_{\ell m}\, Y_{oo}\, Y_{\ell'm'}\, d\underline{\Omega} = \frac{\delta_{\ell\ell'}\delta_{mm'}}{2\sqrt{\pi}}$$

(see Edmonds (1960), p21, equation (2.5.4))

For $n = 3$, $\ell = 0$; $f^{B}_{3so}(\theta,\phi) = -\frac{2^5.3^4.}{\sqrt{3}} \frac{(27K^2 + 16Z^2)}{(9K^2 + 16Z^2)^4}$

$\ell = 1$; $f^{B}_{3pm}(\theta,\phi) = -\frac{2^8.3^3\, i\sqrt{\pi}}{\sqrt{6}.K} \cdot \frac{(27K^2 + 16Z^2)}{(9K^2 + 16Z^2)^4} Y^{*}_{1m}(\theta,0)$

$\ell = 2$; $f^{B}_{3dn}(\theta,\phi) = \frac{2^{11}.3^4.\sqrt{\pi}}{\sqrt{30}} \cdot \frac{1}{(9K^2 + 16Z^2)^4} Y^{*}_{2m}(\theta,0)$

Appendix VII : Evaluation of the Polarized-Born Scattering Amplitude:

$$f^{PB}_{n\ell m}(\theta,\phi)$$

Equation (2.56) defines $f^{PB}_{n\ell m}(\theta,\phi)$ thus:

$$f^{PB}_{n\ell m}(\theta,\phi) = f^{B}_{n\ell m}(\theta,\phi) + \delta f^{PB}_{n\ell m}(\theta,\phi)$$

where

$$\delta f^{PB}_{n\ell m}(\theta,\phi) = \frac{2}{3\sqrt{\pi}} \int \frac{e^{i\underline{K}.\underline{r}_2}}{r_2^{\,2}} \sum_{\mu=-1}^{1} \mathcal{J}_{n\ell m}(2,\mu)\, Y^{*}_{1\mu}(\underline{\Omega}_2)\, d\underline{r}_2$$

and

$$\mathcal{J}_{n\ell m}(2,\mu) = \int_{\underline{\Omega}_1} \int_0^{r_2} \phi^{*}_{n\ell m}(\underline{r}_1) \left(\frac{1}{r_{12}} - \frac{1}{r_2}\right) u_{1s\to p}(r_1)\, r_1 dr_1\, Y_{1\mu}(\underline{\Omega}_1)\, d\underline{\Omega}_1$$

Using the expansion for $\frac{1}{r_{12}}$ (see (A1.10))

$$\mathcal{J}_{n\ell m}(r,\mu) = \sum_{\lambda'=1}^{\infty} \sum_{\mu'=-\lambda'}^{\lambda'} \frac{4\pi}{(2\lambda'+1)} \int_0^{r} R_{n\ell}(t) u_{1s\to p}(t) \gamma_{\lambda'}(t,r) t\, dt \times$$

$$\int_{\Omega_1} Y_{\lambda'\mu'}(\underline{\Omega}_1)\; Y^{*}_{\ell m}(\underline{\Omega}_1)\, Y_{1\mu}(\underline{\Omega}_1) d\underline{\Omega}_1\, Y^{*}_{\lambda'\mu'}(\underline{\Omega}_2)$$

Integrating over $\underline{\Omega}_1$:

$$= (-1)^m \sum_{\lambda'=1}^{\infty} \sum_{\mu'=-\lambda'}^{\lambda'} \left[\frac{12(2\ell+1)\pi}{(2\lambda'+1)}\right]^{\frac{1}{2}} V^{\lambda'}_{n\ell}(r) \begin{pmatrix} \ell & 1 & \lambda' \\ -m & \mu & \mu' \end{pmatrix} \begin{pmatrix} \ell & 1 & \lambda' \\ 0 & 0 & 0 \end{pmatrix} Y^{*}_{\lambda'\mu'}(\underline{\Omega}_2)$$

(see Edmonds (1960), p.63, equation (4.6.3))

where

$$V^{\lambda'}_{n\ell}(r) = \int_0^{r} R_{n\ell}(t)\, u_{1s\to p}(t) \gamma_{\lambda'}(t,r) t\, dt$$

Now,

$$Y^*_{\lambda'\mu'}(\underline{\Omega}_2)\, Y^*_{1\mu}(\underline{\Omega}_2) = (-1)^{\mu+\mu'} \sum_{\ell_o,m_o} \left[\frac{3(2\lambda'+1)(2\ell_o+1)}{4\pi}\right]^{\frac{1}{2}} \times$$

$$\begin{pmatrix} \ell_o & 1 & \lambda' \\ m_o & -\mu & -\mu' \end{pmatrix} \begin{pmatrix} \ell_o & 1 & \lambda' \\ 0 & 0 & 0 \end{pmatrix} Y^*_{\ell_o m_o}(\underline{\Omega}_2)$$

(see: Edmonds (1960), p.63, equation (4.6.5))

and

$$\sum_{\mu,\mu'} \begin{pmatrix} \ell & 1 & \lambda' \\ -m & \mu & \mu' \end{pmatrix} \begin{pmatrix} \ell_o & 1 & \lambda' \\ m_o & -\mu & -\mu' \end{pmatrix} = \frac{(-1)^{\ell+1+\lambda'}}{(2\ell+1)} \delta_{\ell\ell_o}\, \delta_{mm_o}\, \delta(\ell,1,\lambda')$$

(see: Edmonds (1960), p.47, equation (3.7.8))

where $\delta(\ell,1,\lambda')$ is the triangular condition.

So

$$\sum_{\mu=-1}^{1} \mathcal{J}_{n\ell m}(r,\mu)\, Y^*_{1\mu}(\underline{\Omega}_2) = 3 \sum_{\lambda'=1}^{\infty} V^{\lambda'}_{n\ell}(r) \begin{pmatrix} \ell & 1 & \lambda' \\ 0 & 0 & 0 \end{pmatrix}^2 Y^*_{\ell m}(\underline{\Omega}_2)$$

Therefore

$$\delta f^{PB}_{n\ell m}(\theta,\phi) = \frac{2}{\sqrt{\pi}} \sum_{\lambda'=1}^{\infty} \int \frac{e^{i\underline{K}.\underline{r}_2}}{r^2} V^{\lambda'}_{n\ell}(r_2) \begin{pmatrix} \ell & 1 & \lambda' \\ 0 & 0 & 0 \end{pmatrix}^2 Y^*_{\ell m}(\underline{\Omega}_2)\, d\underline{r}_2$$

Expanding $e^{i\underline{K}.\underline{r}_2}$ according to (AVI.1)

$$\delta f^{PB}_{n\ell m}(\theta,\phi) = 8\sqrt{\pi} \sum_{\ell'=0}^{\infty} \sum_{\lambda'=1}^{\infty} \sum_{m'=-\ell'}^{\ell'} i^{\ell'} \begin{pmatrix} \ell & 1 & \lambda' \\ 0 & 0 & 0 \end{pmatrix}^2 \times$$

$$\int j_\ell(Kr_2)\, V^{\lambda'}_{n\ell}(r_2)\, dr_2 \times \int Y^*_{\ell m}(\underline{\Omega}_2)\, Y_{\ell' m'}(\underline{\Omega}_2)\, d\underline{\Omega}_2\, Y^*_{\ell' m'}(\theta,0)$$

The integral over $\underline{\Omega}_2$ is non-zero for $\ell' = \ell$ and $m' = m$ only.

so

$$\delta f^{PB}_{n\ell m}(\theta,\phi) = 8\sqrt{\pi} \sum_{\lambda'=1}^{\infty} i^{\ell} \begin{pmatrix} \ell & 1 & \lambda' \\ 0 & 0 & 0 \end{pmatrix}^2 \int j_\ell(Kr_2) V^{\lambda'}_{n\ell}(r)\, dr\, Y^*_{\ell m}(\theta,0)$$

The sum over λ' is restricted to the non-zero values of the 3-j Wigner coefficient, thus:

$$\sum_{\lambda'} \begin{pmatrix} \ell & 1 & \lambda' \\ 0 & 0 & 0 \end{pmatrix}^2 V_{n\ell}^{\lambda'}(r) = \frac{\lambda'}{(2\lambda'+1)(2\ell+1)} V_{n\ell}^{\lambda'}(r) \left(\delta_{\lambda'\ell-1} + \delta_{\lambda'\ell+1}\right)$$

substituting for $R_{n\ell}(r)$, $u_{ls\to p}(r)$ and $\gamma(t,r)$ in $V_{n\ell}^{\lambda'}(r)$:

$$V_{n\ell}^{\lambda'}(r) = \frac{1}{r^{\lambda'+1}} \left(\frac{2}{n}\right)^{\ell+2} \frac{\left[(n-\ell-1)!(n+\ell)!\right]^{\frac{1}{2}}}{2} \sum_{s=o}^{n-\ell-1} \frac{\left(-\frac{2}{n}\right)^s}{s!(2\ell+1+s)!(n-\ell-1-s)!} \times$$

$$\int_0^r t^{\lambda'+\ell+s+3} \left(1 + \frac{t}{2}\right) e^{-\gamma t}\, dt$$

and so

$$\int j_\ell(Kr)\, V_{n\ell}^{\lambda'}(r)\, dr = \left(\frac{2}{n}\right)^{\ell+2} \frac{\left[(n-\ell-1)!(n+\ell)!\right]^{\frac{1}{2}}}{2} \sum_{s=0}^{n-\ell-1} \frac{\left(-\frac{2}{n}\right)^s}{s!(2\ell+1+s)!(n-\ell-1-s)!}$$

$$\times \int_0^\infty \frac{j_\ell(Kr)}{r^{\lambda'+1}} \int_0^r t^{\lambda'+\ell+s+3} \left(1 + \frac{t}{2}\right) e^{-\gamma t}\, dt\, dr$$

letting $t = ry$

$$= \left(\frac{2}{n}\right)^{\ell+2} \frac{\left[(n-\ell-1)!(n+\ell)!\right]^{\frac{1}{2}}}{2} \sum_{s=o}^{n-\ell-1} \frac{\left(-\frac{2}{n}\right)^s}{s!(2\ell+1+s)!(n-\ell-1-s)!}$$

$$\times \int_0^\infty \int_0^1 j_\ell(Kr)\, r^{\ell+s+3}\, y^{\lambda'+\ell+s+3} \left(1 + \frac{yr}{2}\right) e^{-\gamma r y}\, dy dr$$

and by changing the order of integration

$$= \left(\frac{2}{n}\right)^{\ell+2} \frac{\left[(n-\ell-1)!(n+\ell)!\right]^{\frac{1}{2}}}{2} \sum_{s=0}^{n-\ell-1} \frac{\left(-\frac{2}{n}\right)^{s}}{s!(2\ell+1+s)!(n-\ell-1-s)!}$$

$$\times \int_0^1 y^{\lambda'+\ell+s+3} \left[\int_0^\infty j_\ell(Kr)\ (r^{\ell+s+3} + \frac{yr^{\ell+s+4}}{2})\ e^{-\gamma r y}\ dr\right] dy$$

For the states of interest here, $\ell = 0, 1, 2$

and

$$j_o(Kr) = \frac{\text{Sin } Kr}{Kr}$$

$$j_1(Kr) = \frac{\text{Sin } Kr}{K^2r^2} - \frac{\text{Cos } Kr}{Kr}$$

$$j_2(Kr) = \left(\frac{3}{K^2r^3} - \frac{1}{Kr}\right) \text{Sin } Kr - \frac{3}{K^2r^2} \text{Cos } Kr$$

now

$$\int_0^\infty \left\{\begin{matrix}\text{Sin}\\ \text{Cos}\end{matrix}\right\}(kr)\ r^\alpha e^{-\gamma y r}\ dr = \frac{\Gamma(\alpha+1)}{(\beta^2y^2+K^2)^{\frac{\alpha+1}{2}}} \left\{\begin{matrix}\text{Sin}\\ \text{Cos}\end{matrix}\right\}((\alpha+1)\theta)$$

where

$$\sin\theta = \frac{K}{(\gamma^2y^2+K^2)^{\frac{1}{2}}}$$

using these results, and the fact that the states of interest are those for which $n = 3$, leads to

$$\delta f^{PB}_{3s0}(\theta,\phi) = \frac{16\sqrt{3\pi}}{27K} Y^*_{oo}(\theta,\phi) \int_0^1 \frac{y^4}{(\gamma^2y^2+K^2)^{3/2}} \left(2\sin3\theta - \frac{3}{4}\sin4\theta\cos\theta\right.$$

$$\left. - \frac{7}{2}\sin5\theta\cos^2\theta + \frac{15}{8}\sin6\theta\cos^3\theta\right) dy$$

$$\delta f^{PB}_{3pm}(\theta,\phi) = \frac{64\sqrt{6\pi}}{45x27K^2} iY^*_{1m}(\theta,\phi) \int_0^1 \frac{y^6}{(\gamma^2y^2+K^2)^{3/2}} \left(2\sin3\theta + \frac{3}{2}\cos4\theta\cos\theta\right.$$

$$\left. - \frac{9}{8}\sin5\theta\cos^2\theta - 6\sin\theta\cos4\theta - 6\sin\theta\cos5\theta + \frac{45}{8}\sin\theta\cos^2\theta\cos6\theta\right) dy$$

$$\cos\theta$$

$$\delta f^{PB}_{3dm}(\theta,\phi) = -\frac{32\sqrt{\pi}}{405\sqrt{30}K^3}\, Y^*_{2m}(\theta,\phi) \int_0^1 \frac{(14y^6 + 9y^8)}{21(\gamma^2y^2 + K^2)^{3/2}} \left(6\sin 3\theta + \frac{27}{4}\cos 4\theta\cos\theta\right.$$

$$\left. - 18\sin\theta\cos 4\theta - 27\cos 5\theta\sin\theta\cos\theta - 24\sin^2\theta\sin 5\theta - 45\cos\theta\sin^2\theta\sin 6\theta\right) dy$$

with $\gamma = \frac{4}{3}$

by means of the transformation $\gamma y = K \tan\beta$ ($\therefore \cos\theta = \sin\beta$, $\sin\theta = \cos\beta$), these expressions becomes

$$\delta f^{PB}_{3so}(\theta,\phi) = \frac{16\sqrt{3\pi}K}{27\gamma^5} \int_0^{\tan^{-1}\frac{\gamma}{K}} \frac{\sin^4\beta}{\cos^2\beta} \left(-2 + \frac{15\sin^2\beta}{2} + \frac{189\sin 4\beta}{4}\right.$$

$$\left. - 116\sin^6\beta + 60\sin^8\beta\right) d\beta\, Y^*_{oo}(\theta,\phi)$$

letting:

$$Q_n = \int_0^{\beta'} \frac{\sin^{2n}\beta}{\cos^2\beta}\, d\beta \qquad \beta' = \tan^{-1}\left(\frac{\gamma}{K}\right)$$

then:

$$Q_{n+1} = -\frac{\sin^{2n+1}\beta}{2n\cos\beta} + \frac{(2n+1)}{2n}\, Q_n$$

and

$$Q_1 = \int \tan^2\beta\, d\beta = \tan\beta' - \beta'.$$

$$\therefore\ \delta f^{PB}_{3so}(\theta,\phi) = \left[\frac{46\sqrt{3\pi}\,K}{9\gamma^5} \tan^{-1}\frac{\gamma}{K} - \frac{2\sqrt{3\pi}}{27\gamma^4(\gamma^2+K^2)^5} \times\right.$$

$$\left.(26\gamma^{10} + 161\gamma^8K^2 + 522\gamma^6K^4 + 592\gamma^4K^6 + 322\gamma^2K^8 + 69K^{10})\right] Y^*_{oo}(K)$$

similarly:

$$\delta f^{PB}_{3pm}(\theta,\phi) = \frac{64\sqrt{6\pi}\,K^2}{45x27\gamma^5} \int_0^{\tan^{-1}\frac{\gamma}{K}} \frac{\sin^4\beta}{\cos^2\beta} \left(-8 + \frac{21}{4}\sin^2\beta + 204\sin^4\beta\right.$$

$$\left. - 180\sin^6\alpha\right) d\beta\, i\, Y^*_{1m}(\theta,\phi)$$

$$= \left[\frac{-32\sqrt{\pi}\,K^2\tan^{-1}}{9\sqrt{6}\,\gamma^7} \frac{\gamma}{K} + \frac{32\sqrt{\pi}.K}{405\sqrt{6}\,\gamma^6(\gamma^2+K^2)^5} (85\gamma^{10} + 128\gamma^8K^2 + 334\gamma^6K^4\right.$$

$$\left. + 384\gamma^4K^6 + 210\gamma^2K^8 + 45K^{10})\right] i\, Y^*_{1m}(K).$$

and, finally:

$$\delta f^{PB}_{3dm}(\theta,\theta) = \frac{-16 \times 32\sqrt{\pi}\, K}{7\times 405\sqrt{30}\ \gamma^9}\left\{14\gamma^2 \int_0^{\tan^{-1}\frac{\gamma}{K}} (30\sin^{10}\beta - \sin^8\beta - \sin^6\beta)d\beta \right.$$

$$\left. + 9K^2 \int_0^{\tan^{-1}\frac{\gamma}{K}} \frac{\sin^8\beta}{\cos^2\beta}\,(30\sin^4\beta - \sin^2\beta - 1)d\beta\right\}$$

$$= \left[-\frac{16\sqrt{\pi}\, K}{27\sqrt{30}\ \gamma^9}\,(29\gamma^2 - 210K^2)\tan^{-1}\frac{\gamma}{K} - \frac{16\sqrt{\pi}\, K^2}{2835\sqrt{30}\ \gamma^8(\gamma^2+K^2)^5} \times\right.$$

$$\left.(-1435\gamma^{10} + 44544\gamma^8K^2 + 139916\gamma^6K^4 + 173950\gamma^4K^6 + 99855\gamma^2K^8 + 22050K^{10})\right] \times$$

$$Y^*_{2m}(\theta,\phi).$$

Appendix AVIII: Parameters for Radiation From the n = 3 states of Hydrogen

AVIII.1 Branching ratios for 3p - 2s and 3p - 1s transitions

These ratios are given by the relative probabilities of transitions to the 2s and 1s states and can be expressed in terms of the Einstein A coefficient:

$$B_m = \frac{A(3^2P \to m^2S)}{A(3^2P \to 1,2^2S)} = \frac{\sigma_{m3}^3 \, S(3^2P \to m^2S)}{\sigma_{13}^3 \, S(3^2P \to 1^2S) + \sigma_{23}^3 \, S(3^2P \to 2^2S)}$$

where $m = 1$ or 2, S is the line strength for radiation from a state n to state m and the wave number σ_{mn} is given by:

$$\sigma_{mn} = R\left(\frac{1}{m^2} - \frac{1}{n^2}\right)$$

(R is Rydberg's constant).

Using Condon and Shortley (1963) p.134, we obtain

$$B_1 = 0.882$$

$$B_2 = 0.118$$

AVIII.2 Absolute Values for the Einstein A Coefficients and Line Widths

The line width, Γ, is related to the A coefficient by

$$\Gamma = A/2\pi c$$

thus, we obtain (see Condon and Shortly (1963), p.134):

Transition	A coefficient (sec^{-1})	Transition	Line width Γ (cm^{-1})
$3^2D_{5/2} - 2^2P_{3/2}$	6.468,7		
$3^2D_{3/2} - 2^2P_{3/2}$	1.078,7	$3^2D - 2^2P$	3.434,-4
$3^2D_{3/2} - 2^2P_{1/2}$	5.390,7		
$3^2P_{3/2} - 2^2S_{1/2}$	2.246,7	$3^2P - 2^2S$	1.192,-4
$3^2P_{1/2} - 2^2S_{1/2}$	2.246,7		
$3^2S_{1/2} - 2^2P_{1/2}$	2.105,6	$3^2S - 2^2P$	0.335,-4
$3^2S_{1/2} - 2^2P_{3/2}$	4.211,6		

AVIII.3 Fine and Hyperfine Structure Splitting

The table below shows the energies, separations, fine structure splittings in cm^{-1}, and hyperfine splittings.

State	Energy[1] (GHz)	Separation (GHz) δE	Fine Structure (cm^{-1}) $= \delta E/c$	ΔE[2] (MHz)	Hyperfine Structure (cm^{-1})
$3^2D_{5/2}$	4.32789	1.08327	0.1084	2.690	8.973,-5
$3^2D_{3/2}$	3.24462			4.185	1.396,-4
$3^2P_{3/2}$	3.24993	3.24993	0.0361	6.973	2.326,-4
$3^2P_{1/2}$	0.0			17.436	5.816,-4
$3^2S_{1/2}$	0.31481			52.283	1.744,-3.

(1) J.D. Garcia and J.E. Mack, (1965)

(2) H. Bethe and E.E. Salpeter (1957) p.110.

Appendix AIX The Polarization Formulae

As explained in Chapter 5, for the calculation of the polarization formulae three states are identified - an initial state α, the excited state β, and the final state γ. Throughout the work below, we follow Percival and Seaton (1958) (referred to as PS). The polarization fraction is given by:

$$P = 100 \frac{(3K_z - K)}{K_z + K} \qquad \text{(AIX.1)}$$

The exact form of K and K_z is dependent on the inclusion of hyperfine splitting.

AIX.1 Excluding hyperfine splitting

In this case α, β and γ are given by:

$$\begin{aligned} \alpha &= \Delta', S'L'J'M_J' \\ \beta &= \Delta, SLJM_J \\ \gamma &= \Delta'', S''L''J''M_J'' \end{aligned} \qquad \text{(AIX.2)}$$

(equation (5.5))

where Δ', Δ and Δ'' refer to non-relevant quantum numbers. Since the interaction potential is assumed not to include spin co-ordinates then it follows that

$$S = S' = S'' \qquad \text{(AIX.3)}$$

Under this description of the quantum states, PS equation (3.33) for K_z applies, thus:

$$K_z(SL \to SL'') = \frac{v_a A(SL \to SL'')}{A(SL)(2S+1)}(2L+1) \sum_{JJ''M_J} (2J''+1) \left[\sum_{M_S M_L} C^{SLJ}_{M_S M_L M_J} C^{J''1J}_{M_J'' 0 M_J} W(LJL''J'';S1) \right]^2 \sigma_{|M_L|} \qquad \text{(AIX.4)}$$

where v_a is the velocity of the impact electron, $C^{J_1J_2J_3}_{M_1M_2M_3}$ and $W(J_1J_2J_3J_4;J_5J_6)$ are Clebsch-Gordon 3-j and Wigner 6-j vector-coupling coefficients respectively, evaluated using Edmonds (1960), and $\sigma_{|M_L|}$ is the cross section for excitation of the $n\ell m_L$ sub-level.

The function $K(SL \rightarrow SL'')$ is obtained by summing PS equation (3.32) over J and J" to give:

$$K(SL \rightarrow SL'') = \frac{v_a\, A(SL \rightarrow SL'')}{(2L+1)(2S+1)A(SL)} \sum_{J,M_L} (2J+1)\,\sigma_{|M_L|} \qquad \text{(AIX.5)}$$

This is used in preference to PS equation (3.34) which does not include the factor $\frac{\sum(2J+1)}{(2L+1)}$ and which leads to erroneous results.

After some algebra, we obtain for hydrogen:

1a) For $^2P \rightarrow {}^2S$ transitions:

$$K_z(^2P \rightarrow {}^2S) = \frac{v_a A(^2P \rightarrow {}^2S)}{9A(^2P)} (5\sigma_{npo} + 4\sigma_{npl}) \qquad \text{(AIX.6)}$$

$$K(^2P \rightarrow {}^2S) = \frac{v_a A(^2P \rightarrow {}^2S)}{A(^2P)} (\sigma_{npo} + 2\sigma_{npl}) \qquad \text{(AIX.7)}$$

Thus:

$$P(^2P \rightarrow {}^2S) = \frac{300(\sigma_{npo} - \sigma_{npl})}{(7\sigma_{npo} + 11\sigma_{npl})} \%$$

(in exact agreement with PS).

1b) For $^2D \rightarrow {}^2P$ transitions:

$$K_z(^2D \rightarrow {}^2P) = \frac{v_a A(^2D \rightarrow {}^2P)}{75A(^2D)} (44\sigma_{ndo} + 69\sigma_{ndl} + 12\sigma_{nd2}) \qquad \text{(AIX.9)}$$

$$K(^2D \rightarrow {}^2P) = \frac{v_a . A(^2D \rightarrow {}^2P)}{2A(^2D)} (\sigma_{ndo} + 2\sigma_{ndl} + 2\sigma_{nd2}) \qquad \text{(AIX.10)}$$

Thus:

$$P(^2D \rightarrow {}^2P) = 5700\ \frac{(\sigma_{ndo} + \sigma_{nd1} - 2\sigma_{nd2})}{(119\sigma_{ndo} + 219\sigma_{nd1} + 162\sigma_{nd2})}\ \% \qquad \text{(AIX.11)}$$

AIX.2 Including hyperfine splitting

In this case α, β and γ are given by equation (5.6):

$$\alpha = \Delta', SL'J'IF'M_F'$$

$$\beta = \Delta, SLJIFM_F \qquad \text{(AIX.12)}$$

$$\gamma = \Delta'', SL''J''IF''M_F''$$

where $\underline{F} = \underline{J} + \underline{I}$.

2a) For $^2P \rightarrow {}^2S$ transitions:

PS include an explicit calculation for this situation and obtain for hydrogen (where the nuclear spin, I, = $\frac{1}{2}$):

$$K_z(^2P_{1/2} \rightarrow {}^2S) = \frac{v_a}{9}(\sigma_{npo} + 2\sigma_{npl})$$

$$K_z(^2P_{3/2} \rightarrow {}^2S) = \frac{v_a}{36}(13\sigma_{npo} + 11\sigma_{npl})$$

$$\therefore \quad K_z(^2P \rightarrow {}^2S) = \frac{v_a}{36}(17\sigma_{npo} + 19\sigma_{npl}) \qquad \text{(AIX.13)}$$

Similarly $$K(^2P_{1/2} \rightarrow {}^2S) = \frac{v_a}{3}(\sigma_{npo} + 2\sigma_{npl})$$

$$K(^2P_{3/2} \rightarrow {}^2S) = \frac{2v_a}{3}(\sigma_{npo} + 2\sigma_{npl})$$

$$\therefore \quad K(^2P \rightarrow {}^2S) = v_a(\sigma_{npo} + 2\sigma_{npl}) \qquad \text{(AIX.14)}$$

thus: $$P(^2P_{1/2} \rightarrow {}^2S) = 0 \qquad \text{(AIX.15)}$$

$$P(^2P_{3/2} \rightarrow {}^2S) = \frac{15(\sigma_{npo} - \sigma_{npl})}{(37\sigma_{npo} + 59\sigma_{npl})} \qquad \text{(AIX.16)}$$

and $$P(^2P \rightarrow {}^2S) = \frac{15(\sigma_{npo} - \sigma_{npl})}{(53\sigma_{npo} + 91\sigma_{npl})} \qquad \text{(AIX.17)}$$

2b) For $^2D \rightarrow {}^2P$ transitions:

In case 2a) above, Percival and Seaton were able to use the unitarity properties of the transformations employed and thus obtain greatly simplified expressions for $K_z(SLJ \rightarrow SL)$ when only two magnetic substate excitation cross-sections are involved. When more substates are included this simplification does not occur so that the problem must be tackled from first principles.

The relevant relations to be noted are:

$$K(\beta) = v_a\, \sigma(\beta) \qquad \text{(PS equation (2.12))}$$

$$K_z(\beta) = v_a\, \frac{A_z(\beta)}{A(b)}\, \sigma(\beta) \qquad \text{(PS equation (2.15))}$$

$$\sigma(\beta) = \frac{(2J+1)}{(2I+1)(2S+1)} \sum_{T,M_T M_L} (2T+1) \times \left[W(SLIF;JT)\; C^{TLF}_{M_T M_L M_F} \right]^2 \sigma_{|M_L|} \qquad \text{(PS equation (3.20))}$$

$$A_z(\beta) = (2J+1)(2L+1)A \sum_{J''F''M''_F} (2F''+1)(2J''+1) \times \left[C^{F''1F}_{M''_F 0 M_F}\; W(JFJ''F'';I1) \times W(LJL''J'';S1) \right]^2$$

(PS equations (3.24), (3.29) and (3.30))

and in this case $A = A(^2D \rightarrow {}^2P)$.

After some manipulation, we find that:

$$K(^2D_J) = \frac{(2J+1)}{10}\, v_a\, (\sigma_{ndo} + 2\sigma_{nd1} + 2\sigma_{nd2}) \qquad \text{(AIX.18)}$$

$$K(^2D) = v_a(\sigma_{ndo} + 2\sigma_{nd1} + 2\sigma_{nd2})$$

and

$$K_z(^2D_{3/2} \rightarrow {}^2P) = \frac{v_a}{120}\ (23\sigma_{ndo} + 39\sigma_{ndl} + 18\sigma_{nd2})$$

$$K_z(^2D_{5/2} \rightarrow {}^2P) = \frac{v_a}{15}\ (5\sigma_{ndo} + 8\sigma_{ndl} + 2\sigma_{nd2})$$

$$\therefore\quad K_z(^2D \rightarrow {}^2P) = \frac{v_a}{120}\ (63\sigma_{ndo} + 103\sigma_{ndl} + 34\sigma_{nd2}) \qquad \text{(AIX.19)}$$

Thus:

$$P(^2D_{3/2} \rightarrow {}^2P) = \frac{2100(\sigma_{ndo} + \sigma_{ndl} - 2\sigma_{nd2})}{(71\sigma_{ndo} + 135\sigma_{ndl} + 114\sigma_{nd2})} \qquad \text{(AIX.20)}$$

$$P(^2D_{5/2} \rightarrow {}^2P) = \frac{300(\sigma_{ndo} + \sigma_{ndl} - 2\sigma_{nd2})}{(7\sigma_{ndo} + 13\sigma_{ndl} + 10\sigma_{nd2})} \qquad \text{(AIX.21)}$$

$$P(^2D \rightarrow {}^2P) = \frac{6900(\sigma_{ndo} + \sigma_{ndl} - 2\sigma_{nd2})}{(183\sigma_{ndo} + 343\sigma_{ndl} + 274\sigma_{nd2})} \qquad \text{(AIX.22)}$$

AIX.3 Percival and Seaton "Exact" Formulae

It is explained in Chapter 5 that the "exact" PS formulation is required in the two possibly ambiguous cases when the fine structure separation is of similar order to the line width or when the hyperfine splittings are of the same order as the line width.

In the former case, if $\varepsilon = \varepsilon_\ell$ is the ratio of fine structure splitting to line width, then:

$$K_z^{(\varepsilon)} = \frac{K_z^{(0)} + \varepsilon^2 K_z^{(\infty)}}{1 + \varepsilon^2} \qquad \text{(AIX.23)}$$

where $K_z^{(0)}$ and $K_z^{(\infty)}$ are the results obtained via Oppenheimer-Penney theory when fine structure are excluded or included respectively. $K_z^{(\infty)}$ corresponds exactly to section AIX.1 above.

In the latter case, similar expressions apply where $\varepsilon = \varepsilon_J = \frac{2\pi\Delta E_J}{A}$, (i.e. the ratio of hyperfine splitting to line width) and $K_z^{(0)}$ and $K_z^{(\infty)}$ are the Oppenheimer-Penney results including fine structure but excluding or including hyperfine structure respectively. Thus $K_z^{(0)}$ and $K_z^{(\infty)}$ correspond exactly to sections AIX.1 and AIX.2 respectively.

Since, for the $n = 3$ levels of hydrogen, hyperfine structure is of the same order as line width, the results obtained using the expressions in the second situation above are presented here.

3a) For $^2P \rightarrow {}^2S$ transitions.

Letting $\varepsilon_1 = \varepsilon_{J=1/2}$ and $\varepsilon_2 = \varepsilon_{J=3/2}$:

$$K_z^{\varepsilon_1}(^2P_{1/2} \rightarrow {}^2S) = \frac{v_a}{9}(\sigma_{npo} + 2\sigma_{npl})$$

$$K_z^{\varepsilon_2}(^2P_{3/2} \rightarrow {}^2S) = \frac{v_a}{36(1+\varepsilon_2^2)}\left[(16 + 13\varepsilon_2^2)\sigma_{npo} + (8 + 11\varepsilon_2^2)\sigma_{npl}\right]$$

$$\therefore \quad K_z(^2P \rightarrow {}^2S) = \frac{v_a}{36(1+\varepsilon_2^2)}\left[(20 + 17\varepsilon_2^2)\sigma_{npo} + (16 + 19\varepsilon_2^2)\sigma_{npl}\right] \qquad \text{(AIX.24)}$$

The expressions for $K(^2P_{1/2} \rightarrow {}^2S)$, $K(^2P_{3/2} \rightarrow {}^2S)$ and $K(^2P \rightarrow {}^2S)$ remain unchanged from (AIX.14)

$$\therefore \quad P(^2P_{1/2} \rightarrow {}^2S) = 0 \qquad \text{(AIX.25)}$$

$$P(^2P_{3/2} \rightarrow {}^2S) = \frac{(24 + 15\varepsilon_2^2)(\sigma_{npo} - \sigma_{npl})}{\left[(40 + 37\varepsilon_2^2)\sigma_{npo} + (56 + 59\varepsilon_2^2)\sigma_{npl}\right]} \% \qquad \text{(AIX.26)}$$

and

$$P(^2P \rightarrow {}^2S) = \frac{(24 + 15\varepsilon_2^2)(\sigma_{npo} - \sigma_{npl})}{\left[(56 + 53\varepsilon_2^2)\sigma_{npo} + (88 + 91\varepsilon_2^2)\sigma_{npl}\right]} \% \qquad \text{(AIX.27)}$$

Values for ε_1 and ε_2 for the 3p state are given in table T5.1 obtained from appendix AVIII and final forms for the polarization formulae shown in T5.2.

3b) For $^2D \rightarrow {}^2P$ transitions, letting $\varepsilon_1 = \varepsilon_{J=3/2}$ and $\varepsilon_2 = \varepsilon_{J=5/2}$, we obtain:

$$K_z^{\varepsilon_1}(^2D_{3/2} \rightarrow {}^2P) = \frac{v_a}{600(1+\varepsilon_1^2)}\left[(136 + 115\varepsilon_1^2)\sigma_{ndo} + (216 + 195\varepsilon_1^2)\sigma_{ndl} + (48 + 90\varepsilon_1^2)\sigma_{nd2}\right]$$

$$K_z^{\varepsilon_2}(^2D_{5/2} \rightarrow {}^2P) = \frac{v_a}{75(1+\varepsilon_2^2)}\left[(27 + 25\varepsilon_2^2)\sigma_{ndo} + (42 + 40\varepsilon_2^2)\sigma_{ndl} + (6 + 10\varepsilon_2^2)\sigma_{nd2}\right]$$

$$K_z(^2D \rightarrow {}^2P) = K_z^{\varepsilon_1}(^2D_{3/2} \rightarrow {}^2P) + K_z^{\varepsilon_2}(^2D_{5/2} \rightarrow {}^2P) \qquad \text{(AIX.28)}$$

The expressions for $K(^2D_J \rightarrow {}^2P)$, $K(^2D \rightarrow {}^2P)$ are given in (AIX.18),

$$\therefore \quad P(^2D \rightarrow {}^2P) = \frac{100a_o(\sigma_{ndo} + \sigma_{ndl} - 2\sigma_{nd2})}{(a_1\sigma_{ndo} + a_2\sigma_{ndl} + a_3\sigma_{nd2})} \ \% \qquad \text{(AIX.29)}$$

where

$$a_o = 456 + 345\varepsilon_1^2\varepsilon_2^2 + 393\varepsilon_1^2 + 408\varepsilon_2^2$$

$$a_1 = 952 + 915\varepsilon_1^2\varepsilon_2^2 + 931\varepsilon_1^2 + 936\varepsilon_2^2$$

$$a_2 = 1752 + 1715\varepsilon_1^2\varepsilon_2^2 + 1731\varepsilon_1^2 + 1736\varepsilon_2^2$$

$$a_3 = 1296 + 1370\varepsilon_1^2\varepsilon_2^2 + 1338\varepsilon_1^2 + 1328\varepsilon_2^2$$

By using the relevant values for ε_1 and ε_2 from Table T5.1, the expressions for the 3d states are obtained and shown in T5.2.

Appendix AX: Coincidence Parameters for the n = 3 States of Hydrogen

In Chapter 6 the coincidence parameters $A_{qq'}$, $(q,q' = 0, \pm 1)$ are defined:

$$A_{qq'} = \sum_{J,M_L,M_L'} \frac{(2L+1)(2J+1)^2}{(2S+1)\gamma} (-1)^{q+L_o-M_L} \langle a_{M_L'} a_{M_L} \rangle \sum_{\chi,\nu} (2\chi+1) \times$$

$$\begin{Bmatrix} L & L & \chi \\ J & J & S \end{Bmatrix}^2 \begin{Bmatrix} L & L & \chi \\ 1 & 1 & L_o \end{Bmatrix} \times \begin{pmatrix} L & L & \chi \\ -M_L' & M_L & \nu \end{pmatrix} \begin{pmatrix} 1 & 1 & \chi \\ q & -q' & \nu \end{pmatrix}$$

Using elementary algebraic methods gives for each transition $n\ell \to n\text{-}1\ \ell'$

1. $3s \to 2p$

$$A_{qq'} = \frac{2}{\gamma} (-1)^{q+1} \langle a_o a_o \rangle \sum_{\chi} (2\chi+1) \begin{Bmatrix} 0 & 0 & \chi \\ \frac{1}{2} & \frac{1}{2} & \frac{1}{2} \end{Bmatrix}^2 \begin{Bmatrix} 0 & 0 & \chi \\ 1 & 1 & 1 \end{Bmatrix} \begin{pmatrix} 0 & 0 & \chi \\ 0 & 0 & 0 \end{pmatrix} \times$$

$$\begin{pmatrix} 1 & 1 & \chi \\ q & -q' & 0 \end{pmatrix} = \sigma_{3s}/3\gamma \cdot \delta_{qq'}$$

2. $3p \to 2s, 1s$

$$A_{qq'} = \frac{3}{2\gamma} \sum_{\substack{J=1/2,3/2 \\ M_L,M_L'}} (-1)^{q-M_L} (2J+1) \langle a_{M_L'}, a_{M_L} \rangle \sum_{\chi,\nu} (2\chi+1) \begin{Bmatrix} 1 & 1 & \chi \\ J & J & \frac{1}{2} \end{Bmatrix}^2 \times$$

$$\begin{Bmatrix} 1 & 1 & \chi \\ 1 & 1 & 0 \end{Bmatrix} \begin{pmatrix} 1 & 1 & \chi \\ -M_L' & M_L & \nu \end{pmatrix} \begin{pmatrix} 1 & 1 & \chi \\ q & -q' & \nu \end{pmatrix}$$

Summing over J and substituting for the 6-j vector coupling coefficients (see Edmonds (1960)).

gives

$$A_{qq'} = \sum_{M_L M'_L} (-1)^{q-M_L} \frac{\langle a_{M'_L} a_{M_L} \rangle}{9\gamma} \sum_{\chi,\nu} (2\chi+1)(9-\chi-\chi^2) \begin{pmatrix} 1 & 1 & \chi \\ M_L & -M'_L & \nu \end{pmatrix} \begin{pmatrix} 1 & 1 & \chi \\ q & -q' & \nu \end{pmatrix}$$

$$\therefore \quad A_{oo} = \frac{1}{9\gamma} (5\sigma_{3po} + 4\sigma_{3p1})$$

$$A'_{11} = \frac{1}{9\gamma} (2\sigma_{3po} + 7\sigma_{3p1})$$

$$A_{1-1} = -\frac{\sigma_1}{3\gamma}$$

$$A_{o1} = \frac{5}{9\gamma} \langle a_1 a_o \rangle - \frac{2}{9\gamma} \langle a_o a_1 \rangle$$

$$= \frac{1}{3\gamma} \text{ Re } \langle a_1 a_o \rangle + \frac{7i}{9\gamma} \text{ Im} \langle a_1 a_o \rangle$$

3. <u>3d → 2p</u>

$$A_{qq'} = \frac{5}{2\gamma} \sum_{\substack{J=3/2,5/2 \\ M_L, M'_L}} (-1)^{1+q-M_L} (2J+1)^2 \langle a_{M'_L} a_{M_L} \rangle \sum_{\chi,\nu} (2\chi+1) \begin{Bmatrix} 2 & 2 & \chi \\ J & J & \frac{1}{2} \end{Bmatrix}^2 \times$$

$$\begin{Bmatrix} 2 & 2 & \chi \\ 1 & 1 & 1 \end{Bmatrix} \begin{pmatrix} 2 & 2 & \chi \\ -M'_L & M_L & \nu \end{pmatrix} \begin{pmatrix} 1 & 1 & \chi \\ q & -q' & \nu \end{pmatrix}$$

summing over J, and substituting for the 6-j coupling coefficients gives

$$A_{qq'} = \frac{1}{300\gamma} \sum_{M_L, M'_L} (-1)^{1+q-M_L} \langle a_{M'_L} a_{M_L} \rangle \sum_{\chi,\nu} (2\chi+1)(25-\chi-\chi^2) \Big[(\chi+5)(\chi+4)(4-\chi) \times$$

$$(3-\chi) \Big]^{\frac{1}{2}} \times \begin{pmatrix} 2 & 2 & \chi \\ M_L & -M'_L & \nu \end{pmatrix} \begin{pmatrix} 1 & 1 & \chi \\ q & -q' & \nu \end{pmatrix}$$

and therefore:

$$A_{oo} = \frac{1}{75\gamma} \left(44\sigma_{3do} + 69\sigma_{3d1} + 12\sigma_{3d2}\right)$$

$$A_{11} = \frac{1}{150\gamma} \left(31\sigma_{3do} + 81\sigma_{3d1} + 138\sigma_{3d2}\right)$$

$$A_{1-1} = \frac{1}{150\gamma} \left(38\sqrt{6}\ \ \mathrm{Re}\langle a_2 a_o\rangle - 57\sigma_{3d1}\right)$$

$$A_{o1} = \frac{1}{150\gamma} \left(57\sqrt{2}\ \ \mathrm{Re}\langle a_2 a_1\rangle + 19\sqrt{3}\ \ \mathrm{Re}\langle a_1 a_o\rangle + 69\sqrt{2}\ i\ \mathrm{Im}\langle a_2 a_1\rangle + 69\sqrt{3}\ i\ \mathrm{Im}\langle a_1 a_o\rangle\right)$$

Appendix AXI: The Excitation, Electric Field Mixing and Decay Matrices: F, A and G; Appearing In the Asymmetry Calculation In the n = 3 States of Hydrogen.

Considering in particular the n = 3 states of hydrogen, then the intermediate states, β, β' and δ can take any of 18 distinct values given by $3\ell jm_j$: $\ell = 0, 1$ and 2; $j = |\underline{j}|$, $\underline{j} = \underline{s} + \underline{\ell}$, $s = |\underline{s}| = \frac{1}{2}$. The ground state α is represented by $1s\ \frac{1}{2} \pm \frac{1}{2}$ and γ, the final states, by $2\ell jm_j$. With this representation the F, A and G matrices can be calculated as follows:

AXI.1 The Excitation Matrix, F.

This 18 x 18 matrix is given by:

$$F_{\beta\beta'}(\alpha, \hat{\underline{K}}) \sim f_{\beta}(\alpha,\hat{\underline{K}})\ f^{*}_{\beta'}(\alpha,\hat{\underline{K}})$$

However, it is not necessary to compute all the 324 terms since only diagonal terms and the terms representing the coherent excitation of closely adjacent terms are considered for the analysis here. These 12 adjacent terms are: $\beta \leftrightarrow \beta' \equiv s\frac{1}{2} \pm \frac{1}{2} - p\frac{1}{2} \pm \frac{1}{2}$; $p3/2 \pm 3/2 - d3/2 \pm 3/2$; $p3/2 \pm \frac{1}{2} - d3/2 \pm \frac{1}{2}$, and of the twelve, only three distinct elements need be computed since

$$f_{3\ell jm_j}\ f^{*}_{3\ell' jm_j} = (f_{3\ell' jm_j}\ f^{*}_{3\ell jm_j})^{*}$$

and

$$f_{3\ell jm_j}\ f^{*}_{3\ell' jm_j} = (f_{3\ell j\ -m_j}\ f^{*}_{3\ell' j-m_j})^{*}$$

of the eighteen diagonal terms, only nine are distinct since

$$f_{3\ell jm_j}\ f^{*}_{3\ell jm_j} = f_{3\ell j-m_j}\ f^{*}_{3\ell j\ -\ m_j}$$

making a total of twelve separate elements in all to be calculated.

The angular dependence may be separated from the scattering amplitudes and then the $1s - 3\ell m_\ell$ amplitudes may be rewritten thus:

$$f_{3s} = - G_{3s}$$

$$f_{3pm_\ell} = - G_{3p}\, i\, Y^*_{1m_\ell}(\hat{\underline{K}})$$

$$f_{3dm_\ell} = G_{3d}\, Y^*_{2m_\ell}(\hat{\underline{K}})$$

The scattering amplitudes used here are either Born or polarized-Born:- expressions for either approximation are given in appendices AVI and AVII in which the $G_{3\ell}$ terms can be identified easily. Using Condon and Shortley (1953) (and in particular their equations (8a) and (8b) p.123), the coupled $f_{3\ell jm_j}$ are obtained in terms of the $f_{3\ell m_\ell}$. The table below gives all the elements of F:

$$f_{3s\frac{1}{2}\pm\frac{1}{2}} f^*_{3p\frac{1}{2}\pm\frac{1}{2}} = - f_{3p\frac{1}{2}\pm\frac{1}{2}} f^*_{3s\frac{1}{2}\pm\frac{1}{2}} = \mp \frac{i}{\sqrt{4\pi}}\, G_{3s}\, G_{3p} \cos\theta$$

$$f_{3p3/2\pm 3/2} f^*_{3d3/2\pm 3/2} = - f_{3d3/2\pm 3/2} f^*_{3p3/2\pm 3/2} = \mp \frac{3i}{8\pi}\, G_{3p} G_{3d} \cos\theta\sin^2\theta$$

$$f_{3p3/2\pm\frac{1}{2}} f^*_{3d3/2\pm\frac{1}{2}} = - f_{3d3/2\pm\frac{1}{2}} f^*_{3p3/2\pm\frac{1}{2}} = \mp \frac{i}{8\pi}\, G_{3p}\, G_{3d} \cos\theta(9\cos^2\theta - 5)$$

$$|f_{3s\frac{1}{2}\pm\frac{1}{2}}|^2 = G^2_{3s}$$

$$|f_{3p\frac{1}{2}\pm\frac{1}{2}}|^2 = \frac{1}{4\pi} G^2_{3p}$$

$$|f_{3p3/2\pm 3/2}|^2 = \frac{3}{8\pi} G^2_{3p} \sin^2\theta$$

$$|f_{3p3/2\pm\frac{1}{2}}|^2 = \frac{1}{8\pi} G^2_{3p} (1 + 3\cos^2\theta)$$

$$|f_{3d3/2\pm 3/2}|^2 = \frac{3}{8\pi} G^2_{3d} \sin^2\theta$$

$$|f_{3d3/2 \pm \frac{1}{2}}|^2 = \frac{1}{8\pi} G_{3d}^2 (1 + 3\cos^2\theta)$$

$$|f_{3d5/2 \pm 5/2}|^2 = \frac{15}{32\pi} G_{3d}^2 \sin^2\theta$$

$$|f_{3d5/2 \pm 3/2}|^2 = \frac{3}{32\pi} G_{3d}^2 \sin^2\theta (1 + 15\cos^2\theta)$$

$$|f_{3d5/2 \pm \frac{1}{2}}|^2 = \frac{3}{16\pi} G_{3d}^2 (5\cos^4\theta - 2\cos^2\theta + 1)$$

The integral $\int_{Kmin}^{Kmax} \int_0^{2\pi} F\, KdK\, d\phi$ $(= 2\pi \int_{Kmin}^{Kmax} F\, KdK)$ is simply evaluated for Born scattering amplitudes - however the integration is more complicated for the polarized Born case and therefore a numerical integration package (DOlACF) was used to calculate the twelve elements of the F matrix by quadrature. This program package is available on the NAG3F system library of the University of London Computer Centre CDC 7600 Computer.

AXI.2 The Electric Field Mixing Matrix, A.

The elements of this matrix are given by equation (7.3). To derive the functions $a_{\beta\delta}(\underline{E},t)$, it is necessary to obtain the solutions to the equations (7.4) and (7.5). By means of the tranformations

$$a_1 = b_1 \exp\left(\frac{iE_2 t}{\hbar}\right)$$

and

$$a_2 = b_2 \exp\left(\frac{iE_2 t}{\hbar}\right)$$

these equations may be written:

$$\frac{da_1}{dt} = \left(-\frac{iE_{12}}{\hbar} - \frac{\Gamma_1}{2}\right)a_1 - ifa_2$$

$$\frac{da_2}{dt} = ifa_1 - \frac{\Gamma_2}{2} a_2$$

where

$$f = f_{12} = f_{21} = \langle u_1 | \frac{eE_z}{h} | u_2 \rangle$$

$$E_{12} = E_1 - E_2$$

The convention adopted in the work below is that state 1 has orbital angular momentum = ℓ and state 2 has orbital angular momentum = $\ell - 1$.

There exists two sets of boundary conditions which yield four solutions, $a_{ij}(t)$, $(i,j = 1,2)$: the value of i corresponds to the boundary conditions adopted and j to the state amplitudes. These boundary conditions together can be used to describe the mixing process as intermediate to the individual conditions:

a) $a_{11}(0) = 1$, $a_{12}(0) = 0$ i.e. only state 1 is excited initially

b) $a_{11}(0) = 0$, $a_{12}(0) = 1$ i.e. only state 2 is excited initially.

Mahan (thesis 1974) has obtained the solutions $a_{ij}(t)$. These are:

$$a_{11}(t) = \frac{\beta_-}{\gamma} \exp(\alpha_+ t) + \frac{\beta_+}{\gamma} \exp(\alpha_- t)$$

$$a_{12}(t) = \frac{-if}{\gamma} \exp(\alpha_+ t) + \frac{if}{\gamma} \exp(\alpha_- t)$$

$$= a_{21}(t)$$

$$a_{22}(t) = \frac{\beta_+}{\gamma} \exp(\alpha_+ t) + \frac{\beta_-}{\gamma} \exp(\alpha_- t)$$

where

$$\omega_{12} = \frac{E_{12}}{h}, \quad \Gamma_\pm = \Gamma_1 \pm \Gamma_2,$$

$$\gamma = \sqrt{\left(\frac{\Gamma_-^2}{4} - 4f^2 - \omega_{12}^2 + i\omega_{12}\Gamma_-\right)},$$

$$\alpha_\pm = -\frac{\Gamma_+}{4} \pm \frac{\gamma}{2} - \frac{i\omega_{12}}{2},$$

$$\beta_\pm = \pm\frac{\Gamma_-}{4} + \frac{\gamma}{2} \pm \frac{i\omega_{12}}{2}.$$

The physical explanation of the $a_{ij}(t)$ is that they describe the amount of state j created by the effect of the field at time t when state

i was initially excited.

Strictly, $A_{\beta\delta\beta'\delta}(\underline{E},t)$ is defined in terms of the amplitudes $b_{ij} = a_{ij} \exp(-iE_2 t/h)$ but the exponential terms is always removed in the full expression (7.3) and therefore in the following the relations for a_{ij} only are retained.

Coherence mixing occurs since not all the integrals:

$$\int a_{\beta\delta}\, a^{*}_{\beta\delta}\, dt,$$

where $\delta \neq \beta$, are zero. The signal asymmetry arises in turn since not all the integrals:

$$\int a_{\beta\delta}\, a^{*}_{\beta'\delta}\, dt,$$

where $\beta \neq \beta'$, are zero. Since only two state mixing is considered here, then either $\beta = \delta$ or $\beta' = \delta$ in this latter integral.

An example of the mixing between the $3s_{\frac{1}{2}\pm\frac{1}{2}}$ and $3p_{\frac{1}{2}\pm\frac{1}{2}}$ is provided below. The $3p_{\frac{1}{2}\pm\frac{1}{2}}$ is referred to as state 1 and the $3s_{\frac{1}{2}\pm\frac{1}{2}}$ as state 2. There are five distinct terms for $A_{\beta\delta\beta'\delta}$ in this case, which are:

a) $\beta = \beta' = \delta = 3s_{\frac{1}{2}\pm\frac{1}{2}}$

$$A = \int_0^{\infty} a_{22}\, a^{*}_{22}\, dt = -\frac{1}{|\gamma|^2}\left\{\frac{|\beta_+|^2}{2\mathrm{Re}(\alpha_+)} + 2\mathrm{Re}\left[\frac{\beta_+\beta^{*}_-}{\alpha_+ + \alpha^{*}_-}\right] + \frac{|\beta_-|^2}{2\mathrm{Re}(\alpha_-)}\right\}$$

b) $\beta = \beta' = \delta = 3p_{\frac{1}{2}\pm\frac{1}{2}}$

$$A = \int_0^{\infty} a_{11}\, a^{*}_{11}\, dt = -\frac{1}{|\gamma|^2}\left\{\frac{|\beta_-|^2}{2\mathrm{Re}(\alpha_+)} + 2\mathrm{Re}\left[\frac{\beta_+\beta^{*}_-}{\alpha^{*}_+ + \alpha_-}\right] + \frac{|\beta_+|^2}{2\mathrm{Re}(\alpha_-)}\right\}$$

c) $\beta = \beta' = s_{\frac{1}{2}\pm\frac{1}{2}}$, $\delta = p_{\frac{1}{2}\pm\frac{1}{2}}$

$$A = \int_0^{\infty} a_{21}\, a^{*}_{21}\, dt = -\frac{f^2_{sp}(m_j)}{|\gamma|^2}\left\{\frac{1}{2\mathrm{Re}(\alpha_+)} - 2\mathrm{Re}\left[\frac{1}{(\alpha_+ + \alpha^{*}_-)}\right] + \frac{1}{2\mathrm{Re}(\alpha_-)}\right\}$$

and since $a_{21} = a_{12}$ this is equivalent to the case when

$$\beta = \beta' = p_{\frac{1}{2}} \pm \tfrac{1}{2}, \quad \delta = s_{\frac{1}{2}} \pm \tfrac{1}{2}.$$

(d) $\beta = \delta = s_{\frac{1}{2}} \pm \tfrac{1}{2}$. $\beta' = p_{\frac{1}{2}} \pm \tfrac{1}{2}$

$$A = \int_0^\infty a_{22}\, a_{12}^*\, dt = \mp \frac{i f_{sp}(m_j)}{|\gamma|^2} \left\{ \frac{\beta_+}{2\mathrm{Re}(\alpha_+)} - \frac{\beta_+}{(\alpha_+ + \alpha_-^*)} + \frac{\beta_-}{(\alpha_- + \alpha_+^*)} - \frac{\beta_-}{2\mathrm{Re}(\alpha_-)} \right\}$$

$$\left[= \left(\int_0^\infty a_{12}\, a_{22}^*\, dt \right)^* \right.$$

$$\left. = A^*_{\beta\delta\beta'\delta} \quad \text{where} \quad \beta' = \delta = s_{\frac{1}{2}} \pm \tfrac{1}{2}, \quad \beta = p_{\frac{1}{2}} \pm \tfrac{1}{2} \right]$$

(e) $\beta = s_{\frac{1}{2}} \pm \tfrac{1}{2}$; $\beta' = \delta = p_{\frac{1}{2}} \pm \tfrac{1}{2}$.

$$A = \int_0^\infty a_{21}\, a_{11}^*\, dt = \pm \frac{i f_{sp}(m_j)}{|\gamma|^2} \left\{ \frac{\beta_-^*}{2\mathrm{Re}(\alpha_+)} - \frac{\beta_-^*}{(\alpha_+^* + \alpha_-)} + \frac{\beta_+^*}{(\alpha_-^* + \alpha_+)} - \frac{\beta_+^*}{2\mathrm{Re}(\alpha_-)} \right\}$$

$$\left[= \left(\int_0^\infty a_{11}\, a_{21}^*\, dt \right)^* \right.$$

$$\left. = A^*_{\beta\delta\beta'\delta} \quad \text{where} \quad \beta = \delta = p_{\frac{1}{2}} \pm \tfrac{1}{2}. \quad \beta' = s_{\frac{1}{2}} \pm \tfrac{1}{2} \right]$$

Similar expressions for $p3/2 \pm 3/2$ - $d3/2 \pm 3/2$ and $p3/2 \pm \frac{1}{2}$ - $d3/2 \pm \frac{1}{2}$ two state mixing are obtained by referring to the states $p3/2 \pm 3/2$ or $p3/2 \pm \frac{1}{2}$ as state 2 and to the $d3/2 \pm 3/2$ or $d3/2 \pm \frac{1}{2}$ states as state 1 where appropriate. The remaining states of which account remains to be included are $3d5/2 \pm m_j$. These states are not mixed into any others and the amount of each state depends only on its lifetime thus:

(f) $\beta = \beta' = \delta = 3d5/2 \pm m_j$ ($m_j = \frac{1}{2}$, 3/2 or 5/2).

$$= \frac{1}{\Gamma_D}$$

Using Condon and Shortley 1963 (pps 123 and 132) we obtain:

$$f_{12} = \langle u_1 | \frac{eE_z}{\hbar} | u_2 \rangle$$

$$= \frac{eE}{\hbar} \langle n\ell j m_j | \frac{r\cos\theta}{\hbar} | n\ell\text{-}1\ j m_j \rangle$$

$$= \frac{3eE}{2\hbar} \cdot \frac{n\sqrt{(n^2-\ell^2)}}{(4\ell^2-1)} \left\{ \left[\ell^2-(\pm m_j + \tfrac{1}{2})^2\right]^{\frac{1}{2}} \left[\ell^2-(m_j - \tfrac{1}{2})^2\right]^{\frac{1}{2}} - \left[\ell^2-(\pm m_j - \tfrac{1}{2})^2\right]^{\frac{1}{2}} \left[\ell^2-(m_j + \tfrac{1}{2})^2\right]^{\frac{1}{2}} \right\}$$

and, explicitly:

$$f_{sp}(m_j) = 6\sqrt{2} m_j \frac{eE}{\hbar} \qquad (m_j \neq \pm\tfrac{1}{2})$$

$$f_{pd}(m_j) = 0.6\sqrt{5} m_j \frac{eE}{\hbar} \qquad (m_j = \pm\tfrac{1}{2}, \pm 3/2)$$

By referring to (a) - (e) above the field dependent terms can be identified. The terms in (c) give a symmetric field dependence since this varies as E^2. The terms in (d) and (e) are those which lead to the asymmetry since they vary only as E and thus are dependent on the sign of E. It should be noted that no complex terms arise in the final evaluation of (7.1) since complex cross-mixing terms such as (e) or (d) are matched with imaginary terms of the excitation matrix F and when the summations are completed the final result will be wholly real.

AXI.3 The Decay Matrix G.

The radiation matrix elements of interest are:

$$G_\delta = \sum_\gamma G_{\delta\gamma}(\hat{e})$$

$$\sim \sum_\gamma g_{\delta\gamma}(\hat{e})\, g^*_{\delta\gamma}(\hat{e})$$

As explained in Chapter 7, these elements include the transition probabilities together with a correction term to allow for the observation position. These correction terms can be calculated for each transition by considering the separate non-zero contributions to the radiation

intensity from three dipoles aligned along the x, y and z directions and then calculating the reduced intensity which would arise if the dipole aligned in the x direction is removed.

Thus, for example, considering radiation from the state $\delta = 3s_{\frac{1}{2}\frac{1}{2}}$: the total intensity is given by:

$$I^T = \sum_\gamma I_{\delta \to \gamma}$$

$$= I_{\delta \to 2p_{\frac{1}{2}\frac{1}{2}}} + I_{\delta \to 2p_{\frac{1}{2}-\frac{1}{2}}} + I_{\delta \to 2p3/23/2} + I_{\delta \to 2p3/2_{\frac{1}{2}}} + I_{\delta \to 2p3/2-\frac{1}{2}}$$

(note that $I_{\delta \to 2p3/2-3/2}$ is ommitted since this is a forbidden transition). Defining

$$W^{n'\ell'm}_{n\ell m} = (n'\ell'm'|w|\ n\ell m)$$

and

$$P^{n'\ell'}_{n\ell} = \int_0^\infty r^3 R_{n'\ell'}(r)\, R_{n\ell}(r)\, dr$$

where w can be x, y or z (and then W = X, Y or Z respectively). Then W gives the intensity strength for dipoles in each of the x, y or z directions. The function $R_{n\ell}(r)$ is the radial part of the $n\ell$ state Hydrogen wavefunction.

If P is the interaction, using Condon and Shortley (1963):

$$I_{\delta \to 2p_{\frac{1}{2}\frac{1}{2}}} \alpha \ |(2p_{\frac{1}{2}\frac{1}{2}}|\underline{P}|3s_{\frac{1}{2}\frac{1}{2}})|^2.$$

$$= \frac{1}{3} |(2p0|\underline{P}|3s0)|^2$$

$$= \frac{1}{3} (Z^{2p0}_{3s0})^2$$

$$= \frac{1}{9} (R^{2p}_{3s})^2$$

$$I_{\delta \to 2p_{\frac{1}{2}-\frac{1}{2}}} \alpha \ |(2p_{\frac{1}{2}-\frac{1}{2}}|\underline{P}|3s_{\frac{1}{2}\frac{1}{2}})|^2$$

$$= \frac{2}{3} |(2p-1|\underline{P}|3s0)|^2$$

$$= \frac{2}{3} \left[(X^{2p-1}_{3s0})^2 + (Y^{2p-1}_{3s0})^2\right]$$

$$= \frac{2}{9} (R^{2p}_{3s})^2$$

$$I_{\delta\to 2p3/23/2} \propto |(2p_{3/23/2}|\underline{P}|3s_{\frac{1}{2}\frac{1}{2}})|^2$$

$$= |(2p1|\underline{P}|3s0)|^2$$

$$= \left[(X^{2p1}_{3s0})^2 + (Y^{2p1}_{3s0})^2\right]$$

$$= \frac{1}{3}(R^{2p}_{3s})^2$$

$$I_{\delta\to 2p3/2\frac{1}{2}} \propto |(2p_{3/2\frac{1}{2}}|\underline{P}|3s_{\frac{1}{2}\frac{1}{2}})|^2$$

$$= \frac{2}{3}|(2p0|P|3s0)|^2$$

$$= \frac{2}{3}(Z^{2p0}_{3s0})^2$$

$$= \frac{2}{9}(R^{2p}_{3s})^2$$

$$I_{\delta\to 2p3/2-\frac{1}{2}} \propto |2p_{3/2-\frac{1}{2}}|\underline{P}|3s_{\frac{1}{2}\frac{1}{2}})|^2$$

$$= \frac{1}{3}|(2p-1|\underline{P}|3s0)|^2$$

$$= \frac{1}{3}\left[(X^{3p-1}_{3s0})^2 + (Y^{2p-1}_{3s0})^2\right]$$

$$= \frac{1}{9}(R^{2p}_{3s})^2$$

Therefore the corrected signal (i.e. that ignoring any contribution due to $X^{n'\ell'm'}_{n\ell m}$ terms in the above) is given by:

$$I^C \propto (\frac{1}{9} + \frac{1}{9} + \frac{1}{6} + \frac{2}{9} + \frac{1}{18})(R^{2p}_{3s})^2$$

$$= \frac{2}{3}(R^{2p}_{3s})^2,$$

the total signal is:

$$I^T \propto (\frac{1}{9} + \frac{2}{9} + \frac{1}{3} + \frac{2}{9} + \frac{1}{9})(R^{2p}_{3s})^2$$

$$= (R^{2p}_{3s})^2$$

and thus the correction factor is:

$$I^C/I^T = \frac{2}{3}.$$

The correction factors for the remaining transitions are calculated in the same way and we find (in agreement with the values reported by Mahan (thesis, 1974))

$$G_{3s\frac{1}{2}+\frac{1}{2}} = \frac{2}{3} \sum_{\gamma} A(3s_{\frac{1}{2}} \pm \tfrac{1}{2} \rightarrow \gamma)$$

$$G_{3p\frac{1}{2}\pm\frac{1}{2}} = \frac{2}{3} \sum_{\gamma} A(3p_{\frac{1}{2}} \pm \tfrac{1}{2} \rightarrow \gamma)$$

$$G_{3p\frac{1}{2}\pm\frac{1}{2}} = \frac{1}{2} \sum_{\gamma} A(3p_{3/2} \pm 3/2 \rightarrow \gamma)$$

$$G_{3p3/2\pm\frac{1}{2}} = \frac{5}{6} \sum_{\gamma} A(3p_{3/2} \pm \tfrac{1}{2} \rightarrow \gamma)$$

$$G_{3d3/2\pm3/2} = \frac{11}{20} \sum_{\gamma} A(3d_{3/2} \pm 3/2 \rightarrow \gamma)$$

$$G_{3d3/2\pm\frac{1}{2}} = \frac{47}{60} \sum_{\gamma} A(3d_{3/2} \pm \tfrac{1}{2} \rightarrow \gamma)$$

$$G_{3d5/2\pm5/2} = \frac{1}{2} \sum_{\gamma} A(3d_{5/2} \pm 5/2 \rightarrow \gamma)$$

$$G_{3d5/2\pm3/2} = \frac{7}{10} \sum_{\gamma} A(3d_{5/2} \pm 3/2 \rightarrow \gamma)$$

$$G_{3d5/2\pm\frac{1}{2}} = \frac{4}{5} \sum_{\gamma} A(3d_{5/2} \pm \tfrac{1}{2} \rightarrow \gamma)$$

The values for the transition probabilities, $A(\delta \rightarrow \gamma)$, are given in appendix AVIII.

The calculated values for the intensity at different values of the field and for different impact electron energies are computed by summing the expression (7.1) over α, β, β', δ and γ as necessary.

Appendix AXII Born R-Matrix Elements for the Hydrogen n = 3 Levels.

The elements of the reactance matrix are given by (see Seaton (1961) p.191, Lawson et al. (1961) and Somerville (1963)):

$$R(n\ell_1 k\ell_2 L, n'\ell_1' k'\ell_2' L) = -2(kk')^{\frac{1}{2}} \sum_{\lambda} f_\lambda(\ell_1\ell_2\ell_1'\ell_2';L)\, I_{\ell_2\ell_2'\lambda}(n\ell_1 n'\ell_1')$$

where: the coefficients

$$f_\lambda(\ell_1\ell_2\ell_1'\ell_2';L) = (\ell_1\ell_2 L|P_\lambda|\ell_1'\ell_2' L)$$

are tabulated by Percival and Seaton (1957); and

$$I_{\ell_2\ell_2'\lambda}(n\ell_1 n'\ell_1') = (n\ell_1 k\ell_2|\Gamma_\lambda(r_1,r_2)|n'\ell_1' k'\ell_2')$$

$$= \int_0^\infty \int_0^\infty P_{n\ell_1}(r_1) j_{\ell_2}(kr_2) \Gamma_\lambda(r_1,r_2) P_{n'\ell_1'}(r_1) j_{\ell_2'}(k'r_2) r_2^2 dr_1 dr_2$$

$$\Gamma_\lambda(r_1,r_2) = \gamma_\lambda(r_1,r_2) - \frac{\delta_{\lambda o}}{r_2}$$

(and $\gamma_\lambda(r_1,r_2)$ is defined in equation (2.25)).

$$P_{n\ell}(r) = rR_{n\ell}(Z,1) \qquad \text{(see equation (2.12))}$$

and $j_\ell(x)$ is a spherical Bessel function.

The Born R-matrix elements presented here are those for the $3\ell_1 \rightarrow 3\ell_1'$ transitions and for which $k = k'$. Furthermore, the fact that the long range parts of the potential dominate can be used to greatly simplify the calculations. Thus:

$$I_{\ell_2\ell_2'\lambda}(3\ell_1,3\ell_1') = \int_0^\infty \int_0^\infty P_{3\ell_1}(r_1)P_{3\ell_1'}(r_1)\gamma_\lambda(r_1,r_2)j_{\ell_2}(kr_2)j_{\ell_2'}(kr_2)r_2^2 dr_2 dr_1$$

$$- \int_0^\infty j_{\ell_2} j_{\ell_2'} r_2 dr_2 \, \delta_{\lambda o}\delta_{\ell_1\ell_1'}$$

$$= \int_0^\infty T_\lambda(3\ell_1,3\ell_1')j_{\ell_2} j_{\ell_2'} r_2^2 \, dr_2$$

and therefore

$$T_\lambda(3\ell_1,3\ell_1') = \frac{1}{r_2^{\lambda+1}} \int_0^{r_2} P_{3\ell_1}P_{3\ell_1'} r_1^\lambda dr_1 + r_2^\lambda \int_{r_2}^\infty \frac{P_{3\ell_1}P_{3\ell_1'}}{r_1^{\lambda+1}} dr_1 - \frac{\delta_{\ell_1\ell_1'}\delta_{\lambda_o}}{r_2}$$

$$\underset{r_2\to\infty}{\to} \frac{1}{r_2^{\lambda+1}} \int_0^\infty P_{3\ell_1}P_{3\ell_1'} r_1^\lambda \, dr_1 - \frac{\delta_{\ell_1\ell_1'}\delta_{\lambda_o}}{r_2} + O(r_2^{-\lambda-2})$$

The parameter λ is such that

$$|\ell_2 - \ell_2'| \leq \lambda \leq \ell_2 + \ell_2' \qquad \ell_2 + \ell_2' + \lambda = \text{even integer}$$

$$|\ell_1 - \ell_1'| \leq \lambda \leq \ell_1 + \ell_1' \qquad \ell_1 + \ell_1' + \lambda = \text{even integer.}$$

There are nine angular momentum states for given total angular momentum L given by:

label:	1	2	3	4	5	6	7	8	9
state $3\ell_1$:	3s	3p	3p	3p	3d	3d	3d	3d	3d
electron angular momentum ℓ_2:	L	L-1	L+1	L	L-2	L-1	L+2	L+1	L

The parity conservation condition requires that:

$$(-1)^{\ell_1+\ell_2} = (-1)^{\ell_1' + \ell_2'}$$

so that the states 1, 2, 3, 5, 7 and 9 all have one parity and states 4, 6, and 8 have the other parity: since there is no coupling between states in opposite groupes, the total number of separate R-matrix elements to be calculated is greatly reduced.

The asymptotic forms of $T_\lambda(3\ell_1,3\ell_1')$ are given below.

$T_o(3s,3s) \to 0$

$T_1(3s,3p) \to \frac{-18}{\sqrt{2}r^2}$

$T_2(3s,3d) \to \frac{45\sqrt{10}}{r^3}$

$T_o(3p,3p) \to 0$

$T_2(3p,3p) \to \frac{180}{r^3}$

$T_1(3p,3d) \to -\frac{9\sqrt{5}}{2r^2}$

$T_3(3p,3d) \to -\frac{945\sqrt{5}}{r^4}$

$T_o(3d,3d) \to 0$

$T_2(3d,3d) \to \frac{126}{r^3}$

$T_4(3d,3d) \to \frac{25515}{r^5}$

The integrals including the spherical Bessel functions can be obtained from:

$$\int_0^\infty \frac{1}{t^{\lambda-1}} j_\mu(kt) j_{\mu'}(kt)\, dt = \frac{\pi}{2k} \int_0^\infty \frac{1}{t^\lambda} J_{\mu+\frac{1}{2}}(kr) J_{\mu'+\frac{1}{2}}(kt)\, dt.$$

$$= \frac{\pi}{2k} \cdot \frac{k^{\lambda-1}}{2^\lambda} \cdot \frac{\Gamma(\lambda)\Gamma(\frac{\mu+\mu'+2-\lambda}{2})}{\Gamma(\frac{\mu-\mu'+\lambda+1}{2})\Gamma(\frac{\mu'-\mu+\lambda+1}{2})} \cdot \frac{1}{\Gamma(\frac{\mu+\mu'+\lambda+2}{2})}$$

(see Abramowitz and Stegun (1968), equations (11.4.33), (11.4.34) and (15.1.20)). This yields, for the integrals here:

$$\int_0^\infty j_\mu\, j_{\mu-1}\, dr = \frac{1}{2k\mu}$$

$$\int_0^\infty \frac{1}{r^2}\, j_\mu\, j_{\mu-1}\, dr = \frac{k}{3(\mu+1)\mu(\mu-1)}$$

$$\int_0^\infty \frac{1}{r}\, j_\mu\, j_{\mu-2}\, dr = \frac{1}{6\mu(\mu-1)}$$

$$\int_0^\infty \frac{1}{r^3}\, j_\mu\, j_{\mu-2}\, dr = \frac{k^2}{5(\mu+1)\mu(\mu-1)(\mu-2)}$$

$$\int_0^\infty \frac{1}{r}\, j_\mu\, j_\mu\, dr = \frac{1}{2\mu(\mu+1)}$$

$$\int_0^\infty \frac{1}{r^3}\, j_\mu\, j_\mu\, dr = \frac{k^2}{3(\mu+2)(\mu+1)\mu(\mu-1)}$$

$$\int_0^\infty \frac{1}{r^2}\, j_\mu\, j_{\mu-3}\, dr = \frac{k}{15\mu(\mu-1)(\mu-2)}$$

$$\int_0^\infty \frac{1}{r^3}\, j_\mu\, j_{\mu-4}\, dr = \frac{k^2}{35\mu(\mu-1)(\mu-2)(\mu-3)}$$

Writing:

$$R_{\ell_2\ell_2'}(3\ell_1, 3\ell_1') = R(3\ell_1 k\ell_2\, L, 3\ell_1' k\ell_2' L),$$

and using the results above leads directly to:

$$R_{LL}(3s,3s) = 0$$

$$R_{LL-1}(3s,3p) = \frac{18}{\sqrt{[6L(2L+1)]}}$$

$$R_{LL+1}(3s,3p) = \frac{-18}{\sqrt{[6(L+1)(2L+1)]}}$$

$$R_{LL-2}(3s,3d) = \frac{-15\sqrt{3}k}{\sqrt{[L(L-1)(2L-1)(2L+1)]}}$$

$$R_{LL}(3s,3d) = \frac{45\sqrt{2}k}{\sqrt{[L(L+1)(2L-1)(2L+3)]}}$$

$$R_{LL+2}(3s,3d) = \frac{-15\sqrt{3}k}{\sqrt{[(L+1)(L+3)(2L+1)(2L+3)]}}$$

$$R_{L-1L-1}(3p,3p) = \frac{-36k}{L(2L+1)}$$

$$R_{L-1L+1}(3p,3p) = \frac{36k}{(2L+1)\sqrt{[L(L+1)]}}$$

$$R_{L-1L-2}(3p,3d) = \frac{9}{\sqrt{[2(2L-1)(L-1)]}}\left[1 + \frac{30k^2}{\sqrt{[L(2L+1)]}}\right]$$

$$R_{L-1L}(3p,3d) = \frac{-9\sqrt{[(L+1)(2L+3)]}}{2L\sqrt{[3(2L-1)(2L+1)]}}\left[1 + \frac{180k^2}{(L+1)(2L+3)}\right]$$

$$R_{L-1L+2}(3p,3d) = \frac{135k^2\sqrt{2}}{(2L+1)\sqrt{[L(L+1)(L+2)(2L+3)]}}$$

$$R_{L+1L+1}(3p,3p) = \frac{-36k}{(L+1)(2L+1)}$$

$$R_{L+1L-2}(3p,3d) = \frac{-135k^2\sqrt{2}}{(2L+1)\sqrt{[L(L+1)(L-1)(2L-1)]}}$$

$$R_{L+1L}(3p,3d) = \frac{9\sqrt{[L(2L-1)]}}{2(L+1)\sqrt{[3(2L+1)(2L+3)]}}\left[1+\frac{180k^2}{L(2L-1)}\right]$$

$$R_{L+1L+2}(3p,3d) = \frac{-9}{\sqrt{[2(2L+3)(L+2)]}}\left[1+\frac{30k^2}{(L+1)(2L+1)}\right]$$

$$R_{L-2L-2}(3d,3d) = \frac{-36k}{(L-1)(2L-1)}\left[1+\frac{135k^2}{4L(2L+1)}\right]$$

$$R_{L-2L}(3d,3d) = \frac{6k\sqrt{[6(L+1)(2L+3)]}}{L(2L-1)\sqrt{[(L-1)(2L+1)]}}\left[1+\frac{405k^2}{2(L+1)(2L+3)}\right]$$

$$R_{L-2L+2}(3d,3d) = \frac{-1215k^3}{(2L+1)\sqrt{[(2L-1)(2L+3)(L+2)(L+1)(L-1)L]}}$$

$$R_{LL}(3d,3d) = \frac{18k(2L-3)(2L+5)}{L(L+1)(2L-1)(2L+3)}\left[1-\frac{405k^2}{(2L-3)(2L+5)}\right]$$

$$R_{LL+2}(3d,3d) = \frac{6k\sqrt{[6L(2L-1)]}}{(2L+3)(L+1)\sqrt{[(L+2)(2L+1)]}}\left[1+\frac{405k^2}{2L(2L-1)}\right]$$

$$R_{L+2L+2}(3d,3d) = \frac{-36k}{(L+2)(2L+3)}\left[1+\frac{135k^2}{4(L+1)(2L+1)}\right]$$

$$R_{LL}(3p,3p) = +\frac{36k}{L(L+1)}$$

$$R_{LL-1}(3p,3d) = \frac{9\sqrt{(L-1)}}{2L\sqrt{(2L+1)}}\left[1-\frac{60k^2}{(L-1)(L+1)}\right]$$

$$R_{LL+1}(3p,3d) = -\frac{9\sqrt{(L+2)}}{2L\sqrt{(2L+1)}}\left[1-\frac{60k^2}{L(L+2)}\right]$$

$$R_{L-1L-1}(3d,3d) = \frac{18k(L+5)}{L(L-1)(2L+1)}\left[1+\frac{135k^2}{(L+1)(L+5)}\right]$$

$$R_{L-1L+1}(3d,3d) = \frac{18k\sqrt{[(L-1)(L+2)]}}{L(L+1)(2L+1)}\left[1-\frac{135k^2}{(L-1)(L+2)}\right]$$

$$R_{L+1L+1}(3d,3d) = \frac{18k(L-4)}{(L+1)(L+2)(2L+1)}\left[1+\frac{135k^2}{L(L-4)}\right]$$

REFERENCES

Abramowitz M. and Stegun I.A.,1968, 'Handbook of Mathematical Functions', Dover Publications Inc., New York

Bates D.R.,1962, in: 'Atomic and Molecular Processes', ed: D.R.Bates, Academic Press (New York)

Bates D.R.,Fundaminsky A.,Leech J.W., and Massey H.S.W., 1950, Phil Trans Roy Soc A243, pps 93-143

Baye D. and Heenen P.H.,1974, J Phys B 7, p 928

Beigman I.L. and Shevel'ko V.P.,1974, Opt Spectrosc 37, p 353

Belling J.A., 1968, J Phys B 2, p 136

Bethe H.A. and Salpeter E.E.,1957, 'Quantum Mechanics of One and Two Electron Atoms', Springer - Verlag (Berlin)

Bhadra K. and Ghosh A.S.,1971, Phys Rev Lett 26, p737

Bransden B.H. and Coleman J.P.,1972, J Phys B 5, p 537

Bransden B.H.,Coleman J.P. and Sullivan J.,1972, J Phys B 5, p 546

Bransden B.H.,McDowell M.R.C.,Noble C.J. and Scott T.,1976, J Phys B 9, p 1301

Bransden B.H. and Noble C.J.,1976, J Phys B 9, p 1507

Burgess A.,1963, Proc Phys Soc (Lond) 81, p 442

Burgess A.,Hummer D.G. and Tully S.A.,1970, Phil Trans Roy Soc A266, p 255

Burke P.G.,Schey H.M. and Smith K.,1963, Phys Rev 129, p 1258

Burke P.G.,Ormonde S. and Whittaker W.,1967, Proc Phys Soc (Lond) 92, p 319

Callaway J.,LaBahn R.W.,Pöe R.J. and Duxler W.,1968, Phys Rev 168, p 12

Condon E.U. and Shortley G.H., 1963, 'The Theory of Atomic Spectra', Cambridge University Press (Cambridge)

Drachman R.J. and Temkin A., 1972, in: 'Case studies in Atomic Collision Physics 2', (p 401), eds: E.W.McDaniel and M.R.C.McDowell, North Holland (Amsterdam)

Duxler W., Pöe R.J. and LaBahn R.W., 1971, Phys Rev A4, p 1935

Dwight H.B., 1961, 'Tables of Integrals and Other Mathematical Data', MacMillan (New York)

Edmonds A.R., 1960, 'Angular Momentum in Quantum Mechanics', Princeton University Press,

Eminyan M., McAdam K.B., Slevin J. and Kleinpoppen H., 1973, Phys Rev Lett 31, p 576

---- 1974, J Phys B 7, p 1519

Fano U. and Macek J.H., 1973, Rev Mod Phys 45, p 553

Fon W.C., Kingston A.E. and Burke P.G., 1975, 'Proc 9th Int Conference on Physics of Electronic and Atomic Collisions', Seattle, vol 2, (Seattle: University of Washington) p 669

Flannery M.R. and McCann K.J., 1974, J Phys B 7, L522

Garcia J.D. and Mack J.E., 1965, J Opt Soc Am 55, p 654

Goldberger and Watson , 1964, 'Collision Theory', Wiley (New York)

Gordon, 1928, Zeits fur Physik 48, p 180

Gradsteyn I.S. and Ryzhiz I.M., 1965, 'Tables of Integrals, Series and Products', Academic Press (New York)

Gumble R.S., 1969, J Phys Soc Japan 27, p 973

Holt A.R. 1969, J Phys B 2, p 1202

Inokuti M. and McDowell M.R.C., 1974, J Phys B 7, p 2382

Kleinpoppen H. and Kraiss E., 1968, Phys Rev Lett 20, p 361

Kleinpoppen H., Kruger H. and Ulmer R., 1962, Phys Lett 2, p 78

Krotkov R., 1975, Phys Rev A12, p 1793

Landau L.D. and Lifshitz E.M., 1958, 'Quantum Mechanics', Pergamon (New York)

Lawson J.,Lawson W. and Seaton M.J.,1961, Proc Phys Soc (Lond) 77, p 192

Lloyd D. and McDowell M.R.C.,1969, J Phys B 2, p 1313

McDowell M.R.C. and Coleman J.P.,1969, 'Introduction To The Theory of Ion - Atom Collisions', North Holland (Amsterdam)

McDowell M.R.C.,Morgan L.A. and Myerscough V.P.M.,1973, (IA), J Phys B 6, p 1435

---- 1974, (IB), Comput Phys Commun 7, p 38

---- 1975a, (III), J Phys B 8, p 1053

---- 1975b, (V), J Phys B 8, p 1838

McDowell M.R.C., Myerscough V.P.M. and Narain U.,1974, (II), J Phys B 7, L195

Macek J. and Jaecks D.H.,1971, Phys Rev A4, p 2288

Mahan A.H.,1974, PhD Thesis, University of Colorado

Mahan A.H.,Gallagher A. and Smith S.J.,1976, Phys Rev A13, p 156

Mandelberg H.I.,1970, Phys Rev A2, p 1372

Mittleman M.H. and Pöe R.J.,1962, Phys Rev 126, p 370

Moiseiwitsch B.L. and Smith S.J.,1968, Rev Mod Phys 40, p238

Morgan L.A. and McDowell M.R.C.,1975, (IV), J Phys B 8, p1073

Morrison D.J.T. and Rudge M.R.H.,1966, Proc Phys Soc (Lond) 89, p 45

Mott N. and Massey H.S.W.,1971,'The Theory of Atomic Collisions', Oxford University Press, Oxford

Ochkur V.J.,1964, Sov Phys JEPT 18, p 503

Oppenheimer J.R.,1927a, Zeits fur Physik 43, p 27

---- 1927b, Proc Nat Acad Sci 13, p 800

---- 1928, Phys Rev 32, p 361

Ott W.O.,Kauppila W.E. and Fite W.L.,1970, Phys Rev A1, p 1089

Penney W.G.,1932, Proc Nat Acad Sci 18, p 231

Percival I.C. and Seaton M.J.,1957, Proc Camb Phil Soc 53, p 654

---- 1958, Phil Trans Roy Soc A251, p 113

Rudge M.R.H.,1965a, Proc Phys Soc (Lond) 85, p 607

---- 1965b, Proc Phys Soc (Lond) 86, p 763

Scott T. and McDowell M.R.C.,1975, J Phys B 8, p 1851

Seaton M.J.,1961, Proc Phys Soc (Lond) 77, p 174

Smith S.J.,1975, in: 'Electron and Photon Interactions With Atoms', eds: H.Kleinpoppen and M.R.C.McDowell, Plenum (New York)

Somerville W.B.,1963, Proc Phys Soc (Lond) 82, p 446

Sternheimer R.M.,1954, Phys Rev 96, p 951

Syms R.F.,McDowell M.R.C.,Morgan L.A. and Myerscough V.P.,1975, (VI) J Phys B 8, p 2817

Tai H.,Bassel R.H.,Gerjuoy E. and Franco V.,1970, Phys Rev A1, p 1819

Temkin A.,1959, Phys Rev 116, p 358

Temkin A. and Lamkin ,1961, Phys Rev 121, p 788

Vainshtein L.A.,1961, Opt Spectrosc (USSR) 11, p 163

---- 1965, Opt Spectrosc (USSR) 18, p 538

Vainshtein L.A. and Presnyakov L.,1969, Sov Phys JEPT 28, p 156

Walker J.D. and St John R.M.,1974, J Chem Phys 61, p 2394

Walters H.R.J.,1976, J Phys B 9, p 221

Wiese, Smith and Glennon,1966, 'Atomic Transition Probabilities - 1: Hydrogen through Neon',NSRDS-NBS-4, US Govt Printing Office

Williams J.F. and Willis B.A.,1975, J Phys B 8, p 1641

Woollings M.J. and McDowell M.R.C.,1973, J Phys B 6, p 450

Wu T-Y and Ohmura T., 1962, "Quantum Theory of Scattering", Prentice-Hall Int. (London)

J. Phys. B: Atom. Molec. Phys., Vol. 8, No. 17, 1975. Printed in Great Britain.

Electron impact excitation of H and He^+ VI. Excitation of the $n = 3$ levels

R F Syms†, M R C McDowell†, L A Morgan‡ and V P Myerscough§

† Mathematics Department, Royal Holloway College, Egham Hill, Egham, Surrey TW20 0EX

‡ Department of Computer Science, Royal Holloway College, Egham Hill, Egham, Surrey TW20 0EX

§ Department of Applied Mathematics, Queen Mary College, Mile End Road, London E1 4NS

Received 23 June 1975

Abstract. Electron impact excitation of the $n = 3$ levels of atomic hydrogen is investigated by generalizing the DWPO II approximation (McDowell *et al*) to $1s \rightarrow nlm_l$ transitions. Results are presented, at energies from threshold to 500 eV, for total cross sections for each $1s \rightarrow 3l$ ($l = 0, 1, 2$) transition, total $n = 3$ cross sections, and the cross section for Hα production. They are compared, where possible, with experiment.

Results for the polarization of Hα emitted at 90° to the incident beam are given in Born and DWPO II models, and shown to be inconsistent with experiment.

Differential cross sections for individual and total $n = 3$ transitions are tabulated at selected angles and energies. Further experimental and theoretical work is suggested.

1. Introduction

We extend our earlier work (McDowell *et al* 1973, 1974, 1975a, b, Morgan and McDowell 1975, papers I–V of the present series) on application of the distorted wave polarized orbital approximation (DWPO) to the transition

$$e + H(1s) \rightarrow e + H(3l; l = 0, 2). \tag{1}$$

There is little published theoretical work on these transitions except in the first Born approximation; a modified Born approximation (Morrison and Rudge 1966), a two-state distorted wave approximation (Vainshtein 1961) and the Glauber approximation (Tai *et al* 1970, Bhadra and Ghosh 1971). In our first paper (McDowell *et al* 1973) we gave DWPO results for $1s \rightarrow 3s$ excitation, neglecting target distortion (DWPO I), while Woollings and McDowell (1973) gave results for $1s \rightarrow 3d$ in a simplified second Born approximation. There are some close-coupling results near threshold (Burke *et al* 1963).

The lack of theoretical interest in the $n = 3$ transitions has undoubtedly been partially due to the paucity of reliable experimental data. This situation has now changed. The measurement of the total Hα production cross section (see below) by Kleinpoppen and Kraiss (1968) has now been repeated by Walker and St John (1974), who claim an absolute calibration. At the same time Mahan has used an elegant and sophisticated technique to obtain cross sections for the individual $1s \rightarrow nl$ ($l = 0, 1, 2$) transitions (relative to the Born approximation for $1s \rightarrow 3p$ at 500 eV) and has discovered some interesting asymmetries (Mahan 1974, Mahan *et al* 1975, Smith 1975,

see also Krotlzov 1975). The only measurements of the optical polarization of the Balmer α line are those of Kleinpoppen and his collaborators (Kleinpoppen and Kraiss 1968, Kleinpoppen *et al* 1962).

A knowledge of the total and differential cross sections for the magnetic sublevels (l, m_l) will enable a study to be made of orientation and alignment effects detectable by coincidence experiments (Eminyan *et al* 1974, Morgan and McDowell 1975, IV) and this study will be described in a subsequent paper.

In the present paper we give a unified treatment of our DWPO models for the general $1s \rightarrow nlm_l$ transition in hydrogenic systems, (§ 2). A computer program (POLORB 2) embodying the results of this analysis is being prepared for publication elsewhere (Morgan *et al* 1975). Details of the analysis are given by Syms (1975). Our results for total cross sections for $n = 3$ are presented in § 3 while in § 4 we consider the optical polarization of Hα, and the total Hα production cross section. A selected set of values of differential cross sections are given in § 5. Finally we present our conclusion in § 6.

2. General theoretical formulation

Adopting the notation of our earlier papers, the cross section for the $1s \rightarrow nlm_l$ transition in atomic hydrogen may be written

$$Q(1s \rightarrow nlm_l, k_i^2) = \frac{1}{2\pi^2 k_i^2} \int_{K_{min}}^{K_{max}} |T_{if}|^2 K \, dK \; (\pi a_0^2) \tag{2}$$

where

$$|T_{if}(K)|^2 = \tfrac{1}{4}(|T_{if}^+|^2 + 3|T_{if}^-|^2) \tag{3}$$

(plus and minus signs referring to singlet and triplet respectively).

2.1. The DWPO I model

In the DWPO I approximation which neglects target distortion,

$$T_{if}^{\pm}(K) = \langle \phi_{nlm_l}(Z, 1)\chi_{k_f}(z, 2)|V_f|(1 \pm P_{12})\phi_{1s}(1)F^{\pm}(2)\rangle. \tag{4}$$

The scattering function $F^{\pm}(2)$ is expanded in partial waves, and evaluated in the exchange adiabatic approximation (I, equation (11)). We work in an uncoupled representation, and expand $T_{if}^{\pm}$ in terms of the partial waves λ' of the scattered electron,

$$T_{if}^{\pm}(K) = \sum_{\lambda'=0}^{\infty} C_{\lambda'}^{\pm}(m_l) P_{\lambda'}^{|m_l|}(\cos\theta) = \mathscr{C}_{m_l}^{\pm} + i\mathscr{D}_{m_l}^{\pm}. \tag{5}$$

Then after some algebra we find

$$C_{\lambda'}^{\pm}(m_l) = \frac{4\pi}{[(2l+1)k_i]^{1/2}} \sum_{\lambda=0}^{\infty} i^{\lambda-\lambda'} e^{i\xi_{\lambda\lambda'}^{\pm}} \chi_{\lambda\lambda'}^{lm_l} \left[I^{\pm}(\lambda, \lambda') \pm \frac{(2l+1)}{(2\lambda'+1)} \times \left(J^{\pm}(\lambda, \lambda') - \delta_{\lambda' 0}\delta_{m_l 0}\delta_{\lambda l} \frac{2Z^{3/2}}{(Z^2 + k_f^2)} d(\alpha_f) K^{\pm}(l, 0) \right) \right] \tag{6}$$

with

$$\chi^{lm_l}_{\lambda\lambda'} = (2\lambda+1)(2\lambda'+1)\left(\frac{(\lambda'-|m_l|)!}{(\lambda'+|m_l|)!}\right)^{1/2}\begin{pmatrix}\lambda' & l & \lambda\\ m_l & -m_l & 0\end{pmatrix}\begin{pmatrix}\lambda' & l & \lambda\\ 0 & 0 & 0\end{pmatrix}, \tag{7}$$

the other factors being generalizations of those defined in III.

2.2. *The* DWPO II *model*

In this model we take account of target distortion in the direct term of the T matrix, but, consistent with neglecting exchange polarization terms in solving for the scattering function, we neglect it in the exchange term. To be precise, we allow the initial state of the target to be perturbed by the dipole component of the interaction with the incident electron, to first order in the interaction, provided that electron is farther away from the nucleus than the bound electron. Thus we obtain

$$\tilde{T}^{\pm}_{\mathrm{if}}(K) = T^{\pm}_{\mathrm{if}}(K) + \langle \phi_{nlm_l}(Z,1)\chi_{k_\mathrm{f}}(z,2)|V_\mathrm{f}|\phi_{\mathrm{pol}}(1,2)F^{\pm}(2)\rangle \tag{8}$$

where $\phi_{\mathrm{pol}}(1,2)$ is defined in II. The only effect is to modify (6) above by replacing $I^{\pm}(\lambda,\lambda')$ by $\tilde{I}(\lambda,\lambda')$ as in III, but now

$$t_{1\mathrm{s},nl}(r) = \left(\frac{2l}{(l-1)}k^{(l-1)}_{1\mathrm{s},nl} + \frac{2(l+1)}{(2l+3)}k^{(l+1)}_{1\mathrm{s},nl}\right)r. \tag{9}$$

The kernel functions $k^{(l')}_{1\mathrm{s},nl}$ are given by (see also appendix)

$$\begin{aligned} k^{(l')}_{1\mathrm{s},nl}(r) &= -\frac{1}{r^{l'+3}}\int_0^r t^{l'+1}U_{1\mathrm{s}\to\mathrm{p}}(t)R_{nl}(t)\,\mathrm{d}t, \qquad l' > 0\\ &= 0, \qquad l' \leqslant 0 \end{aligned} \tag{10}$$

and $U_{1\mathrm{s}\to\mathrm{p}}(r)$ is the Sternheimer function defined in II. This is equivalent to replacing $rf_{1\mathrm{s},nl}(r)$ in $I^{\pm}(\lambda,\lambda')$ by $rf_{1\mathrm{s},nl}(r)+t_{1\mathrm{s},nl}(r)$. The leading term of $k^{(1)}_{1\mathrm{s},ns}$ is, of course, of polarization form; $k^{(1)}_{1\mathrm{s},ns}(r) \simeq -c/r^4$.

2.3. *Total and differential cross sections*

With the above definitions the total cross section may be written

$$\sigma(1\mathrm{s}\to nlm_l;k_\mathrm{i}^2) = \frac{1}{4\pi^2}\frac{k_\mathrm{f}}{k_\mathrm{i}}\sum_{\lambda'=0}^{\infty}\frac{(\lambda'+|m_l|)!}{(\lambda'-|m_l|)!}\frac{1}{(2\lambda'+1)}(|C^+_{\lambda'}(m_l)|^2+3|C^-_{\lambda'}(m_l)|^2) \tag{11}$$

while the corresponding differential cross section is

$$\frac{\mathrm{d}\sigma}{\mathrm{d}\Omega}(m_l) = \frac{1}{16\pi^2}\frac{k_\mathrm{f}}{k_\mathrm{i}}[|T^+_{\mathrm{if}}(m_l,K)|^2+3|T^-_{\mathrm{if}}(m_l,K)|^2] \tag{12}$$

$$= \frac{1}{16\pi^2}\frac{k_\mathrm{f}}{k_\mathrm{i}}[\mathscr{C}^{+2}_{m_l}+\mathscr{D}^{+2}_{m_l}+3(\mathscr{C}^{-2}_{m_l}+\mathscr{D}^{-2}_{m_l})] \tag{13}$$

and may be readily summed over m_l to give the corresponding cross sections for $1\mathrm{s}\to nl$ transitions.

In practice, rather than evaluating the T-matrix elements via (5) above, we choose some λ'_0 such that for $\lambda' > \lambda'_0$ the Born approximation to the direct terms of the partial wave T matrix differs from the DWPO approximation by a pre-assigned small amount.

Then

$$T_{if}^{\pm} = \sum_{\lambda'=0}^{\lambda'_0} (C_{\lambda'}^{\pm}(m_l) - C_{\lambda'}^{B}(m_l)) P_{\lambda'}^{|m_l|}(\cos\theta) + T_{if}^{B} \tag{14}$$

where $C_{\lambda'}^{B}(m_l)$ is the Born approximation to $C_{\lambda'}^{\pm}(m_l)$ obtained by replacing $U_{\lambda'}^{\pm}(k_i, r)$ by a Coulomb (or Bessel) function, and T_{if}^{B} is the Born T matrix.

Let $\sigma_{\lambda'_0}$ be the approximation to σ (equation (11)) obtained by summing up to λ'_0 only, and let $\sigma_{\lambda'_0}^{B}$ be the approximation obtained by summing up to λ'_0 only and replacing distorted by undistorted waves: then

$$\sigma(1s \rightarrow nlm_l, k_i^2) = \sigma_{\lambda'_0} - \sigma_{\lambda'_0}^{B} + \sigma_B(nlm_l) \tag{15}$$

where $\sigma_B(nlm_l)$ is the Born approximation total cross section for the $1s \rightarrow nlm_l$ transition.

For s–s transitions, exchange is important even for $\lambda' > \lambda'_0$, and we adopt a similar procedure except that σ_B is replaced by the Born–Oppenheimer cross section σ_{BO}. For $z > 0$, we approximate Coulomb waves by plane waves. This is precisely the large λ' correction introduced by Burgess *et al* (1970), and is justified provided $\xi_{\lambda\lambda'}^{\pm}$ is negligible for such λ'. We therefore choose λ'_0 such that

$$\xi_{\lambda\lambda'_0}^{\pm} \leqslant 10^{-3}.$$

3. Results

3.1. Total cross sections for individual 1s → nlm$_l$ transitions

Our calculated total cross sections for the individual transitions

$$e + H(1s) \rightarrow e + H(3l), \qquad l = 0, 1, 2$$

are shown in figure 1. The 3p cross section is by far the largest, but the DWPO II results, which include the effects of polarization distortion of the target, are approximately 10% lower than the DWPO I values over the energy range from 20 to 200 eV. At high energies, σ(3p, DWPO I) tends to the Born approximation, but σ(3p, DWPO II) approaches the polarized-Born approximation. This is defined (McDowell *et al* 1975b) by the T matrix

$$T_{if}^{PB} = \langle \phi_{nlm_l}(Z, 1)\chi_{k_f}(z, 2) | V_f | (\phi_{1s0}(Z, 1) + \phi_{pol}(1, 2))\chi_{k_i}(z, 2) \rangle \tag{16}$$

and introducing an antisymmetrizer, one similarily obtains a polarized-Born–Oppenheimer approximation. Results in this approximation can be obtained in closed form and do not approach the Born result until very high impact energies. They provided a close check on the detailed DWPO II calculations. The 3s cross section is small at all energies and polarization distortion effects were found to be insignificant above 100 eV. However while σ(3d, DWPO I) is comparable in magnitude to the 3s cross section, polarization distortion effects are now very large. Thus σ(3d, DWPO II) is 50% smaller than the DWPO I result at 200 eV and at high energies, the DWPO II results, which are equivalent above 200 eV to the polarized-Born results, continue to be significantly below the Born approximation (figure 4(b)). Similar conclusions have been reached independently by Beigman in an investigation of electron impact induced inelastic transitions in the alkalis (Beigman and Shevel'ko 1974). Non-adiabatic distortions may significantly reduce this effect at higher energies.

Our 3s results are compared with those of other workers in figure 2. The experimental results shown are the relative measurements of Mahan (Mahan 1974, Mahan *et al*

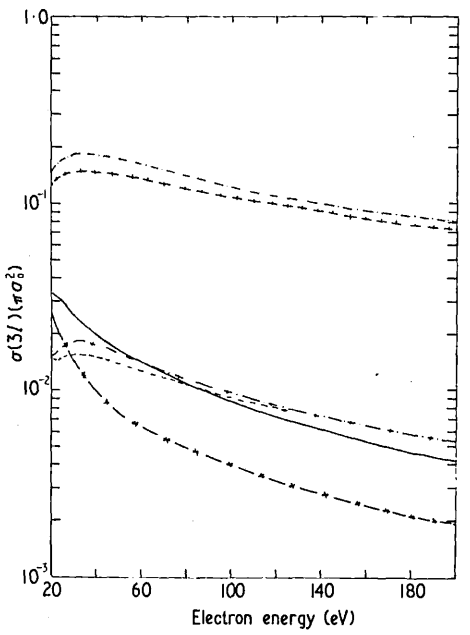

Figure 1. Total $3l$ ($l = 0, 1, 2$) cross sections in units of πa_0^2 for impact electron energy in the range 20 to 200 eV. $-\cdot+\cdot-\cdot+\cdot$, 3s DWPO I approximation; ————————, 3s DWPO II approximation; $\cdot-\cdot-\cdot-\cdot-\cdot-$, 3p DWPO I approximation; + + + + + + + +, 3p DWPO II approximation; ————————, 3d DWPO I approximation; $-*-*-*-*-*$, 3d DWPO II approximation.

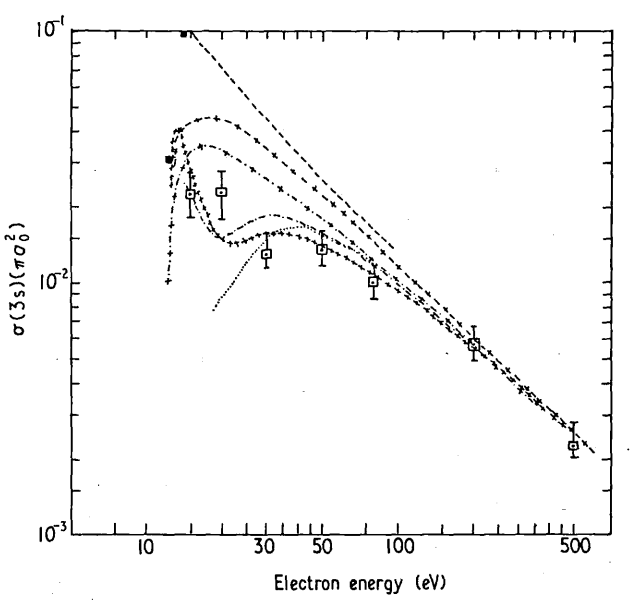

Figure 2. Total 3s cross sections in units of πa_0^2 for impact electrons energies from threshold to 500 eV. ■, Burke *et al* (1967) (six-state close-coupling); ————————, Vainshtein (1961) (distorted wave); + − + − + − + −, Born approximation; + + + + + + + +, DWPO II approximation; $-\cdot-\cdot-\cdot-\cdot-\cdot-$, DWPO I approximation; $-\cdot+\cdot-\cdot+\cdot$, Morrison and Rudge (1966) (modified Born); ·····, Tai *et al* (1970) (Glauber); ⊡, Mahan (1974).

1975), obtained via a normalization to the Born 3p cross section at 500 eV. Our results are in excellent agreement with this experiment throughout the energy range. The Glauber calculations of Tai *et al* (1970) are also in good accord with experiment at energies above 30 eV. The Born cross section and the modified Born results of Morrison and Rudge (1966) substantially overestimate the cross section at energies below 150 eV. We also show an early distorted wave calculation of Vainshtein (1961).

The calculated values of $\sigma(3p)$ are compared with those of other workers, and with the experimental values (Mahan 1974) in figure 3. Our DWPO II results are in good

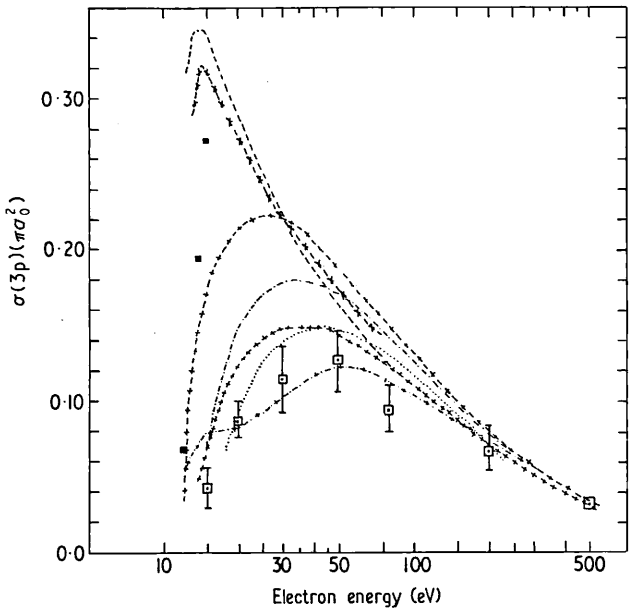

Figure 3. Total 3p cross sections in units of πa_0^2 for impact electron energies from threshold to 500 eV. The meaning of the curves is the same as in figure 2, with – * – * – * –, Burke *et al* (1963) (two-state close-coupling).

general agreement with experiment when this is renormalized to our $\sigma(3p)$ value at 500 eV, rather than to the Born value which is 8% higher. However, with this renormalization we lie slightly above Mahan's estimated RMS errors below 40 eV. The modified Born results of Morrison and Rudge (1966) are, however, in excellent agreement with experiment above 20 eV. Of the other available theoretical results only the Glauber (Tai *et al* 1970) gives reasonable accord, in shape and magnitude, with the experimental values. In particular the two-state close-coupling calculation of Burke *et al* (1963) yields very large values of $\sigma(3p)$, in total disagreement with experiment at energies below 50 eV. This may be partly because inclusion of only the 1s and 3p states in a close-coupling expansion does not account for much of the ground state polarizability. Burke *et al* (1967) give six-state close-coupling results for $1 \rightarrow 3$ transitions below the $n = 4$ threshold. Their results for $\sigma(3p)$ which are also shown in figure 3 increase very rapidly above threshold and again appear in disagreement with experiment. Burke *et al* remark that they believe their results to be of doubtful validity (due to resonances below the $n = 4$ threshold whose effect is not included) except at $k_i^2 = 0{\cdot}9$ au. An eleven-state 'pseudostate' calculation, combined with our DWPO II values for partial

wave contributions $L > 3$, is in hand (cf Callaway *et al* 1976) and may help to resolve this discrepancy.

Finally our calculated 3d values are shown in figure 4(*a*), (*b*). We first compare our DWPO I and DWPO II results with Mahan's experimental values (normalized to the Born 3d at 500 eV), and with certain other theoretical calculations. Mahan's results have an energy dependence which differs substantially from that of the first Born approximation and his results lie 50% above the first Born approximation at its maximum. However, both the shape and the magnitude of the experimental results are correctly given by σ(3d, DWPO I) at all energies. The simplified second Born calculation of Woolings and McDowell (1973) and the Glauber results of Bhadra and Ghosh (1971) are in very close agreement with each other, tend to the first Born approximation at high energies, but lie a factor of two below experiment (normalized as above) at its maximum: that is, they also show an energy dependence which differs from the experimental one. The modified Born results (Morrison and Rudge 1966) give substantially lower values near the maximum of the cross section, and again tend to the Born at high energies. As we have already remarked, the effect of polarization distortion of the target on the calculated cross sections is large in this case. The DWPO II results (which agree above 200 eV with the polarized-Born results) are shown in figure 4(*b*).

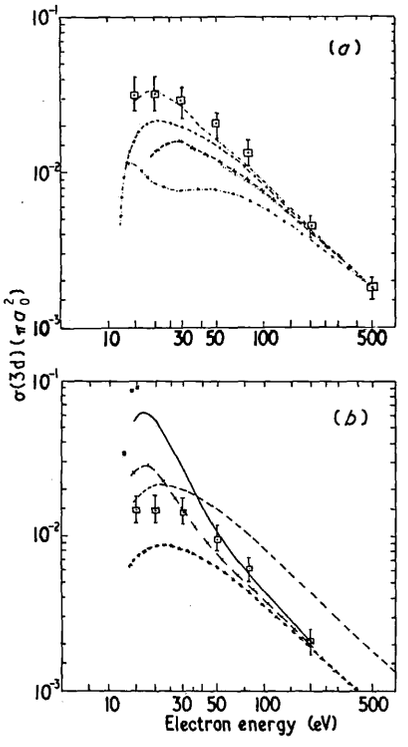

Figure 4. Total 3d cross sections in units of πa_0^2 for impact electron energies from threshold to 500 eV. (*a*) − + − + − + − +, Born approximation; − · − · − · −, DWPO I approximation; − * − * − * − *, Bhadra and Ghosh (1971) (Glauber); − · + · − · + ·, Morrison and Rudge (1966) (modified Born); ⊡, Mahan (1974), normalized to Born 3d at 500 eV. (*b*) ————, Born–Oppenheimer II (includes target distortion); + + + +, DWPO II approximation; − − − −, Born; ********, Born II (includes target distortion); ■, Burke *et al* (1967) (six-state close-coupling); ⊡, Mahan (1974), normalized to Born II at 500 eV.

At 480 eV they lie a factor of 2·4 below the first Born values, and even at 5 keV are still almost a factor of two lower. Similar results were found for σ(2p, DWPO II) by McDowell *et al* (1975b) and for several s–p transitions in the alkalis by Beigman and Shevel'ko (1974). This effect does not disappear, though it may be reduced, in higher order calculations when non-adiabatic effects are included. Extension of the three-state close-coupling calculation to high energies (Fon *et al* 1975) produces results for σ(2p) appreciably below the first Born results.

We therefore believe that our values of σ(3d, DWPO II) are superior to the first Born approximation at 500 eV and choose to renormalize the experimental values to them at this energy (figure 4(*b*)).

Our calculated values remain in accord with the renormalized experiment at energies $E_i > 30$ eV. We also show the results of a Born–Oppenheimer calculation, modified as in DWPO II to include polarization distortion of the target. This always gives values greater than those obtained in DWPO II, the effect being a factor of two at the maximum of the cross section. This comparison shows that while target distortion lowers the calculated cross section at high energies, it is distortion of the incident wave which has the dominant effect at energies below 100 eV.

The calculations reported here do not allow for p–d coupling, which may be important. This may be investigated by the unitarization (R matrix) technique suggested by Seaton (1961), and will be reported on in a later paper.

The effect of renormalization of the measured relative 3d cross section to the DWPO II result, rather than to the first Born, at 500 eV is that, contrary to the assumption of Mahan in other work, the 3d cross section nowhere exceeds the Born value. This is of importance in analysing measurements of the optical polarization of Hα (§ 4 below) and in interpreting the asymmetry in the Hα intensity in an applied static electric field reported by Mahan (Mahan *et al* 1975, Smith 1975). Our analysis of this latter experiment will be reported elsewhere.

3.2. Total $n = 3$ and total Hα cross sections

Mahan (1974) actually measured the total Hα cross section

$$\sigma(\mathrm{H}\alpha) = \sigma_{3s} + 0{\cdot}12\sigma_{3p} + \sigma_{3d} \tag{17}$$

relative to the Born value at 500 eV, together with a measurement of the ratios $\sigma_{3s}/\sigma(\mathrm{H}\alpha)$, $\sigma_{3p}/\sigma(\mathrm{H}\alpha)$ and $\sigma_{3d}/\sigma(\mathrm{H}\alpha)$. From the values of the individual cross sections he obtained (see above), we computed the total $n = 3$ cross section

$$\sigma(n = 3) = \sigma_{3s} + \sigma_{3p} + \sigma_{3d}. \tag{18}$$

These results for this cross section (which are shown in figure 5) are insensitive to our suggested renormalization of his 3d value at 500 eV. They lie between our DWPO II result and the modified Born calculation of Morrison and Rudge. The sum of the individual Glauber cross sections (Tai *et al* 1970, Bhadra and Ghosh 1971) also gives a result in good agreement with experiment for $E_i > 20$ eV. Neglect of target distortion in our model (DWPO I) gives results which, while lower than the first Born approximation, are nevertheless much too large at energies below 150 eV.

The total Hα cross section σ(Hα) is of more interest, since the contribution of σ(3p) no longer dominates. The available theoretical results are shown in figure 6(*a*). Our DWPO II results are in good agreement with those obtained using the individual cross sections presented by Morrison and Rudge, though they behave quite differently at very

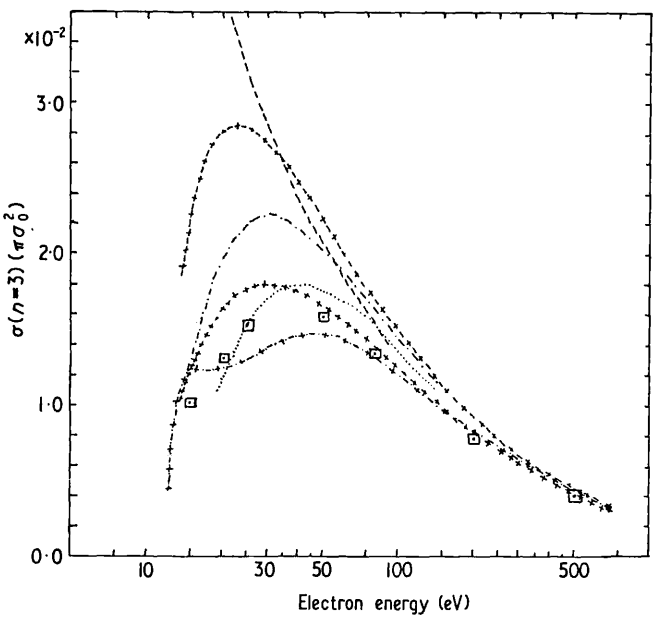

Figure 5. Total cross sections for the process $e + H(n = 1) \rightarrow e + H(n = 3)$ in units of πa_0^2 for impact energies from threshold to 500 eV. – – – – – –, Vainshtein (1961) (distorted wave); – + – + – + – +, Born approximation; + + + + + + + + +, DWPO II approximation; –·–·–·–·–·–·, DWPO I approximation; – · + · – · + · –, Morrison and Rudge (1966) (modified Born); ·····, Glauber approximation (Tai *et al* 1970, Bhadra and Ghosh 1971); □, Mahan (1974).

low energies (less than 15 eV) where neither approach is likely to be valid. The Glauber cross sections of Tai *et al* (1970) and of Bhadra and Ghosh (1971) lead to values of $\sigma(H\alpha)$ in good agreement with our DWPO I values at energies above 70 eV, but show a maximum at 35 eV and as is usual with Glauber calculations, yield very small cross sections below this energy. The other theoretical models (Born, DWPO I, Born–Oppenheimer, distorted wave) for which results are available give cross sections about 50% higher than our DWPO II results at intermediate energies ($15 < E_i < 100$ eV).

We compare our DWPO II results with the Glauber values and the available experimental data in figure 6(*b*). The only absolute experiment is that of Walker and St John (1974). These results are uncorrected for cascade, or for the optical polarization (cf § 4 below). Both these corrections, which are energy dependent, would reduce the quoted values at energies below 200 eV. The remaining experiments (Kleinpoppen *et al* 1962, Kleinpoppen and Kraiss 1968, Mahan 1974) are relative measurements, originally normalized to the first Born Hα cross section at either 200 or 500 eV. We have renormalized them to our DWPO II result at this energy, which lies about 8% below the Born value. When this is done the results of Mahan (Mahan 1974, Mahan *et al* 1975) remain in agreement with our calculated values at all energies above 20 eV. This suggests that Mahan's 3p results may be 20% too low at energies below 150 eV, and that his 3d values may be 50% high over this energy range, though his total cross section is accurate.

The earlier measurements of Kleinpoppen and his colleagues (Kleinpoppen *et al* 1962, Kleinpoppen and Kraiss 1968) remain in good agreement with our theoretical

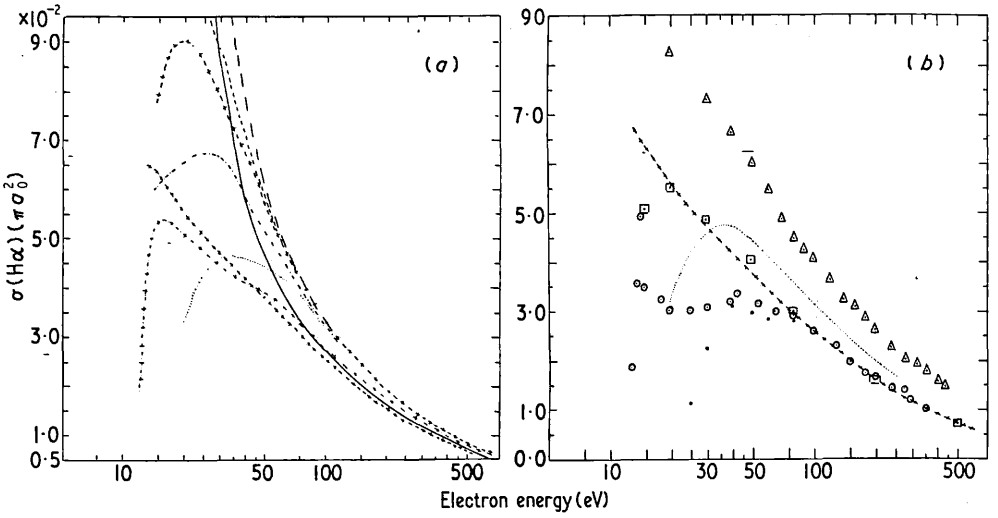

Figure 6. Total Balmer α production cross section in units of πa_0^2 for impact electron energies from threshold to 500 eV. (*a*) — — — —, Born–Oppenheimer; ————, Born–Oppenheimer II (includes target distortion); – – – – – – – –, Vainshtein (1961) (distorted wave); + – + – + – +, Born approximation; – · – · – · –, DWPO I; + + + + + + + + +, DWPO II; – · + · – · + · –, Morrison and Rudge (1966) (modified Born); · · · · · · · ·, Glauber (Tai *et al* 1970, Bhadra and Ghosh 1971). (*b*) △, Walker and St John (1974); ⊡, Mahan (1974) normalized to DWPO II at the highest energy of the experiment points; ⊙, Kleinpoppen *et al* (1962) normalized as above; ●, Kleinpoppen and Kraiss (1968) normalized as above; + + + + + + + + +, DWPO II; · · · · · · · ·, Glauber (Tai *et al* 1970, Bhadra and Ghosh 1971).

results and the experiment of Mahan *et al* at energies above 80 eV, but show almost no energy dependence below this energy. These measurements carry large errors (which may be as much as ±25%) but the general trend is nonetheless incompatible with that found by Mahan *et al* or by Walker and St John, or with our theoretical results.

As will be seen below, the polarization correction to be applied to Walker's data is quite small at all energies, so that it is tempting to attribute the whole difference between our results (or Mahan's) and those of Walker and St John to cascade effects. This difference is close to 50% of our Hα cross section at 20 eV increasing to 80% at 500 eV. However, Mahan (1974) has attempted a direct experimental determination of the percentage cascade correction to σ(Hα) as a function of energy, by using the different frequency response to an applied RF field of the states with $n \geqslant 4$ and finds that this percentage correction decreases from 9·3% at 500 eV to 4·4% at 15 eV. If these results are confirmed, then there exists a serious discrepancy between our results, and those of Mahan (however normalized), with the measurements of Walker and St John.

4. Polarization of Hα

The optical polarization of Hα photons observed at 90° to the incident electron beam can be expressed in terms of the total Hα cross section, and that cross section $\sigma_{90}(\mathrm{H}\alpha)$ which would be measured at 90°. Thus:

$$P_{90}(\mathrm{H}\alpha) = 3[1-\sigma(\mathrm{H}\alpha)/\sigma_{90}(\mathrm{H}\alpha)] \tag{19}$$

where

$$\sigma_{90}(\mathrm{H}\alpha) = \sigma_{90}(3s) + 0{\cdot}12\sigma_{90}(3p) + \sigma_{90}(3d) \tag{20}$$

and the individual 90° cross sections $\sigma_{90}(3l)$ ($l = 0, 1, 2$) are defined in terms of the 90° polarization of photons emitted from those states by

$$\sigma_{90}(3l) = \sigma(3l)[1 - \tfrac{1}{3}P_{90}(3l)]^{-1}. \tag{21}$$

Expressions for $P_{90}(3l)$ in terms of the cross sections for exciting the magnetic sublevels $\sigma(3lm_l)$, on the assumption that hyperfine-structure effects can be neglected, may be obtained from the work of Percival and Seaton (1958). We find

$$\begin{aligned} P_{90}(3s) &= 0, \qquad P_{90}(3p) = \frac{3(\sigma(3p0) - \sigma(3p1))}{7\sigma(3p0) + 11\sigma(3p1)}, \\ P_{90}(3d) &= 57\frac{(\sigma(3d0) + \sigma(3d1) - 2\sigma(3d2))}{119\sigma(3d0) + 219\sigma(3d1) + 162\sigma(3d2)} \end{aligned} \tag{22}$$

in agreement with the results of Mahan (1974), after correcting some misprints in Percival and Seaton's paper.

From these results we obtain expressions for the perpendicular cross sections.

$$\begin{aligned} \sigma_{90}(3s) &= \sigma(3s), \qquad \sigma_{90}(3p) = \frac{7\sigma(3p0) + 11\sigma(3p1)}{6}, \\ \sigma_{90}(3d) &= \frac{119\sigma(3d0) + 219\sigma(3d1) + 162\sigma(3d2)}{100}. \end{aligned} \tag{23}$$

These may now be used to calculate the polarization of the Hα line radiation,

$$P_{90}(\mathrm{H}\alpha) = \frac{1}{\sigma_{90}(\mathrm{H}\alpha)} \sum_{l=0}^{2} B_l \sigma_{90}(3l) P_{90}(3l) \tag{24}$$

where B_l is the proportion of emissions from the $3l$ state to the $n = 2$ state.

Our results for $P_{90}(3l)$ and $P_{90}(\mathrm{H}\alpha)$ in the DWPO II model are tabulated, and compared with the Born results, in table 1. The overall effect of including distortion and exchange

Table 1. Polarization fractions for 3p and 3d states and for Hα radiation.

E (eV)	Born $P_{90}(3p)$	DWPO II $P_{90}(3p)$	Born $P_{90}(3d)$	DWPO II $P_{90}(3d)$	Born $P_{90}(\mathrm{H}\alpha)$	DWPO II $P_{90}(\mathrm{H}\alpha)$
15	0·3570	0·3230	0·3999	0·3879	0·1859	0·2159
20	0·2794	0·2832	0·3087	0·3577	0·1590	0·2468
25	0·2291	0·2459	0·2447	0·3126	0·1347	0·2034
30	0·1929	0·2153	0·1958	0·2632	0·1143	0·1643
40	0·1434	0·1725	0·1245	0·1719	0·8294, −1	0·1124
50	0·1103	0·1435	0·7401, −1	0·1085	0·6005, −1	0·8515, −1
80	0·5281, −1†	0·8906, −1	−0·1914, −1	−0·3232, −2	0·1730, −1	0·4232, −1
100	0·3026, −1	0·6561, −1	−0·5773, −1	−0·4728, −1	−0·2588, −3	0·2617, −1
150	−0·4540, −2	0·2725, −1	−0·1209	−0·1160	−0·2824, −1	0·1522, −1
200	−0·2515, −1	0·3188, −2	−0·1604	−0·1559	−0·4478, −1	−0·1706, −1

† In this table and the following tables the abbreviation 0·5281, −1 ≡ $0{\cdot}5281 \times 10^{-1}$ is adopted.

is to increase the calculated polarization at all energies. The results for $P_{90}(H\alpha)$ are shown in figure 7. The behaviour of the calculated values is very similar to that found for Lyα (McDowell *et al* 1975a), except that the polarization goes negative about 50 eV

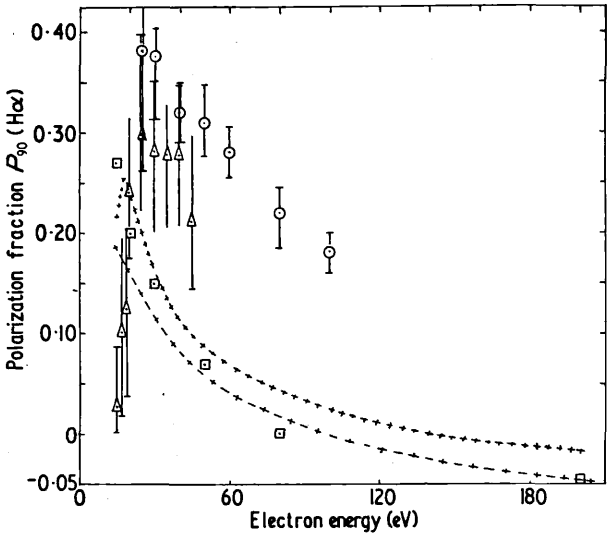

Figure 7. 90° polarization fraction of the Balmer α line for impact electron energies from threshold to 200 eV. ⊙, Kleinpoppen *et al* (1962); △, Kleinpoppen and Kraiss (1968); ⊡, Mahan (1974); + + + + + + + +, DWPO II; − + − + − + − +, Born.

lower in energy. However, while our DWPO II Lyα polarization results were in complete agreement, at energies above 20 eV, with the measured values of Ott *et al* (1970) our present results for Hα are in strong disagreement with the measurements of Kleinpoppen and his colleagues (Kleinpoppen *et al* 1962, Kleinpoppen and Kraiss 1968). Kleinpoppen believes that the latter experiment carries errors of at least 25% (1975 private communication), but this does not bring them into agreement with theory. The values given by Mahan (1974) do not represent an independent measurement of polarization, but rather are calculated values in which the Born $\sigma(nl)$ cross sections are replaced with his measured values, but the $\sigma(nlm_l)$ Born results are retained.

5. Differential cross sections

Differential cross sections for the individual $1s \rightarrow 3l$ transitions have been calculated using (12)–(14), and summed to give total $n = 3$ differential cross sections at selected energies. The individual and summed results at 100 and 200 eV are shown in figures 8(*a*), (*b*), 9(*a*) and (*b*), the values shown being obtained in the DWPO II model. At small angles ($\leqslant 45°$) the 3p transition dominates, but above 45° the 3s cross section contribution is also significant. Glauber 3p cross sections for $\theta \leqslant 50°$ have been given by Tai *et al* (1970) at 100 eV and are very close to our results in the forward direction, though they lie somewhat higher at intermediate angles (figure 8(*b*)). The Glauber 3s differential cross section at 100 eV is lower than our result in the forward direction ($\theta < 20°$) and somewhat higher at larger angles ($20° < \theta < 50°$), but the differences are small. For the 3d case, Glauber values have been given by Bhadra and Ghosh (1971) at both 100

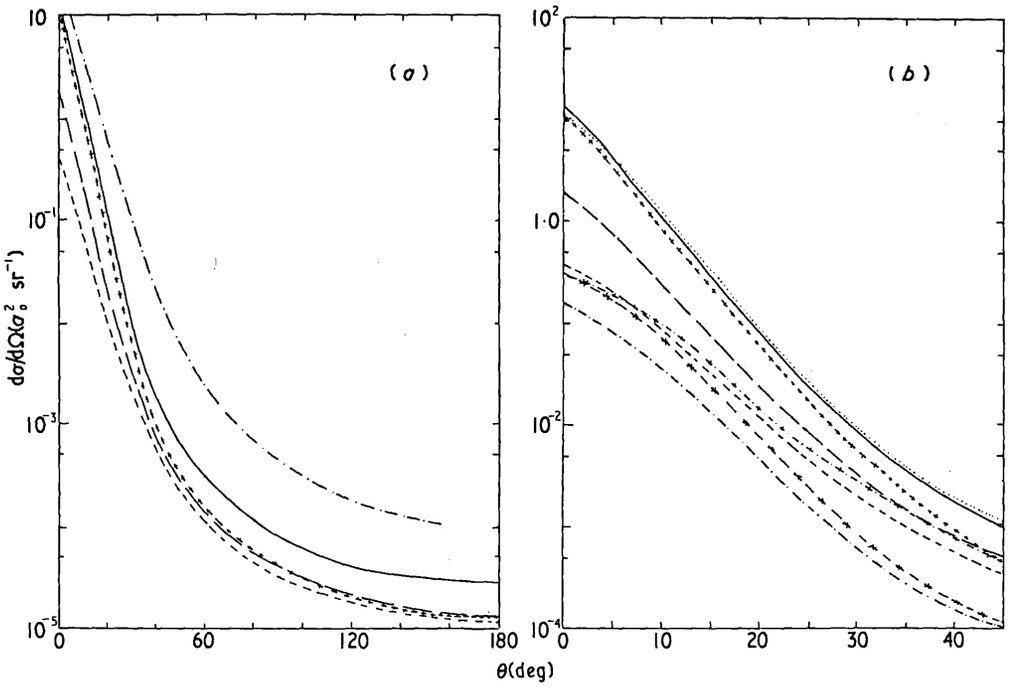

Figure 8. Differential cross sections in units of $a_0^2\ sr^{-1}$. (*a*) At 100 eV, for electron angles of 0° to 180°. ————, total $n = 3$ DWPO II; — — — —, Balmer α DWPO II; + + + + + +, 3p DWPO II; – – – – – –, 3s DWPO II; – · – · – ·, 3d DWPO II ($\times 10^2$). (*b*) At 100 eV, for electron angles of 0° to 45°. ————, total $n = 3$ DWPO II; — — — —, Balmer α DWPO II; + + + + + + + +, 3p DWPO II; · · · · · · · ·, 3p Glauber (Tai *et al* 1970); – · + · – · + ·, 3s Glauber (Tai *et al* (1970); – – – – – – – –, 3s DWPO II; – · – · – · –, 3d DWPO II; * – * – * – * –, 3d Glauber (Bhadra and Ghosh 1971).

and 200 eV for $\theta < 50°$. They find a forward value a factor of two higher than we obtain in the DWPO II approximation, but the difference is small at larger angles in this range (figures 8(*b*) and 9(*b*)).

Results, in our model, over the complete angular range are presented in figures 8(*a*) and 9(*a*). There is some numerical instability in our 3d result for $\theta > 120°$. At large angles the calculated cross section is many orders of magnitude greater than that obtained in the first Born approximation. Comparison of the predictions of the DWPO II model for $1s \rightarrow n = 2$ transitions in hydrogen (McDowell *et al* 1975b) with the experiments of Williams and Willis (1975) indicate that our failure to incorporate final channel distortion leads to an underestimate of $d\sigma/d\Omega$ ($n = 2$) in the backward direction by about a factor of two. This was confirmed by comparison of our results with experiment for $e + He(1\ ^1S) \rightarrow e + He(n\ ^1S)$, $n = 2, 3$ (Scott and McDowell 1975). We conclude that while our current differential cross sections are superior to previously published values for the $n = 1$ to $n = 3$ transition in atomic hydrogen, they may well be substantially too low at large angles. They might well be susceptible to improvement using a unitarization procedure to couple the $n = 3$ states (Fon *et al* 1975, Callaway *et al* 1976).

Values of the total $n = 3$ and Hα differential cross sections at 50, 100, 150 and 200 eV at selected angles are given in table 2 for future reference; values at other angles and energies will be published elsewhere (Syms 1975).

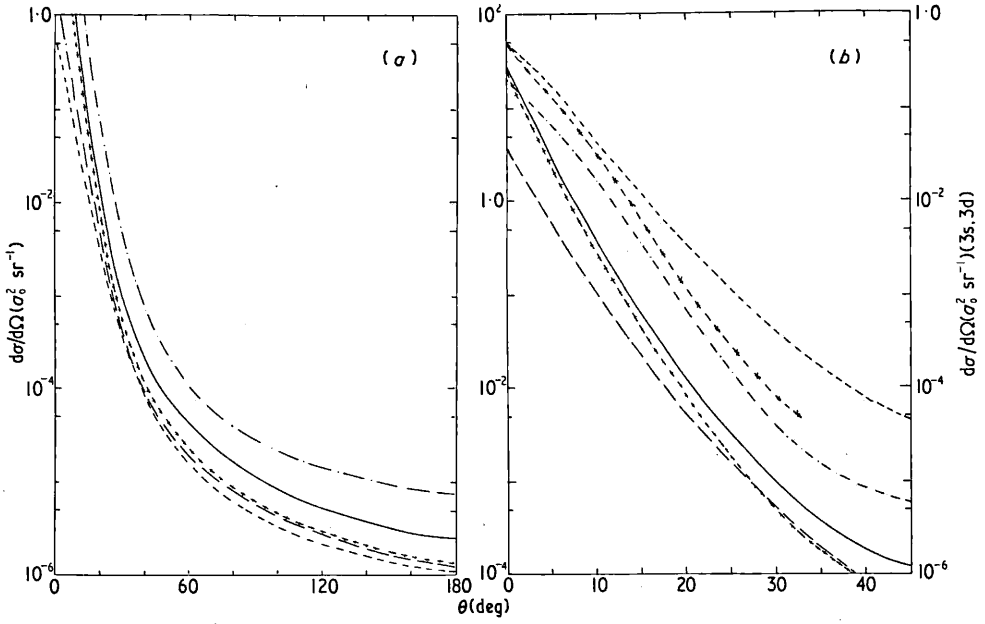

Figure 9. Differential cross sections in units of $a_0^2\,sr^{-1}$. (*a*) At 200 eV for electron angles of 0° to 180°. The meaning of the curves is the same as in figure 8(*a*). (*b*) At 200 eV for electron angles of 0° to 45°. ————, total $n = 3$ DWPO II; — — — —, Balmer α DWPO II; + + + + + + + +, 3p DWPO II; – – – – – – – –, 3s DWPO II; –·–·–·–·–, 3d DWPO II; *–*–*–*–*–, 3d Glauber (Bhadra and Ghosh 1971). (Note that the scales for the 3s and 3d cross sections are on the right-hand side.)

6. Conclusions

We have presented a study of the cross sections for the reactions

$$e + H(1s) \rightarrow e + H(nl) \qquad (l = 0, 1, 2)$$

evaluated in the DWPO II model.

Our calculated total Hα cross sections agree well in shape with the recent relative measurement of Mahan. They do not agree with the intermediate energy relative experiments of Kleinpoppen and Kraiss (1968). The absolute but uncorrected measurements by Walker and St John appear incompatible with our theoretical values when proper allowance is made for polarization and cascade effects.

Mahan (Mahan 1974, Mahan *et al* 1975) has used an RF technique to obtain cross sections for the individual $1s \rightarrow 3l$ ($l = 0, 1, 2$) levels from his normalized total Hα measurement. Our theoretical values are in excellent agreement with these results for $l = 0$, but at energies below 50 eV our 3p results lie 20% above the maximum uncertainty on Mahan's results, with a corresponding very substantial decrease in the calculated 3d values compared to the experimental ones. The latter discrepancy may be removed by renormalizing the experimental 3d values (which are small compared with $\sigma(3p)$) to our result at 500 eV, without significantly affecting $\sigma(H\alpha)$. We have also calculated the optical polarization of Hα emitted at 90° to the incident beam and find, in agreement with Mahan (1974), values of $P_{90}(H\alpha)$ much smaller at energies above 20 eV than those reported by Kleinpoppen and his colleagues (Kleinpoppen *et al* 1962, Kleinpoppen

Table 2. Differential cross sections (DWPO II approximation).

(*a*) 50 eV

θ (deg)	$d\sigma_{3s}/d\Omega$	$d\sigma_{3p}/d\Omega$	$d\sigma_{3d}/d\Omega$	$d\sigma(H\alpha)/d\Omega$	$d\sigma(n=3)/d\Omega$
0	0·2207	0·4271, +1	0·1098	0·8345	0·4602, +1
15	0·5276, −1	0·5418	0·2719, −1	0·1439	0·6218
30	0·6591, −2	0·4434, −1	0·5533, −2	0·1736	0·5646, −1
45	0·2104, −2	0·5795, −2	0·1881, −2	0·4669, −2	0·9780, −2
60	0·1017, −2	0·1546, −2	0·6136, −3	0·1813, −2	0·3177, −2
90	0·2658, −3	0·2447, −3	0·5520, −4	0·3499, −3	0·5657, −3
120	0·1526, −3	0·1394, −3	0·3231, −4	0·2014, −3	0·3243, −3
150	0·1603, −3	0·1641, −3	0·2381, −4	0·2038, −3	0·3482, −3
180	0·1697, −3	0·1771, −3	0·1987, −4	0·2104, −3	0·3667, −3

(*b*) 100 eV

0	0·3647	0·1092, +2	0·1554	0·1809, +1	0·1144, +2
15	0·2931, −1	0·2224	0·1300, −1	0·6855, −1	0·2647
30	0·2133, −2	0·6001, −2	0·6277, −3	0·3469, −2	0·8762, −2
45	0·3400, −3	0·4599, −3	0·1090, −3	0·5033, −3	0·9089, −3
60	0·1150, −3	0·1479, −3	0·2526, −4	0·1577, −3	0·2882, −3
90	0·3302, −4	0·4037, −4	0·4330, −5	0·4211, −4	0·7772, −4
120	0·1713, −4	0·1990, −4	0·1756, −5	0·2123, −4	0·3869, −4
150	0·1270, −4	0·1439, −4	0·1074, −5	0·1547, −4	0·2816, −4
180	0·1189, −4	0·1352, −4	0·8526, −6	0·1434, −4	0·2626, −4

(*c*) 150 eV

θ(deg)	$d\sigma_{3s}/d\Omega$	$d\sigma_{3p}/d\Omega$	$d\sigma_{3d}/d\Omega$	$d\sigma(H\alpha)/d\Omega$	$d\sigma(n=3)/d\Omega$
0	0·4379	0·1774, +2	0·1733	0·2705, +1	0·1835, +2
15	0·1677, −1	0·1009	0·6563, −2	0·3523, −1	0·1272
30	0·8302, −2	0·1393, −2	0·1268, −3	0·1121, −2	0·2350, −2
45	0·9897, −4	0·1317, −3	0·1833, −4	0·1328, −3	0·2490, −3
60	0·3402, −4	0·4964, −4	0·2520, −5	0·4240, −4	0·8618, −4
90	0·1021, −4	0·1462, −4	0·8776, −6	0·1281, −4	0·2571, −4
120	0·4903, −5	0·6623, −5	0·5422, −6	0·6627, −5	0·1207, −4
150	0·3343, −5	0·4384, −5	0·4612, −6	0·4322, −5	0·8188, −5
180	0·3246, −5	0·4817, −5	0·4422, −6	0·4257, −5,	0·8505, −5

(*d*) 200 eV

0	0·4831	0·2410, +2	0·1842	0·3511, +1	0·2477, +2
15	0·1062, −1	0·5115, −1	0·3405, −2	0·2006, −1	0·6518, −1
30	0·3786, −3	0·4804, −3	0·3313, −4	0·4683, −3	0·8921, −3
45	0·4241, −4	0·6311, −4	0·5632, −5	0·5549, −4	0·1112, −2
60	0·1504, −4	0·2350, −4	0·9825, −6	0·1880, −4	0·3952, −4
90	0·4494, −5	0·6841, −5	0·2398, −6	0·5541, −5	0·1157, −4
120	0·2009, −5	0·2891, −5	0·1354, −6	0·2489, −5	0·5035, −5
150	0·1384, −5	0·2087, −5	0·9498, −7	0·1725, −5	0·3566, −5
180	0·1444, −5	0·1323, −5	0·7308, −7	0·1675, −5	0·2842, −5

and Kraiss 1968). These experiments are difficult, and subject to error due to the large background. More accurate results might now be obtained using coincidence techniques.

Such coincidence measurements (of Lyα and Hα photons emitted subsequent to excitation of the $n = 3$ levels, in coincidence with the scattered electron) are in hand in at least one laboratory, and our theoretical predictions for the Fano–Macek parameters (Fano and Macek 1973, Morgan and McDowell 1975) which allow a complete description of such experiments will be given in a subsequent paper.

Acknowledgment

One of us (RFS) was the holder of an SRC Research Studentship during the course of this work.

Appendix. A general form for $f_{1s,nl}(r)$ and $k_{1s,nl}(r)$

Taking

$$R_{nl}(Z,r) = 2Z^{3/2}\left(\frac{(n-l-1)!(n+l)!}{n^4}\right)^{1/2}\left(\frac{2Zr}{n}\right)^{l} e^{-Zr/n}\sum_{s=0}^{n-l-1}\frac{(-2Zr/n)^s}{s!(n-l-1-s)!(2l+1+s)!}$$

we obtain, setting $\gamma = (n+1)/n$,

$$rf_{1s,nl}(r) = \left(\frac{2}{n}\right)^{l+2}\frac{[(n-l-1)!(n+l)!]^{1/2}}{(\gamma Zr)^l}\sum_{s=0}^{n-l-1}\frac{(-2/n)^s(2l+s+2)}{s!(n-l-1-s)!}\gamma^{-(l+s+3)}$$
$$\times\left\{1-e^{-\gamma Zr}\left[\sum_{p=0}^{2l}\frac{(\gamma Zr)^p}{p!}+\sum_{p=2l+1}^{2l+2+s}(\gamma Zr)^p\left(\frac{1}{p!}-\frac{(s+1)!}{(2l+2+s)!(p-2l-1)!}\right)\right]\right\}.$$

Similarly, for $l' = l\pm 1$,

$$rk^{(l')}_{1s,nl}(r) = \frac{1}{4}\left(\frac{2}{n}\right)^{l+2}\frac{[(n-l-1)!(n+l)!]^{1/2}}{(\gamma Zr)^{l'+2}Z}\sum_{s=0}^{n-l-1}\frac{(-2/n)^s(2l+2+s)w_s(l,l')}{s!(n-l-1-s)!\gamma^{l+s+3}}$$
$$\times\left\{-1+e^{-\gamma Zr}\left[\sum_{p=0}^{l+l'+s+3}\left(\frac{(\gamma Zr)^p}{p!}\right)+\frac{(\gamma Zr)^{l+l'+s+4}}{(l+l'+s+3)!(l+l'+s+4+2\gamma)}\right]\right\}$$

with

$$w_s(l,l') = \begin{cases}(l+l'+s+4+2\gamma), & l' = l-1\\ (l+l'+s+2)(l+l'+s+3)(l+l'+s+4+2\gamma), & l' = l+1.\end{cases}$$

For small Zr,

$$rk^{(l')}_{1s,nl}\underset{Zr\to 0}{\to} -\frac{1}{2Z}\left(\frac{2}{n}\right)^{l+2}[(n-l+1)!(n+l)!]^{1/2}$$
$$\times\sum_{s=0}^{n-l-1}\frac{(-2/n)^s(Zr)^{l+s+2}}{s!(n-l-1-s)!(2l+1+s)!(l+l'+s+4)}$$
$$\times\left(1+\sum_{p=0}^{p_0}\frac{(-\gamma Zr)^{p+1}(l+l'+s+4)(2\gamma-p-1)}{2\gamma(p+1)!(l+l'+s+p+5)}\right).$$

Note added in proof. Professor M R Flannery has brought to our attention a paper by Flannery and McCann (1974, *J. Phys.* B: *Atom. Molec. Phys.* **7** L522) containing results for the 3s and 3p excitation processes, obtained in a seven-channel (1s, 2s, 2p, 3s, 3p) eikonal treatment. As can be seen from table A.1 below, these results are in excellent agreement with ours above 20 eV, and with experiment. However, the polarization fractions for the 3p states obtained by using their reported values for $\sigma(3p0)$ and $\sigma(3p1)$ in equation (22) (see table A.2) would imply a serious discrepancy between their individual magnetic sub-levels contributions and ours.

Table A.1. Total 3s and 3p cross sections in units of $10^{-2}\pi a_0^2$.

	FMcC[a]		DWPO I		DWPO II		Experiment[b]	
eV	3s	3p	3s	3p	3s	3p	3s	3p
15	—	—	2·28	7·97	2·86	7·04	2·16	4·07
16·5	1·41	7·23	1·84	10·7	2·20	9·25	—	—
20·0	1·78	10·9	1·52	14·8	1·51	12·5	2·16	8·06
30·0	1·87	14·8	1·81	18·0	1·55	14·8	1·29	11·4
50·0	1·46	14·6	1·57	17·0	1·39	14·4	1·36	12·7
80·0	—	—	1·15	14·1	1·07	12·2	0·97	9·15
100·0	0·90	11·1	0·97	12·5	0·93	11·0	—	—
200·0	0·50	7·42	0·54	8·10	0·54	7·27	0·58	6·79

[a] Flannery and McCann (1974).
[b] Mahan (1974).

Table A.2. Polarization fractions for the 3p state.

eV	FMcC[a] $P_{90}(3p)$	Born $P_{90}(3p)$	DWPO II $P_{90}(3p)$
15	—	0·36	0·32
16·5	0·25	—	—
20	0·19	0·28	0·28
30	0·11	0·19	0·22
50	0·04	0·11	0·14
100	−0·04	0·03	0·07
200	−0·09	−0·03	0·0

[a] Flannery and McCann (1974).

References

Beigman I L and Shevel'ko V P 1974 *Opt. Spectrosc.* **37** 353–5
Bhadra K and Ghosh A S *Phys. Rev. Lett.* **26** 737–9
Burgess A 1963 *Proc. Phys. Soc.* **81** 442–52
Burgess A, Hummer D G and Tulley S A 1970 *Phil. Trans. R. Soc.* A **266** 255–79
Burke P G, Ormonde S and Whitaker W 1967 *Proc. Phys. Soc.* **92** 319–35
Burke P G, Schey H M and Smith K 1963 *Phys. Rev.* **129** 1258–74
Callaway J, McDowell M R C and Morgan L A 1976 *Bull. Am. Phys. Soc.* in press
Eminyan M, McAdam K B, Slevin J and Kleinpoppen H 1974 *J. Phys.* B: *Atom. Molec. Phys.* **7** 1519–42

Fano U and Macek J H 1973 *Rev. Mod. Phys.* **45** 553–73
Fon W C, Kingston A E and Burke P G 1975 *Proc. 9th Int. Conf. on Physics of Electronic and Atomic Collisions, Seattle* vol 2 (Seattle: University of Washington) pp 669–70
Kleinpoppen H and Kraiss E 1968 *Phys. Rev. Lett.* **20** 361–3
Kleinpoppen H, Kruger H and Ulmer R 1962 *Phys. Lett.* **2** 78–9
Krotlzov R 1975 *Phys. Rev.* in press
McDowell M R C, Morgan L A and Myercough V P 1973 *J. Phys.* B: *Atom. Molec. Phys.* **6** 1435–51
—— 1975a *J. Phys.* B: *Atom. Molec. Phys.* **8** 1053–72
—— 1975b *J. Phys.* B: *Atom. Molec. Phys.* **8** 1838–50
McDowell M R C, Myerscough V P and Narain U 1974 *J. Phys.* B: *Atom. Molec. Phys.* **7** L195–7
Mahan A H 1974 *PhD Thesis* University of Colorado
Mahan A H, Gallaher A and Smith S 1975 *Phys. Rev.* to be published
Morgan L A and McDowell M R C 1975 *J. Phys.* B: *Atom. Molec. Phys.* **8** 1073–81
Morgan L A, McDowell M R C, Stauffer A D and Syms R F 1975 *Comput. Phys. Commun.* to be submitted
Morrison D J T and Rudge M R H 1966 *Proc. Phys. Soc.* **89** 45–53
Ott W R, Kaupilla W E and Fife W L 1970 *Phys. Rev.* A **1** 1089–98
Percival I C and Seaton M J 1958 *Phil. Trans. R. Soc.* A **251** 113–38
Scott T and McDowell M R C 1975 *J. Phys.* B: *Atom. Molec. Phys.* **8** 1851–65
Seaton M J 1961 *Proc. Phys. Soc.* **77** 174–83
Smith S J 1975 *Electron and Photon Interactions with Atoms* ed H Kleinpoppen and M R C McDowell (New York: Plenum) in press
Syms R F 1975 *PhD Thesis* University of London, in preparation
Tai H, Bassel R H, Gerjuoy E and Franco V 1970 *Phys. Rev.* A **1** 1819–35
Vainshtein L A 1961 *Opt. Spectrosc.* **11** 163
Walker J D and St John R M 1974 *J. Chem. Phys.* **61** 2394–407
Williams J F and Willis B A 1975 *J. Phys.* B: *Atom. Molec. Phys.* **8** 1641–70
Woolings M J and McDowell M R C 1973 *J. Phys.* B: *Atom. Molec. Phys.* **6** 450–61